ERDC/GSL TR-04-4

Geotechnical and Structures Laboratory

US Army Corps of Engineers®
Engineer Research and Development Center

A Partially Saturated Constitutive Theory for Compacted Fills

Ernest S. Berney IV

June 2004

ERDC/GSL TR-04-4
June 2004

A Partially Saturated Constitutive Theory for Compacted Fills

Ernest S. Berney IV

Geotechnical and Structures Laboratory
U.S. Army Engineer Research and Development Center
3909 Halls Ferry Road
Vicksburg, MS 39180-6199

Final report

Prepared for U.S. Army Corps of Engineers
Washington, DC 20314-1000

ABSTRACT: Partially saturated soil is the most common material encountered in the field of geotechnical engineering. Yet, mechanics of partially saturated soil lags far behind that of saturated soil. A partially saturated soil is a complex multiphase system consisting of air, water, and solid material whose response is a function of the stress state, moisture condition, and other internal variables present within the soil. From a thermodynamic viewpoint, a partially saturated soil can be best described by the free energy associated with each component of the soil and water mixture.

It is noted that many thermodynamic formulations have been proposed for soil plasticity. In the current research, a theory to capture the mechanical response of partially saturated materials was constructed from a saturated soil model by adding a term for the free energy of the capillary phase that includes coupling between the solid and water phases. In defining the free energy, a distinction is made between water in the capillary phase and mobile water that flows as an independent phase. This inherent relationship between the variables appearing in the free energy expression and their conjugate stress terms obviates the traditional problem of defining the effective stress. The principles of the theory are illustrated by extending an existing plasticity model for saturated soils, which is based on an internal variable formulation, by adding terms that account for free energy of the capillary phase. The model exhibits the tendency of partially saturated soil to either swell or collapse, depending on the compaction state. Simulations of consolidated-undrained triaxial tests demonstrate the proper relationship between strength and the state as described by water content, void ratio, and total confining stress.

TABLE OF CONTENTS

Page

Page

Page

PREFACE

The research reported herein was sponsored by the U.S. Army Corps of Engineers, through the Research, Development, Testing and Evaluation (RDT&E) Program, Pavements Research Work Package, AT40. The research was conducted at the U.S. Army Engineer Research and Development Center (ERDC), Geotechnical and Structures Laboratory (GSL), Engineering Systems and Materials Division (ESMD), Airfield and Pavements Branch (APB), Vicksburg, MS.

The study was conducted under the general supervision of Dr. David Pittman, Acting Director, GSL, Dr. Albert Bush, Chief, ESMD, and Mr. Don R. Alexander, Chief, APB. Drs. John F. Peters and Donald M. Smith, APB Analytical Modeling Team, provided technical direction. Drs. Thomas D. White, Mississippi State University, and John E. Haddock, Purdue University, provided much insight and guidance as committee chairmen during the testing, analysis, and publication phases of this research. Dr. Sam Berney and Mses. Cindy Berney and Ginger Berney provided enduring support toward the completion of this research. Messrs. Dan Leavell, Charles Carter, Tommy Carr, and Larry Dunbar, and Ms. Judy Hudnall provided assistance during the testing and analysis phases of this research. Dr. Ernest S. Berney IV was the project principal investigator and author of this report. This report was submitted by Dr. Ernest S. Berney IV to and accepted by the Graduate School, Purdue University, in partial fulfillment for the degree of Doctor of Philosophy.

COL James R. Rowan, EN, was Commander and Executive Director of ERDC, and Dr. James R. Houston was Director.

CHAPTER I
Introduction

1.1 Background

Partially saturated, compacted fills are used widely throughout civil engineering construction. One of the most common uses of a compacted fill is as a foundation for highway and airfield pavements. Compacted soil as a foundation for pavements improves the distribution of applied stresses thereby reducing the magnitude of strain experienced within the pavement system under trafficking. The challenge to current civil engineers is no longer simply the design of pavement systems, but prediction of their performance under repeated loads. To complicate the issue of modeling pavement foundations is the need to account for moisture influencing the stress-strain response of not only the compacted layers, but also the in-situ ground beneath the pavement system. This thesis will provide a material model to capture the response of partially saturated, compacted fills accounting for changes in density and moisture as conditions dictate.

Airfield pavement design is a complex blend of relatively simple linear elastic theory, fatigue concepts, empirical relationships derived from small and full-scale tests, and pragmatic adjustments to reflect observations of in-service pavements. This philosophy served the design community well for many years as it allowed total thickness, asphalt concrete pavement thickness, and material requirements for constituent layers in the pavement to be determined to avoid a pre-selected level of distress in the pavement. For flexible pavement airfields, this level of distress at "design" failure was selected to be one inch of shear rutting in the subgrade or fatigue cracking of the asphalt concrete.

Predicting pavement performance is a far more complex task than simply providing safe thickness of the layers. To deal with this new challenge, the design community must have material models that predict cumulative deformations under repetitive aircraft loads and account for environmental changes occurring over the lifetime of the pavement system. With heavy loading, such as may be encountered with many airfields, nonlinear response of base course and subgrade materials must be considered when predicting pavement performance. With seasonal variations, the moisture condition of unbound aggregates and soils influences their strength and deformation responses. The sensitivity of compacted soils to moisture condition continues to be a difficult problem to model. However, a material model accounting for the moisture effects is critical to predicting performance of any pavement system containing layers of partially saturated unbound aggregates or soil. Furthermore, to apply such a material model, mechanical response data are required to calibrate the necessary parameters, Barker and Gonzalez (*1991*).

A partially saturated soil is a complex multi-phase system consisting of air, water and solid material whose response is a function of not only the external and internal stress state but as well the moisture condition present within the soil. In traditional soil mechanics, this moisture effect has largely been ignored to produce a conservative design that always assumes the worst-case scenario whereby a fully saturated soil is present. A soil in a saturated state is typically at its weakest strength condition and is the least susceptible to swelling effects due to changes in its water content. This conservative approach to design has been used for nearly a century and has proven to produce stable structures and edifices. However when analysis is sought on existing structures, the use of current design models is woefully inadequate to predict future performance. Therefore there is a need to understand the mechanics of the partially saturated system as a step forward in the knowledge base of material responses. This will allow the analyst greater insight into the observed mechanical behavior of loaded soil systems under a condition of partial saturation.

1.2 Objective

The objective of this research is to provide a predictive method for modeling response of compacted fine-grained soil layers in pavements subjected to aircraft loads and changes in moisture. Essential features of soil response that are required from a constitutive model include non-linear elastic response, permanent or plastic deformation resulting from yield, hysteresis, strain softening/hardening, shear-dilatancy and shrink-swell effects due to changes in moisture. These features must also reflect the influence of partial saturation. The constitutive model should be simple in operation, calibration and implementation into an effective stress model capable of handling aircraft loading. The model must also be capable of predicting performance of partially saturated compacted fills for a pavement structure subject to traffic loading.

1.3 Originality

The research involves development, implementation, and evaluation of a constitutive theory based upon the thermodynamic behavior of partially saturated soils. A capability will be provided to predict strain and associated stress in compacted pavement fills for current and future aircraft loads and for seasonal variations in moisture condition.

1.4 Scope of Work

This research was conducted as a five-phase effort.

Phase 1: State of the Art Review and Assessment: This phase included a review of related publications, research, and test results. Candidate theories including a discussion of the constitutive model framework chosen for this project, models, test methods, data sets and a thorough history of concept development were identified in this review. *Chapter III.*

Phase 2: Model Development: In this phase a candidate constitutive model was developed from fundamental thermodynamic principles of a three-phase soil to capture the effects of moisture and plasticity within a compacted fill.
Chapter IV.

Phase 3: Model Integration: In this phase, the candidate constitutive model was implemented within a single finite-element constitutive driver entitled the Multi-Mechanical Model (MMM) (*Smith, 2000 and Smith, et al., 2001*).
Chapter V.

Phase 4: Model Calibration: In this phase, a suite of laboratory tests was conducted to obtain data to calibrate the saturated and partially saturated response of compacted fill material model. Historical test data was acquired and new tests were conducted where necessary.
Chapters VI, VII.

Phase 5: Model Verification, Evaluation and Documentation: In this phase, the newly calibrated thermodynamic model was exercised and results compared against laboratory test data to assess its predictive capability. The partially saturated model was implemented into the MMM effective stress constitutive driver to carry out model simulations. Strengths and weaknesses of the response model and calibration parameter relationships were evaluated and documented.
Chapter VIII.

CHAPTER II
Problem Statement

One of the most common uses of compacted soils is as a foundation for highway and airport/aircraft pavements. Pavements designed for military aircraft commonly consist of a thin asphalt concrete (AC) layer supported by relatively thick layers of bound or unbound granular base and compacted fill over a deep foundation. Portland cement concrete pavements are relatively thick surface layers also supported by bound and unbound granular base and compacted fill. These thick soil fill layers reduce stresses applied by traffic at the pavement surface. Current military trends dictate a need to accurately characterize and predict pavement response for both surfaced (AC, PCC) and unsurfaced airfield pavements. This need requires the ability to accurately model stress-strain response of pavement foundations. To attain this goal, material models for the foundation layers must be capable of accounting for changes in stress-strain response with density as well as soil moisture.

Magnitude and frequency of airfield pavement loading are very different from typical highway pavements. Heavy static aircraft loads are the most critical to pavement structures. Load repetitions applied to airfield pavements are several orders of magnitude less than that applied to highway pavements. A high-volume highway may experience 10's of millions of load repetitions, while a high volume airfield may only experience 250,000 aircraft coverages over a 20-year period. The airfield pavement community has been required to broaden its focus of analytical research to predict performance of the supporting structural layers including the partial saturation effects of compacted fill.

The structural components of pavement foundations are highly nonlinear elastic-plastic materials. This non-linear response is greatly apparent within the pavement foundation when subjected to heavy aircraft loading and therefore is essential to consider

when predicting pavement performance. The foundation soils are also susceptible to seasonal changes in moisture within the layers since changes in moisture lead to variability of mechanical response that needs to be accounted for when predicting performance. The problem of modeling a pavement system is further complicated by the fact that each surface pass applied by an aircraft changes the characteristics of its behavior due to the accumulation of plastic strain; therefore it is critical to develop an understanding of the physics dictating the observed response.

A promising research effort into the modeling of nonlinear elastic-plastic response of two-phase, saturated foundation materials has been demonstrated through implementation in a commercial analysis tool by Smith (*2000*). The current research enables analysis of the more complex, three-phase soil stress-strain constitutive behavior, its coded implementation into the existing model by Smith along with a definition of its physical response. To date the ability to incorporate a three-phase soil system model into an analysis program has not been sufficiently demonstrated.

The objective of this research is to derive a fundamental thermodynamic model to allow a prediction of partially saturated response for compacted fine-grained soil layers typically found in pavements subjected to aircraft loads. Essential features of soil response are non-linear elastic response, permanent or plastic deformation resulting from yield, hysteresis, strain softening/hardening, shear-dilatancy, and moisture induced shrink-swell effects, all of whose effects are influenced by partial saturation. A model capable of being incorporated into any effective stress model is anticipated that will be simple in operation, calibration and implementation. The model must be capable of predicting both response and performance of partially saturated compacted fills within a compacted fill under aircraft traffic loading.

CHAPTER III

Literature Review

The literature review will focus on cohesive, fine-grained soils such as clays and mixtures of clay with other coarser materials such as silt, sand and gravel. A review of early work on the effect of moisture on soil response through soil fabric followed by a review of the suction concept and early work concerning its role in the effective stress relationship originally proposed by Terzaghi in 1943. An overview will be provided on empirical work related to volume change of partially saturated soil independent of strength. A summary of modeling efforts to estimate the combined constitutive response of partially saturated soils begun in the mid 1960's through to the late 1990's will finalize the chapter.

3.1 Definition of a Partially Saturated Soil

A partially saturated soil (PSS) is defined as a material which is made up of three phases, air, water and solids (Figure 3-1). Almost any surface material which is not inundated with water and lies above the groundwater table is a partially saturated soil. The use of fill material in embankments, roadways, earthen dams, backfill and landfill liners is always partially saturated at the time of construction. With time, inundation with water can cause these constructions to become saturated leading to a loss of strength and the potential for shrink/swell. Therefore it is important to understand the mechanical behavior of a PSS to extend the capabilities of existing saturated soil models.

3.2 The Role of Partially Saturated Soil in Construction

Compacted soil in embankments, dams, slopes, pavement foundations and subgrades, building foundations and deep fills are constructed at moisture conditions at or near optimum moisture content but ultimately partially saturated. The benefits of this were documented by Proctor (*1933*) who noted that by compacting soil at water contents less than saturation, a greater density and therefore better performance was obtained. Soon thereafter the advent of the California Bearing Ratio (CBR) test (*Porter, 1942*) allowed a shearing type test to be conducted on compacted soil at varying densities specified by Proctor. From these early tests it was shown that the strength of a soil improved when not completely saturated and that an ideal soil would have an optimum water content coupled with a maximum dry density at which the soil would achieve its highest strength potential. From CBR tests strength was related to placement density and water content, these early tests laid the groundwork for future researchers to explore details behind this unique relationship.

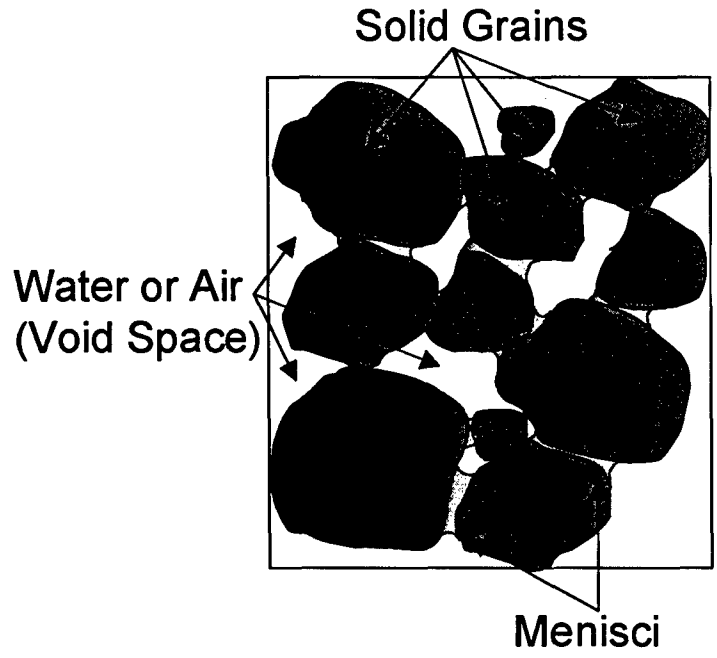

Figure 3-1: Diagram of partially saturated soil components

In the early 1950's researchers began to quantify the strength and deformation response of partially saturated soils. Partially saturated cohesive soils have a tendency to swell or increase in volume when water content increases and shrink or decrease in volume when dried as water content is reduced. Wilson (*1952*) showed that soils compacted dry of optimum water content could sustain higher loads than those wet of optimum for an equivalent change in volume (*Leonards, 1952*). However when the soil was soaked by inundation with water, the dry specimens experienced a rapid decrease in volume that collapsed to the volume of a saturated specimen under the same load. This collapse phenomena has been documented extensively by other researchers in a one-dimensional test apparatus (*Jennings, 1962; Barden, 1969, 1973; Blight, 1965; Dudley, 1970; Cox, 1978*) and in a triaxial device (*Lawton, 1986, 1989*) and traditionally occurs when a soil is compacted in a very loose state or is supporting a pressure greater than its saturated strength owing to the increase in strength from partial saturation.

A formal study on the role of shear strength of compacted soils was conducted by Seed (*1959, 1960*) which showed that the unconfined shear strength of a partially saturated soil was greatest just prior to the optimum water content, reduced in strength as the sample dried out further and significantly lost strength when failed at water contents wetter than optimum approaching saturation. To examine the volumetric response of partially saturated soils when the water content was increased to saturation, Seed (*1962*) illustrated that in unconfined cohesive soils, the volume increases during inundation with water reaching a maximum change at a water content slightly drier than optimum, eventually reaching minimal swell at water contents near saturation. The early work of both Seed and Wilson illustrated a coupling of behavior between both strength and deformation and a dependence of each on water content that had otherwise not been addressed.

Being able to predict either strength or volume change behavior of partially saturated soil poses a great challenge to the soils engineer. Terzaghi (*1943*) introduced the concept of effective stress to represent the response of soils fully saturated either with water or air as follows:

$$\sigma_{ij}' = \sigma_{ij} - u_w \delta_{ij} \qquad (3.1)$$

σ_{ij}' = Effective or intergranular stress

σ_{ij} = Cauchy or boundary stress

u_w = pore water pressure *(or zero for air saturation)*

This model of soil strength behavior and volumetric response is based upon a two-phase material. To include water content and air within a partially saturated three-phase soil system requires definition of water content interaction with both soil and air phases.

3.3 Soil Suction

As early as 1897, Briggs introduced the concept of water existing within soil in three distinct phases: gravitational, capillary and hygroscopic. Gravitational water is the free water in the pore spaces of a soil structure that is free draining under influence of gravity. Capillary water is water that forms capillaries or menisci between adjacent soil grains (see Figure 3-1). Hygroscopic water is bound water attracted to the soil particle surface dependent on soil mineralogy. Gravitational water contributes to the pore pressure defined in Terzaghi's effective stress definition. The capillary water generates the soil suction defined as the difference between atmospheric pressure and the pressure in the free water. Lastly, hygroscopic water is that volume of water causing a cohesive soil to swell or shrink with changes in water as the volume is adsorbed or removed from the mineral lattice.

The importance of soil suction for construction of highways and airfields was noted by Croney (*1948*). Because of seasonal changes in climate, the moisture regime beneath a pavement structure can change with an increase or decrease in precipitation or with changes in temperature that cause moisture vapor to rise into the upper layers of a pavement (moisture vapor migrates from warm to cold regions). This change in moisture results in changes in soil suction that can alter the soil's mechanical behavior.

Total soil suction can be divided into two separate but additive suction values, osmotic suction and matric suction (*Bolt, 1958*). Matric suction is that portion of energy

potential derived from physical bonding between capillaries and solid grains of soil providing a tensile resistance at the contacts. Osmotic suction is the chemical interaction between the pore fluid and the soil grains that generates a secondary bonding between particles that have attractive chemical charges. The difference between total and matric suction is negligible up to very high (1000 atm) suction pressures (*Coleman 1959*) suggesting only a small osmotic suction influence in most soils. For a given soil, the osmotic remains constant whereas the variation in measured total suction will originate only from changes in matric suction due to changes in water volume within the soil (*Aitchison, 1960*). Therefore total suction can be taken as equal to matric suction (*Coleman, 1959*) and literature almost universally reports a measured value of total suction for use in analyses of soil strength. Any measured values of suction used in this thesis will be assumed to be the total suction and will be referred to in this thesis as the suction or suction potential.

3.4 Suction as a Parameter

The first approach to account for the effect of partial saturation in modeling was to incorporate soil suction as a parameter affecting the soil response. Soil suction varies with degree of saturation and therefore represents an indirect means to incorporate water content into the analysis. Hilf, Aitchison and Bishop (*1956, 1960, 1960*) studied the effects of soil suction and defined the role of pore pressure of partially saturated soils. Hilf (*1956*) in his work on the axis translation technique for triaxial testing of partially saturated soils, showed that soil matric suction is the change in air pressure from water pressure ($u_a - u_w$), and if both are increased at the same rate, the suction and therefore the material response will not change. This established that suction was a controllable quantity, and through its variation, the soil response will change. Bishop (*1960*) and Aitchison (*1960*) used this information to construct equations of effective stress that were dependent on water content to the extent that they would consider this new suction parameter.

Their goal was to create a single valued equation relating the degree of saturation to the percentage of matric suction that contributed to the pore pressure response in the classical Terzaghi definition of effective stress. Bishop (*1960*) proposed a model to predict soil strength based upon soil suction potential within a partially saturated soil. Below is an outline of the idealized formulation used by Bishop:

$$\sigma_{ij}' = \sigma_{ij} - u_a\delta_{ij} + \chi(u_a - u_w)\delta_{ij} \qquad (3.2)$$

σ_{ij}' = effective stress as defined by Terzaghi

σ_{ij} = Cauchy or boundary stress

δ_{ij} = Kronecker delta

u_a = pore air pressure

u_w = pore water pressure

χ = parameter influenced by soil structure and type, cycle of wetting/drying and stress change

This expression states that the matric suction (u_a - u_w) contributes to an increase in the effective stress, and that the increase varies by a parameter χ unique for a given soil. The factor χ is dependent on the type of soil and is an empirical, non-linear function with respect to degree of saturation. The goal of Bishop's work was to introduce this new definition of effective stress into the existing formulae for determining strength and volume change to account for the suction potential. Unfortunately, while it was possible to account for the increase in strength, the shortcoming of Bishop's effective stress model was that it failed to predict the volume change response adequately since saturated soils do not experience swelling or collapse typically found in partially saturated soils. This deficiency was identified by Jennings and Burland (*1962*) and Burland (*1965*). As well, Leavell, et al., (*1987*) showed that partially saturated soils tend to fracture at failure rather than shear, offering a different failure mechanism than that assumed by the effective stress strength theory.

The idea that suction acted as an independent stress variable from the applied stress, $(\sigma - u_a)$ began with work by Matyas and Radakrishna (*1968*), who conducted a series of isotropic triaxial tests looking at the volumetric strain occurring in cohesive soils under varying suction conditions. Their work built upon early work by Biot (*1941*) and Coleman (*1962*) to identify and separate principal stress variables that influence volumetric behavior of partially saturated soil. The stress variables were defined as $(\sigma - u_w)$, $(\sigma - u_a)$ and $(u_a - u_w)$. Radakrishna (*1967*) found that applied stress, $(\sigma - u_a)$ and suction, $(u_a - u_w)$ are fundamentally different mechanisms that both contribute to the volume change. From their research, they were able to predict isotropic volume change and shear strength behavior from independent measurements of the two stress variables (*Matyas, 1968*). The relationships can be represented in a three dimensional plot with axes of volume change, net stress and suction to create the first constitutive surface for partially saturated soils. This was a breakthrough in the development of a critical state model for unsaturated soil, however its usefulness was limited, because the results included only isotropically increasing loading and continued wetting of soil and did not address unloading and drying. As a result, the surface fails to account for hysteretic effects of the wetting/drying cycle or the soil swell/collapse behavior.

From Matyas and Radarkrishna's work, the ability to use independent stress and suction variables to predict isotropic volume response through an incremental stress-strain law was established. Use of degree of saturation, stress and void ratio allowed researchers to begin describing a partially saturated soil and to mechanically analyze its response. As with saturated soils, recoverable elastic strains in compression varied according to stress state and previous stress history. Hysteretic effects due to saturation/desaturation of the soil induce non-uniqueness in stress-void ratio relationships.

Matyas and Radarkrishna's work led to a theoretical framework of unsaturated soil behavior by Fredlund in the late 1970's. Fredlund (*1977*) studied the influence of the three primary stress variables defined as $(\sigma - u_w)$, $(\sigma - u_a)$ and $(u_a - u_w)$. In a series of null tests for isotropic consolidation, he varied total stress, σ, air pressure and water pressure in equal increments and noted that the volume change remained constant. From this he

was able to ascertain that any two of the three stress variables are required to describe the volumetric response and the third would be redundant. His methodology was to take these two stress state variables and rewrite existing saturated mechanics laws with respect to these two variables. He then added coefficients where appropriate, labeling them as being relevant to either suction or net stress behavior (*Fredlund, 1993*).

Fredlund's models justified in theory that prediction of the constitutive behavior of unsaturated soils was feasible. The drawback to his formulation was that the expressions contained a considerable number of soil parameters many of which would be difficult to measure. The models needed to be simplified enough to allow their use in practice and computer applications.

Fredlund also introduced a means to predict soil shear strength in a manner similar to that defined by Terzaghi (*1943*):

$$\tau = (\sigma_{ij} - u_w \delta_{ij}) \tan \phi' + c' \qquad (3.3)$$

ϕ' = *friction angle associated with soil grains*

τ = *shear stress*

c' = *cohesion for fine grained soils*

σ_{ij}, u_w, δ_{ij} = same as in equation 3.2

Fredlund's shear strength relationship evolved by treating soil suction as an increase in cohesion that varied with suction magnitude. His expression appeared as follows:

$$\tau = (\sigma_{ij} - u_a \delta_{ij}) \tan \phi' + (u_a - u_w) \delta_{ij} \tan \phi'' + c' \qquad (3.4)$$

τ = *shear stress*

ϕ' = *friction angle of the soil grains*

ϕ'' = *friction angle associated with suction*

σ_{ij}, u_w, u_a, δ_{ij} = same as in equation 3.2

where the value of ϕ'' could be obtained from laboratory investigation.

This approach provided a rational means to account for increasing shear strength with increasing suction that is typical of partially saturated soils. The value of ϕ'' could be obtained from comparing shear stresses at failure under a constant applied stress with varying suction, and the resultant trend in strength increase expressed as a constant slope. However data used by Fredlund and additional data from direct shear tests conducted by Escario and Saez (*1986, 1987*) showed that the rate of the strength increase from suction is non-linear. At low suction values, ϕ'' is equal to ϕ' but at high suctions, ϕ'' decreases to the strength at saturation. The response matches that of the curved failure envelope for a granular saturated soil.

3.5 Volume Change Behavior

As discussed above, volume change of partially saturated soils is complex where volume changes can occur due to changes in applied stress and/or suction potential and can lead to either swell or collapse. A number of researchers have conducted one-dimensional consolidation tests (*Barden 1969, 1973; Dudley, 1970; Booth, 1977*) and later isotropic triaxial compression tests (*Lawton, 1989*) on compacted cohesive soils to quantify their volumetric response. Their research identified important soil properties in predicting the way in which a partially saturated soil would tend to deform. It was found that initial density and water content were primary factors in determining behavior. The researchers showed that strength increase due to suction enables a relatively loose PSS grain structure to sustain loads much greater than would otherwise be possible in a saturated state. As s result, the grain structure is in a very unstable state and will collapse with loss of suction, i.e. inundation with water. Conversely, if a soil is in a very dense state, but very dry it will tend to swell upon inundation. Collective results showed that for a constant density, the magnitude of swell increased with reduction in water content and for a constant water content, the magnitude of collapse increased with reduction in density.

Cox (*1978*) introduced the idea that swelling can occur simultaneously with collapse as observed in field measurements of deep fills by Brandon (*1990*) and Maswowse (*1992*). The intergranular structure of partially saturated soils is typically that of a series of small packets of soil at a much higher degree of saturation than the global soil matrix (*Brackley, 1975*) as shown in Figure 3-2. The overall response therefore is a combination of the response of the individual packets mixed with the global tendency of the soil state which dictates whether swell or collapse will be the resultant effect. This interdependence is more pronounced in soils of high plasticity since variations in suction potential throughout a soil sample can have a greater variability due to the soil's reduced permeability, whereas in more granular media such as sands, the global structure of the soil tends to control response.

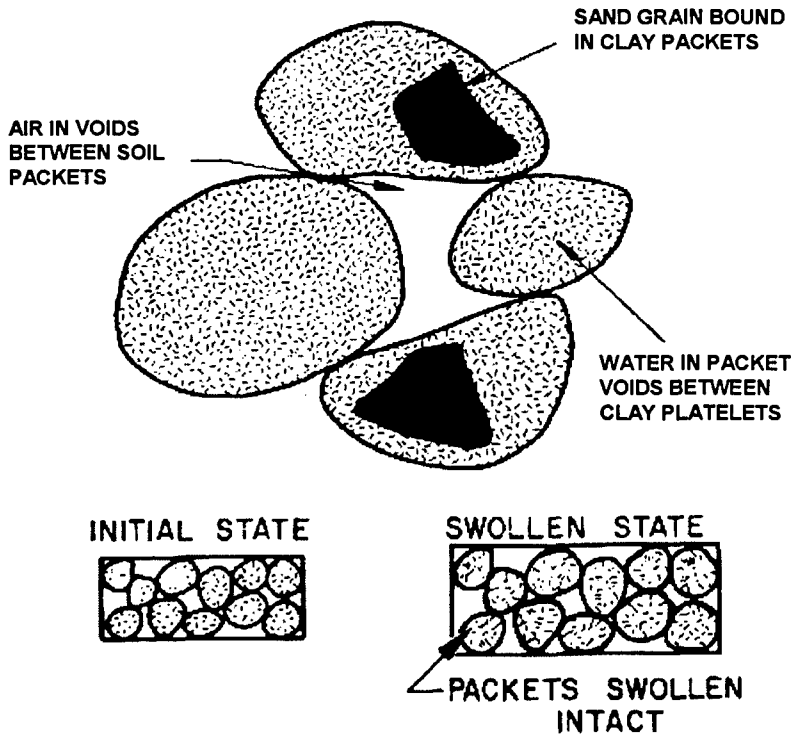

Figure 3-2: Illustration of microstructure of partially saturated soil (Brackley, 1975)

The importance of being able to distinguish volumetric response for varying pressures and moisture contents throughout the life of a structure has great importance for

soil structures such as pavement foundations. In the 1990's, a number of field studies (*Brandon, 1990; Noorany, 1992; Kropp, 1994; Vicente, 1994*) were conducted on deep fills in the southwestern United States. Observations were made on swelling and collapse of cohesive soils within the same fill at differing depths that resulted in catastrophic damage to surface structures. For a compacted soil structure that typically has a design life of many years, the seasonal and groundwater variations will inevitably change the soil moisture regime and alter its strength and volume with time. It is important that a model for partially saturated soils be able to simulate this response with time and for the most critical response, i.e. when the soil is inundated.

3.6 Constitutive Modeling

Coupling of volume change and strength proposed by Matyas and Fredlund inspired several researchers from the late 1980's on to construct constitutive models for PSS (*Alonso, et al., 1990; Toll, 1990; Sivakumar, 1993; Wheeler, et al., 1995*). Researchers focused on implementing the concept of two independent stress variables, (σ - u_a) and ($u_a - u_w$) into the saturated, critical state soil model developed by Scholfield, et al., (*1968*). Critical state soil mechanics (CSSM) is well developed and represents a formal way to predict soil constitutive response for a wide range of volumetric states. The model accounts for well documented soil behavior such as cohesion, non-linear failure envelopes, shear-volumetric strain coupling , influence of volumetric state on the soil stiffness and the strength and volume limit conditions that soils tend to at large deformations known as the critical state.

Alonso, et al. (*1990*) implemented suction into the critical state framework for non-expansive soils. He analyzed laboratory data taken on partially saturated soil (*Josa, 1988*) and developed a critical state plasticity model based on isotropic strain hardening using the two stress state variables which converge to the effective stress CSSM upon saturation. Alonso defines a non-associated flow rule which builds on the traditional saturated failure surface for effective stress by expanding the yield surface proportionate to the magnitude of both boundary stress and suction. The yield criteria is based upon the

concept of using two yield surfaces, one associated with the loading or boundary stress response and the other being a suction cap to provide an additional upper bound to the strength based on the suction potential. The yield surfaces are assumed parabolic and their movement in space is controlled by suction dependent hardening and flow rules, which also expand in tension due to the suction potential that is treated like a cohesive intercept. Strains from both suction and boundary stress are determined independently and then summed based on location within the yield space. A departure from the CSSM is Alonso's introduction of volumetric stiffness as a function of the suction suggesting that the soil's menisci increase its resistance to strain by creating an overconsolidating effect on the soil.

One drawback of the Alonso model is an inability to account for swelling strains due to changes in water content. To account for swelling properties of expansive clays, an extension of the model was suggested (*Gens, et al., 1992*) to incorporate a term for microstructural swelling as a secondary effect. The term adjusts the slope and location of the yield surface associated with changes due to suction. However, this enhanced model was never formally developed, nor numerically incorporated into a predictive tool.

Another drawback to the Alonso and Gens plasticity model is its use of isotropic strain hardening which fails to account for the accumulation of plastic strain during cyclic loading. Once the yield surface is defined in space, any stress paths that occur beneath this surface are treated as elastic. This would then fail to capture both the cyclic swelling found during seasonal moisture changes (*Subba Rao, 2000*) and the repetitive loading present within pavement structures.

Calibration of the model requires knowledge of traditional saturated critical state soil parameters found readily enough in standard laboratory tests. However a series of partially saturated triaxial tests are required which are difficult and time consuming to conduct. Only a handful of soil laboratories worldwide can produce this type of data. The tests define volumetric stiffness over the potential range of suction during the isotropic triaxial test and changes in compressibility with suction during consolidation. Results of this test is a term that adjusts cohesion with suction and a term that adjusts the flow rule to determine shear strain based upon Jaky's (*1948*) K_o response.

Validation of the Alonso and Gens model to predict stress and strain paths of data used in the calibration worked satisfactorily for the soil and stress paths of interest, but failed to predict the volumetric stiffness even given the vast amount of partially saturated calibration data used in the model. While the Alonso and Gens work lacked a readily applicable model for analysis, it did provide insight into global behavior of partially saturated soil, as well as a platform from which future researchers would continue their work.

Toll (*1990*) focused on defining how suction influenced the critical states occurring at large deformations within the CSSM model rather than developing a complete predictive model. Using a low plasticity soil exhibiting little swelling, he separated out a critical state stress ratio based on total stress (σ- u_a) and suction ($u_a - u_w$) as separate entities much in the way Alonso defined the strength and volume relationships separately. His goal was to find relationships based on globally observed response for the effect of suction on the shape of the regression curves used to define the strain and strength envelopes for the critical state model.

Toll conducted a series of triaxial strength tests on saturated and partially saturated clay gravel. Critical state values at the residual strength were obtained and plotted versus degree of saturation. Using the CSSM he proposed expressions for the shear stress, q, and volume, v, at the critical states such that the contribution of total stress, σ and suction ($u_a - u_w$) to shear stress can be expressed as two individual stress ratios M_a and M_w both of which are dependent on degree of saturation.

$$q = M_a(\sigma - u_a) - M_w(u_a - u_w) \tag{3.5}$$

Likewise a similar expression representing the volume change can be expressed as an intercept, Γ_{aw} and slopes, λ_a and λ_w all of which are functions of saturation.

$$v = \Gamma_{aw} - \lambda_a \ln(\sigma - u_a) - \lambda_w \ln(u_a - u_w) \tag{3.6}$$

A true critical state was not achieved in the unsaturated tests as they continued to dilate even at large strains, but the stress and volume conditions when each sample was removed from the apparatus were assumed as the critical state. This led to the finding that the individual parameters M_a and M_w approach the critical state stress ratio, M_c defined by Scholfield, et al., (*1968*) when the sample approaches saturation. This suggests a coupling exists between suction and total stress response as will be explored within the context of this thesis.

Toll (*1990*) hypothesized that there was a limitation to the approach of defining response of partially saturated soils solely on the basis of a modified CSSM. The limitation arises because the soil fabric or grain arrangement during shear does not change, being held in place by the menisci. This is counter to the behavior of saturated soils, whose grain structure reaches some equilibrium state at the critical state condition. Therefore it is difficult to define a partially saturated critical state volume relationship because the fabric is not destroyed upon failure.

One of Toll's more important observations was that once the degree of saturation of a soil drops below 55 percent, the suction potential no longer has an influence on the shear stress of the soil. This suggests that at low saturation, the menisci are no longer distributed throughout the entire volume of material, but are constrained to a few isolated pockets. As a result, they no longer contribute to the soil's global response. This supports the microstructure viewpoint of Brackley (Figure 3-2) and provides a magnitude of water content at which this effect can begin to be observed.

Sivakumar (*1993*) built on the concepts developed by both Alonso for the definition of critical state stress ratio and the approach of Toll to define the critical state volume, but instead of using suction or degree of saturation as the controlling variable, he uses volumetric water content. He notes that by defining the water within the soil relative to a volume is important in developing the constitutive relationships. This is because changes in volumetric water content are correctly associated with suction. And when multiplied together, a component of work per unit volume of soil is obtained. In a similar fashion as volumetric strain and shear strain increments produce work when multiplied by their respective stress magnitudes. Unfortunately, this work concept is not put to use

in the theoretical development of his model, but is the foundation of the work presented in this thesis.

Sivakumar used an elasto-plastic, parabolic yield surface which has a cohesive intercept associated with suction. The yield criterion has a tensile cut-off limiting its strength in tension similar to that of the Griffith theory in rock mechanics (*Lee, et al., 1968*) and extended to cohesive soils by Bishop, et al., (*1969*) and Peters, et al., (*1988*). Unlike Alonso, he used an associated flow rule, simplifying his model development and calibration but sacrificing accuracy. His work involved an extensive series of partially saturated triaxial tests on a low plasticity clay to develop six relationships between water content and the slopes and intercepts for the critical state. He discovered, as Toll did, that it is difficult to achieve a critical state behavior in unsaturated triaxial tests. His model does not take into account swelling behavior of plastic soils, nor hardening associated with accumulation of plastic strain observed during cyclic loading typical of stress paths experienced by pavement foundations. Sivakumar observed from the triaxial tests that the shear modulus, G, varied with both mean stress and suction. However, this detail was not included in his model. This detail is addressed in the current work, as the modulus is assumed dependent on both mean stress and suction.

3.7 Particle and Micro-Mechanical Modeling

The constitutive models presented in the previous section assume that the soil behaves as a continuum. This simplification allows the modeler to define the soil behavior in terms of equations of equilibrium and associated kinematics. The parameters which shape and give magnitude to these equations are the only means to distinguish behavior from one continuum (or soil) to another, since a continuum represents only a volume of "stuff" that inherently has no properties until defined by a constitutive model. The constitutive model then links stresses to strains within the system to capture the response of a soil body such as the CSSM. Dividing a continuum into sections as is done in a finite element program allows more complicated soil body geometries and

boundary/loading conditions to be modeled by assuming the soil body consists of many smaller continua interacting with one another.

There is another competing modeling field known as particle modeling (*Cundal, 2002*). The particle modeling approach represents the soil as an assemblage of individual particles that each transmit forces and allow sliding and rotation between grains. The interaction laws defining the contact and rotational behavior of the grains dictates the behavior of a larger number of particles. This approach provides very accurate representations of observed soil behavior and has led to great insight into soil micro behavior. The limitation to this approach is that in order to model a volume of material for even a common laboratory specimen, literally thousands to millions of soil grains are must be included. Tremendous computer processing power is required to accomplish a single simulation. In addition, there is the added complication of adding water and menisci to the soil grain structure. At the time of this writing, the computational tools available are incapable of handling the large number of calculations needed to represent the number of soil particles present within a laboratory soil specimen. As well, numerical codes lack the ability to effectively add water to the grain structure to account for pore pressures and the tensile effect of partial saturation.

To overcome this limitation a mixture of constitutive and particle modeling has emerged known as micro-mechanical modeling (e.g. *Tordesillas and Walsh, 2002*). Originating with the interaction laws at a particle level, virtual work associated with the forces and their associated deformations are formulated with the help of evolution laws to develop a thermodynamic theory that then can describe the macro-behavior of the soil. This allows a synthesis between the definition of the important particulate variables from particle modeling and the evolution equations to convert these variables to stresses and strains used in constitutive modeling. The limitation to this approach is that the model is only as good as the constitutive or evolution law that bounds the material behavior. The same restrictions common to plasticity and hardening laws such as the inability to capture accumulation of plastic strain, cyclic loading and effects of partial saturation limit the effectiveness of many of these proposed models.

Benefits of micro-mechanical modeling are that great insight is provided into physical workings of the soil at the grain level, which can be extrapolated to explain nuances in soil behavior observed during laboratory testing. An excellent example of this is the work by Brackley (*1975*) who envisioned the grain structure of a partially saturated soil and therefore a means to explain the various swell and collapse phenomena that were observed (Figure 3-2).

Research into micro-mechanical modeling began as early as 1907 when Buckingham presented his theory on a means to determine water tension from a uniform set of soil grains based on the geometry of the water menisci at the microscopic level. Later, Biot in 1941 proposed a general theory on consolidation which was based on soil physics at the micro-structural level and extended to the global response. Throughout much of the 1950's into the 1970's significant effort was directed toward constitutive modeling with plasticity models and means to predict observed global response by observing macro-behavior. Biot (*1977*) published his work on the physics of porous media that led to a rebirth of micro behavioral research. From the 1980's on and especially into the new century, work advanced through use of computers for numerical modeling. Researchers such as Coussy (*1989, 1995*) formalized a much more in depth description of the thermodynamics of porous media as a foundation for future modeling efforts. Recent work (*Houslby, 1997; Li, 2003; Molenkamp, et al. 2003*) has begun to investigate the role of the menisci and the effect of partial saturation on the thermodynamics of porous media. This is the focus of this thesis and the basis of the theoretical development to incorporate energy or virtual work associated with the menisci into the soil global response.

CHAPTER IV

Theory of Partially Saturated Soil Response

4.1 Problem Definition

Within the field of geotechnical engineering, partially saturated soil is the most common material encountered. A partially saturated soil is a complex multi-phase system consisting of air, water and solid material whose response is a function of not only the external and internal stress state but as well the moisture condition present within the soil. As a first step in developing a constitutive model for multi-phase partially saturated soil, a thermodynamic interpretation of the interaction among the three components, soil, air and water (Figure 4-1) will be presented. The discussion will focus on establishing the basis of a free energy expression in terms of strain and water content for a soil restricted to thermoelastic behavior. The discussion will then be extended to inelastic behavior by introducing internal variables to account for the plastic behavior in the solid phase. The relevance and calibration of the various parameters and coefficients associated with the partially saturated model will be discussed, setting up the implementation of the model into a constitutive driver outlined in Chapter V.

4.2 Formulation of Thermoelastic Partially Saturated Soil

The analysis begins with an idealization of soil as a thermoelastic material for which behavior is governed by the first and second laws of thermodynamics. The first law asserts that there exists a state variable U (internal energy density) such that:

$$\frac{d}{dt}\int_V \rho U dV = R + P_e \tag{4.1}$$

ρ = mass density of the soil

P_e = external power of the soil

R = heat flow in the soil

t = time

V = total volume of soil skeleton

The heat flow, R is equal to:

$$R = \int_V \rho r dV - \int_S h dS \tag{4.2}$$

h = heat outflow per time

r = soil heating

Using Gauss's thereom:

$$R = \int_V \left(\rho r - \frac{\partial h_i}{\partial x_i} \right) dV \quad \text{and} \quad \rho r - \frac{\partial h_i}{\partial x_i} = 0 \quad \text{for an adiabatic system.}$$

Any heat generated within the specimen, ρr is offset by the heat flux from the specimen. This allows the first law to be written as:

$$\rho \dot{U} - P_e = 0 \tag{4.3}$$

The second law of thermodynamics states that there exists a state function $\eta(U, \varepsilon)$ such that for a thermoelastic body $d\eta/dt = 0$ in an adiabatic process (*Lubliner, 1990*). The thermodynamic state can also be expressed in terms of the Helmholtz free energy, $W = W(T, \varepsilon_{ij}, \varepsilon^w, \varepsilon^a, \theta) = U - T\eta$ where T = absolute temperature and ε_{ij}, ε^w, ε^a, and θ

represent the small strain tensors associated with the soil skeleton, water, air and menisci surface as shown in Figure 4-1. Note that the temperature $T = \partial U/\partial \eta$. Given that the temperature T is always a positive quantity the thermodynamic state can be given in terms of either of the state functions entropy or free energy. It follows that the free energy can be expressed as:

$$\frac{\partial W}{\partial T}\dot{T} + \frac{\partial W}{\partial \varepsilon_{ij}}\dot{\varepsilon}_{ij} + \frac{\partial W}{\partial \varepsilon^{w}}\dot{\varepsilon}^{w} + \frac{\partial W}{\partial \varepsilon^{a}}\dot{\varepsilon}^{a} + \frac{\partial W}{\partial \theta}\dot{\theta} = \dot{U} - \dot{T}\eta - \dot{\eta}T \tag{4.4}$$

To arrive at the constitutive relationship between stress and strain for the solid, water and air phases of the soil, the two equations from the first and second laws must be satisfied simultaneously. Therefore an expression for the external power of the soil in terms of stress and strain must be derived.

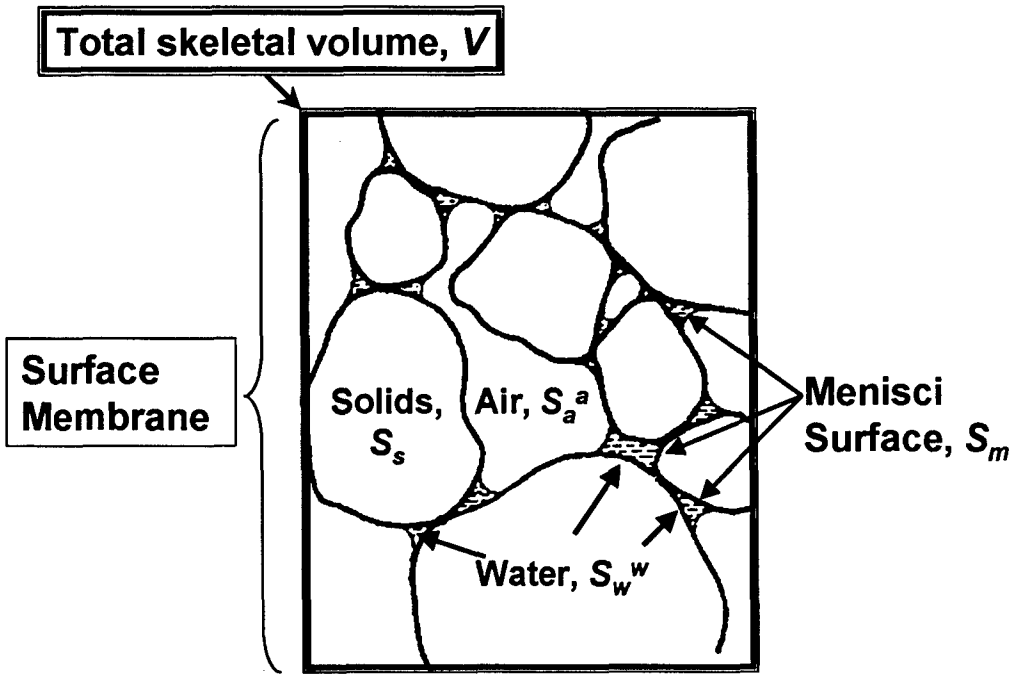

Figure 4-1: Sketch of three phase soil matrix and accompanying surfaces

A partially saturated soil from a thermodynamic formulation consists of three phases, soil solids, water and air. Measured stresses within a soil body are taken at the surface of the soil at the membrane interface that is in contact with all three soil phases as shown in Figures 4-1 and 4-2. The average Cauchy stress, σ_{ij} acting on the boundary of the soil specimen is measured as a sum of the tractions in contact with the membrane, t_i^s which act at the particle to particle contacts surfaces, S_s , $t_i^a = u_a n_i$ which act over the surface in contact with the air, S_a^a, and $t_i^w = u_w n_i$, which acts over the surface area in contact with the water, S_w^w. The average Cauchy stress can be represented as:

$$\frac{1}{V}\int_V \sigma_{ij} dV = \frac{1}{V}\left(\int_{S_s} t_i^s x_j dS_s + \int_{S_a} t_i^a x_j dS_a + \int_{S_w} t_i^w x_j dS_w \right) \tag{4.5}$$

he left hand side of the equation can be obtained through Gauss's theorem as shown in Appendix C. It is assumed for a partially saturated soil that the air and water stresses, u_a and u_w are uniform within the soil body and the solid grains are incompressible.

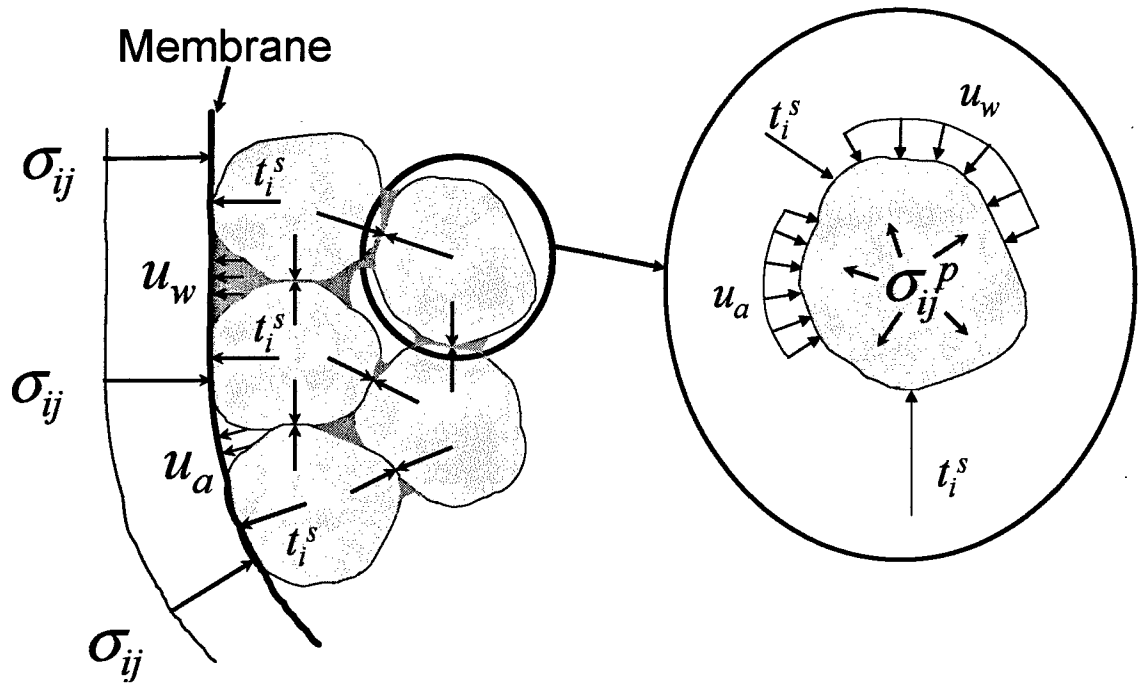

Figure 4-2: Definition of stress within a partially saturated soil

For this example, the tangential components of the traction, t_i acting on the membrane surface are zero, $S_{ij} = 0$, therefore the stress transfer at the surface of the membrane is simply, $\sigma_{ij} = u\delta_{ij}$:

$$\sigma_{ij} = S_{ij} + u\delta_{ij} = u\delta_{ij} \tag{4.6}$$

The air and water surfaces, S_a and S_w include both those in contact with the surface membrane (menisci) and internal to the respective volume. Accordingly, the air and water surfaces are subdivided further into two components as shown below, where $S_a{}^a$ and $S_w{}^w$ are surfaces associated with the pure phase of each material and $S_a{}^m$ and $S_w{}^m$ are surfaces bounded by the air-water menisci as illustrated in Figure 4-1.

$$S_w = S_w^w + S_w^m \tag{4.7a}$$

$$S_a = S_a^a + S_a^m \tag{4.7b}$$

It is further noted that the surface of the meniscus is equally shared between the air and water meniscus surfaces such that $S_m = S_w^m = S_a^m$.

The components influencing power within a soil system are those observable and measurable from the exterior of a soil body that include soil particles, air and water. The external power, P_e for each of the three phases can be broken down into a body force, ρbv driven by gravity and tractions acting on the surface of each phase.

$$P_e = \int_{V_s} \rho_s b_i v_i^s dV_s + \int_{V_w} \rho_w b_i^w v_i^w dV_w + \int_{V_a} \rho_a b_i^a v_i^a dV_a + \int_{S_s} t_i^s v_i^s dS_s + \int_{S_w^w} t_i^w v_i^w dS_w^w + \int_{S_a^a} t_i^a v_i^a dS_a^a \tag{4.8}$$

The surface tractions can also be expressed as follows:

$$t_i^s = \sigma_{ij}{}^s n_j \qquad t_i^w = \sigma_{ij}{}^w n_j = u_w n_i \qquad t_i^a = \sigma_{ij}{}^a n_j = u_a n_i$$

From which the following relationships are provided from Gauss's theorem for the influence of the soil, water and air surface tractions acting over the entire surface of each individual phase:

$$\int_{V_s} \frac{\partial \sigma_{ij}^s}{\partial x_j} v_i dV_s = -\int_{V_s} \sigma_{ij}^s \frac{\partial v_i^s}{\partial x_i} dV_s + \int_{S_s} t_i^s v_i^s dS_s \tag{4.9a}$$

$$\int_{V_w} \frac{\partial u_w}{\partial x_i} v_i^w dV_w = -\int_{V_w} u_w \frac{\partial v_i^w}{\partial x_i} dV_w + \int_{S_w} t_i^w v_i^w dS_w \tag{4.9b}$$

$$\int_{V_a} \frac{\partial u_a}{\partial x_i} v_i^a dV_a = -\int_{V_a} u_a \frac{\partial v_i^a}{\partial x_i} dV_a + \int_{S_a} t_i^a v_i^a dS_a \tag{4.9c}$$

Substituting equations 4.9 into equation 4.8 and accounting for the subdivision of the air and water surfaces yields:

$$P_e = \int_{V_s} \left(\frac{\partial \sigma_{ij}^s}{\partial x_j} - \rho_s b_i \right) v_i^s dV_s + \int_{V_w} \left(\frac{\partial u_w}{\partial x_i} - \rho_w b_i^w \right) v_i^w dV_w + \int_{V_a} \left(\frac{\partial u_a}{\partial x_i} - \rho_a b_i^a \right) v_i^a dV_a$$
$$+ \int_{V_s} \sigma_{ij}^s \frac{\partial v_i^s}{\partial x_i} dV_s + \int_{V_w} u_w \frac{\partial v_i^w}{\partial x_i} dV_w + \int_{V_a} u_a \frac{\partial v_i^a}{\partial x_i} dV_a + \int_{S_w^m} u_w n_i v_i^w dS_w^m + \int_{S_a^m} u_a n_i v_i^a dS_a^m \tag{4.10}$$

The first three terms of equation 4.10 represent the equilibrium relationship for each phase and each is identically equal to zero as shown in equation 4.11 resulting in an expression containing only surface tractions expressed as volume integrals in equation 4.12.

$$\frac{\partial \sigma_{ij}^s}{\partial x_j} + \rho_s b_i = 0 \tag{4.11a}$$

$$\frac{\partial u_w}{\partial x_i} + \rho_w b_i^w = 0 \tag{4.11b}$$

$$\frac{\partial u_a}{\partial x_i} + \rho_a b_i^a = 0 \tag{4.11c}$$

$$P_e = \int_{V_s} \sigma_{ij}^s \frac{\partial v_i^s}{\partial x_i} dV_s + \int_{V_w} u_w \frac{\partial v_i^w}{\partial x_i} dV_w + \int_{V_a} u_a \frac{\partial v_i^a}{\partial x_i} dV_a + \int_{S_w^m} u_w n_i v_i^w dS_w^m + \int_{S_a^m} u_a n_i v_i^a dS_a^m \tag{4.12}$$

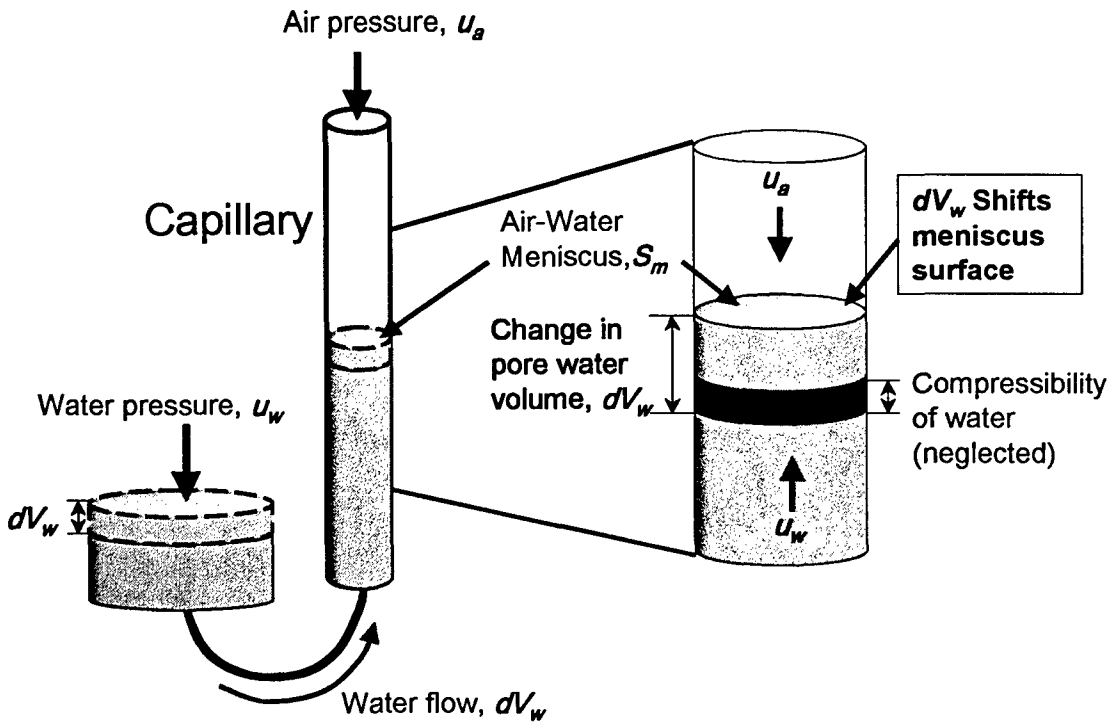

Figure 4-3: Movement of air-water interface due to the change in water volume, dV_w

In equation 4.12 the volume integral, V refers to the total skeletal volume of the soil mass (Figure 4-1), therefore a volumetric term can be derived for the air and water phases to allow inclusion of their volume states into a single integral. Using porosity, n times degree of saturation, S for the air and water phases, $nS_w = V_w/V$ and $nS_a = V_a/V$ and noting that $v_i^a = -v_i^w = v_m$ equation 4.12 can be rewritten as:

$$P_e = \int_V \left(\sigma_{ij}^s \frac{\partial v_i^s}{\partial x_i} + u_w \mathrm{nS_w} \frac{\partial v_i^w}{\partial x_i} + u_a \mathrm{nS_a} \frac{\partial v_i^a}{\partial x_i} \right) dV + (u_a - u_w) \int_{S_m} v_i n_i dS_m \tag{4.13}$$

As Figure 4-3 illustrates, the movement of the menisci surface, S_m due to a change in water volume, dV_w results in a change in volume associated with S_m. This volume can be approximated as the total change in water volume, dV_w, neglecting the compressibility of water. As such equations 4.14 and 4.15 show that the surface integral associated with the menisci can be included as a volume integral with the remaining soil components creating a four-phase soil system.

$$P_e = \int_V \left(\sigma_{ij}^s \frac{\partial v_i^s}{\partial x_i} + u_w \mathrm{nS_w} \frac{\partial v_i^w}{\partial x_i} + u_a \mathrm{nS_a} \frac{\partial v_i^a}{\partial x_i} \right) dV + (u_a - u_w) dV_w \tag{4.14}$$

$$\dot{\varepsilon}^w = \mathrm{nS_w} \frac{dv_i^w}{dx_i}$$

$$\dot{\varepsilon}^a = \mathrm{nS_a} \frac{dv_i^a}{dx_i}$$

$$dV_w = V d\theta = \int_V d\theta dV$$

$$P_e = \int_V \left(\sigma_{ij}^s \dot{\varepsilon}_{ij} + u_w \dot{\varepsilon}^w + u_a \dot{\varepsilon}^a + (u_a - u_w) \dot{\theta} \right) dV \tag{4.15}$$

The constitutive relationship above can be expressed as functions of the internal energy by substitution of equation 4.15 into equation 4.3:

$$\rho \dot{U} = \sigma_{ij}^s \dot{\varepsilon}_{ij} + u_w \dot{\varepsilon}^w + u_a \dot{\varepsilon}^a + (u_a - u_w) \dot{\theta}$$

or,

$$\dot{U} = \rho^{-1} \left[\sigma_{ij}^s \dot{\varepsilon}_{ij} + u_w \dot{\varepsilon}^w + u_a \dot{\varepsilon}^a + (u_a - u_w) \dot{\theta} \right] \tag{4.16}$$

It is necessary at this point to replace the dependency of the constitutive relationship on internal energy with the Helmholtz free energy, W from the earlier discussion by substitution of equation 4.16 into equation 4.4.

$$\dot{W} = \rho^{-1}\left[\sigma_{ij}^{s}\dot{\varepsilon}_{ij} + u_w\dot{\varepsilon}^{w} + u_a\dot{\varepsilon}^{a} + (u_a - u_w)\dot{\theta}\right] - T\dot{\eta} - \eta\dot{T} \tag{4.17}$$

The soil matrix is assumed to be elastic such that $\dot{\eta} = 0$. Therefore, the free energy is a function of only strain and temperature as follows and like terms can be grouped to provide a relationship between the free energy and the stress variables:

$$\left[\frac{1}{\rho}\sigma_{ij}^{s} - \frac{\partial W}{\partial \varepsilon_{ij}}\right]\dot{\varepsilon}_{ij} + \left[\frac{1}{\rho}u_w - \frac{\partial W}{\partial \varepsilon^{w}}\right]\dot{\varepsilon}^{w} + \left[\frac{1}{\rho}u_a - \frac{\partial W}{\partial \varepsilon^{a}}\right]\dot{\varepsilon}^{a} + \left[\frac{1}{\rho}(u_a - u_w) - \frac{\partial W}{\partial \theta}\right]\dot{\theta} - \left[\eta + \frac{\partial W}{\partial T}\right]\dot{T} = 0 \tag{4.18}$$

Because each term outside of the brackets is independent, each component within the square brackets must identically be equal to zero resulting in the existence of constitutive relationships for each phase of a PSS:

$$\sigma_{ij}^{s} = \rho\frac{\partial W}{\partial \varepsilon_{ij}} \tag{4.19a}$$

$$u_w = \rho\frac{\partial W}{\partial \varepsilon^{w}} \tag{4.19b}$$

$$u_a = \rho\frac{\partial W}{\partial \varepsilon^{a}} \tag{4.19c}$$

$$(u_a - u_w) = \rho\frac{\partial W}{\partial \theta} \tag{4.19d}$$

Equation 4.19 defines the conjugate variables for each phase of a PSS: stress transfer in the soil grains, σ_{ij}^{s} is conjugate to soil skeleton strain, ε_{ij}, stress transfer in the

water, u_w is conjugate to the strain in the water phase, ε_w stress transfer in the air, u_a is conjugate to the strain in the air phase, ε_a and stress transfer in the menisci, suction, $(u_a - u_w)$, is conjugate to the change in volumetric water content, θ. Suction is defined as the variable, $p = (u_a - u_w)$ which is the stress associated with the tensile strength of the water menisci between soil grains.

It is assumed that only small changes in total mass density, ρ occur during experimentation, therefore it is included in the free energy term. This then allows definition of the external Helmholtz free energy, W_E of the system as:

$$W(\varepsilon,\theta) = W_s + W_w + W_a + W_\theta \tag{4.20}$$

where W_θ is equal to the energy associated with the air-water interface

Suction is assumed to be an isotropic second order tensor and since it produces a stress acting between grains it influences the intergranular stress. This suggests that a coupling is necessary in the definition of the free energy to combine the effects of the soil skeleton response and the suction as follows:

$$W(\varepsilon,\theta) = W_{s\theta}(\varepsilon_v,\theta) + W_w(\varepsilon^w) + W_a(\varepsilon^a) \tag{4.21}$$

The following quadratic expression is used to relate the coupled free energy term, $W_{s\theta}$:

$$W_{s\theta}(\varepsilon_v,\theta) = \frac{1}{2}K_1(\varepsilon_v)^2 + K_2\varepsilon_v\theta + \frac{1}{2}K_3\theta^2 \tag{4.22}$$

Where $K_{1,2,3}$ represent coefficients to be determined from laboratory tests and ε_v is the volumetric strain of the soil skeleton. This equation represents the simplest coupling of the two energies. However, this is not the only possible relationship, as higher order terms could be added to represent more complex associations between terms.

The constants K_1, K_2 and K_3 are not independent but must satisfy $W_{s\theta} > 0$ for all ε_v and θ. The interdependence of the K constants can be determined by evaluating $W_{s\theta}$ at

two extremes, $\varepsilon_v = 0$ and $\theta = 0$. For the specific condition of saturation ($b = 0$) for a condition of $\varepsilon_v = 0$, K_3 must be a positive coefficient. Likewise K_1 must have a positive value when θ approaches zero. Accordingly set $b = \varepsilon_v/\theta$ such that b approaches zero at water saturation, $\varepsilon_v = 0$, and b approaches infinity at air saturation, $\theta = 0$. For equation 4.23 to be definite it is required that b be imaginary and for positive definiteness the eigenvalues must all be positive. The restriction on K_2 follows from:

$$K_1 b^2 + 2K_2 b + K_3 \geq 0 \tag{4.23}$$

$$b = \frac{-2K_2 \pm \sqrt{4K_2^2 - 4K_1 K_3}}{2K_1} \tag{4.24}$$

To ensure that the free energy not equal zero, b must be imaginary and therefore the discriminate must be less than zero:

$$K_2^2 - K_1 K_3 < 0 \qquad \text{or} \qquad K_2^2 < K_1 K_3 \tag{4.25}$$

Therefore, for the second inequality of 4.25 to be true, given K_3 and K_1 are positive, K_2 can take on any value within the limitation of equation 4.30. For the purposes of the model development, K_2 will be defined as a positive value.

Furthermore, by differentiating the free energy, $W_{s\theta}$, a matrix of the coefficients is obtained:

$$\frac{\partial W_{s\theta}}{\partial \varepsilon_{ij}} = \sigma_{ij}^s = K_1 \varepsilon_v + K_2 \theta \tag{4.26}$$

$$\frac{\partial W_{s\theta}}{\partial \theta} = p = K_2 \varepsilon_v + K_3 \theta \tag{4.27}$$

yielding: $$\begin{Bmatrix} \sigma_{ij}^{s} \\ p \end{Bmatrix} = \begin{bmatrix} K_1 & K_2 \\ K_2 & K_3 \end{bmatrix} \begin{Bmatrix} \varepsilon_v \\ \theta \end{Bmatrix}$$

Where σ_{ij}^{s} is the fraction of the Cauchy stress, σ_{ij} transmitted to the grains at the soil membrane as seen in Figure 4-1, 4-2 and 4-4.

The resulting stiffness matrix satisfies the condition of a non-singular, positive definite matrix, as the matrix contains positive terms in the diagonal, is a symmetric matrix, and the diagonal terms are the largest values.

Note that equations 4.26 and 4.27 obviate the need for a formal decomposition of stress into total and effective stresses. However, it is conceptually useful to note that at suction equal to zero, $K_1\varepsilon_v$ represents the Terzaghi effective stress. In the general case, this represents an intergranular stress, Q_{ij} that is the result of ε_v alone (Figure 4-4). $K_2\theta$ is the stress component that results from changes in water content.

To determine the Cauchy stress of a three phase soil acting on the membrane surface of the soil body shown in Figure 4-4, the inclusion of the partial pore pressures, u_w and u_a which act on their respective volumes, are necessary along with the stress, σ_{ij}^{s}.

The definition of pore pressure requires the evaluation of the two independent components, air and water pressure, u_w and u_a which combined, are the stresses that resist the distribution of the Cauchy stress to the intergranular contacts defined in section 4.4 and shown in Figure 4-4.

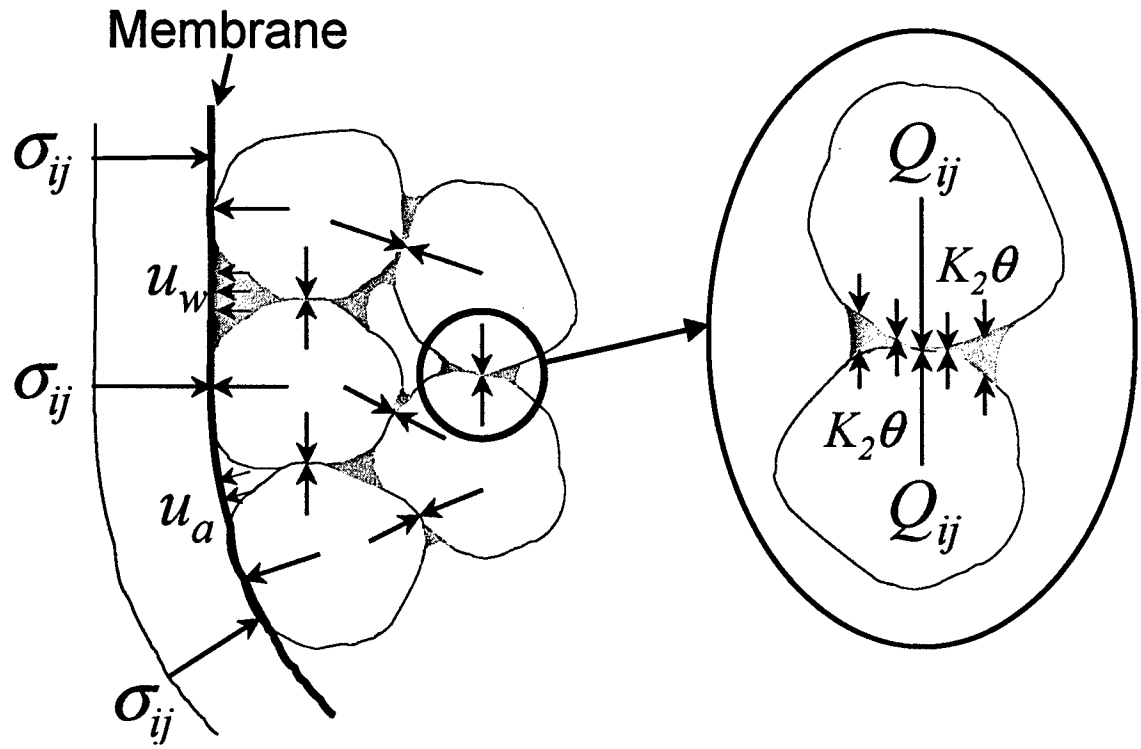

Figure 4-4: Internal and external stress and pore pressure relationships

The total Helmholtz energy, $W(\varepsilon,\theta)$ from equation 4.20 can be expanded in equation 4.28, and the Cauchy stress obtained from the differential shown in equation 4.29 which reveals the definition of partial pore pressures, u_w^* and u_a^* in equation 4.30.

$$W(\varepsilon,\theta) = \tfrac{1}{2} K_1(\varepsilon_v)^2 + K_2\varepsilon_v\theta + \tfrac{1}{2} K_3\theta^2 + \tfrac{1}{2} K_w(\varepsilon_w)^2 V_w + \tfrac{1}{2} K_a(\varepsilon_a)^2 V_a \qquad (4.28)$$

$$\sigma_{ij} = \frac{\partial W}{\partial \varepsilon_{ij}} = \frac{\partial W}{\partial \varepsilon_{kl}^{s\theta}}\frac{\partial \varepsilon_{kl}^{s\theta}}{\partial \varepsilon_{ij}} + \frac{\partial W}{\partial \varepsilon_{kl}^{w}}\frac{\partial \varepsilon_{kl}^{w}}{\partial \varepsilon_{ij}} + \frac{\partial W}{\partial \varepsilon_{kl}^{a}}\frac{\partial \varepsilon_{kl}^{a}}{\partial \varepsilon_{ij}} \qquad (4.29)$$

$$\sigma_{ij} = K_1\varepsilon_v + K_2\theta + u_w^*\delta_{ij} + u_a^*\delta \qquad (4.30)$$

Equation 4.35 shows that the Cauchy stress is a function of both the volumetric strain and the volumetric water content. Research has shown that K_2 is a function of both the initial

mean stresses and the suction condition and therefore a coupling between the effective stress and suction is implied.

4.3 Determining the Pore Pressures

In order to calculate pore pressure response, a partially saturated sample is assumed to have finite masses of solids, air and water, all of which are fixed values for the duration of the experiment. The solids volume is assumed incompressible and therefore fixed. However, the volume of air and water are allowed to change such that the total change in volume of the three components is always equal to the applied volumetric strain.

To quantify air and water pressures within the soil sample, the masses of the air and water are defined (*note the change in nomenclature from that of a surface defined in section 4.2*) in terms of their density (ρ), porosity ($n = V_v/V_T$) and degree of saturation (S) of each of the phases as follows:

$$m_w = \rho_w \cdot n \cdot S_w \tag{4.31}$$

$$m_a = \rho_a \cdot n \cdot S_a \tag{4.32}$$

where masses of both air and water are constant. By differentiating the masses with respect to the individual components results in:

$$nS_w \frac{d\rho_w}{\rho_w} + S_w dn + n dS_w = 0 \tag{4.33}$$

$$nS_a \frac{d\rho_a}{\rho_a} + S_a dn + n dS_a = 0 \tag{4.34}$$

By definition, the air and water degrees of saturation must sum to unity. This relationship is combined with equations 4.33 and 4.34 to obtain:

$$S_a \frac{d\rho_a}{\rho_a} + S_w \frac{d\rho_w}{\rho_w} = -\frac{dn}{n} \tag{4.35}$$

In order to introduce pore pressure into the equations, the compressibility of air and water can be related to the change in density as follows:

$$\frac{d\rho_w}{\rho_w} = C_w du_w \qquad \text{where } C_w = 4.58 \text{ x } 10^{-7} \text{ 1/kPa} \tag{4.36}$$

$$\frac{d\rho_a}{\rho_a} = C_a du_a \qquad \text{where } C_a = 4.94 \text{ x } 10^{-3} \text{ 1/kPa} \tag{4.37}$$

Where C_w and C_a represent water and air compressibility, respectively and u_w and u_a are the pore pressures for both water and air (*Fredlund & Rahardjo, 1993*). To obtain a more accurate compressibility for the air phase, the ideal gas law is necessary to account for the current pressure and the volume occupied by the air in the sample. However, this correction has been ignored resulting in the use of a constant air compressibility to simplify the simulations.

The relationship between air and water pressure can be defined in terms of the suction potential, p, measured within the soil where:

$$dp = du_a - du_w \tag{4.38}$$

$$p = u_a - u_w \tag{4.39}$$

Substituting the suction (eq. 4.38) and compressibility relationships (eq. 4.36 & 4.37) into equation 4.35 yields the expression for the change in pore water pressure for any change in suction or porosity (volume):

$$du_w = \frac{-(S_a C_a dp + dn/n)}{S_w C_w + S_a C_a} \tag{4.40}$$

The change in air pressure, du_a, can be obtained from the difference expressed in equation 4.38, which is the change in suction applied to the system and the change in pore water pressure (equation 4.40). Once the differential pore pressures are known, the final pore pressures can then be determined:

$$u_w = u_{wo} + du_w \tag{4.41}$$

$$u_a = u_{ao} + du_a \tag{4.42}$$

4.4 Internal Variables for 3-Phase Plastic Model

At this point the constitutive relationships have been developed for a partially saturated soil from an ideal elastic standpoint. The true response of a soil is that of an elastic-plastic material, where free energy is dissipated within the system due to irrecoverable plastic deformation of the soil skeleton, $d\eta / dt \geq 0$. To account for this free energy loss within the soil system, internal variables are introduced and defined as a mechanism that accounts for the accumulation of plastic strain through the dissipation of energy.

The theory of internal variables for solid mechanics was introduced for viscoelastic materials following Onsager's original work of the 1930's (see *Valanis, 1968*), although the mathematical foundation is generally credited to papers by Colman and Gurtin (*1967*). Essentially the same formulation was produced by the

contemporaneous work of Valanis (*1968*) who later put the theory on a firm footing for rate independent plasticity by introduction of intrinsic time (*Valanis, 1971, 1980*). Valanis (*1971*) recognized the validity of the second law of thermodynamics does not depend on the definition of time as Newtonian. Rather, each material has it own sense of time that is tied to internal changes through evolution of the internal variables. Accordingly, it is admissible to write evolution equations in terms of any monotonically increasing parameter. Specifically, Valanis (*1971*) showed that definition of a time parameter based on the distance in plastic strain space could reproduce self-consistent isotropic and kinematic hardening plasticity that could accurately reproduce hysteresis loops after many cycles of loading (see *Valanis and Lee, 1984*). The theory was extended to geologic materials including concrete (*Valanis and Reed, 1986*) and soils (*Valanis and Peters, 1991*). Internal variable theory for plastic materials can likewise be developed without introducing internal time (e.g. *Herrmann and Bertholf, 1983, Holsby and Puzrin, 2000*). Such models lack the mathematical compactness of endochronic models but can be simpler to calibrate and implement in computer codes. This thesis builds on a model that is a simplification of the theory of Valanis and Peters (*1991*) that was applied to pavement analysis by Smith et al. (*2000*).

The assumptions made in application of internal variables are that the response of water, air, and suction are reversible and elastic in nature. Therefore the loss terms are only associated with the soil skeleton strain tensor, ε_{ij}. Additionally, early development of internal variables (*Coleman, 1967*) and (*Valanis, 1980*) assumed they acted within a continuous constitutive function. The simplification by Valanis and Peters (*1991*) allows the use of a finite number of internal variables for application in the MMM further described in Chapter V. In the equation derivations to follow, the summation sign will be used to represent the summation effect of a finite number (r) of internal variables versus a more theoretical integration over a continuous function.

Internal variables are related to the non-affine motion of particles within a body (*Valanis, 1980*). Their effects are averaged out by the use of global strain terms such as shear strain or volumetric strain. However, to satisfy the first and second laws of

irreversible thermodynamics, the internal variables are necessary in the formal definition of the paired constitutive equations.

An internal variable represents that fraction of the strain tensor that involves plastic strain or permanent deformation symbolized by q_{ij}^{r} and is associated with only the effects of the soil skeleton, ε_{ij} and soil skeleton stress, σ_{ij}^{s}. The Helmholtz free energy can be expressed as a function of strain, temperature and internal variables $W = W(\varepsilon, T, q^{r})$.

For a system in which the change in entropy is no longer zero, heat flow R takes on a value from equation 4.2 and is then included in equation 4.1 as:

$$T\rho\dot{\eta} = \rho\dot{U} - \sigma_{ij}^{s}\dot{\varepsilon}_{ij} = \rho r - \operatorname{div}\mathbf{h} \tag{4.43}$$

Expressing the entropy density function $\eta = \eta(U, \varepsilon)$ and defining $T^{-1} = d\eta/dU$ yields:

$$\dot{\eta} = \frac{\partial\eta}{\partial U}\dot{U} + \frac{\partial\eta}{\partial\varepsilon_{ij}}\dot{\varepsilon}_{ij} = \frac{1}{T}\dot{U} - \frac{1}{T\rho}\sigma_{ij}^{s}\dot{\varepsilon}_{ij} = \frac{1}{T\rho}(\rho r - \operatorname{div}\mathbf{h}) \tag{4.44}$$

Let the total entropy within the system be defined as M:

$$M = \int_{V}\rho\eta dV \tag{4.45}$$

$$\dot{M} = \int_{V}\rho\dot{\eta}dV = \int_{V}T^{-1}(\rho r - \operatorname{div}\mathbf{h})dV \tag{4.46}$$

and substituting in the relationship from equation 4.44:

$$\dot{M} = \int_{V}\left[\rho\frac{r}{T} - \operatorname{div}\left(\frac{\mathbf{h}}{T}\right) + \mathbf{h}\cdot\nabla T^{-1}\right]dV \tag{4.47}$$

and using the divergence theorem, equation 4.47 can be expanded as follows:

$$\dot{M} = \int_V \rho \frac{r}{T} dV - \int_S \frac{h(\mathbf{n})}{T} dS + \int_V \mathbf{h} \cdot \nabla T^{-1} dV \tag{4.48}$$

It follows from the experimental fact $\mathbf{h} \cdot \nabla T^{-1} \geq 0$ Lubliner (1990)

$$\dot{M} - \left(\int_V \rho \frac{r}{T} dV - \int_S \frac{h(\mathbf{n})}{T} dS \right) = \Gamma \geq 0 \tag{4.49}$$

This relationship is known as the Clausius-Duhem inequality, where Γ is the internal entropy production and can be assumed to be given by:

$$\Gamma = \int_V \rho \gamma dV$$

where γ is the internal entropy production per unit mass. This along with the divergence theorem allows equation 4.49 to be rewritten as:

$$\int_V \left[\rho \dot{\eta} - \rho \frac{r}{T} + \nabla \cdot \left(\frac{\mathbf{h}}{T} \right) - \rho \gamma \right] dV = 0 \tag{4.50}$$

Finally the local Clausius-Duhem inequality is obtained when it is assumed that the term inside the bracket for any volume, V, must be equal to zero:

$$\rho \dot{\eta} - T^{-1} (\rho r + \nabla \cdot \mathbf{h}) - \mathbf{h} \cdot \nabla T^{-1} = \rho \gamma \geq 0 \tag{4.51}$$

This allows substitution of equation 4.44 into the term in parenthesis and substitution of equation 4.4 for $\dot{\eta}$ yields:

$$\mathbf{h}\cdot\nabla T^{-1}-\rho T^{-1}\left(\dot{W}+\eta\dot{T}-\frac{1}{\rho}\sigma_{ij}^{s}\dot{\varepsilon}_{ij}\right)\geq 0 \tag{4.52}$$

Furthermore, the external power incorporating the internal variables can be expressed as:

$$\dot{W}=\frac{\partial W}{\partial \varepsilon_{ij}}\dot{\varepsilon}_{ij}+\frac{\partial W}{\partial \varepsilon^{w}}\dot{\varepsilon}^{w}+\frac{\partial W}{\partial \varepsilon^{a}}\dot{\varepsilon}^{a}+\frac{\partial W}{\partial \theta}\dot{\theta}\frac{\partial W}{\partial T}\dot{T}+\sum_{r}\frac{\partial W}{\partial q^{r}}\dot{q}^{r}$$

This can be substituted into equation 4.52 to obtain:

$$\mathbf{h}\cdot\nabla T^{-1}-\rho T^{-1}\left(\left(\frac{\partial W}{\partial \varepsilon_{ij}}-\rho^{-1}\sigma_{ij}^{s}\right)\dot{\varepsilon}_{ij}+\left(\frac{1}{\rho}u_{w}-\frac{\partial W}{\partial \varepsilon^{w}}\right)\dot{\varepsilon}^{w}+\left(\frac{\partial W}{\partial \varepsilon^{a}}-\rho^{-1}u_{a}\right)\dot{\varepsilon}^{a}+\left(\frac{\partial W}{\partial \theta}-\rho^{-1}\left(u_{a}-u_{w}\right)\right)\dot{\theta}+\left(\frac{\partial W}{\partial T}+\eta\right)\dot{T}+\sum_{r}\frac{\partial W}{\partial q^{r}}\dot{q}^{r}\right)\geq 0 \tag{4.53}$$

For the particular case where the internal variables are not allowed to change, such that $\dot{q}^{r}=0$, then the quantities multiplying $\dot{\varepsilon}_{ij}$, $\dot{\varepsilon}^{w}$, $\dot{\varepsilon}^{a}$, $\dot{\theta}$ and $\dot{T}$ likewise must be zero in general. Therefore, if the internal variables are allowed to change, then the following inequality must be true:

$$\mathbf{h}\cdot\nabla T^{-1}-\rho T^{-1}\sum_{r}\frac{\partial W}{\partial q^{r}}\dot{q}^{r}\geq 0$$

Since the first term in equation 4.53 must be greater than zero, so too must the second term in the equation giving us the dissipation (Kelvin) inequality for the internal variables:

$$\sum_{r}\frac{\partial W}{\partial q^{r}}\dot{q}^{r}\geq 0$$

And from this relationship, there emerges the conjugate stress associated with each internal variable labeled the intergranular stress, $Q_{ij} = f\left(\dot{q}_{ij}^r\right)$:

$$Q_{ij} = -\frac{\partial W}{\partial q_{ij}^r} \tag{4.54}$$

In the particular case of a granular media, Q_{ij}^r represent the forces occurring between grains of soil. These forces are the combined effects of boundary loadings and tensile forces imparted by the menisci.

For simplicity, the internal variables are only considered for the soil skeleton. For a complete description of the system, internal variables would need to be associated with the water phase as well, a fact well verified by experiment (Figure 6-34). Therefore, the only free energy term influenced by the internal variables is $W_{s\theta}$ which is defined as:

$$W_{s\theta} = \frac{1}{2}\sum K_1^r \left(\varepsilon_{ij} - q_{ij}^r\right)^2 + \theta \sum K_2^r \left(\varepsilon_{ij} - q_{ij}^r\right) + \frac{1}{2} K_3 \theta^2 \tag{4.55a}$$

The conjugate pair $\boldsymbol{q}^r$ and $\boldsymbol{Q}^r$ can also be decomposed respectively into a hydrostatic (h) scalar and deviatoric (s) tensor components, q_h^r, Q_h^r, and $\mathbf{q}_s^r$, $\mathbf{Q}_s^r$, as follows:

$$W_{s\theta} = \frac{1}{2}\sum K_1^r \left(\varepsilon_v - q_h^r\right)^2 + \theta \sum K_2^r \left(\varepsilon_v - q_h^r\right) + \frac{1}{2} K_3 \theta^2 + \frac{1}{2}\sum 2G^r \left\|\gamma_{ij} - \mathbf{q}_s^r\right\|^2 \tag{4.55b}$$

Taking the partial differential of the coupled energy expression, the stress tensor $\boldsymbol{Q}$ can be related to the internal variables and the strain tensor as follows:

$$-\frac{\partial W_{s\theta}}{\partial \mathbf{q}_s^r} = Q_s^r = 2G^r \left\|\gamma_{ij} - \mathbf{q}_s^r\right\| \tag{4.56}$$

$$-\frac{\partial W_{s\theta}}{\partial \mathbf{q}_h^r} = Q_h^r = K_1^r \left(\varepsilon_v - q_h^r\right) \tag{4.57}$$

$$\frac{\partial W_{s\theta}}{\partial \gamma_{ij}} = \tau_{ij} = \mathbf{Q}_s = \sum 2G^r \left(\gamma_{ij} - \mathbf{q}_s^r\right) \tag{4.58}$$

where: $$\tau_{ij} = \sigma_{ij} - \frac{1}{3}\sigma_{kk}\delta_{ij}$$

$$\frac{\partial W_{s\theta}}{\partial \varepsilon_v} = \sigma_{ij}^s = \sum K_1^r \left(\varepsilon_v - q_h^r\right) + K_2\theta \tag{4.59}$$

where: $$Q_h = \sum K_1^r \left(\varepsilon_v - q_h^r\right) \tag{4.60}$$

Equation 4-60 represents the definition of total intergranular stresses (normal stress), Q_h used to define the potential strength between grain contacts in place of the effective stress concept used in classical saturated soil mechanics. Additionally the stress definitions follow where the sum of all hydrostatic and shear components produce the second order intergranular stress tensor, Q_{ij}:

$$Q_{ij} = Q_h + \mathbf{Q}_s \tag{4.61}$$

The intergranular stress tensor is related to the soil skeleton stress as:

$$\sigma_{ij}^s = Q_{ij} + K_2\theta \tag{4.62}$$

Leading to the definition of Cauchy stress on the membrane surface as:

$$\sigma_{ij} = Q_{ij} + u_w\delta_{ij} + u_a\,\delta_{ij} \tag{4.63}$$

Note that in the definition of soil skeleton stress, the internal variables are tied to the volumetric strain of the soil skeleton, but are independent of the suction response. This supports the assumption that the suction is considered a reversible energy given the appropriate change in volumetric water content, θ.

4.5 Definition of the K Moduli

4.5.1 Introduction

To complete the introduction of the constitutive response it is necessary to define the coefficients $K_{1,2,3}$ and show the means by which they are determined from laboratory experiments. The free energy expression, $W_{s\theta}$ involves a complex interaction of four variables: effective stress, suction, strain and volumetric water content. In order to understand their interactions, a series of experiments was designed to isolate those specific variables. Tests conducted were the constant volume swell test, one-dimensional consolidation test, one-dimensional free swell test and from literature, the psychrometer test (*Peterson, 1990*),

The psychrometer test provides a direct determination of the relationship between volumetric water content and suction potential for a given specimen. A psychrometer test correlates the relative humidity within a soil specimen to a magnitude of suction obtained from a previous calibration with a salt or material of known suction potential. The volumetric water content, θ is obtained as the ratio of the measured volume of water in the specimen over the total volume of the specimen calculated. The definition of K_3 follows from the introduction of two parameters associated with the slope of the p-θ conjugate variable relationship, a slope κ and a compatibility term defined as α, two parameters that will be clearly defined later in the chapter.

A constant volume swell test involves changing the soil skeleton stress, suction and volumetric water content under a zero-stain condition. At the limit condition when the soil becomes saturated the soil skeleton stress is equal to the applied boundary stress. Because volumetric water content affects both soil skeleton stress and suction simultaneously, a relationship can be obtained that isolates the suction and soil skeleton stress variables. The constant volume swell test provides a ratio of the two coefficients K_2 and K_3 from the boundary conditions present for a constant volume swell test.

In a drained condition, the Cauchy stress and intergranular stress are equivalent for a one dimensional consolidation test conducted on a saturated soil specimen. This

isolates the effective stress-volumetric strain relationship and these experiments lead to determining K_1 for an elastic condition.

The one-dimensional free swell test involves changing suction, strain and volumetric water content for a constant Cauchy stress condition. At the limit when the sample is saturated, the intergranular stress will equal the measured Cauchy stress. Because the volumetric water content affects both strain and suction simultaneously, a relationship can be obtained between the changes in suction with changes in strain. The use of this test in identifying the relevant coefficients comes in the limit condition when the response at saturation is compared to the response at saturation for a constant volume swell test. A linear relationship is assumed between swell stresses and swell strains which establishes an equivalence between the three K moduli affecting the test. In this case K_2 is actually a function of both K_1 and K_3. The benefit of this knowledge is that within these four tests, the system is over-determined. And the ability to determine the coefficients in the lab becomes a simpler process by requiring fewer combinations of experiments.

The Multi-Mechanical Model was developed as a tension positive convention, which means that compressive strains and stresses will be assigned a negative value. To continue with the derivations for the various parameters associated with the constitutive relationship, the values of intergranular stress, Q and suction, p are used both as variables and as parameters. When used as parameters, Q and p take on an absolute value or magnitude to produce the logarithmic response observed between the stress-strain and suction-water content conjugate pairs.

4.5.2 Generalizing the Constitutive Equations

Beginning from the idealized relationships in equations (4.30) and (4.31) which define the soil skeleton stress and suction, the following differential expressions will illustrate relationships between the K coefficients, use of Q and p as parameters and the need to incorporate a coupling factor from which to create a consistency between both the free swell and constant volume swell tests.

From equations (4.26) and (4.27) we can take the double partial differential of the free energy for each term as follows:

$$d\sigma_{ij}^{s} = \frac{\partial^2 W}{\partial \varepsilon_{ij}^2} d\varepsilon_{kl} + \frac{\partial^2 W}{\partial \varepsilon_{ij} \partial \theta} d\theta \tag{4.64}$$

$$dp = \frac{\partial^2 W}{\partial \varepsilon_{ij} \partial \theta} d\varepsilon_{ij} + \frac{\partial^2 W}{\partial \theta^2} d\theta \tag{4.65}$$

Three unique partial differentials corresponding to a modulus relating a change in stress to a change in strain or similarly a change in suction potential to a change in volumetric water content are defined as follows:

$$\frac{\partial^2 W}{\partial \varepsilon_{ij}^2} = K_1 = K_1^o |Q| \tag{4.66}$$

$$\frac{\partial^2 W}{\partial \varepsilon_{ij} \partial \theta} = K_2 = -K_2^o \sqrt{|Qp|} \tag{4.67}$$

$$\frac{\partial^2 W}{\partial \theta^2} = K_3 = K_3^o |p| \tag{4.68}$$

The $K^o_{1,2,3}$ terms represent the numeric constants that are determined from regression analysis on data obtained from the laboratory. The $K_{1,2,3}$ moduli incorporate intergranular stress and suction as parameters to account for the non-linearity of the elastic constitutive response. The form of the $K_{1,2,3}$ moduli are such that they capture the semi-logarithmic behavior observed from laboratory investigation. Specifically, for the case of $d\theta = 0$, the consolidation response is semi-logarithmic and therefore Q is used as a parameter. For the case of $d\varepsilon = 0$, the suction-volumetric water content response is semi-logarithmic and therefore p is used as a parameter.

The following system of equations represents the basis for the partially saturated model in an idealized case where no internal variables are present. In this case the system is reversible:

$$d\sigma^s = K_1^o |Q| d\varepsilon_v - K_2^o \sqrt{|Qp|} d\theta \tag{4.69}$$

$$dp = -K_2^o \sqrt{|Qp|} d\varepsilon_v + K_3^o |p| d\theta \tag{4.70}$$

To create a system of equations which observes dissipation of free energy during cycles of loading, equations (4-69) and (4-70) can be rewritten including the hydrostatic internal variables as:

$$d\sigma^s = |Q| \sum K_1^{or} (d\varepsilon_v - dq_h^r) - K_2^o \sqrt{|Qp|} d\theta \tag{4.71}$$

$$dp = -\sqrt{|Qp|} \sum K_2^{or} (d\varepsilon_v - dq_h^r) + K_3^o |p| d\theta \tag{4.72}$$

Equations (4.71) and (4.72) will be used in the proof of concept of the partially saturated soil model. In doing so the assumption is made that the K moduli are calculated based on data taken over the entire range of strain applied therefore providing an average value for the strain range of interest. The following illustrates the fit between the observed test data and the determination of the variables described in the preceding equations.

4.5.3 Solving for the Coefficients

<u>One Dimensional Consolidation Test:</u>

The one-dimensional consolidation test or oedometer test is a very common laboratory test used in many conventional soil designs. An oedometer test measures the

magnitude of volume change of a short, cylindrical soil specimen during application of a series of increasing or decreasing vertically applied loads (Figure 4-5). Constraints of the test are that no lateral strain is allowed due to the confining ring that around the specimen. As a result, only vertical deformation occurs, which is proportional to the total volume change. The applied loading occurs is vertical, so measured stresses during the test are of the major principal stress (σ_1) acting in a direction normal to the surface of the soil specimen. As well, the specimen is tested saturated and drained so that any excess water pressure incurred during loading is allowed to dissipate with time. This ensures that applied stresses, σ_{ij} are equal to the intergranular stresses, Q_{ij} which support the entire load.

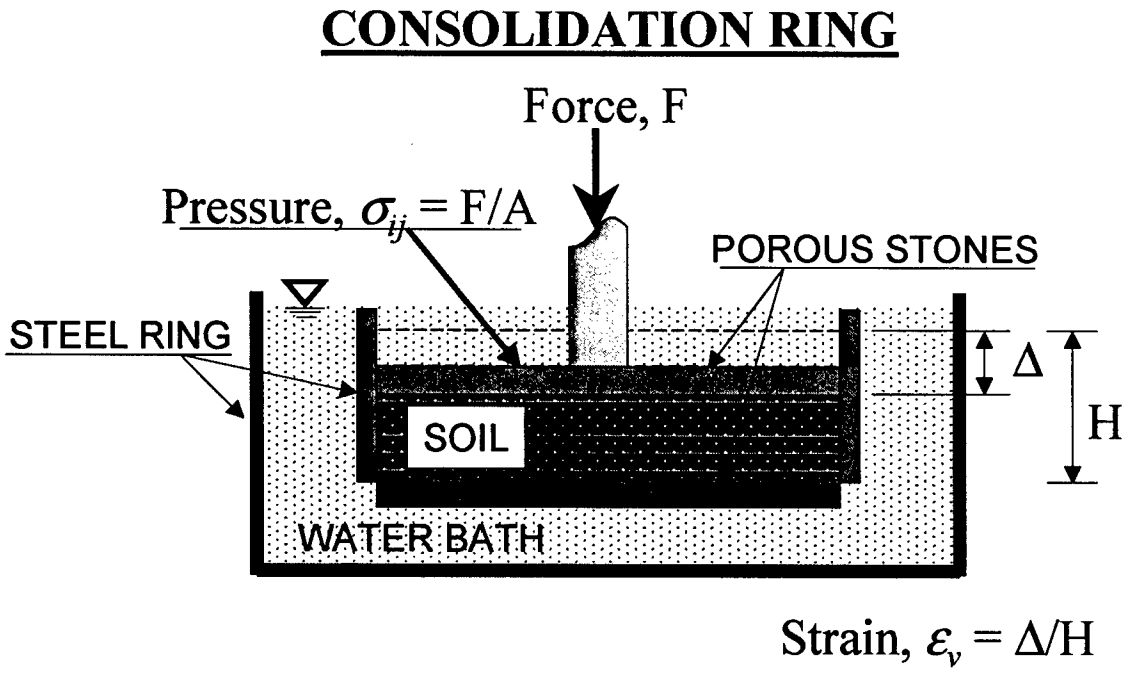

Figure 4-5: Diagram of Consolidation Ring used in one-dimensional consolidation, constant volume swell and free swell testing

Typically when a soil specimen is loaded, both elastic and plastic volumetric strain occurs in the system. The elastic strain is recoverable upon unloading of the soil and the plastic strain is permanent, unrecoverable deformation. Therefore, the oedometer

test can be used to define the magnitude of K_1^o, which relates the changes in elastic volumetric strain to the changes in intergranular stress.

If the test conditions for the oedometer are: $dp = 0$, $d\theta = 0$ and $d\sigma' = dQ$, equations (4.71) and (4.72) are reduced to the following:

$$dQ = K_1^o |Q| d\varepsilon \tag{4.73}$$

Since any compacted soil has some initial strain, a better means to identify an origin for changes in volume is to use the state variable, void ratio to express the initial volume of the soil specimen. The conversion from volumetric strain to void ratio, e, maintaining a compressive strain negative convention is as follows:

$$d\varepsilon = -\frac{de}{1+e_0} \tag{4.74}$$

Which when substituted into equation (4.73) allows the following expression to be obtained:

$$dQ = -K_1^o |Q| \frac{de}{1+e_0} \tag{4.75}$$

The limits of the test range from an initial void ratio of the specimen e_o, and an initial confining pressure, Q_0, on the soil to some final void ratio, e, and a final confining pressure, Q, after unloading:

$$\int_{Q_0}^{Q} \frac{dQ}{|Q|} = -\frac{K_1^o}{1+e_0} \int_{e_0}^{e} de \tag{4.76}$$

After integration, the following expressions for the elastic relationship between volumetric strain (void ratio) and confining/intergranular stress are:

$$\ln\left(\frac{Q}{Q_0}\right) = K_1^o \frac{e_0 - e}{1 + e_0} \tag{4.77}$$

$$Q = Q_0 \exp\left(K_1^o \frac{e_0 - e}{1 + e_0}\right) \tag{4.78}$$

Equation (4.79) below is obtained from taking the square root on both sides of equation (4.78) and will be used later in deriving an expression for a term which provides compatibility between the free swell and constant volume swell tests α.

$$\frac{\sqrt{Q}}{\sqrt{Q_0}} = \exp\left(\frac{K_1^o}{2} \frac{e_0 - e}{1 + e_0}\right) \tag{4.79}$$

Constant Volume Swell Test:

The constant volume swell (CV) test is similar to the one-dimensional consolidation test in that it uses the same size specimens and apparatus (Figure 4-5). The exception is that the soil is initially in an unsaturated condition. Through suction, water contained within the reservoir is drawn into the specimen with time. The same constraints used in the oedometer test apply to the CV test with no lateral strain allowed and the measured stress is the vertical confining pressure generated by prevention of vertical strain, $\varepsilon_v = 0$, by locking the piston in place. This transfers the suction potential into a pressure felt on the surface of the piston.

The CV test operates on the principle that as a soil specimen is wetted from an unsaturated to a saturated condition, the release of free energy stored by the suction potential will be transferred to the boundary stresses, increasing the stress exerted by the piston to maintain the soil at a constant volume. Since the stress transfer during this test is from the suction to the Cauchy stress, the intergranular stress represents the transition stress. The intergranular stress at the end of the test is equal to the final Cauchy stress, $\sigma_{sw} = Q_{sw}$, because the system becomes saturated at zero suction. Since no additional

Cauchy stress is added to the soil during the test, the intergranular stress originates solely from the suction component at the beginning of the test. This allows a direct relationship between the magnitudes of intergranular stress as result of a given suction.

If the test conditions for the CV test are: $d\varepsilon_v = 0$ (a constrained test sample), equation (4.71) reduces to:

$$d\theta = -\frac{d\sigma^s}{K_2^o\sqrt{|Qp|}} \tag{4.80}$$

Substitution into equation (4.72) yields:

$$dp = -\frac{K_3^o}{K_2^o}\frac{|p|}{\sqrt{|Qp|}}d\sigma^s \tag{4.81}$$

The limits of integration are from an initial suction value of the unsaturated specimen of p_{sw} and an initial confining pressure, $\sigma^s = 0$ (unconfined), to a final suction, $p = 0$ (at saturation) and a confining pressure equal to the swell pressure of the sample, $-\sigma_{sw}$:

$$\int_{p_{sw}}^{0}\frac{dp}{|p|} = -\frac{K_3^o}{K_2^o}\frac{1}{\sqrt{|Q|}}\int_{0}^{-\sigma_{sw}} d\sigma \tag{4.82}$$

The initial intergranular stress within the specimen, Q_{sw}, is assumed to be equivalent to the final intergranular stress and therefore equal to the boundary stress, σ_{sw}, measured on the face of the piston after the specimen has reached full saturation:

$$-\frac{2(-p_{sw})}{\sqrt{|-p_{sw}|}} = -\frac{K_3^o}{K_2^o}\frac{-\sigma'_{sw}}{\sqrt{|Q_{sw}|}} \tag{4.83}$$

This results in a final expression relating the initial suction prior to wetting, p_{sw}, to the contribution of intergranular pressure resulting from that suction prior to the application of water, Q_{sw}:

$$\sqrt{p_{sw}} = \frac{1}{2}\frac{K_3^o}{K_2^o}\sqrt{Q_{sw}} \tag{4.84}$$

Equation (4.84) is called the Constant Volume Swell Pressure Relationship.

Free Swell Test:

The Free Swell test (FS) is similar to both the CV test and the one-dimensional consolidation test. In the FS test, changes in volume of a soil specimen are determined relative to changes in saturation or suction rather than to changes in Cauchy stress. In the case of the FS test, the specimen and apparatus (Figure 4-5) are similar to the above tests and the sample begins in a partially saturated state with some initial suction and water content. The soil specimen is then wetted while allowing only a vertical strain to occur due to the release of free energy from the suction potential in the soil. The vertical Cauchy stress is held constant at some relatively small value (or zero) and the specimen swells until a condition of full saturation occurs. The assumption is that upon completion of the test, where the suction approaches zero, the intergranular stress would equal the applied seating load or boundary stress on the soil. This finalizes the transfer of free energy from the suction to the swelling of the soil skeleton.

In the FS test, the goal is to find a correlation between changes soil suction to changes in volumetric strain dependent on the current stress and volume state of the specimen. Coupling the behavior determined in a FS test to that of the CV test provides a means to define a term α. This coupling term, α, ensures a reversibility between the volumetric strain and swell pressure from the behavior of the free swell and constant volume swell tests.

If the test conditions for a free swell test are: $d\sigma^s = 0$, equation (4.71) reduces to:

$$d\theta = \frac{K_1^o |Q|}{K_2^o \sqrt{|Qp|}} d\varepsilon \tag{4.85}$$

and substituting into equation (4.72) results in:

$$dp = -K_2^o \sqrt{|Qp|} d\varepsilon + \frac{K_1^o K_3^o}{K_2^o} \frac{|Qp|}{\sqrt{|Qp|}} d\varepsilon \tag{4.86}$$

$$\frac{dp}{\sqrt{|p|}} = \left(\frac{K_1^o K_3^o}{K_2^o} - K_2^o \right) \sqrt{|Q|} d\varepsilon \tag{4.87}$$

From the one-dimensional consolidation test, equation 4.79 can be expressed as:

$$\frac{\sqrt{Q}}{\sqrt{Q_{sw}}} = \exp\left(\frac{K_1^o}{2} \frac{e_{sw} - e}{1 + e_{sw}} \right) \qquad \text{where} \qquad \varepsilon_v = \frac{e_{sw} - e}{1 + e_{sw}} \tag{4.88}$$

The subscript *sw*, refers to the initial conditions prior to wetting of swell specimens for either FS of CV tests. Substituting equation (4.88) into (4.87) and integrating over the limit conditions of an initial suction and state, p_{sw} and e_{sw}, and a final suction, p_f, and final swelled volumetric state, e_f, one obtains:

$$\int_{p_{sw}}^{p_f} \frac{dp}{\sqrt{|p|}} = -\left(\frac{K_1^o K_3^o}{K_2^o} - K_2 \right) \frac{\sqrt{|Q_{sw}|}}{1 + e_{sw}} \int_{e_{sw}}^{e_f} \exp\left(\frac{K_1^o}{2} \frac{e_{sw} - e}{1 + e_{sw}} \right) de \tag{4.89}$$

Upon integration the following intermediate expression is found:

$$\frac{2(-p_f)}{\sqrt{|-p_f|}} - \frac{2(-p_{sw})}{\sqrt{|-p_{sw}|}} = -\left(\frac{K_1^o K_3^o}{K_2^o} - K_2 \right) \frac{\sqrt{|Q_{sw}|}}{1 + e_{sw}} \frac{2(1 + e_{sw})}{K_1^o} \left[\exp\left(\frac{K_1}{2} \frac{e_{sw} - e_f}{1 + e_{sw}} \right) - \exp\left(\frac{K_1}{2} \frac{e_{sw} - e_{sw}}{1 + e_{sw}} \right) \right]$$

This results in an expression relating initial suction to final void ratio expected upon wetting a soil specimen to saturation:

$$\sqrt{|p_{sw}|}-\sqrt{|p_f|}=-\left(\frac{K_3^o}{K_2^o}-\frac{K_2^o}{K_1^o}\right)\sqrt{|Q_{sw}|}\left[\exp\left(\frac{K_1^o}{2}\frac{e_{sw}-e_f}{1+e_{sw}}\right)-1\right] \tag{4.90}$$

There should exist a case where an equivalence occurs between the constant volume swell test and the free swell test. For example, the reversibility assumed for this model between these two tests should allow a case where if a specimen of soil was loaded to its swell pressure, and then given access to water, no volume change would occur during free swell. Likewise, if a specimen in a constant volume swell test were to reach a given swell pressure and then the specimen released to strain, it would swell to the void ratio associated with the initial suction of the specimen. This would represent behavior found along the line of reversibility shown in Figure 4-6.

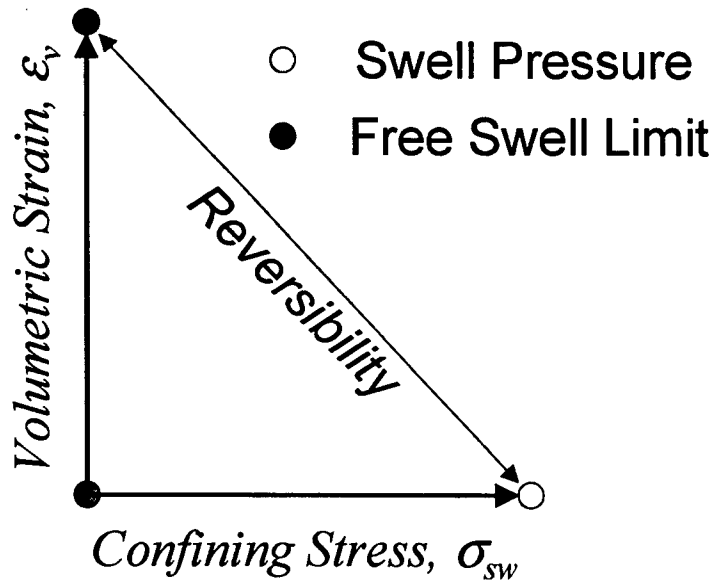

Figure 4-6: Reversibility of the volumetric strain-swell pressure relationship

Substitution of the constant volume swell pressure relationship (eq. 4.84) into the free swell relationship (eq. 4.90) and assuming that during the FS and CV swell tests p_f approaches zero, one obtains:

$$\frac{1}{2}\frac{K_3^o}{K_2^o}\sqrt{|Q_{sw}|} = -\left(\frac{K_3^o}{K_2^o} - \frac{K_2^o}{K_1^o}\right)\sqrt{|Q_{sw}|}\left[\exp\left(\frac{K_1^o}{2}\frac{e_{sw}-e_f}{1+e_{sw}}\right)-1\right]$$

or

$$\frac{1}{2}K_1^o K_3^o = \left(K_2^{o2} - K_1^o K_3^o\right)\left[\exp\left(\frac{K_1^o}{2}\frac{e_{sw}-e_f}{1+e_{sw}}\right)-1\right] \tag{4.91}$$

When the energy model was developed the following inequality $K_2^2 - K_1K_3 < 0$ was derived. This suggests that K_2 is a function of K_1 and K_3, as a result the following expression is proposed, which uses the compatibility coefficient alpha, α, to ensure that the inequality remains true:

$$K_2 = \sqrt{\alpha K_1 K_3} \tag{4.92}$$

To determine the response range of the parameter, α, the substitution for K_2 is made into equation (4.91) and simplified as follows:

$$\frac{1}{2} = (\alpha - 1)\left[\exp\left(\frac{K_1^o}{2}\frac{e_{sw}-e_f}{1+e_{sw}}\right)-1\right] \tag{4.93}$$

From this, one obtains a relationship for α based upon the swelling state of the material as follows:

$$\alpha = \frac{\exp\left(\frac{K_1^o}{2}\frac{e_{sw}-e_f}{1+e_{sw}}\right)-0.5}{\exp\left(\frac{K_1^o}{2}\frac{e_{sw}-e_f}{1+e_{sw}}\right)-1.0} \tag{4.94}$$

The value of the coefficient K_1 can be estimated from the average log-linear slope of the hysteresis during a one-dimensional unloading and reloading test, C^*, and the initial state e_{sw} for a linearized analysis:

$$K_1^o = \frac{2.303(1+e_{sw})}{C^*} \tag{4.95}$$

Substituting equation 4.95 into 4.94, α is determined as a function of the normally consolidated response and the unload-reload elastic response as follows:

$$\alpha = \frac{\exp\left(\frac{1.151}{C^*}(e_{sw}-e_f)\right)-0.5}{\exp\left(\frac{1.151}{C^*}(e_{sw}-e_f)\right)-1.0} \tag{4.96}$$

If the sample exhibits no swelling such that $e_f = e_{sw}$, then α=0.5 representing a maximum stiffness assigned to K_2. If the value of e_f becomes large due to considerable volumetric swelling then the value of α tends towards negative infinity when the exponential approaches one. However it is assumed that K_2 is a positive, real value and therefore from equation (4.92) the lower limit of α is zero.

Psychrometer Test:

The psychrometer test used in this thesis involves preparing a compacted cylindrical soil specimen which by boring a small hole into the top of the cylinder. A psychrometer is inserted and readings of suction are taken. Illustrations of this test can be

found in Chapter VI. Only one psychrometer value is obtained from a given specimen, so for every data point from psychrometer tests, an equal number of compacted specimens in the lab were prepared. In an ideal case, one could alter the moisture content of the specimen by wetting or drying, allow the specimens to shrink or swell and all the while monitor the psychrometer readings to determine the relationship between suction, p, and volumetric water content, θ.

In psychrometer tests allows a value of K^o_3 modulus is determined as result the suction potential and the volumetric water content are coupled. The test also places further limits on the value of the α parameter used to couple the volume change and swell pressures generated due to the presence of partial saturation in the soil. The concept of the ideal test is used to derive the suction-water content relationship as follows:

If the psychrometer test conditions are: $d\sigma' = 0$ (specimen is not confined), equation (4.71) reduces to the following:

$$d\varepsilon = \frac{K_2^o \sqrt{|Qp|}}{K_1^o |Q|} d\theta \tag{4.97}$$

Substituting equation (4.97) into equation (4.72) and simplifying produces an expression relating the change in suction to the change in volumetric water content. The sign convention for the volumetric water content is positive and the sign for suction potential is negative, exhibiting the same convention as a compression negative intergranular stress.

$$dp = -K_2^o \sqrt{|Qp|} \left(\frac{K_2^o \sqrt{|Qp|}}{K_1^o |Q|} d\theta \right) + K_3^o |p| d\theta \quad \text{or}$$

$$\frac{dp}{|p|} = \left(K_3^o - \frac{K_2^{o2}}{K_1^o} \right) d\theta \tag{4.98}$$

The limits of integration for the psychrometer test range from a reference suction, p_r, which represents the suction potential at $\theta = 0$. This is determined from extrapolating the straight-line portion of the suction-water content curve through the x-axis and recording the value of suction obtained, p_r, as illustrated in Figure 4-7. While the value of the reference pressure continues to infinity for very small values of suction the use of this reference pressure bounds the suction similar to the reference void ratio bounds the soil state and allows a single, continuous semi-logarithmic function to define the relationship.

The end limits of the integration are from some value of suction less than the reference pressure and a magnitude of volumetric water content greater than zero:

$$\int_{p_r}^{p} \frac{dp}{|p|} = \left(K_3^o - \frac{K_2^{o2}}{K_1^o} \right) \int_0^{\theta} d\theta \tag{4.99}$$

Making the substitution for K_2^o from equation (4.92) and simplifying produces:

$$\ln\left(\frac{p}{p_r}\right) = \left(\frac{K_1^o K_3^o - \alpha K_1^o K_3^o}{K_1^o} \right) \theta \qquad \text{or}$$

$$\ln\left(\frac{p}{p_r}\right) = (1-\alpha) K_3^o \theta \tag{4.100}$$

Equation (4.100) represents the completed theoretical development of the semi-logarithmic response observed from laboratory data shown in Figure 4-7. Since p/p_r is always less than or equal to one, the logarithm takes on a negative value, α cannot be a value less than zero, since that would make the right hand side of equation 4.100 positive given that θ and K^o_3 are both positive. Combined with the maximum stiffness defined in equation 4.96 the elastic bound of α is:

$$\frac{1}{2} \geq \alpha \geq 0$$

This result matches that determined for a reversible system between the free swell and constant volume swell tests.

To determine the value of K_3^o, a comparison to the laboratory data shown in Figure 4-7 is made. The slope of the relationship between the measured suction and the volumetric water content represented by the semi-logarithmic relationship shown in the following equation with slope κ:

$$\ln\left(\frac{p}{p_r}\right) = -\frac{1}{\kappa}\theta \tag{4.101}$$

In order to determine the value of K_3^o equations 4.100 and 4.101 are equated to obtain:

$$K_3^o(1-\alpha) = -\frac{1}{\kappa} \tag{4.102}$$

Which determines K_3^o as:

$$K_3^o = -\frac{1}{\kappa(1-\alpha)} \tag{4.103}$$

The parameter α must be positive number no greater than 1/2 and the value of κ is negative which defines K_3^o as a positive number.

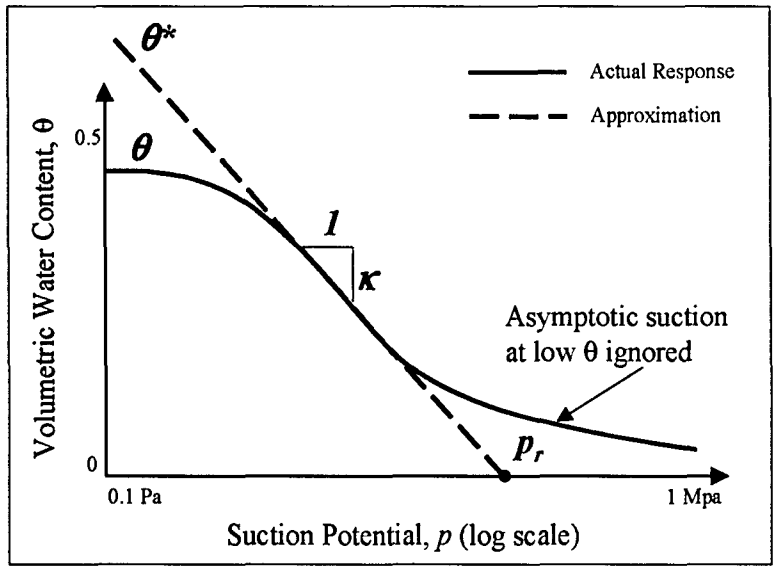

Figure 4-7: Calibration of Volumetric Water Content-Suction Response for Model Development

Taking advantage of the relationships between the K moduli enables determination of the coefficients through various combinations of results from these four tests. There exists one behavior of a partially saturated soil that is not currently accounted for in the derivations previously presented, i.e. a changing suction influences the volumetric stiffness of the soil. The following section will discusses this phenomenon and the means by which its behavior is accounted for in the model development.

4.6 Effect of Suction on Volumetric Stiffness

Researchers have shown (*Wheeler, 1995, Peterson, 1980*) that as suction potential increases for a partially saturated soil, its strength increases. This is evidenced by the shift of the normally consolidated strength line to a higher mean normal stress as the magnitude of suction increases. This is shown in data taken by Sivakumar (*1993*) in Figure (4-8). For suctions greater than zero, the suction is assumed to act isotropically

within the soil, directly influencing the mean stress response and maintaining parallel slopes of constant compression index, C_c.

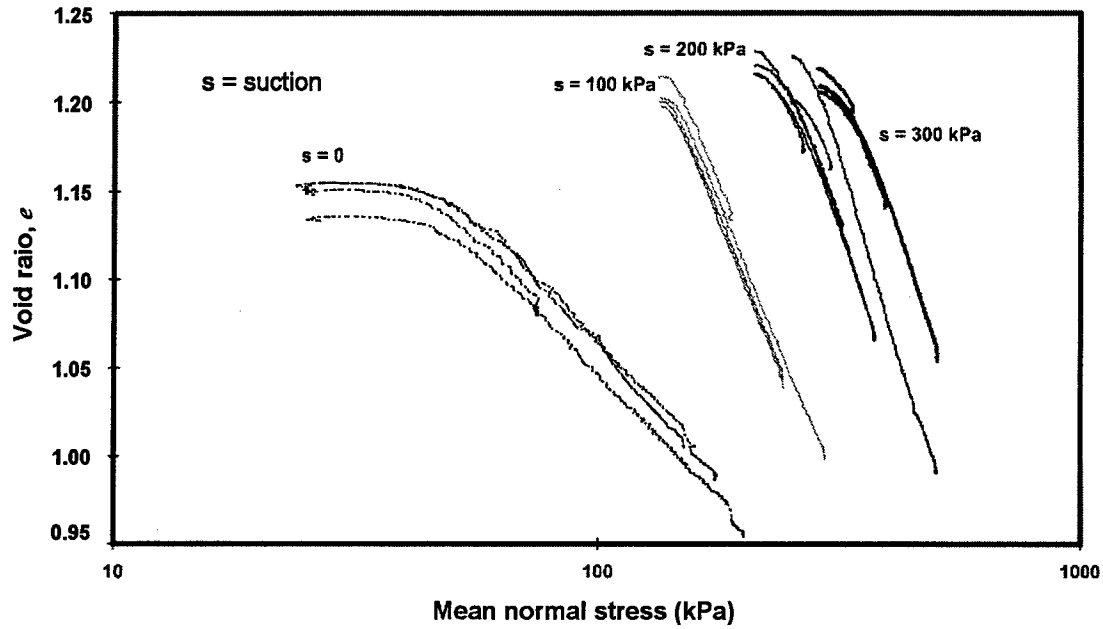

Figure 4-8: Void ratio, e versus mean normal stress at varying suctions for compacted Kaolin (Sivakumar, 1993)

Figure 4-8 illustrates the increase in the volumetric stiffness as a lateral movement of the normally consolidation line as a function of the degree of saturation. As the degree of saturation decreases (suction increases) for a constant void ratio, there is an increase in the preconsolidation pressure, σ_p. Since the mean normal stress felt by the soil at a particular suction is greater than if the soil was saturated, this can be treated as an overconsolidation (OCR) effect. The soil response to suction is the same as that of an overconsolidated material in that its strength increases due to a greater force acting between grains as indicated by the stress value Q_{ij}. The data from Sivakumar (Figure 4-8) shows that the compression index, C_c, for the saturated soil is not the same as that for the unsaturated material, however, there is a parallelism to slopes of the unsaturated curves. It is therefore assumed for simplicity that the unsaturated slopes will be parallel to the saturated slope. As a first concept for developing the model all recompression indices are assumed equal to the saturated state.

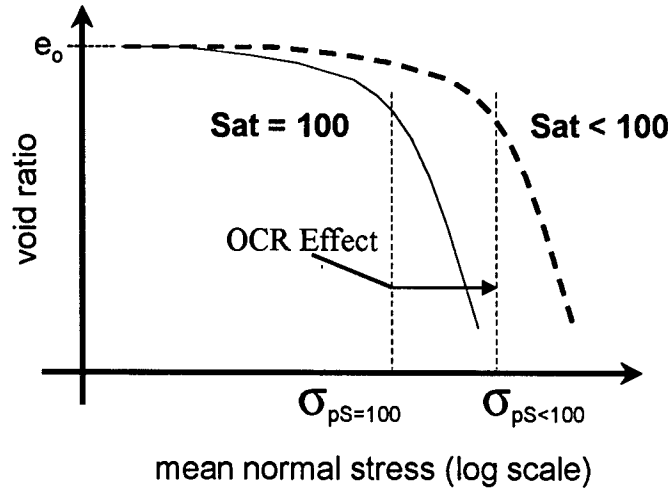

Figure 4-9: Illustration of the effect of saturation on the reference state of a soil

Figures 4-8 and 4-9 suggest that there should be a coupling between the saturation, void ratio, and mean stress for a soil. In essence, there should be a parameter that would account for the lateral shift in the material strength as the degree of saturation decreases. Since the overall shape of the response is similar, then a value taken from critical state soil mechanics can be used as a reference parameter, e_{ref}. The parameter e_{ref} is the largest void ratio a soil can maintain in a virgin consolidated state at a given confining pressure. It is determined by taking a line coincident with the slope, C_c and intersecting it with a reference mean stress as shown in the Figure 4-10:

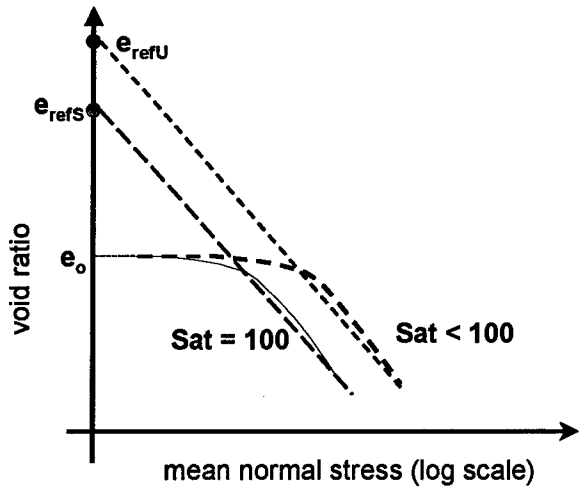

Figure 4-10: Change in reference pressure with degree of saturation

A convenient way to express the increase in volumetric stiffness of a soil with changes in saturation or similarly suction, is to determine a parameter that will shift the reference void ratio e_{refS} with degree of saturation to a new reference pressure e_{refU}.

To generate the data in Figure 4-8 to determine the shift in e_{ref} directly requires a series of complex consolidation tests. Each test would require that either the suction remain a constant, in which case the degree of saturation would decrease as the sample consolidated, or that the suction/saturation be measured at each increment of stress and a series of tests run to construct a family of curves from which to derive the intercepts for e_{refU}. To provide additional support to the work by Sivakumar that this procedure would produce a family of consolidation curves, two sets of data on differing soils were analyzed and plotted to illustrate what the shift parameter would look like.

A limited series of data was utilized for Buckshot clay (*Peterson, 1990*) from a series of consolidation tests run on partially saturated soil specimens. Each specimen began with differing initial water content and suction measured at the beginning of the test. As the specimens were consolidated, the degree of saturation increased as very little water escaped the specimens owing to the loss of air as the principal means of changing pore volume. The raw data from these tests are shown in Figure 4-11.

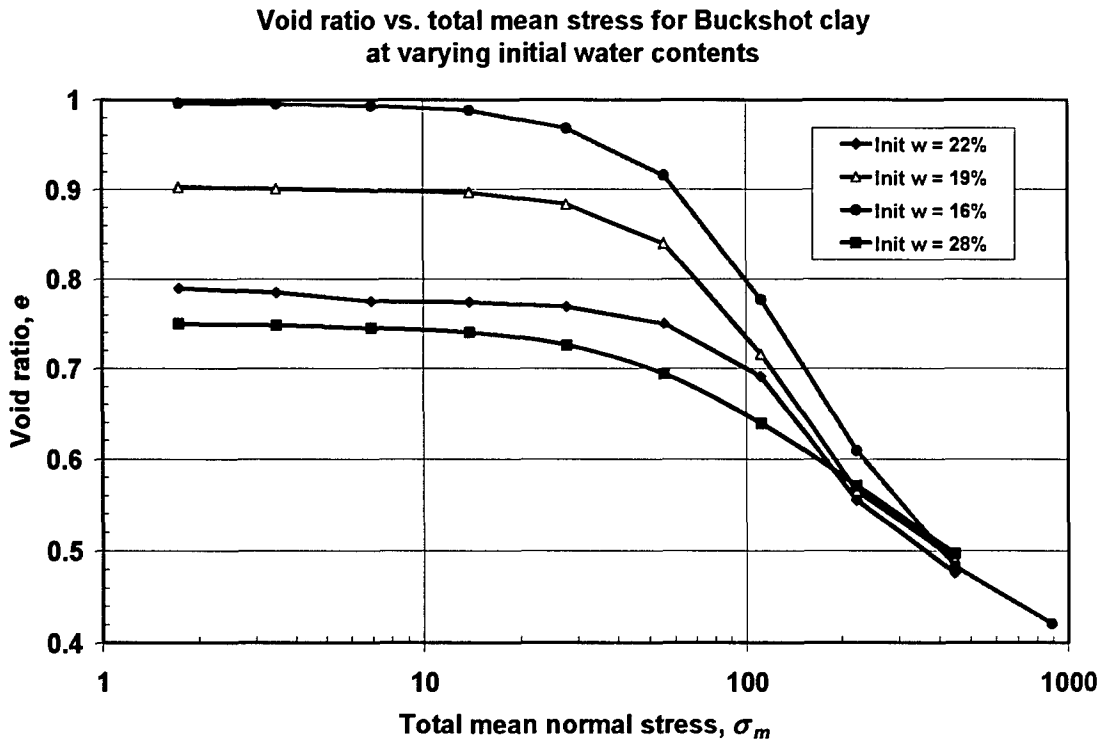

Figure 4-11: Raw consolidation data on partially saturated Buckshot clay specimens from Peterson (1990)

From these tests, the degree of saturation was estimated for each void ratio-mean stress data pair given a constant gravimetric water content and a known volume, e. Taking lines of constant mean stress and projecting the void ratio-saturation data pairs occurring along those lines results in a representation of the data shown in Figure 4-12. A construction of parallel isobars of constant mean stress are drawn through points of void ratio-saturation shown in Figure 4-12 assuming the linearity observed in Figure 4-8. The slope of these lines is taken as a constant labeled as Lambda, λ, where:

$$\lambda = \frac{\Delta e}{\Delta S} \tag{4.104}$$

Lambda now becomes a constant that relates the change in reference void ratio to changes in degree of saturation for a given total mean stress.

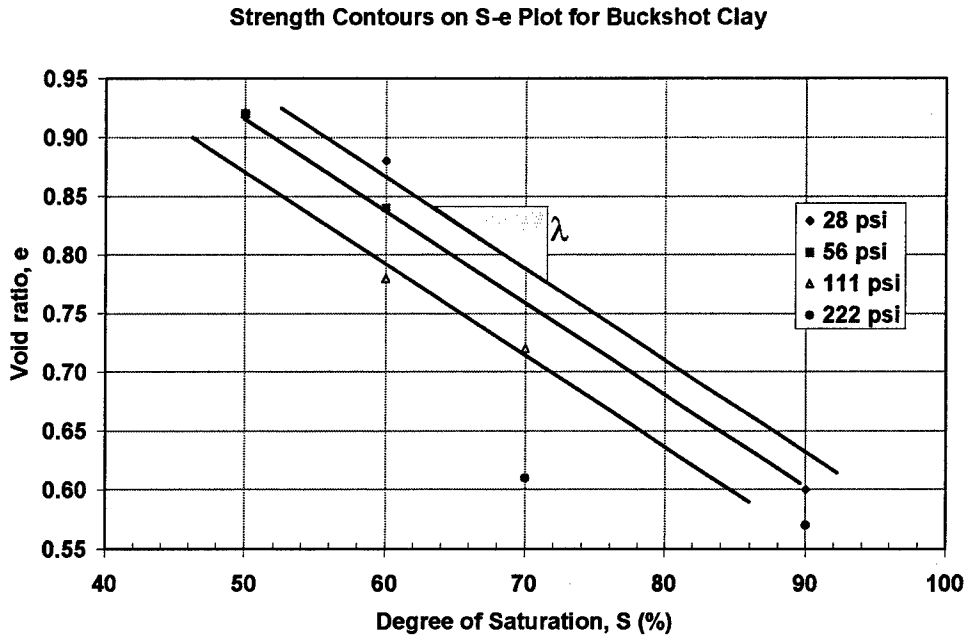

Figure 4-12: Isobars of constant mean stress for Buckshot clay in a void ratio-saturation space to illustrate determination of λ

Data points selected from Figure 4-11 are plotted according to degree of saturation in Figure 4-12. Data lying along constant lines of saturation are replotted in a void ratio-mean stress space in figure 4-13. Interpretation of this data in light of the findings by Sivakumar, show there is a parallelism to the normal consolidation lines over the range of stresses tested such that the value of compression index remains a constant for the Buckshot clay.

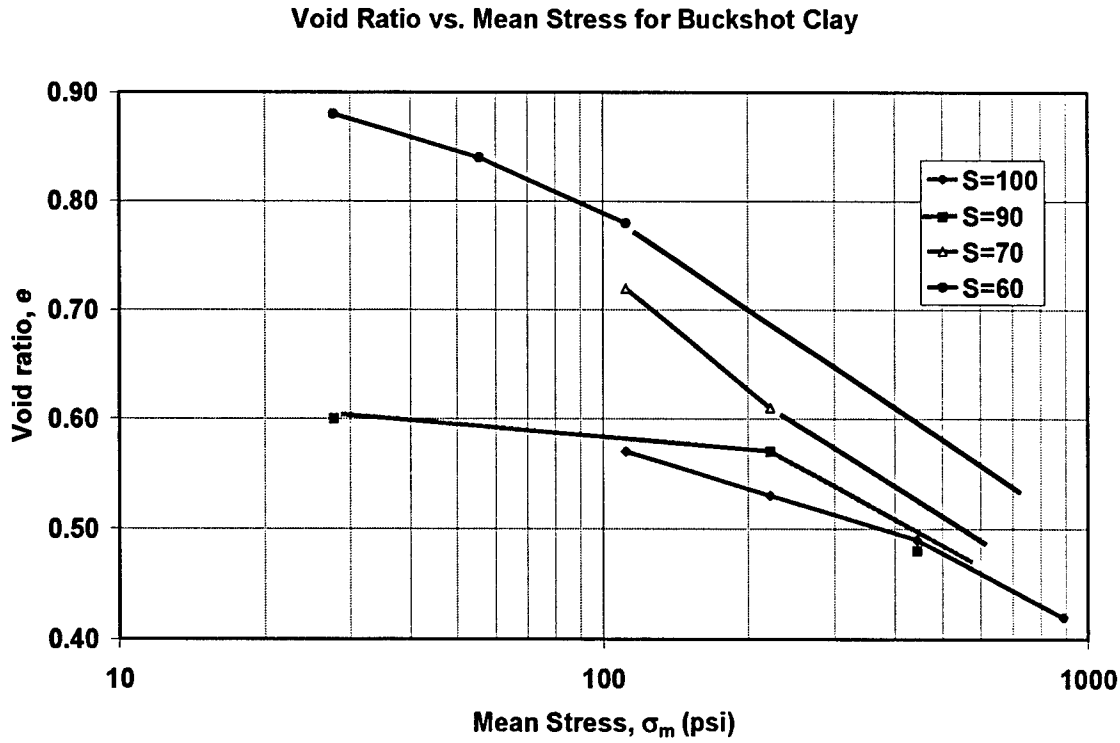

Figure 4-13: Consolidation plot for partially saturated Buckshot clay at constant saturation (suction) values

To extend the anlaysis for another soil using a different test procedure was studied. The soil was a low plasticity silty-clay (CL). The silty-clay was used to study tensile strength of compacted soil specimens (*Peters et al., 1988*). Laboratory specimens were prepared using a static compaction process where the applied stress to produce a desired degree of compaction was measured. Assuming this to be equivalent to a mean stress, each specimen could be referenced to its corresponding void ratio and saturation. Data reduction produced the saturation-void ratio plot and void ratio-mean stress plot as shown in Figures 4-14 and 4-15.

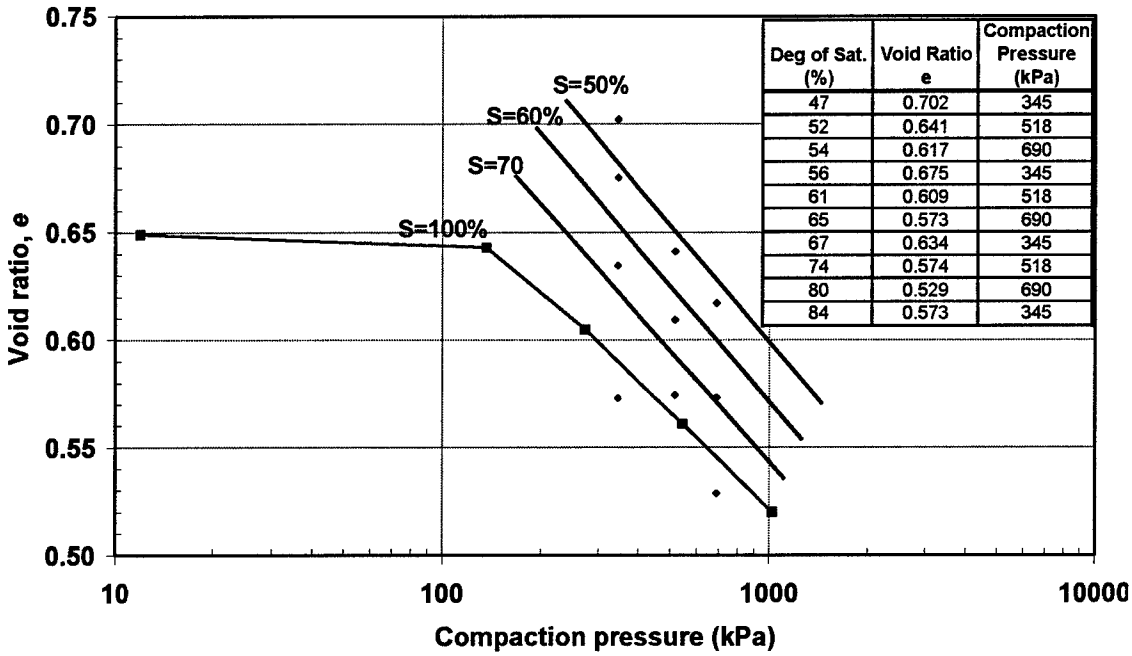

Figure 4-14: Void ratio-mean stress representation of compacted silty-clay specimens

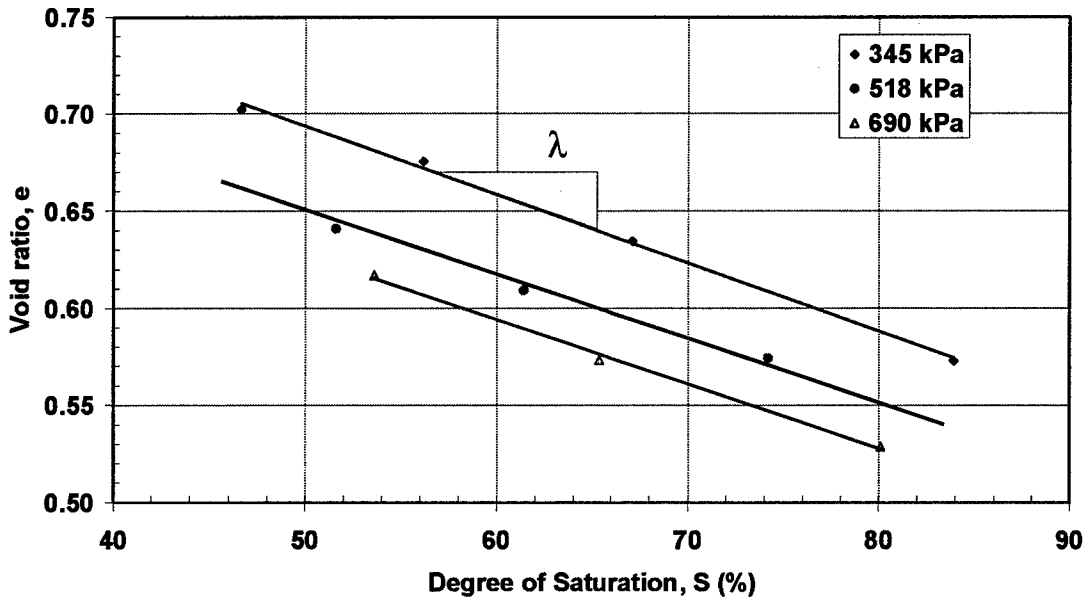

Figure 4-15: Void ratio-saturation plot of compacted silty-clay specimens showing parallel lines of equivalent mean stress

Similar trends as with Buckshot clay are noted, whereby a family of parallel lines connecting isobars of stress are drawn and have a slope, λ. It is noted that the slope, λ, for the silty-clay differs from that of the Buckshot clay suggesting that λ is a function of soil type.

Up to now the effect of increased strength with suction was not accounted for in the thermodynamic model developed earlier. However, the following discussion provides a basis for its incorporation.

The saturated soil model accounts for this increase in strength when normalizing the mean stress acting on the spring-slider elements in the form of a reference pressure, p_e given in equation 4.105. The normalizing effect of the strength response is necessary to predict constitutive response for any volumetric state. Presently, the equation to represent the reference pressure for saturated soil is:

$$p_e = 10^{(e_{ref}-e)/C_c} \tag{4.105}$$

However, the λ factor influences this equation by adjusting the location of e_{ref} by the degree of saturation as in Figure 4.10, so e_{ref} now is defined as e_{refU}:

$$e_{refU} = e_{ref(S=1)} + \lambda \cdot (1-S) \tag{4.106}$$

and, the value of p_e is now defined as the unsaturated reference pressure p_{ew}, that normalizes strength for void ratio and degree of saturation:

$$p_{ew} = 10^{(e_{refU}-e)/C_c} \tag{4.107}$$

A 100% degree of saturation is represented by $S=1$. Reference void ratio, e_{refU} increases with a decreasing saturation as shown in Figure 4-10. As well, when $S = 1$, the value of p_{ew} reduces to the saturated p_e given in equation (4.107). It is important that the strength response be capable of being normalized both in the saturated and unsaturated condition,

so that the predictive model can accommodate partially saturated soil conditions at varying volumetric states.

To show the effectiveness of the proposed concept, tensile strength data from Peters et al., (*1988*), is reproduced in Figure 4-16. According to the researchers' conclusions, tensile strength, or cohesion is a function of degree of saturation represented by the dark circle data set in Figure 4-16. This conclusion was reached by normalizing tensile strength with the saturated reference pressure for each specimen tested. This produced a linear trend whereby normalized strength, T_o/p_e increased with decreasing water content (increasing suction). However by normalizing the silty-clay tensile strength with the unsaturated reference pressure using a value of λ taken from the data in Figure 4-15, T_o/p_{ew} now accounts for the effect of saturation in the soil, and a constant strength ratio is achieved for both varying volumetric states and water contents represented by the triangular data set in Figure 4-16.

This is an important finding, because it provides the final piece of the model to account for all the observed features essential in defining a partially saturated soil. Other researchers have attempted to normalize the critical state reference pressure by adjusting e_{ref} and the slope C_c, however the means to obtain these values requires considerable effort through partially saturated triaxial and consolidation testing.

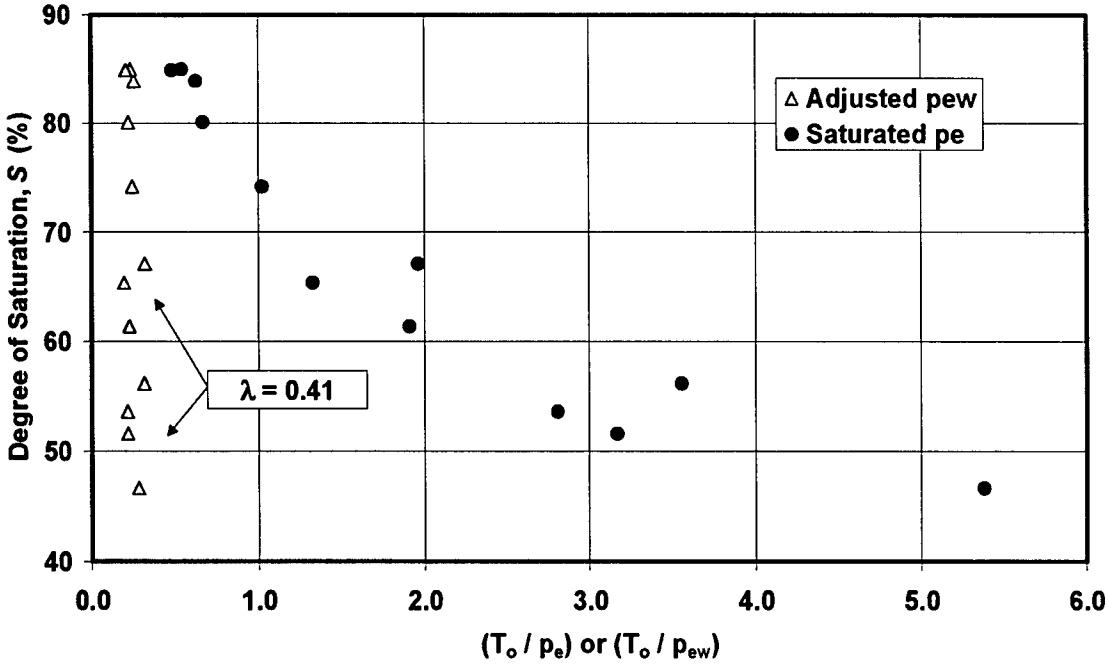

Figure 4-16: Normalized tensile strength for partially saturated silty-clay (CL) from (Peters, et al. 1988)

As noted, tests to determine λ can be extensive and are complex. Therefore a simpler means to determine this parameter was sought. An option are the proctor compacted specimens which provide a measure of the void ratio-saturation-mean stress response. Looking at a standard dry density-water content plot for a compaction test, both axes can be converted into the void ratio and saturation of a point of interest given the specific gravity of the material shown in Figure 4-17.

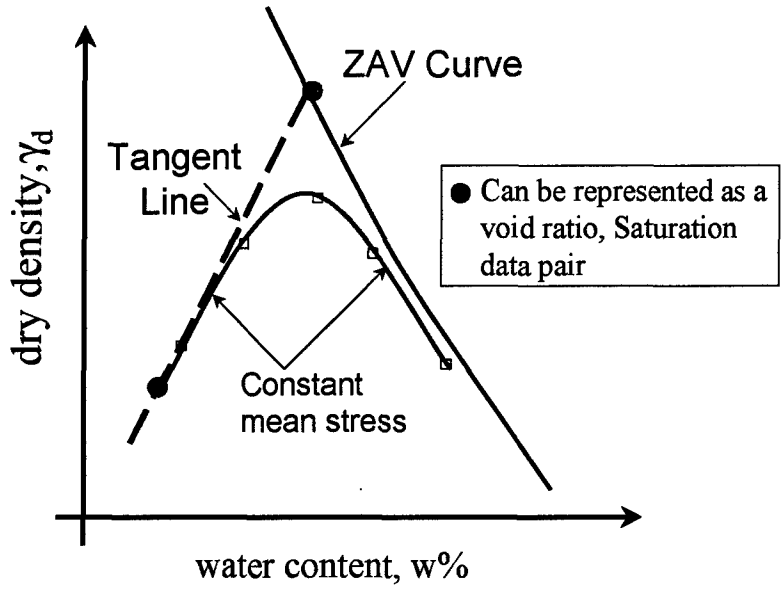

Figure 4-17: Illustration of obtaining the S-e data for computing Lambda from a moisture-density proctor curve

Each compaction curve represents a line of constant applied mean stress given a uniform testing procedure, even if the actual stress value is unknown. By simply drawing a tangent on a compaction curve, data points lying along this line can be converted to void ratio and saturation and the relative differences then used to define λ.

$$e = \frac{\gamma_w \cdot G_s}{\gamma_d} - 1 \tag{4.108}$$

$$Se = G_s w \tag{4.109}$$

The tangent line is drawn through the portion of the compaction curve that has a positive slope and continues up to zero air voids (ZAV) curve. This represents the response of the material as if the water were "soft" or compressible. This is similar to the shape of a kneading compaction test where no excess pore pressure builds up to inhibit densification (*Fenwick, 1968*). For the more traditional Proctor compaction test, which is an impact compaction, fine grained soils of low permeability will observe the concave

downward response once the water content within the specimen exceeds some optimum due to absorption of compaction energy by the water phase instead of the soil skeleton. Physically, at the dry end of the curve where density is the lowest, the material strength due to suction is highest. The strength then steadily decreases as more moisture is added, reducing the suction potential or energy transferred to tension between the grains (*Berney, et al., 2003*).

The technique to obtain λ from this tangent line is to choose a pair, or several pairs of points and convert them to *S-e* pairs of data that can then be used to determine λ. If data points from one of the void-ratio-saturation plots shown previously is plotted on a compaction curve, the points coincide with the slope as shown in Figure 4-17. Data taken from the standard proctor compaction curve for the silty-clay, the slope of λ is found to be 0.40, only slightly off from the value 0.41 determined from the tensile strength tests. For the Buckshot clay data, the value of λ from the standard proctor test is 0.5 which differs from the value of 0.6 to 0.7 obtained from the consolidation estimates in Figure 4-12.

This approach provides an approximation to λ because its behavior in a water content-dry density space does not map linearly to the slope in *S-e* space. To relate the definition of λ to a slope of dry density versus water content shown in Figure 4-17, the following derivation is presented beginning with a differential of equations 4.108 and 4.109:

$$de = -\frac{G_s \gamma_w}{\gamma_d^2} d\gamma_d \tag{4.110}$$

$$dSe + Sde = G_s dw \qquad \text{or} \tag{4.111}$$

$$dSe = G_s dw - Sde$$

substituting equation 4.110 into 4.111 yields:

$$dS = \frac{1}{e}\left(G_s dw + \frac{SG_s\gamma_w}{\gamma_d^2} d\gamma_d \right) \tag{4.112}$$

and substituting in equation 4.108 for e and reducing terms produces an expression for λ:

$$\lambda = \frac{de}{dS} = \frac{\left(1 - \frac{G_s\gamma_w}{\gamma_d}\right)\frac{\gamma_w}{\gamma_d^2}\frac{d\gamma_d}{dw}}{1 + \frac{S\gamma_w}{\gamma_d^2}\frac{d\gamma_d}{dw}} \tag{4.113}$$

This expression for λ is non-linear in a water content-dry density space and is dependent on the $d\gamma_d/dw$ slope of the dry density, γ_d. However, this method does provide a reasonable approximation to the λ value determined on an *S-e* plot. This is advantageous to the modeling effort, since compaction data is readily available for most materials and the range of values for λ is relatively small. Therefore, in the absence of partially saturated consolidation data the proctor curve provides a reasonable engineering approximation to λ.

The empirical factor, λ must be accounted for in the behavior of partially saturated soils. Its formulation stems from observations of the soil's macro behavior where suction is transferred to the soil skeleton. In turn the mean stress influences strength. The parameter λ represents the only empirical parameter of all the material properties that arise from the calibration of the thermodynamic model. Other researchers (*Alonso, et al., 1990, Wheeler, et al., 1995*) have represented the reference pressure and compression index as empirical functions of suction but require numeric calibration based on an extensive laboratory investigation using partially saturated triaxial specimens. The assumption of parallelism of the compression index and the relationship of λ to the compaction curve allows a simple means to capture the strengthening response due to suction.

4.7 Summary

Within the field of geotechnical engineering, partially saturated soil is the most common material encountered. A partially saturated soil is a complex multi-phase system consisting of air, water and solid material whose response is a function of not only the external and internal stress states but as well the soil moisture condition. A constitutive model for multi-phase, partially saturated soil was developed from the laws of thermodynamics and the use of free energy within the soil. Based on the derivation, a free energy expression in terms of strain and water content for a soil restricted to thermoelastic behavior was presented. The model was then extended to inelastic behavior by introducing internal variables to account for the plastic behavior in the solid phase. The advantage of the model over previous model attempts is its fundamental formulation and the definition of the relationship between the soil skeleton, suction and intergranular stress allowing the twin constitutive relationships to be incorporated into any effective stress based model to account for partial saturation.

In order to determine the ability of the model to predict the behavior of real soils for aircraft loading, its implementation into an effective stress model is required. This implementation will be discussed in Chapter V. The relevance and calibration of the various parameters (λ, α, κ) and coefficients ($K_{1,2,3}$) associated with the partially saturated model will be discussed in Chapter VI through VIII.

CHAPTER V
Model Implementation

5.1 Introduction

In Chapter IV, the increment of stress was depicted as consisting of an intergranular stress component proportional to increments in strain and a suction component proportional to increments of water content. It was noted that the intergranular stress component is equivalent to the effective stress when the soil is saturated. It follows that any valid effective stress model can be used to compute the intergranular stress component. This chapter discusses the characteristics desired of an effective stress model, and how the Multi-Mechanical Model (MMM) complies. The MMM is described as a parallel arrangement of Maxwell elements as was used by Smith (*2000*) essentially without modification. A calibration developed for this thesis research is then described based on an equivalent serial arrangement of Kelvin elements. Details are provided on implementation of partial saturation into the MMM, behavior and function of the new partially saturated MMM and calibration requirements.

5.2 Desirable Characteristics of a Constitutive Model

Desired characteristics of a model to implement effects of partial saturation are:

a) The model is strain driven such that inputting an increment of strain produces an increment of stress.

b) Model is intuitive and whose parameters have physical significance. This will minimize empiricism so that the model is not based on the analytic geometry of stress space.

c) Model is modular such that major response components can be separated and operated on independently. The modules should include four basic components: shear response, hydrostatic response, pore pressure response, and shear-volume coupling. The shear-volume coupling should be consistent with shear-dilatancy theories (e.g. critical state soil mechanics (CSSM)) (*Scholfield, et al., 1968*) allowing a link between shear and hydrostatic responses. Pore pressure must be independently determined so that its response can be accounted for by the three other responses.

d) Model must separate saturated phenomenon from phenomenon affected by degree of saturation.

e) Straightforward model calibration scheme that can be accomplished with minimum laboratory effort and be based on traditional geotechnical soil tests.

f) Lastly, the model must be able to be able to capture the unique stress paths and repetitive loading of traffic typically associated with multiple aircraft landings.

5.3 The Multi-Mechanical Model

Recent work (*Smith, 2000*) and (*Smith et al., 2001*) indicates the Multi-Mechanical Model (MMM) has the desired capabilities for an effective stress model. This model satisfies all of the above requirements and was selected for implementation of partial saturation.

The MMM was developed for the U.S. Army Corps of Engineers at the Engineering Research and Development Center (ERDC), Vicksburg, MS for use in

analyzing the complex problem of aircraft loading behavior of pavements. Valanis (*1980*) developed the initial concept, further developed by Valanis and Peters (*1991*) and Peters (*1991*). Subsequently, the model was simplified and adapted by Smith (*2000*) and Smith, et al., (*2001*).

Properties the MMM that satisfy above model requirements defined:

a) The MMM is a strain driven constitutive driver, i.e. given an input strain path will output a stress path.

b) The constitutive behavior of the MMM is based on strength and critical state definitions given by CSSM theory. Each parameter used by the model is based on a physically observable property that is well defined and understood within the soil mechanics community.

c) The MMM consists of a series of subroutines that divide the material behavior into hydrostatic, shear, and shear-volume coupling responses. Prior to current research, the pore pressure module was embedded into the existing subroutines. As part of the current work, the pore pressure module was made an independent module and expanded to include both air and water pressures. Each module can be adjusted to account for the effects of partial saturation independent of one another.

d) The MMM is an non-proprietary source code, and therefore offers the user great flexibility in defining a variety of inputs and outputs depending on the desired properties. Therefore specific suction, saturation and total stress properties can be output either as principal or critical state stress values to evaluate the partially saturated response. As well, the code allows easy implementation of new laboratory tests by enabling code modification to specify new strain paths taken by the soil. This functionality was essential for calibration and verification tests performed in this thesis.

e) Saturated calibration, as was the initial design of the model, is based on use of only laboratory triaxial tests and consolidation tests, both of which are very common geotechnical laboratory tests and can be performed and interpreted by researchers and practicing engineers alike.

f) The foundation of the MMM is a simplification of the endochronic theory viewed as a rheologic model containing a parallel system of elastic-plastic elements that accounts for accumulation of plastic strain from repeated loading. As well, the structure of the model enables it to produce plastic strain at levels commonly associated with heavy aircraft loading.

Lastly, the process of calibration has been streamlined and incorporated into a software package called CModeler, to enable rapid and easy calibration of the relevant rheologic and critical state parameters based on the basic laboratory tests described earlier

5.4 Behavior of the Multi-Mechanical Model

To better understand workings of the MMM, the following section will outline the principal behaviors of the model with an emphasis on those necessary to incorporate the partially saturated components.

5.4.1 Model Description

Computational description of the MMM is a simplification of the endochronic theory viewed as a rheologic model containing a parallel series of elastic-plastic elements divided into an elastic spring and a plastic slider as shown in Figure 5-1. The system contains two sets of four spring-slider systems to account for the hydrostatic and deviatoric response that are coupled by a dilatancy expression linking the plastic volumetric and deviatoric strains in Figure 5-2. This structure provides the desirable

modular system that allows isolation of volumetric and deviatoric behaviors within the model.

Functionally, the application of an increment of strain causes movement in the spring-slider assembly that results in a stress dictated by the shear or bulk modulus in the springs. Accumulation of plastic strain occurs due to yielding of the sliders, allowing movement. If no yielding of the sliders occurs, the motion is considered elastic and is reversible. If plastic strains develop, hysteresis in the constitutive response is captured by the sliders to provide a memory of past strain.

Figure 5-1 contains the stress, strain and internal variable definitions derived in Chapter IV. The spring-slider assembly is operated on by a strain tensor, ε_{ij} that returns a Cauchy stress tensor, σ_{ij}. Stress within each spring-slider element is the intergranular stress, Q_{ij} that is a combination of the effective stress (soil skeleton stress) and the suction for a partially saturated soil. The sliders represent internal variables defined as either, q_h or $\boldsymbol{q_s}$, which dissipate energy and accumulate plastic strain during volumetric or deviatoric loading respectively.

Model response is controlled by distribution of bulk modulus, K, or shear modulus, G, within the springs of each assembly and distribution of friction and mean stress to each slider in the assembly (Figure 5-2). The springs are governed by elasticity and the individual sliders are governed by the yield criteria which is a function of the mechanism intergranular stress, $f(\mathbf{Q}^r)$ set forth by the Matsuoka yield surface (*Matsuoka, 1974*). The Matsuoka surface is defined as the ratio of the eigenvalues of the Cauchy stress tensor which at yield equals a constant $Y^r(\phi)$ for each mechanism:

$$f\left(\mathbf{Q}^r\right)=\frac{I_1 I_2}{I_3}=Y^r\left(\phi\right) \tag{5.1}$$

The eigenvalues are defined in terms of principal stresses as:

$$I_1=\sigma_1+\sigma_2+\sigma_3$$

$$I_2=\sigma_1\sigma_2+\sigma_2\sigma_3+\sigma_1\sigma_3$$

$$I_3 = \sigma_1 \sigma_2 \sigma_3$$

The Matsuoka yield surface was chosen because it represents a continuous surface in a three dimensional space that is a very close approximation to the Mohr-circle yield surface in two-dimensional stress space (*Smith, 2000*) that establishes a simple yield criteria within the MMM. The use of Mohr circle as a criterion for yield is widely used within the geotechnical community and by using the continuous Matsuoka surface it eliminates the singularities found in transitioning the Mohr circle into single function.

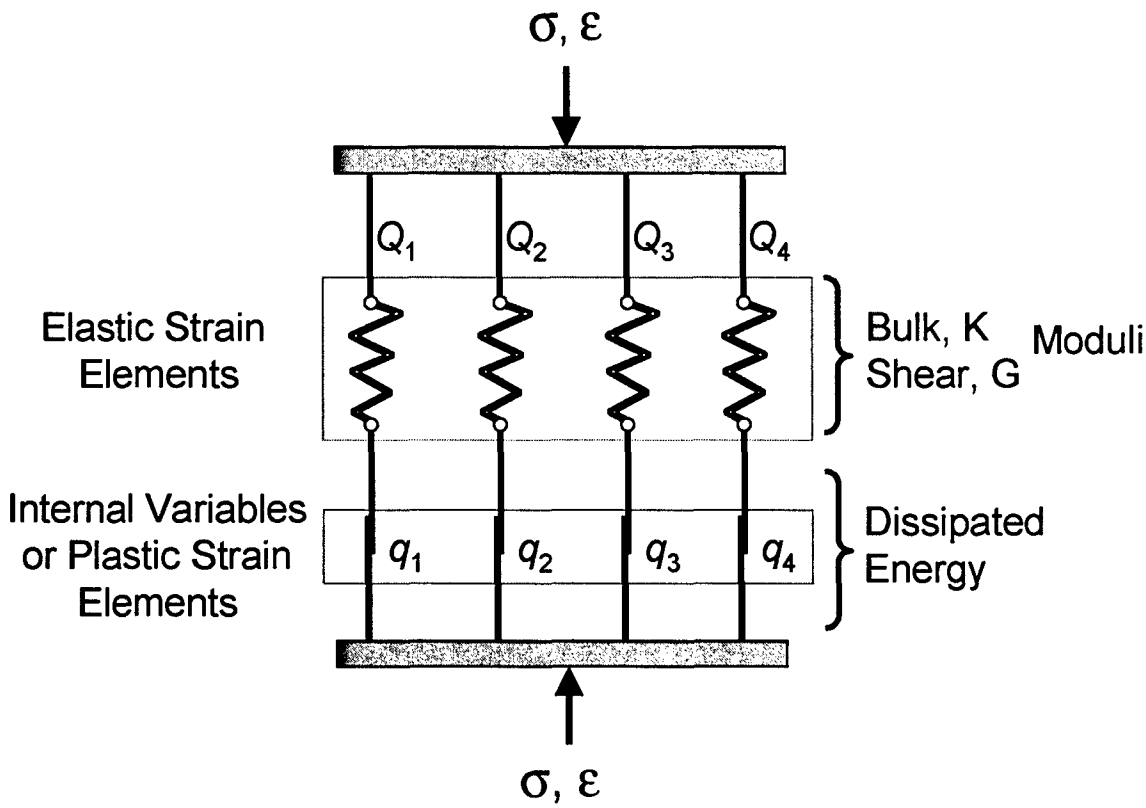

Figure 5-1: Parallel arrangement of spring-slider mechanisms for either hydrostatic or deviatoric response within MMM after Smith et al. (2001)

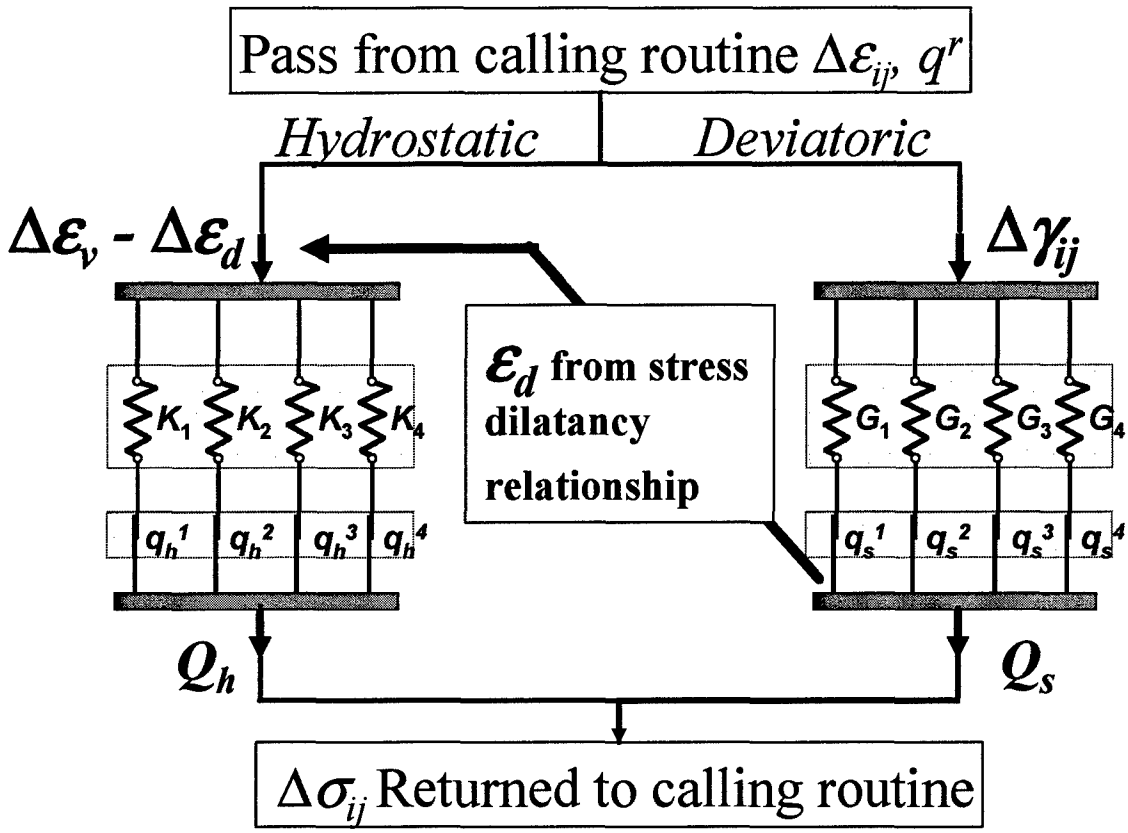

Figure 5-2: Illustration of constitutive driver operation after Smith et al. (2001) for coupled hydrostatic and deviatoric spring-slider assemblies

The following taken from Smith (*2000*) defines the general behavior of the original two-phase saturated model:

General Description

The elastic-perfectly-plastic elements act in parallel by making the total strain common to all mechanisms as represented in Figure 5-1. Thus, each element is computationally independent and can be integrated. The Cauchy stress is the sum of the component intergranular stresses. The shear and hydrostatic mechanisms are independent because they represent different deformation mechanisms (Figure 5-2). A coupling exists between shear and hydrostatic mechanisms in the form of a shear-dilatancy expression (equation 5.11). The

shear-dilatancy imparts a plastic hydrostatic strain increment to the total volumetric strain that is in proportion to the total plastic shear strain produced by the shear mechanisms. The proportionality constant depends on the shear stress to hydrostatic stress ratio in a manner reminiscent of CSSM. In contrast to the CSSM unidirectional dilatancy law, the present model senses the direction of shear loading and correctly predicts the magnitude and sign of plastic volumetric strain during unloading.

Stresses within the mechanism, and the void ratio of the soil describe the material state. The plastic strains are thermodynamic "forces" that retain the effects of the material stress history. The model uses three groups of parameters: stiffness parameters, strength parameters, and a shear-volume coupling parameters. (*Meade, 1998*) (*Peters, 1998*)

Stiffness Parameters

The stiffness parameters are shear modulus, G, for each shear mechanism and bulk modulus, K, for each hydrostatic mechanism. The sum of component stiffness moduli defines the initial elastic stiffness of the material. By distributing the moduli among the mechanisms according to the mechanism's yield strength, the shape of the stress-strain curve can be modeled.

Yield Parameters

The strength parameters define the yield stress for each mechanism. Each mechanism acts as an elastic-plastic component whereby the response is elastic for all stress increments within the yield surface and plastic when the stress point lies on the yield surface. Stress increments that fall outside of the yield surface are then scaled back to the yield surface along a radial line extending from the stress origin.

A friction parameter and cohesion determine the limiting shear stress. The friction is introduced through a yield law of the form:

$$f(\mathbf{Q}^r) = Y^r(\phi) \tag{5.2}$$

where $\mathbf{Q}^r$ is the total intergranular stress for mechanism r defined as:

$$\mathbf{Q}^r = \mathbf{Q}_s^r + \left[\xi^r\right]^r (Q_h + a) \tag{5.3}$$

The shear component $\mathbf{Q}^r{}_s$ is determined from the mechanism constitutive response. The hydrostatic component, $(Q_h + a)$ is distributed from the total hydrostatic stress and cohesion in proportion to the distribution factor ξ^r. Thus the shear mechanism sees the hydrostatic stress as a parameter. The function f is chosen to represent a Mohr-Coulomb-like yield surface with Y^r being the limit parameter for the mechanism that is scaled to the friction angle, ϕ, of the material.

Yield of the hydrostatic mechanisms is scaled by a reference stress that depends on void ratio by:

$$Q_h^r = H^r p_e(e) \tag{5.4}$$

H^r determines the limit stress of hydrostatic mechanism, r. Reference stress, $p_e(e)$, lies on the virgin loading curve at the point corresponding to the prevailing void ratio, e. The effect of void ratio on shear response comes through the dependence of shear yield stress on the hydrostatic stress.

Materials possessing cohesion can withstand some tensile stresses. Tensile strength is accounted for by applying a reduction to the mean stress that is proportional to the material cohesion. Each mechanism is allocated a portion of the tensile strength in proportion to the amount of volumetric stiffness that the mechanism contributes to overall material bulk stiffness.

Shear-Volume Coupling

Magnitude of the shear volume coupling is controlled by two parameters, M_c, the ratio of shear to hydrostatic stress at which a specimen begins to dilate in a monotonic loading test and a parameter, γ, that scales the dilatancy rate as the stress ratio becomes greater. In CSSM, only M_c is used because an assumption is made in the critical state theory that shear stress does not independently influence dilatancy therefore γ=1. The hydrostatic strain "seen" by the hydrostatic mechanisms is distinct from that caused by coupling with shear.

5.4.2 The Series Analogy

In its initial conception, the MMM was treated as a generalized Maxwell system for each set of spring-slider systems. This parallel system was developed first because strain driven constitutive models are more applicable to efficient finite element calculations. Calibration of the model of a strain driven model is difficult because test data is usually given in terms of stress. Therefore the current research converted the spring-slider system into an equivalent serial model representation (Figure 5-4). A serial model representation is desirable for calibration since all the spring-slider pairs are subject to the same stress.

The key component in developing a non-iterative calibration process for the MMM is the ability to derive an equivalent series representation from the parallel spring-slider system. The parallel system model in Figure 5-1 is a generalized Maxwell model consisting of four parallel Maxwell elements where a perfectly plastic slider replaces the viscous dashpot as seen in Figure 5-3. Transformation from a parallel to a series model requires the use of a generalized Kelvin model consisting of three Kelvin-Voigt elements placed within a single Maxwell element (see Figure 5-4). Lee (*1962*) states "*...the generalized Kelvin model is particularly convenient if the stress history is prescribed and the strain response is to be found,*" and likewise a generalized Maxwell model is best for determining stress from a prescribed strain history. It is shown from Lee that the

mathematics of transforming a parallel viscoelastic system to a series system is a linear transformation. In the case of the slider element, this becomes a non-linear system but a solution can be found by assignment of a finite number of elements that average the material's stress-strain response described in Appendix A. It has been shown in electrical systems such as the Norton equivalence, that mathematically both systems can represent the same behavior.

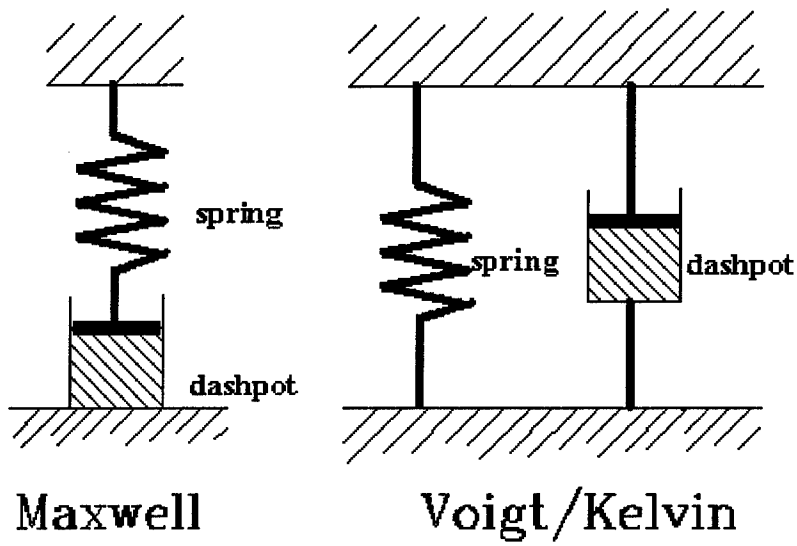

Figure 5-3: Illustration of Maxwell and Kelvin elements

Figure 5-4 demonstrates visually transformation from a parallel arrangement to a series arrangement for the MMM. The critical difference between these two systems is that in parallel, each spring-slider element experiences the same magnitude of strain with a differential stress throughout the mechanisms, whereas in the series arrangement each spring-slider element experiences the same stress with a differential strain throughout the mechanisms. The stress driven behavior of the series arrangement allows a direct, non-iterative calibration process. This process is presented in Appendix A as the origins of the CModeler calibration software.

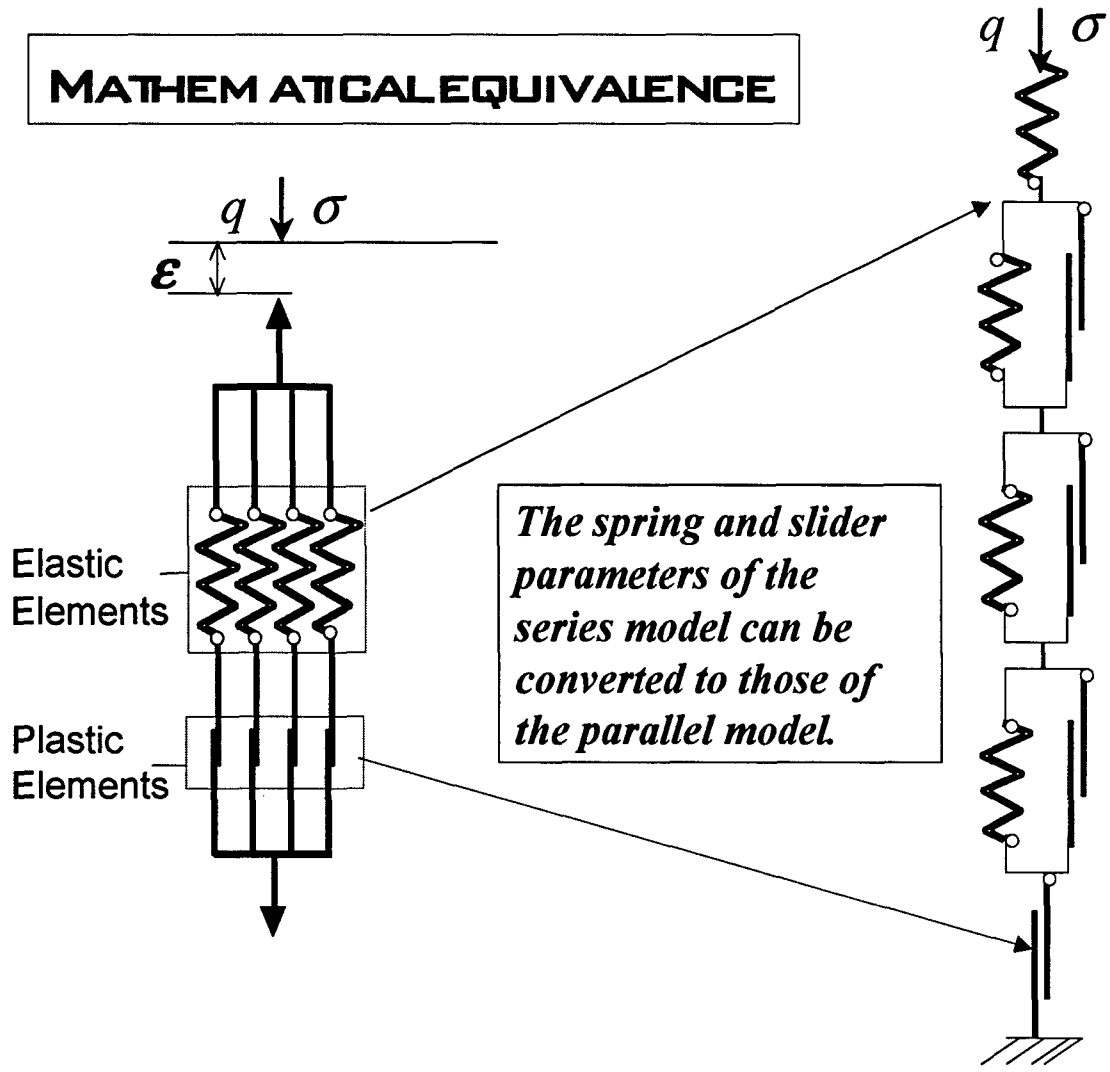

Figure 5-4: Equivalence between Maxwell (parallel) element set and Kelvin-Voight (Series) element set for either volumetric or deviatoric behavior

5.4.3 Global Parameters for Multi-Mechanical Model

There are eighteen global parameters required for operation of the MMM and are listed in Table 5.1. Numbers 1 through 14 represent the original input parameters for the saturated MM. The exception is that number 1 is used to define a stress dependent elastic bulk and shear moduli instead of a constant. Numbers 15 through 18 represent the added parameters that account for the effects of partial saturation, α, κ, λ and p_r.

Table 5.1. Global Properties for MMM

	Name	Code Label	Comments
1	Poissons Ratio, ν	POISSON	Relates Bulk to Shear Modulus
2	Reconsolidation Index	CR	Slope of the reconsolidation line
3	Friction Angle	PHILIM	Maximum Friction Angle of Material
4	Phi Ratio	PHIRATIO	Ratio of minimum to maximum friction angle
5	Over-consolidation Factor	DECAY	Reduces strength with OCR
6	Psi Max	PSIMAX	Maximum angle of critical state line (CSL)
7	Psi Min	PSIMIN	Minimum angle of CSL
8	Curvature of CSL	DECAYV	Curves CSL through Mc point
9	Normalized Cohesion	a	Cohesive intercept for a stress space normalized by reference pressure
10	Hydrostatic Intercept	Fh	Intercept of the NCL with a stress of 1 unit
11	Reciprocal of the Coefficient of Consolidation	BETA	Reciprocal of the slope of the Normal Consolidation Line (NCL)
12	Dilatancy Scaling Factor	GAMMA	Adjusts influence of shear stress on shear-volume coupling
13	Shear Modulus Adjustment	BETAS	Adjusts distribution of shear modulus between springs
14	Bulk Modulus Adjustment	BETAH	Adjusts distribution of bulk modulus between springs
15	Reference Suction	Pr	Defines log-linear suction intercept at 0 volumetric water content
16	Suction-θ Modulus Parameter	Kappa	Log-linear slope between suction and volumetric water content
17	α Parameter	Alpha	Adjusts K moduli for swell strain-stress compatibility
18	λ Parameter	Lambda	Strength parameter for partial saturation

Yield Limits:

PHILIM = Maximum friction angle, ϕ_{max} experienced by the soil during dilation. A constant value taken as the tangent to the maximum curvature of the failure envelope placed on the normalized shear stress-mean stress plot (0 to 90 degrees)

PHIRATIO = Ratio of the minimum friction angle experienced by the soil to the maximum friction angle of the soil, ϕ_{min}/ϕ_{max} where the minimum is typically obtained from the tangent to the curvature of the failure envelope near the critical state point, M_c
(0 to 1)

DECAY = defines the concave downward curvature of the strength envelope with normalized mean stress defining the range of response between maximum and minimum friction angles
(greater than 1) (A value of 1 indicating no curvature similar to a Mohr envelope)

a = normalized cohesion which is the intercept of the yield surface on the normalized shear stress axis accounting for the tensile strength potential gained from cohesion. Typically this value is taken to be a constant, however this model assumes a mean stress dependent cohesion as a function of a and the reference pressure.
(greater than 0)

$$\text{Cohesion} = a * p_e \tag{5.5}$$

An illustration of the determination of the yield limits is found in the triaxial stress space described in Figure 5-5. To properly define the shear strength envelope for a soil in the MMM, limits of the maximum and minimum friction angles, ϕ_{max} and ϕ_{min}, relating the potential shear strength at a given mean stress, must be determined. Slopes of the friction angles are shown as bold lines labeled, ϕ_{min} and ϕ_{max}. For any granular material, friction angle varies with the mean stress in a non-linear fashion owing to the change in dilatancy of a soil with mean stress (*Scholfied, et al. 1968*). Degree of non-linearity or curvature is estimated in the MMM by a variable exponential function dependent on a decay factor as shown below:

$$\phi = \phi_{\min} + (\phi_{\max} - \phi_{\min}) \exp\left(-Decay \cdot \frac{p}{p_e} - a \cdot p_e \right) \tag{5.6}$$

The magnitude of ϕ_{max} and ϕ_{min} are determined from matching the maximum slope of increasing strength gain at small normalized mean stresses, σ_m/p_e, and the minimum slope at a normalized mean stress, q/p_e, near the critical state stress ratio, M_c, where the friction angle reaches a minimum/critical state/steady state value. Decay represents the curvature of the failure envelope in the triaxial stress space. Decay is obtained by adjusting its magnitude until the curvature of the failure envelope over the range of triaxial response measured is bounded.

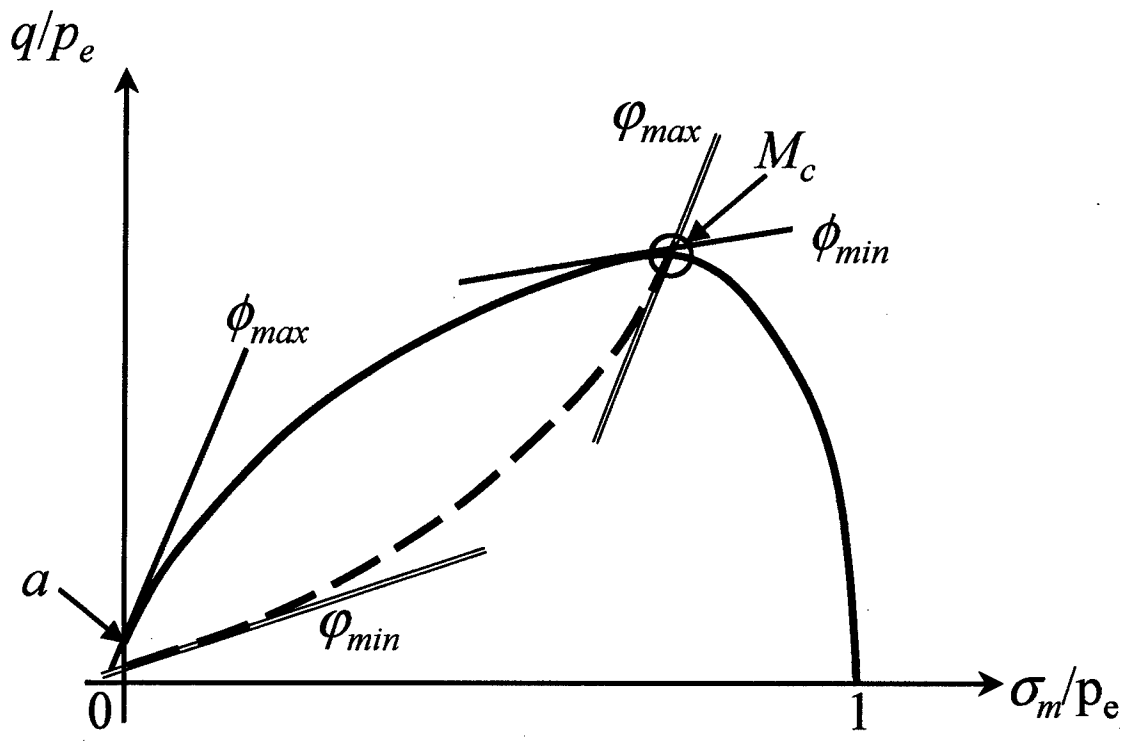

Figure 5-5: Normalized triaxial stress space for calibration of strength and critical state parameters

Critical States:

PSIMAX = Maximum dilation angle, φ_{max} is measured as tangent to the maximum rate of dilation along the critical state line on a normalized shear stress-mean stress plot (Figure 5-5)
(0 to 90 degrees)

PSIMIN = Minimum dilation angle, φ_{min} is measured as tangent to the minimum rate of dilation along the critical state line on a normalized shear stress-mean stress plot (Figure 5-5)
(0 to 90 degrees)

DecayV = defines the concave upward curvature of the critical state envelope with normalized mean stress over the range of response between the maximum and minimum dilation angles
(0 to 1) (1 producing the traditional single valued M_c (*Schofield, et al., 1968*))

To define the dilatant characteristics of a soil, a curved critical state line is envisioned as marking the transition between contraction and dilation for monontically increasing stress paths. An example of this is shown in Section 8.2.1. The curvature of the line is opposite to that of the shear strength envelope discussed above and shown as the dotted line in Figure 5-5. Dilation can be expressed as an angle, φ, which can be converted into a stress ratio, M. The curvature of the line is characterized in the MMM by a variable exponential function dependent on a *DecayV* factor as shown below:

$$\varphi = \varphi_{\max} - (\varphi_{\max} - \varphi_{\min}) \exp\left(-DecayV \cdot \frac{p}{p_e} - a \cdot p_e \right) \tag{5.7}$$

$$M = \frac{6 \sin \varphi}{3 - \sin \varphi} \tag{5.8}$$

The magnitude of φ_{max} and φ_{min} are determined from matching the minimum slope of dilation occurring at a small normalized mean stress and the maximum slope at a normalized mean stress near the critical state stress ratio, M_c. Parameter *DecayV* is obtained by adjusting its magnitude until the curvature of the critical state line gives a reasonable match to the observed boundary between contraction and dilation under monotonic loading.

Volumetric Limits:

BETA = $1/C_c$ = Inverse of the Compression Index, C_c, which is assumed a constant value. This parameter is determined from the one-dimensional or isotropic consolidation test of a specimen.
(greater than 0)

C_r = Reconsolidation index, which is assumed a constant value. This parameter is determined from the one-dimensional unloading of a specimen
(greater than 0)

EREF = saturated reference void ratio at which the line defined by the slope of C_c intercepts the void ratio axis at an effective mean stress of 1 psi from a one-dimensional consolidation plot
(greater than 0)

ν = Poisson's ratio, assumed a constant and used to convert from Bulk to Shear moduli
(-1 to 0.5)

GAMMA = parameter linking the plastic change in shear strain to the change in volumetric strain for the range of strain experienced by a soil.
(0 to 1)

The reference void ratio, EREF, is defined as the intercept of the normal consolidation line (NCL) with slope C_c with the mean stress axis at a value of 1 psi for a saturated soil. These terms are illustrated in Figure 5-6.

As a point of historical interest, the traditional term for expressing the dilatancy relationship within CSSM is given in equation 5.9.

$$\frac{d\varepsilon_v^p}{d\varepsilon_q^p} = M - \frac{q}{\sigma_m} \tag{5.9}$$

Equation 5.9 is derived from the power equation:

$$\sigma_m d\varepsilon_v^p + q d\varepsilon_q^p = M \sigma_m d\varepsilon_q^p \tag{5.10}$$

where:

ε_v^p = plastic volumetric strain

ε_q^p = plastic shear strain

γ = dilatancy parameter

q = σ_1 - σ_3 = shear stress

σ_m = $(\sigma 1 + 2\sigma_3)/3$ = mean stress

M = critical state stress ratio $(q/\sigma_m)_{crit}$

Equation 5.10 is based on the assumption that the rate of energy dissipation does not depend on the level of shear stress. In many soils the stress-dilatancy line is a function of the level of shear stress that is:

$$\frac{d\varepsilon_v^p}{d\varepsilon_q^p} = \gamma\left(M - \frac{q}{p}\right) \tag{5.11}$$

Rearranging terms to produce a corresponding power equation it is seen that introducing γ other than one provides a rate of energy dissipation proportional to a combination of both mean and shear stress as shown in equation 5.12.

$$pd\varepsilon_v^p + qd\varepsilon_q^p = \left[\gamma Mp + (1-\gamma)q\right]d\varepsilon_q^p \tag{5.12}$$

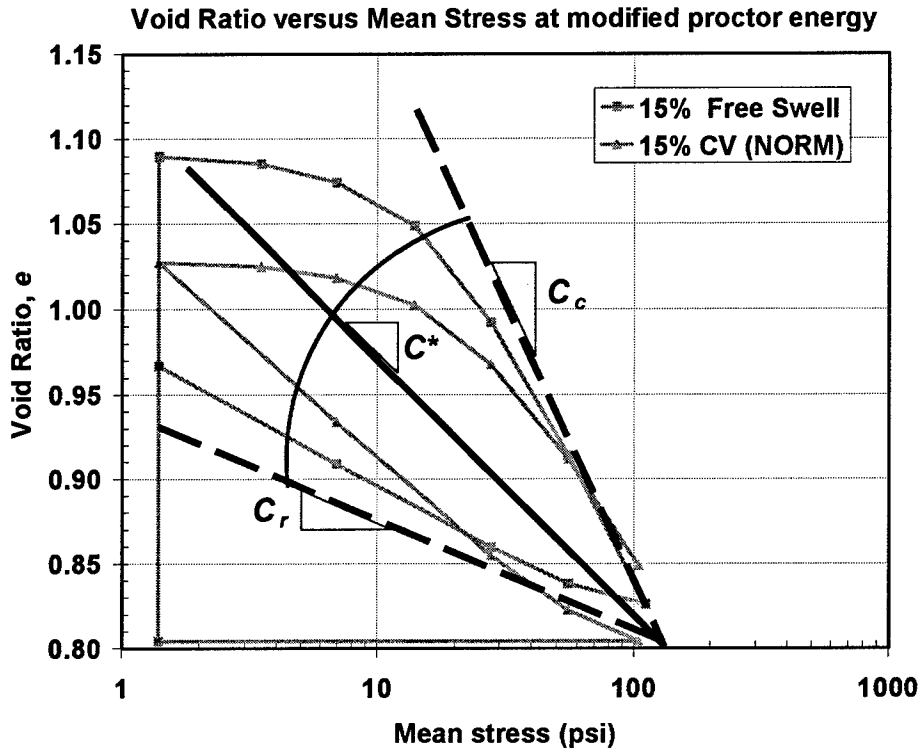

Figure 5-6: Illustration of the C term used in defining K_1^0 and the Bulk Modulus, K used in the model calculations*

An expression was given for the modulus K_1^0 in equation 4.95. The derivation of this expression follows based on the slopes determined from a one-dimensional consolidation test as shown in Figure 5-6.

$$\ln\left(\frac{Q}{Q_o}\right) = K_1^o \frac{e-e_o}{1+e_o} = K_1^o \varepsilon_v \tag{5.13}$$

Traditionally, compression and recompression indices, C_c and C_r are considered constant over the range of void ratios and stresses typically encountered in applied soil structures. Figure 5-6 shows the relative positions of these coefficients on a semi-logarithmic void

ratio-mean stress plot. Given that the compression indices are constant, the modulus K_1^o must be a function of both the initial void ratio and the mean stress as shown in the following derivations.

Compression or recompression indices are defined as follows, where Q represents the mean intergranular stress acting on soil grains:

$$C_r \log_{10}\left(\frac{Q}{Q_o}\right) = e - e_o \qquad C_c \log_{10}\left(\frac{Q}{Q_o}\right) = e - e_o \tag{5.14}$$

Since K_1^o should capture the hysteresis during the loading and unloading response of the material as exhibited during those phases in Figure 5-6, an average constant coefficient between the two, C^*, represents an average secant modulus for the bulk behavior of the soil, where C^* can be assumed the average of both indices:

$$C^* = \frac{1}{2}(C_c + C_r) \tag{5.15}$$

$$C^* \log_{10}\left(\frac{Q}{Q_o}\right) = e - e_o \tag{5.16}$$

Substituting equation 5.15 into 5.16 results in an expression for K_1^o, shown previously in Chapter IV, equation 4.95:

$$K_1^o = \frac{2.303(1+e_o)}{C^*}$$

The approximation of the elastic response between the normally consolidated and over-consolidated phases of the material is represented by the average of the two compression coefficients representing the hysteresis occurring between loading and

unloading of the soil. This means that the stiffness of the material is a function of its initial void ratio, which satisfies the development of a state dependent modulus.

The parameter, C_r, is the slope of the elastic hydrostatic volume change. Use of C_r in the model provides a means to determine and adjust the elastic bulk and shear moduli for varying mean stresses.

Suction Potential:

κ = log-linear slope relating the change in suction potential to volumetric water content. Used in conjunction with α to obtain the modulus K_3
(less than 0)

α = The compatibility term discussed in Chapter 5 that relates the swelling strain to the swelling stress. This parameter is used in conjunction with α to determine K_3 modulus as discussed in equation 4.103.
(0 to 0.5)

p_r = reference suction occurring at zero volumetric water content, $\theta = 0$. This parameter is the intersection of the slope of the semi-log regression line on a p-θ plot with the suction axis.
(0 to infinity)

λ = adjusts location of the normally consolidation line with changes in saturation or suction. This parameter is determined for cohesive soils from either a series of partially saturated consolidation tests or a compaction curve.
(greater than 0)

In summary there are eighteen global soil properties which must be determined for any soil in order to properly calibrate the MMM. Many of the properties can be obtained from the literature and experience working with similar materials. The

following moduli and critical state point definitions are provided to inform the user that these common values are used within the program but are not input as constants by the user, rather they are calculated based on the above inputs:

M_c = Ratio of shear stress to mean stress at the intersection of the failure envelope defined by Phimax/Phimin and the critical state envelope defined by Psimax/Psimin. This parameter is typically assumed a constant but is considered variable for this model. (greater than zero)

K = Bulk modulus. This modulus is assumed to be variable and is determined from the ratio of the intergranular stress, Q_h, divided by the reconsolidation index, C_r:

$$K = \frac{Q_h}{C_r} \tag{5.17}$$

(value greater than 0 in units of stress)

G = Shear modulus. This shear modulus is assumed to be vary linearly with Bulk Modulus and is determined from the Bulk Modulus, K and Poisson's ratio, ν:

$$G = \frac{3K(1-2\nu)}{2(1+\nu)} \tag{5.18}$$

(greater than 0 in units of stress)

5.4.4 Distributed Mechanism Parameters for Multi-Mechanical Model

There are twenty distributed mechanism parameters required for calibration of the Multi-Mechanical Model. They are listed in Table 5.2

Table 5.2. Properties for each Mechanism

Name	Label in code	Comments
Strength factor	PHIFRAC	Scales friction angle
Mean Stress factor	PFACT	Scales mean stress
Shear Stiffness factor	SHEARRATIO	Distributes shear stiffness
Compression limit	HLIMIT	Absolute compression limit
Volumetric Stiffness factor	BULKRATIO	Distributes volumetric stiffness

The following discussion provides an expanded description of the distributed material properties and the way in which they relate to various soil mechanics components necessary to model the soil.

Stress-Strain Points:

SHEARRATIO, PFACT, PHIFRAC: For calibration of the distributed deviatoric model parameters, a selection of four shear stress-shear strain pairs of points that define the initial loading, hardening and ultimate strength of the soil is required. These points are used to generate the distribution of shear modulus, mean stress and friction parameters for each stage of the soil's response
Range (0 to 1)

BULKRATIO, HLIMIT: For calibration of the distributed hydrostatic model parameters, a selection of four void ratio-effective mean stress pairs of points from a one-dimensional consolidation test are required that define the semi-log linear reload and virgin consolidation, and the non-linear hardening of the soil. These points

are used to generate the distribution of bulk modulus and mean stress yield limits over the range of volumetric changes expected by the material.
Range (0 to1)

BETA-S: Fitting parameter that adjusts the magnitude of shear modulus distributed to each of the four shear elements in the MMM.
Range (0 to1)

BETA-H: fitting parameter that adjusts the magnitude of the bulk modulus distributed to each of the four hydrostatic elements of the MMM.
Range (0-1)

The Beta factors are determined based on observed modeling response as curve fitting parameters, but they exhibit little fluctuation in values and can be assumed if necessary. A more complete description of their function is provided in Appendix A.

5.5 Implementation of Partial Saturation into the Model

5.5.1 Incorporate Definition of Intergranular Stress

The original version of the MMM was based upon a classical Terzaghi effective stress model where the intergranular and effective stresses within the system were assumed to be equal. This is of course the case made for a saturated soil system. Furthermore, the Cauchy and effective stresses are equivalent in a drained saturated triaxial simulation, but differ by the pore water pressure for undrained response. The partially saturated MMM requires a distinction between intergranular, effective and Cauchy stress as well as pore air and pore water pressures developed within the system.

The MMM operates on the basis of a defined intergranular stress, be it the intergranular stress derived from the constitutive relationships in Chapter IV or a Terzaghi effective stress. The yield criterion for the slider mechanisms is a function of

either intergranular stress or effective stress. A subroutine, SAND_DRIVER, performs converts a given strain increment to a change in intergranular stress as shown in Figure 5-7. First, the intergranular stress tensor, stain tensor, strain increment and internal variables are input into SAND_DRIVER. Then SAND_DRIVER calculates plastic strain, volumetric strain (from the dilatancy relationship), updates the reference pressure, (p_e or p_{ew}) with void ratio and saturation, and determines a hydrostatic parameter associated with the internal variables for hydrostatic stress. Also, the internal variables for each mechanism are updated at the end of each strain increment.

It is seen from equations 4.71 and 4.72 that to implement partial saturation, the effective stress (soil skeleton stress) in the original model must be replaced with dual constitutive equations to account for the influence of suction potential on the intergranular stress. Therefore, an additional subroutine titled EFF_STRESS is used to produce the dual nature of the constitutive response. This routine is called immediately following any call to SAND_DRIVER so that the updated suction and intergranular stress can be converted into a Cauchy stress as diagrammed in Figure 5-8.

Hydrostatic stresses, applied strain and/or suction increments, and current state variables are input into the subroutine EFF_STRESS. EFF_STRESS then calculates a change in volumetric water content. This in turn is used to update the magnitude of suction, assuming a constant gravimetric water content, the degree of saturation for pore pressure determination and update the suction's contribution to the hydrostatic stress. Subroutine EFF_STRESS returns updated intergranular stress tensor and soil skeleton stress tensors immediately following application of a current strain increment and partially saturated reference pressure, due to changes in void ratio and saturation. The intergranular stress tensor and reference pressure are used to define yield criterion for the next increment of strain applied to SAND_DRIVER. The soil skeleton stress tensor is later combined with the pore pressure calculations to calculate the Cauchy stress.

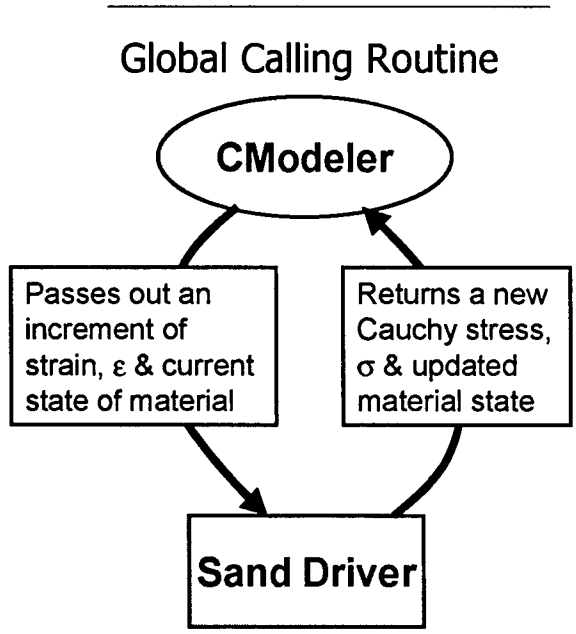

Figure 5-7: Operational diagram of key MMM Components for Saturated Response

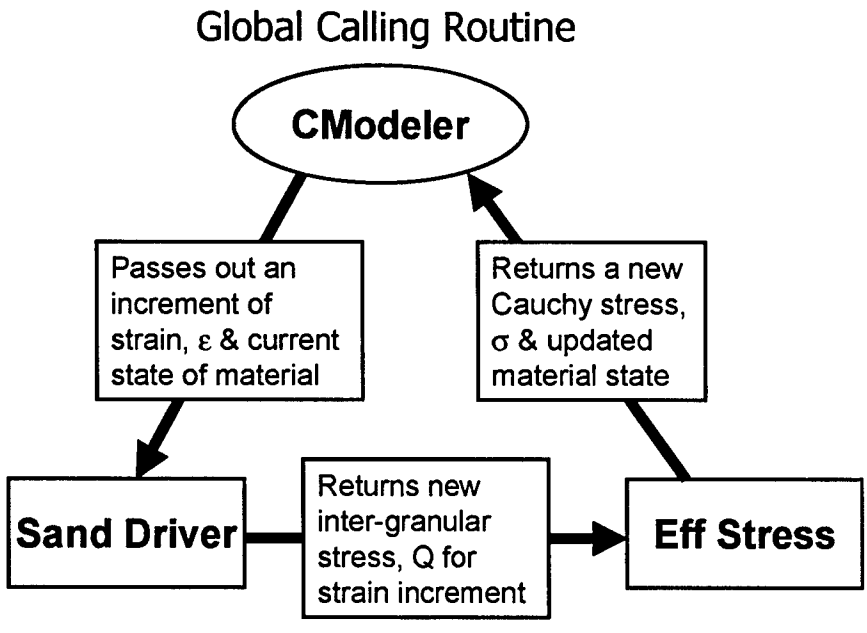

Figure 5-8: Operational diagram of key MMM Components for Partially Saturated Response

Once defined, the intergranular stress and reference pressure operated on within SAND_DRIVER are then shared with subroutines that analyze hydrostatic response and update the yield criteria. Since SAND_DRIVER is based on an intergranular stress, no change in its functionality was necessary, however the constitutive equations in equations 4.71 and 4.72 are necessary to enable an intergranular stress tensor to be operated on by the subroutine. Furthermore, the development of the EFF_STRESS subroutine is necessary to enable an incremental solution to the partially saturated constitutive response.

Soils possessing suction potential can withstand additional tensile stresses. This tensile strength is accounted for in a way that is similar that for cohesion. The mean stress is offset by the initial swell pressure, Q_{sp} determined from the initial suction according to equation 4.84. This is shown in Figure 5-9 on the Mohr's circle plot of hydrostatic intergranular stress, Q_h versus shear stress Q_s. The offset establishes a "cohesive" intercept with the shear stress axis at a condition of $\sigma_{ij} = 0$. This condition indicates the presence of intergranular mean stress resulting exclusively from suction. Each hydrostatic mechanism is then allocated a portion of the tensile strength in proportion to the amount of volumetric stiffness that the mechanism contributes to the overall bulk stiffness of the material. This offset can be considered equivalent to the Fredlund (*1993*) approach to suction induced strength given in equation 3.4.

5.5.2 Modularize the Pore Pressure Response

To account for changes in air and water pore pressures independently within the soil, a subroutine PORE_PRESSUE was developed. The PORE_PRESSURE routine takes the current state variables, air and water pressures and increment of suction from EFF_STRESS and calculates the incremental changes in fluid pressure within the soil matrix. Compressiblites of air and water and the relative saturation levels of each contribute to the amount of pore water pressure developed. This is shown in section 4.4. Pore water pressure is then added to the soil skeleton stress tensor returned from the EFF_STRESS routine to determine the Cauchy stress tensor.

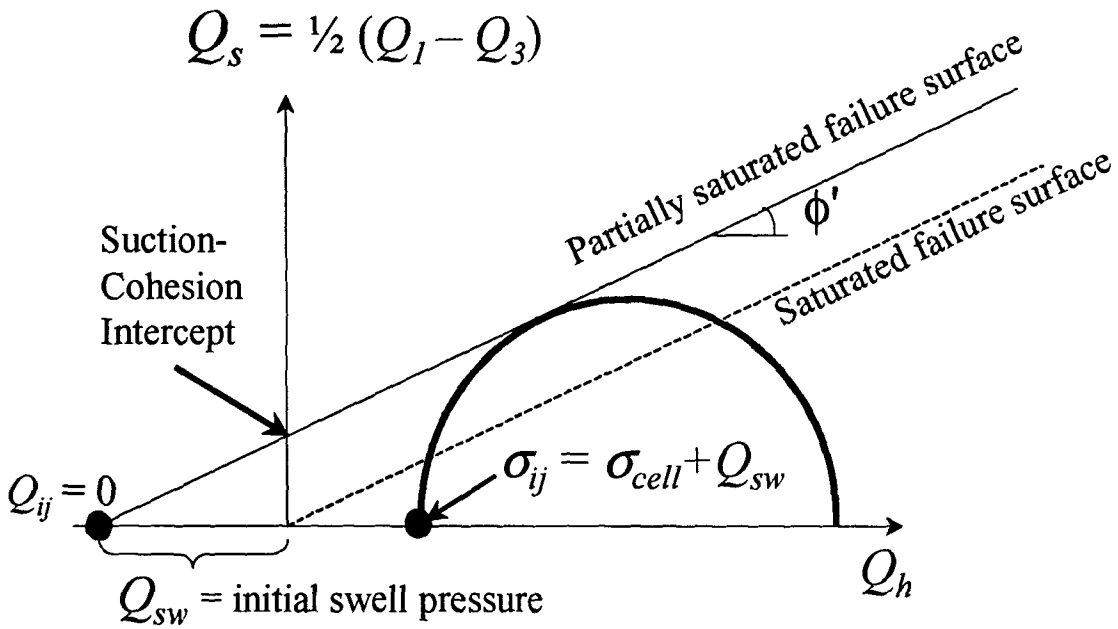

Figure 5-9: Strength increase due to suction represented on Mohr-circle (Matsuoka) failure surface

5.5.3 Initialization of $K_{1,2,3}$

To calibrate the K moduli, the program requires the input parameters κ, α, and initial saturation, S_o. From S_o and e_o the initial volumetric water content is found, θ_o. Knowing, θ_o, the values of κ and α are used to determine the modulus K_3^o from which an initial suction is calculated using equation 4.103. Modulus, K_1^o, is then calculated based on e_o and $C^* = 0.5(C_c + C_r)$ using equation 4.95, where C_c and C_r are the compression and recompression indices respectively described in further detail in section 5.8. Modulus K_2^o can then be computed using equation 4.92.

5.5.4 Initialize Suction in System

To determine contribution to the initial hydrostatic intergranular stress, Q_h derived from the initial suction potential, the constant volume swell relationship (eq. 4.84) is solved using the determined K^o moduli. This suction is then added to the hydrostatic

elements of the Cauchy stress tensor that defines the initial soil boundary stress conditions.

5.5.5 Determine Initial Elastic Moduli

Bulk modulus, K, is then calculated by multiplying K_1^o by the initial mean hydrostatic intergranular stress. The shear modulus, G, is a function of K and Poisson's ratio, ν and is determined from equation 5.18. The magnitudes of both bulk and shear moduli are updated throughout the history of loading as mean intergranular stress and void ratio change.

5.5.6 Calculate Partially Saturated Reference Pressure

The saturated reference pressure, p_e, is determined to define the cohesion for the soil matrix. Parameter, λ, is then used to define the partially saturated reference pressure, p_{ew}, given e_o and S_o according to equation 4.107. The parameter λ is a constant throughout the program influencing the yield criterion of the sliders through its relation with p_{ew}.

5.5.7 Initialize Cohesion in the Soil

The normalized cohesion was shown to be a constant for a material as shown in section 4.7, Figure 4-20. However, the intercept on the normalized shear stress axis for a cohesive material is a function of the saturated reference pressure. Therefore, the definition of cohesion remains the same as prior to introduction of the partially saturated reference pressure.

5.5.8 Redefine the Volumetric Water Content

The definition of volumetric water content needs to be refined to incorporate its value into the PS-MMM. Given the constitutive relationship of an elastic body where a change in strain effects a change in stress, so too must a change in volumetric water content effect a change in suction. In order for this to be possible, volumetric water content is defined as a strain in terms of the degree of water saturation, S, and the porosity (n) or void ratio (e) of the specimen that defines the volume of material influenced by the saturation as follows:

$$\theta = S \cdot n = S\frac{e}{1+e} \tag{5.19}$$

In this expression, both saturation and void ratio are considered positive numbers, as degree of saturation ranges between one and zero. Therefore θ is always a positive number with a magnitude equal to or greater than zero.

An idealized θ-p curve is shown in Figure 5-10. There are four primary features illustrated on this plot based on its curvature: (A) a point near saturation, (B) a point at which air voids appear, (C) the linear portion of the curve and (D) asymptotic behavior of suction as water content approaches zero.

The horizontal line at point A reflects that at low suction potentials, the value of θ remains nearly constant. This suggests that the sample is at a condition of near saturation with very little entrapped air as a result any effect of tensile forces in the water-soil interface is negligible.

At point B, there is an initial break of the response curve. This occurs at point B where air begins to permeate into the void space at a degree of water saturation below 95%. This allows formation of menisci, increasing the rate at which the magnitude of suction potential increases as water content continues to decrease for a constant total volume of material.

The third feature is the linear portion of response characterized by point C. This linear portion of the curve is common to most soil types. For most field applications, this portion of the curve represents the working range of suction which has a direct effect on the strength-deformation response of a soil. Suction potential at levels around points A and B is low enough that the constitutive behavior sees little change in response from a saturated condition. At suction levels characterized by D, suction potential no longer applies to the global soil matrix and so no longer influences the soil's global constitutive response.

Finally, there is asymptotic behavior in the region of point D, where there is large changes in suction for small changes in volumetric water content. Theoretically this is possible, however when the volumetric water content of a soil approaches zero, its dispersion in the soil is no longer uniform. The soil tends to break up into small clods or packets of soil disconnected from the remaining soil mass (*Brackley, 1975*). When this occurs the constitutive response no longer is dependent on suction magnitude since suction no longer contributes to the overall response of the soil mass, i.e. the individual clods begin to act and respond as smaller coarse grained soil material like a weak sand or silt.

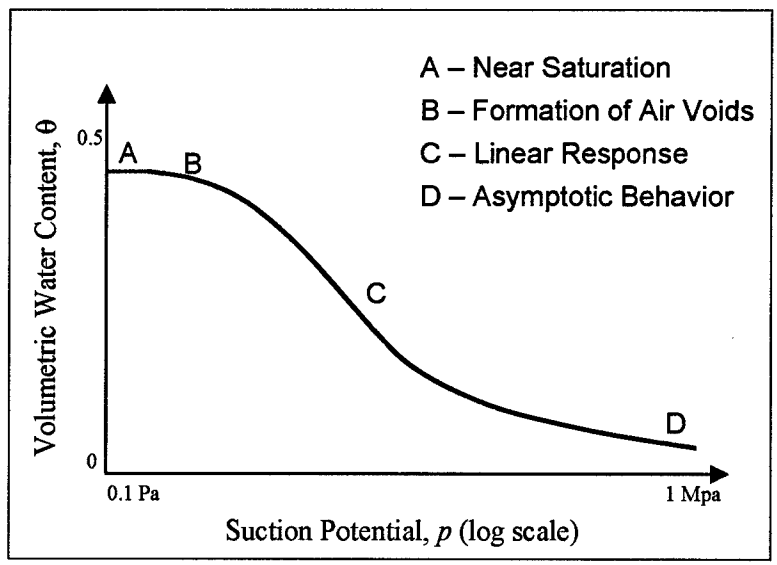

Figure 5-10: Idealized Volumetric Water Content-Suction Curve

In calibrating the MMM, the ideal θ-p curve is approximated with a straight-line regression on a semi-logarithmic plot as shown in Figure 5-11. It is defined by the θ^* variable and the slope of the line, κ. This approximation has a suction intercept, p_r referred to as the reference suction. This reference suction is utilized in the same way as the reference void ratio in the critical state definition of soil behavior. With the limit value to suction, the MMM can initiate calculation representing the constitutive response. As θ increases in a soil, the suction potential decreases. This establishes a negative relationship between changes in volumetric water content and suction. Formulation of a relationship between θ and its conjugate variable suction, p, based on the behavior shown in Figure 5-11 is given below:

$$\frac{dp}{p} = -\frac{1}{\kappa} d\theta^* \tag{5.20}$$

$$\theta^* = -\frac{1}{\kappa} \ln\left(\frac{p}{p_r}\right) \tag{5.21}$$

This means that for a constant volume, where porosity is held constant, and the water saturation decreases in the sample, θ decreases resulting in an increase in the suction. Similarly, as the value of suction approaches zero, θ reaches a limiting value shown in Figure 5-11. Given the logarithmic relationship between suction and volumetric water content (*Fredlund, 1993*), the suction is limited to be greater than one unit of stress. As a result, there may some slight error in the approximation of response for simulations at high water saturation.

The use of a straight line regression is reasonable in calibrating the parameters associated with water content and suction for the MMM because laboratory data on partially saturated soils generally produces this type of relation, point C on Figure 5-10. The drawback to this approach is that mathematically, at very low suctions, the volumetric water content and therefore the saturation of the system will be in error, given θ^* increases to infinity as suction approaches zero. This too violates the mass balance of

the model and therefore adversely affects the free energy response. To correct this problem, it was necessary to redefine the degree of saturation used within the program, or similarly the θ^* such that it becomes a function of the true saturation as displayed in the following expressions.

To begin, let θ^* be equal to a function of water saturation, $f(S)$ which is taken as S^* or a modified saturation:

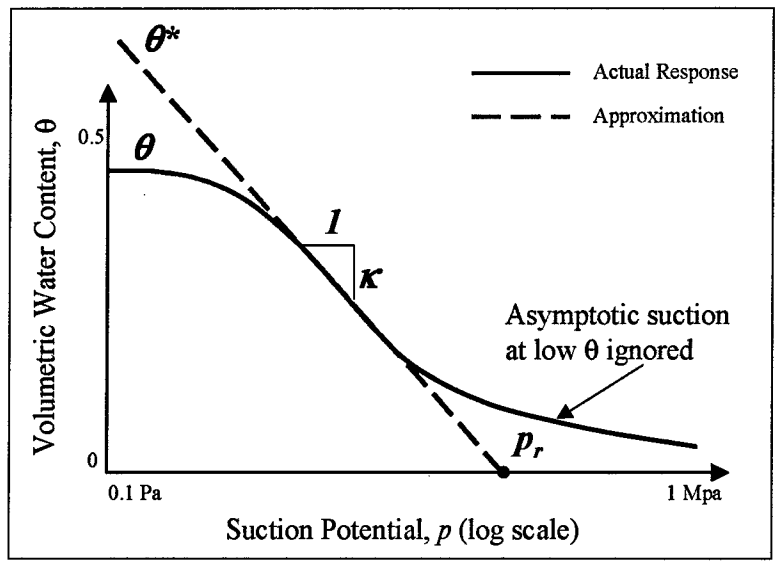

Figure 5-11: Calibration of Volumetric Water Content-Suction Response for Model Development

$$\theta^* = f(S) \cdot n = S^* n \tag{5.22}$$

This function of saturation is a relationship in which the true degree of saturation is equal to the function when the value of S is small, i.e. θ is equal to θ^* for small values of θ^*:

$$f(S) = \frac{\theta^*}{n} = S\left(1 + \frac{a}{1-S}\right) \tag{5.23}$$

To determine the true water content, θ from θ^*, the true value of water saturation is solved for:

$$S^2 - S\left(1 + a + \frac{\theta^*}{n}\right) + \frac{\theta^*}{n} = 0 \tag{5.24}$$

$$S = \frac{1}{2}\left[\left(1 + a + \frac{\theta^*}{n}\right) - \sqrt{\left(1 + a + \frac{\theta^*}{n}\right)^2 - 4\frac{\theta^*}{n}}\right] \tag{5.25}$$

To have a valid solution, only the smaller of the two possible solutions is taken to ensure that saturation remains less than 1. The true saturation can then combined with the volumetric state of the specimen denoted as either porosity or void ratio to define the true volumetric water content of the sample:

$$\theta = Sn = Se(1-n) = S\frac{e}{1+e} \tag{5.26}$$

In this manner, the approximated linear response can be used in the calculations of the constitutive equations 4.71 and 4.72. Also, the function of saturation allows a conversion back to the true water content to allow the current water content and volume state of the sample to be described as shown in Figure (5-12).

In application of the model, a value of $a = 0.005$ is used. As a result, the model matches the linear slope from p_r to the lowest measured suction value, and then levels off at a volumetric water content of approximately 0.45. Engineering judgment can be used to adjust the value of a depending on soil type and the desired range of linear response. Reasonable values for the limit on θ can be obtained from a multitude of published data (*Fredlund, 1993*).

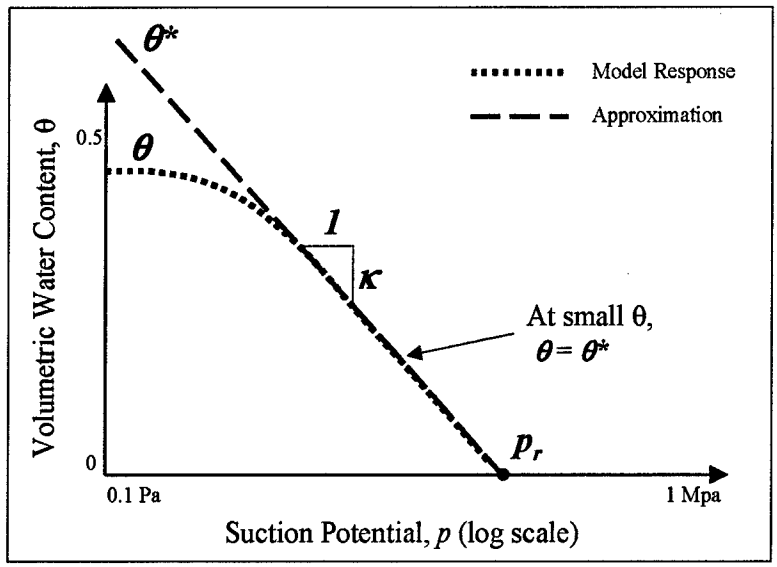

Figure 5-12: Model Approximation of Volumetric Water Content-Suction Response

5.6 A Partially Saturated Multi-Mechanical Model

Above modifications to the MMM result in a model capable of reproducing the unique responses of soils with varying saturation. Original I/O for the MMM remains unchanged. However, addition of mean stress dependent bulk and shear moduli and calibration parameters for partial saturation have been added.

The partially saturated MMM (PS-MMM) is now controlled by either strain or suction and operates by applying small increments of both to adjust the strain and stress tensors as the model progresses to specified end conditions. Suction control capability is necessary to properly simulate laboratory tests than involve wetting, rather than straining the soil specimen. The flowchart in Figure 5-13 illustrates typical model operation for either strain or suction controlled. The complete FORTRAN code detailing the operation of the PS-MMM is given in Appendix B.

5.6.1 Strain Controlled Test

In a strain-controlled test, the model begins with the initial soil state that includes the four variables defined in the incremental relationships derived in Chapter IV: stress tensors, void ratio (strain tensor), suction, and volumetric water content. In a strain-controlled test, an increment of strain (tension or compression) is applied to the spring-slider assemblies with water content held constant. The model determines the incremental change in intergranular stress (SAND_DRIVER) and incremental change in volumetric water content due to the strain (EFF_STRESS). The void ratio and volumetric water content are updated. As a result of change in water content there is a change in suction and the relevant reference pressures are adjusted. Finally, partial pore pressures for the air and water phases are calculated based on the new suction and water content (PORE_PRESSURE) and added to the effective stress tensor to generate the Cauchy stress tensor.

5.6.2 Suction Controlled Test

For a suction-controlled test, the model begins with the initial soil state that includes the four variables defined in the incremental relationships derived in Chapter IV: stress tensors, void ratio (strain tensor), suction, and volumetric water content. For a suction-controlled test, an increment of suction (wetting or drying) is applied to the spring-slider assemblies with strain held constant. The model determines the incremental change in intergranular stress (SAND_DRIVER) and incremental change in volumetric water content due to the suction (EFF_STRESS). The suction and volumetric water content are updated. The change in suction enacts a change in strain which is updated and the relevant reference pressures adjusted. Finally, the partial pore pressures for the air and water phase are calculated based on the new suction, void ratio and water content using subroutine PORE_PRESSURE and are added to the soil skeleton stress tensor to generate the Cauchy stress tensor.

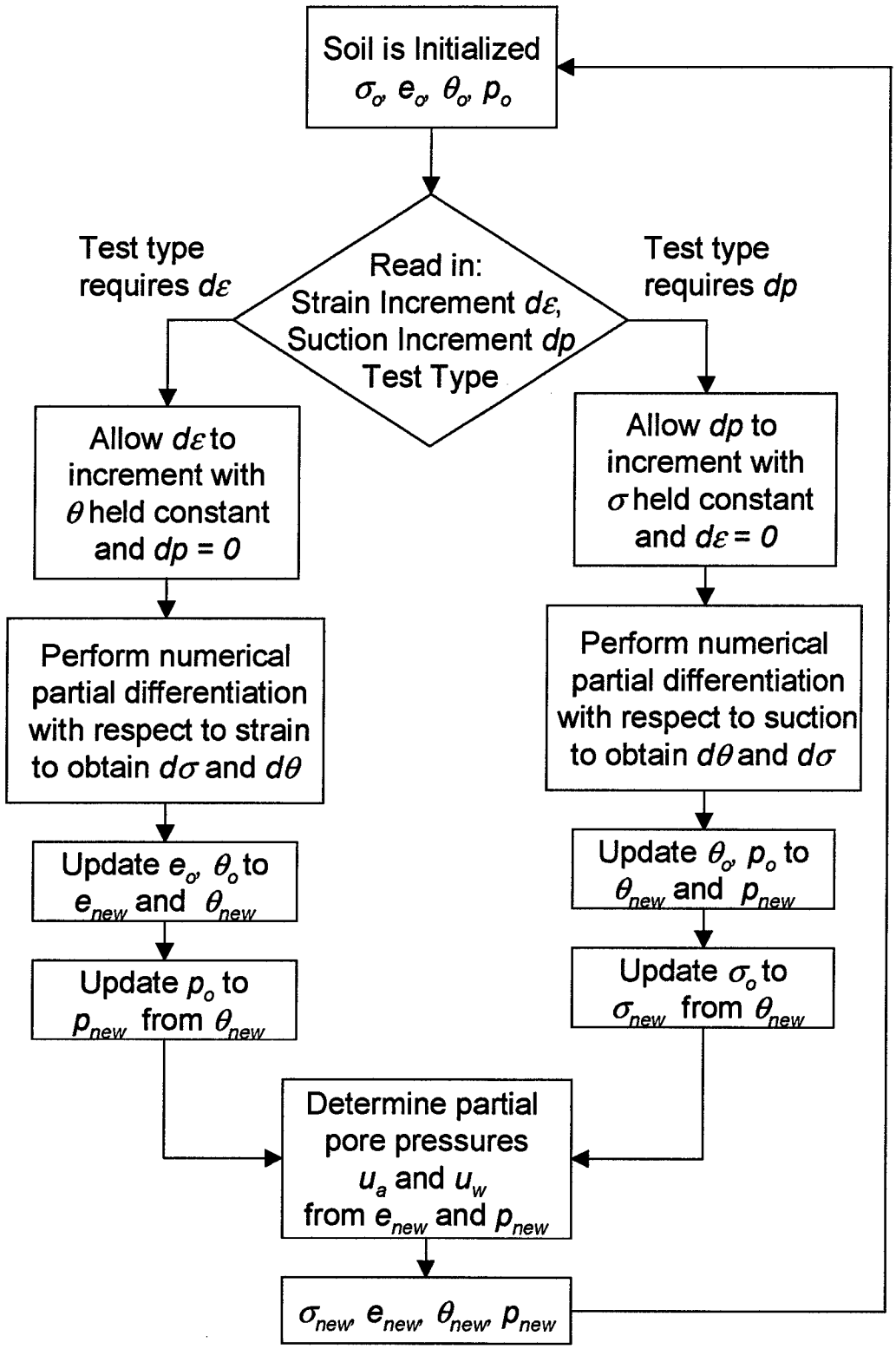

Figure 5-13: Operation of partially saturated MMM

5.7 Benefits of the Improved Model

By incorporating the thermodynamic derivation in the previous chapter and the improved parameter definitions into the existing MMM, the result is a more general soil constitutive model. Whereas the previous MMM could capture only saturated effects and could account for density through the reference pressure, the new MMM now can capture response due to variable saturation as well as density through the partially saturated reference pressure. The previous model was unable to predict collapse or swell phenomenon because there was no mechanism in place within the stress definitions to allow volumetric states to exist above the saturated virgin consolidation line. With introduction of a larger reference pressure, pseudo-stable volumetric states are now possible that upon wetting or loading, can collapse or expand to represent a broader range of in-situ and compacted soils.

Since strength in the saturated MMM could only increase due to external boundary pressures and density, strength increases associated with partial saturation were not possible. The failure envelope shift due to contribution of intergranular mean stress (Figure 5-9) from suction allows an additional condition to increase strength along with density and boundary pressures. In the original MMM constitutive behavior was based on constant bulk and shear elastic moduli. The new model adjusts these moduli for volumetric state and mean stress. As a result, more of the soil's physical properties are incorporated into the simulations. Consequently, a greater range of soil states can now be simulated.

Pore pressure response is now modularized and material specific. Therefore, pore pressure behavior can be modified according to the desired fluid properties, i.e. air and other viscous fluids. Because the model is capable of generating independent pore pressures for the various fluid phases, these magnitudes can be displayed and used to compare to published data allowing a separate calibration of the pore pressure to better suit the material behavior. Finally, the series representation of the spring-slider assembly produces a rapid, direct, linear calibration of the mechanism properties. This was

performed via trial and error in its first attempts (*Smith, 2000*) and an intuitive feel to the calibration was absent.

5.8 General Calibration Requirements

Prior to the current research, calibration of the MMM was a process consisting primarily of engineering judgment (*Smith, 2000*). Appropriate values for the distributive parameters were selected based on knowledge and experience in working with a particular material. And while a value selected for these parameters appeared relatively reliable given a good background in critical state soil mechanics, the parallel arrangement of springs and sliders made an assignment of their proper stiffness and strength values difficult. For example, selection of values involved a trial and error fit whereby all but one of the twenty mechanism properties was held constant and then modified until a portion of the data was matched and then the next parameter was fixed and the process repeated (*Smith, 2000*). The use of engineering judgment and a trial and error process produced a sufficient fit of individual soil response, but it did not represent a unique solution.

This non-systematic approach to calibration was time consuming and did not suffice for describing material condition at various confining pressures. What it did provide was a feel for magnitude and range of expected values to be generated for the various model parameters. The above approach is still useful for unique materials with limited or non-existent laboratory data and allows calibration resulting from trends found during the systematic calibrations performed on other materials. Although not recommended to anyone but those well versed in soil mechanics, this approach can be used, and used only, for problems of a limited scope.

Following is a description of the minimum test data required to generate a reliable material calibration over the range of loads and load patterns expected during the lifetime of the soil structure for an airfield pavement.

At least two cylindrical triaxial tests tested at differing confining pressures either as consolidated drained (CD) or consolidated undrained (CU) are required for evaluation of the saturated critical state and distributed parameters. A schematic of cylindrical triaxial stress conditions is shown in Figure 5-14. Within the design of airfields, triaxial confining pressures for ideally should be conducted over a range that extends from a minimum of 30% of the expected influence of the applied tire pressure at the desired soil depth to at least 150% of the expected pressure, or to the limits of the test equipment. This stress range only ensures that the material properties bound the expected range of response in the field. The triaxial test apparatus should be designed so that measurements of shear strain and volumetric strain (CD) or pore pressure and shear strain (CU) can be determined. Confining pressure and axial load should be measured to determine the shear stress and mean stress applied to the sample.

Loading of triaxial samples should continue until at a minimum, a peak shear stress is achieved and preferably beyond to a critical state condition. The test can be considered complete when the shear and mean stress values are essentially constant and changes in volumetric strain approach zero. Performing tests to these limits, which typically involve shear strain magnitudes on the order of 15-20%, will make predicting the response valid over the entire stress history of the soil.

In order to evaluate the purely hydrostatic volume response, at least one isotropic consolidation test or a one-dimensional consolidation test should be run. In order to ensure that the sample has reached a state of normal consolidation, the chamber pressure (or axial load) should be increased until a definite normally (virgin) consolidated slope can be observed on a void ratio versus mean effective stress, e-log σ', plot. It is preferable to have at least one unload-reload cycle after the specimen has reached normal consolidation to verify the model hysteresis.

For calibration of the PS-MMM, the above tests are required along with, at least one proctor compaction curve. The compaction curve allows λ to be estimated. Laboratory compaction should be at the expected energy level for the field compaction..

Also, at least two pairs of free swell (FS) and constant volume swell (CV) tests are necessary with each pair conducted at a different saturation level but at similar initial

volumetric states. This will provide a minimum of data to evaluate the $K_{1,2,3}$ moduli, κ, α and p_r in concert with the consolidation tests. It is recommended that additional test pairs be run to further establish response curves by regression or acquisition of psychrometer suction-saturation data to directly measure the magnitudes of these parameters. For soils having little swell potential (i.e. sands) it may become mandatory to acquire psychrometer tests or suction-saturation data by some means to estimate the influence of saturation on strength and to evaluate the κ, α and p_r parameters. For this case, the parameter, α, will have a value near 0.5 requiring only the determination of κ and p_r.

5.9 Summary

Formulation of the PS-MMM, produces model output that includes principal Cauchy stresses, principal strains, suction, volumetric water content and pore air and water pressures. These outputs enable comparisons to data obtained in the laboratory on both saturated and partially saturated CV, FS and consolidated undrained triaxial tests for any desired stress or strain definition. To achieve this output, proper calibration of the model is required and the following chapters will detail this process through obtaining, processing and applying the calibration parameters to enable a successful model prediction.

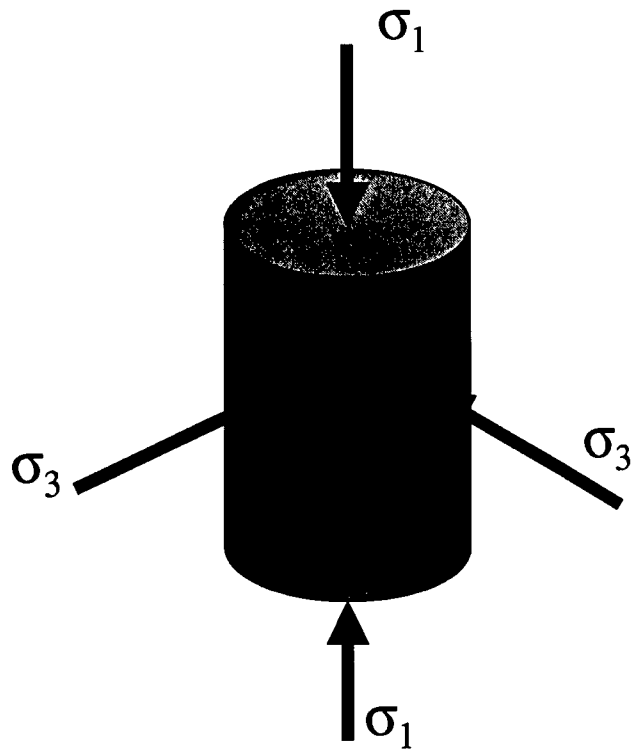

Figure 5-14: Principal stresses acting on cylindrical soil specimen during triaxial shear test

CHAPTER VI
Laboratory Tests and Results

6.1 Overview

In order to apply a constitutive model for prediction of material response under load, the model must be calibrated from laboratory data. The parameters for material strength, failure, deformation and suction defining model properties must be determined. This chapter provides detailed laboratory tests and analyses used to achieve proper calibration for a CH soil (Buckshot clay).

A laboratory test program was undertaken to serve three primary purposes. The first was to establish a similarity with existing laboratory data obtained on Buckshot clay from prior research. Once established common test data from literature could be utilized in the calibration process. Second, fill gaps in the common laboratory data not. Lastly, conduct laboratory tests allowing calibration of the partially saturated soil model developed in this thesis.

6.2 The Material

A heavy clay, commonly referred to as Buckshot clay (CH), was selected as the test material. Its name relates to its consistency at a condition dry of optimum moisture content where it tends to form hard balls or "buckshot". This clay exhibits dramatic changes in strength, swelling and volume change when tested over a wide range of moisture contents. These characteristics make the soil a good choice for evaluating the

partially saturated soil model. These extremes in response allow for a wide band of behavior to be modeled using only a single soil. The soil has uniform consistency from the borrow pit, ensuring a steady supply of clay to work with and the ability to construct repeatable specimens. As well, it has a long history of being utilized in laboratory research by the ERDC.

6.3 The Test Program

An outline of the laboratory work conducted as part of this thesis follows. The laboratory program was begun in April of 2000 and completed in January of 2002. Work was performed at the ERDC soils laboratory by a team of technicians (Larry Dunbar, Judy Hudnall, Charles Carter, and Dan Leavell) with the researcher monitoring and overseeing technique and results. Taking advantage of the technician's experience with working with the Buckshot clay and their various expertise in testing produced expeditious and repeatable tests results from one test series to another.

During the laboratory work, the original stockpile of Buckshot clay was depleted and a second batch was processed for a replicate test series for the partially saturated triaxial, constant volume swell and free swell tests. Table (1) shows a comparison of the index properties between the two batches of Buckshot clay obtained for use. The tests used for calibration of the MMM all originated from the initial batch of clay ensuring consistency in the process.

6.4 Tests Conducted

Atterberg Limits (3) (ASTM D 4318)

1 test run on original Buckshot sample

1 test run on second Buckshot sample

Specific Gravity (2) (ASTM D 854)

1 test run on original Buckshot sample

1 test run on second Buckshot sample

Grain-size Distribution with Hydrometer (1) (ASTM D 422)

1 test run on original Buckshot

Proctor Density Curves (3) (ASTM D 698 and D 1557)

Set of 8 points using Modified energy – 56 blows, 5 layers, 10 lb. hammer

Set of 11 points using Standard energy – 25 blows, 3 layers, 5.5 lb. hammer

Set of 8 points using Light energy – 15 blows, 3 layers, 5.5 lb. hammer

Isotropic Consolidation Test (9) (ASTM D 2435)

Run in conjunction with each CU TX (see below)

test on a Standard energy Proctor sample

CU Triaxial Saturated Test with Pore-pressure measurements (6) (ASTM D 4767)

2 tests run on Standard energy Proctor sample at 15 psi effective confinement

2 tests run on Standard energy Proctor sample at 30 psi effective confinement

2 tests run on Standard energy Proctor sample at 50 psi effective confinement

CD Triaxial Saturated Test (no volume change measurements) (3) (ASTM D 4767)

1 tests run on Standard energy Proctor sample at 15 psi effective confinement

1 tests run on Standard energy Proctor sample at 30 psi effective confinement

1 tests run on Standard energy Proctor sample at 50 psi effective confinement

CU Triaxial Partially Saturated Test (Modified Q-test) (30)

For each of 5 different initial degrees of saturation: 53, 61, 68, 79 and 94%, two samples at each of 3 different confining pressures of 3, 10, 30 psi were run.

Constant-Volume Swell Test (12) *and* Free Swell Test (12) (ASTM D 4829)

All conducted at an initial confining pressure of 1.4 psi = 9.7 kPa

2 specimens at Modified Proctor energy and water content of 15%**

2 specimens at Modified Proctor energy and water content of 19%

2 specimens at Modified Proctor energy and water content of 23.2%

2 specimens at Standard Proctor energy and water content of 23.2%

2 specimens at Standard Proctor energy and water content of 25.2%

2 specimens at Light Proctor energy and water content of 25.2%

6.5 Index Properties

To establish a correlation with existing laboratory data, a series of tests was outlined to allow a one-to-one correspondence with other researchers' findings. Specific gravity, grain size distribution, Atterberg limits, compaction, consolidation, and consolidated undrained (CU) triaxial tests for strength were selected. The three referenced papers concerning previously published Buckshot clay are Peterson, (*1987*), Peters et al., (*1982*) and Freeman et al., (*2004*). Table 6-1 shows a comparison of the relative percent clay, Atterberg limits, specific gravity and compression indices for Buckshot clay tested in the current research (Berney) to that of Peterson, Peters and Freeman. Grain size distribution for the tested Buckshot is shown in Figure (6-1). A discussion of the relevance of the table is given in Chapter VII.

6.6 Compaction

A series of compaction tests was conducted covering a range of moisture contents from 15% to 35%. Three levels of compaction energy were applied with the first two being standard and modified according to ASTM test methods D 698, Method A and D 1557, Method A. The third was a light compaction effort using 15 blows per lift. Figure (6-2) shows a composite of the compaction curves from the three compaction energies.

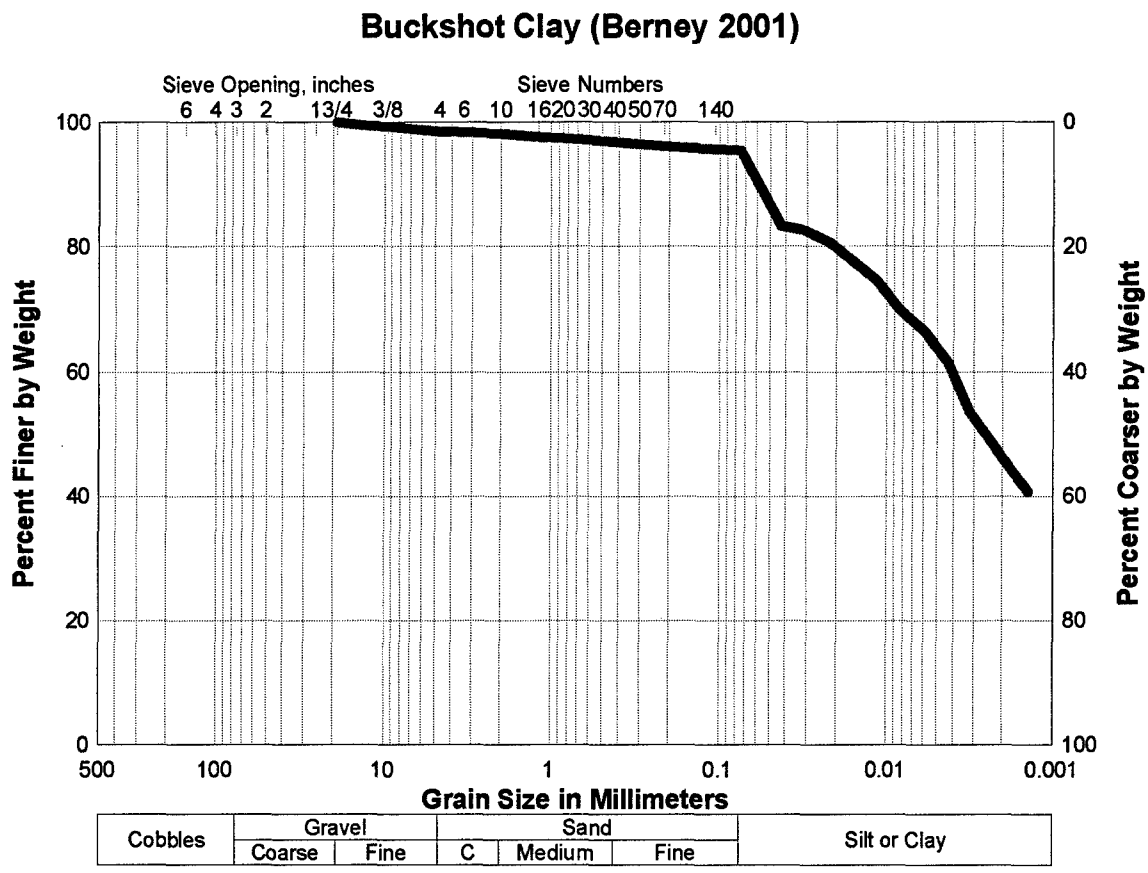

Figure 6-1: Grain Size Distribution for Buckshot Clay

Table 6-1: Summary of Index Properties for Buckshot Clay

Soil Classification = **Grey Clay (CH); Trace of Sand**							
	Berney 2001		**Peterson**	**Peters**	**Freeman**	**Averages**	**St. Dev.**
	Batch 1	Batch 2	1981	1991	1998		
Liquid Limit (LL) =	76	74	56	54	83	68.6	12.9
Plastic Limit (PL) =	24	24	21	17	27	22.6	3.8
Plasticity Index (PI) =	52	50	35	37	56	46	9.4
% Clay =	46		43	40	39	42	3.2
Activity =	1.13		0.81	0.93	1.44	1.08	0.27
Specific Gravity (Gs) =	2.74		2.72	2.74	2.79	2.75	0.030
Cc =	0.325		0.281	0.31		0.229	0.022
Cr =	0.07		0.06	0.05		0.060	0.010

Figure 6-3 combines data from Figure 6-2 with data by Freeman. Freeman's data was obtained using ASTM D 1557, Method C providing three different compaction levels: 12 blows per, 26 blows per and 55 blows per lift. There is agreement in compaction response at the modified energy reflecting consistency in the material's response. This figure helps to illustrate the trend in response of the clay as it approaches conditions considerably dry of optimum moisture content (noted by the circles in Figure 6-2) and its behavior on the wet side of optimum.

On each of the compaction plots, a line of water saturation, $S = 80\%$ is shown which provides an upper bound to the line of optimums. The degree of saturation at optimum dry density and moisture content for the modified test is higher than that of the lower energies which reach optimum near 65 to 70% saturation. As the sample is compacted at ever-decreasing moisture contents, the effect of the suction potential within the soil inhibits compaction and reduces dry density of the compacted clay. There is a limit for which the suction potential influences the compaction response shown as a lower bound line at 55% saturation. Any water content lower than that represented by the 55% degree of saturation line will begin to increase in dry density as the suction no longer influences a large enough volume of material to affect the global material response. A line of zero air voids (ZAV) is provided for reference to show the bounding surface of compaction at a saturation of 100%.

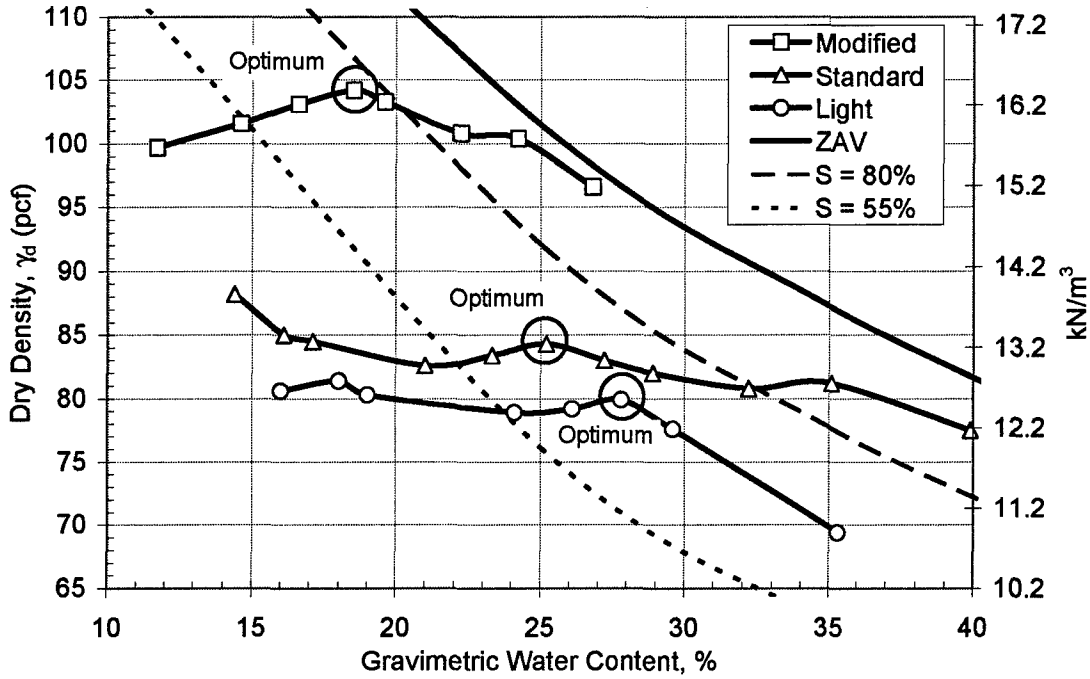

Figure 6-2: Laboratory Compaction Curves for Buckshot Clay

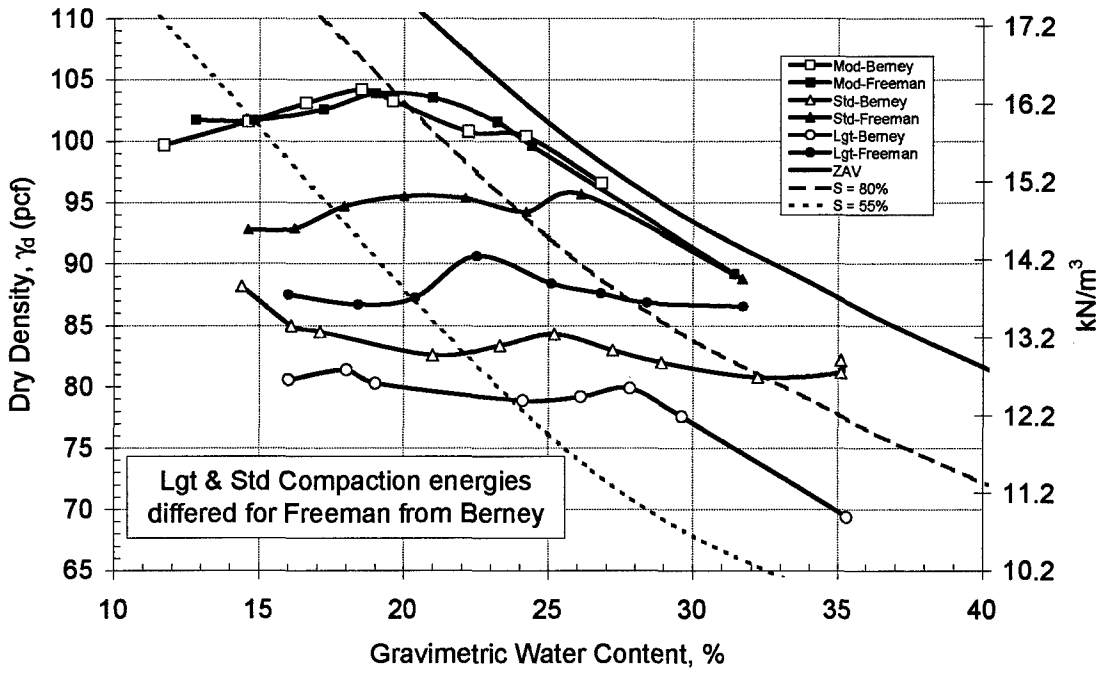

Figure 6-3: Combined Compaction Curves from Berney and Freeman

6.7 Triaxial Consolidated Undrained Test

A cylindrical triaxial test was selected in which a test specimen is subjected simultaneously to axial stress and a radial stress (Figure 5-14). The radial pressure is generated by placing the specimen in a pressurized water bath contained in a chamber enclosed with thick-walled Plexiglas (see Figure 6-8). Axial load is generated by a hydraulic ram incorporated into the vessel. In general, three types of load paths can be obtained from such a device. These can be described in terms of principal stresses σ_1, σ_2, and σ_3 where ($\sigma_1 \geq \sigma_2 \geq \sigma_3$ with compression being a positive value of stress) as follows:

1) hydrostatic (isotropic) compression – the axial stress is equal to the radial stress ($\sigma_1 = \sigma_2 = \sigma_3$)

2) triaxial compression – the axial stress is greater than the radial stress ($\sigma_1 > \sigma_2 = \sigma_3$)

3) triaxial extension – the axial stress is less than the radial stress ($\sigma_1 = \sigma_2 > \sigma_3$)

For the cylindrical triaxial test, two of the three principal stresses are equal at all times. For the research conducted in this thesis, load paths (1) and (2) are considered. The combination of these two tests allows for the determination of strength and deformation properties in both hydrostatic and shear conditions allowing a description of the material response during loading suitable for calibrating the MMM.

6.8 Specimen Preparation

Each triaxial specimen tested in this study was cylindrical in shape, approximately 1.5 inches (38.1 mm) in diameter by 3 inches (76.2 mm) in height. To prepare the specimens an appropriate mass of water was mixed by hand into an air dried sample of finely ground Buckshot clay in a large aluminum mixing bowl shown in Figure 6-4. This

mixture was then sealed in a plastic tub for 7 to 10 days to allow the moisture to come to equilibrium within the mass of soil. The soil was then compacted in a 4 inch (101.6 mm) diameter mold using a standard compaction energy as per ASTM D 698 Method A. The sample was then extruded and sealed in wax for another 5 to 7 days and stored in a humid room to allow further moisture equilibrium before finally being quartered, Figure 6-5, and trimmed with a miter box into 4 similar specimens as shown in Figure 6-6.

Each specimen had its diameter determined as an average of 6 readings found from three positions along its height and at a rotation of 90 degrees. The overall height was 3 inches (76.2 mm) being the height of the miter box used. Specimens were weighed on a digital electronic scale with a maximum range of (1600 g) and an accuracy of +/- 0.01 g. Initial water contents of each specimen were determined from trimmings collected after each specimen was prepared. Specific gravity, height, diameter and the gravimetric water content all were used to calculate the initial void ratio of each specimen prior to any further testing.

Each specimen was fitted with a top and bottom filter paper and porous stone and surrounded by a filter paper cage weighed prior to placement allowing a more rapid movement of pore water to the top and bottom platens of the chamber as shown in Figure 6-7. Each specimen was then wrapped in a 3.5 mil (0.09 mm) thick latex membrane and then double wrapped in a 12 mil (0.3 mm) latex membrane to minimize the influence of air or water permeating into or out of the specimen from the chamber fluid. End platens were placed on the top and bottom of specimens as they were mounted in the chamber and then sealed as shown in Figure 6-8.

The chamber fluid was dyed yellow to differentiate it from the water used within the specimens. This allowed detection of any leaks in the tubing or membrane system. If any leaks were found, the specimens were removed and the set up process begun again unless the specimen had experienced loading beyond the seating stress in which case the specimens were discarded.

The chamber fluid was added to the triaxial chamber until filled at which point a slight chamber pressure of 5 psi (34.5 kPa) was applied while the specimen had an internal pressure of 2 psi (13.8 kPa) applied creating a nominal 3 psi effective mean confining stress on each specimen. Specimens were then de-aired by flushing water through each specimen using a slight vacuum until at least two full burettes (45 cc) of water had been passed through the specimen. Axial deformation of the specimens due to swelling or collapse from de-airing was determined from a rod which was pushed onto the top of each specimen recording the differential movement of the top of the specimen from an initial dial gauge reading. The difference in movement was measured with dial gauges of an accuracy of 0.001 inches (0.025 mm) set on the top of each rod as shown in Figure 6-8.

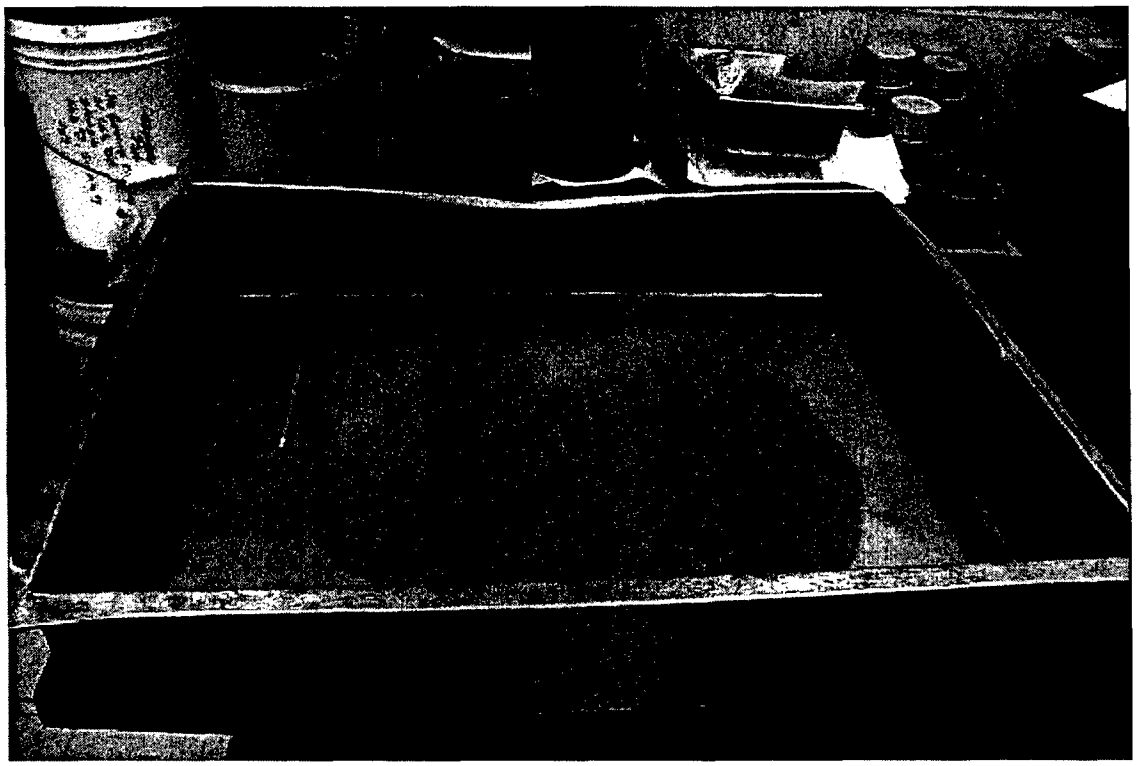

Figure 6-4: Air-dried sample of Buckshot Clay prior to mixing

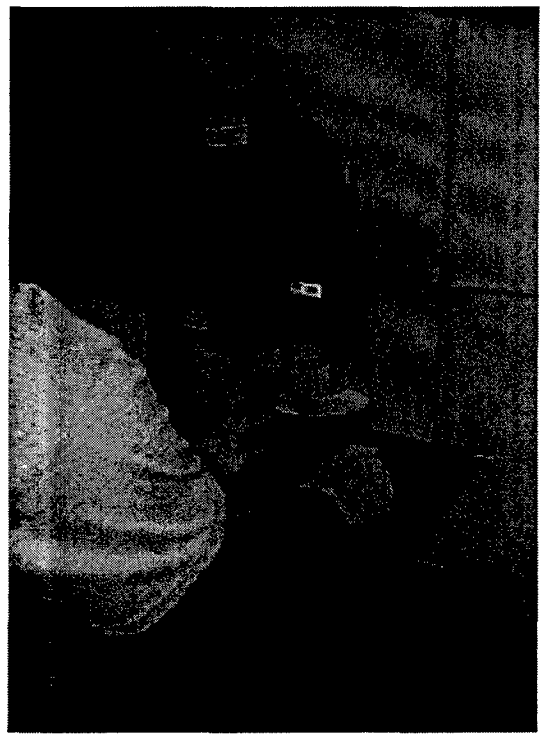

Figure 6-5: Quartering the Compacted sample for CU Triaxial tests

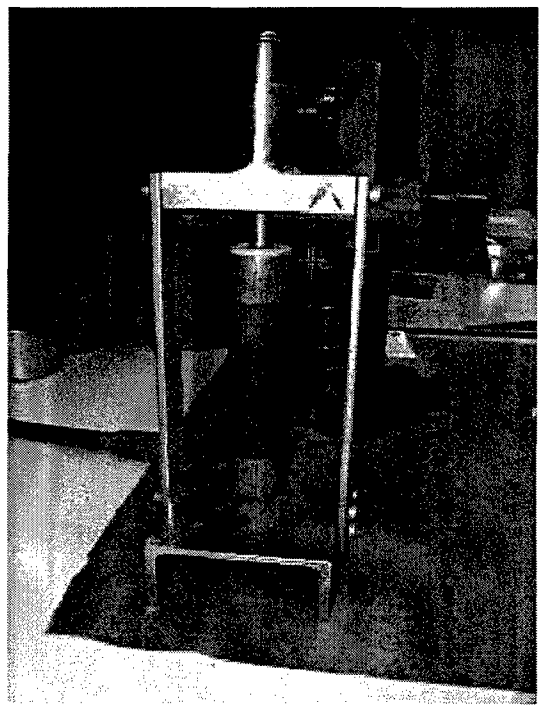

Figure 6-6: Miter box used to trim the Buckshot specimens

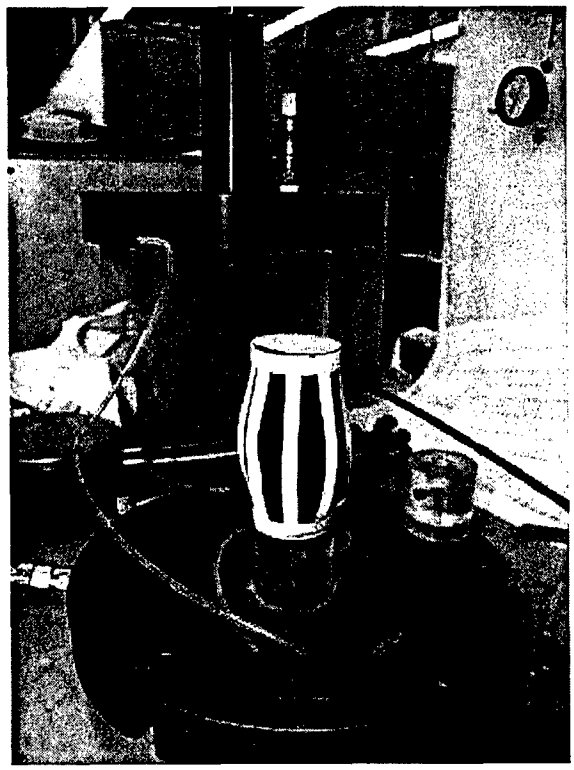

Figure 6-7: Filter Paper Cage for Buckshot Specimen

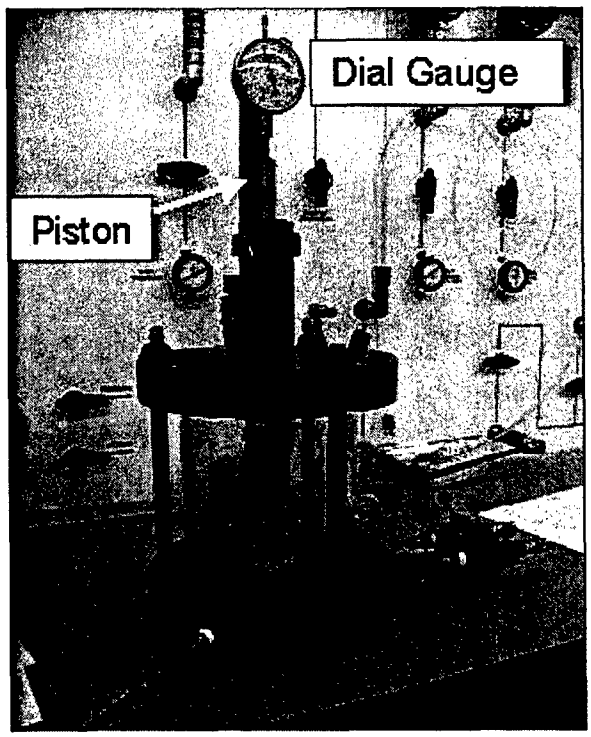

Figure 6-8: Triaxial/Isotropic-Consolidation specimen prior to the application of confining pressure fluid

Once flushing was completed, each sample was backpressure saturated. The chamber pressure and internal water pressure were increased such that the difference was never greater than 3 psi. At 10 psi increments, Skempton's B value was checked to determine whether a value of 0.95 or greater had been achieved. The specimens all required a back pressure between 55 and 65 psi to attain such a B value. Measurements of axial deflection were taken just prior to application of the next increment of confining pressure to observe any changes in sample size occurring during the final wetting stage.

For purposes of developing the critical state strength envelope, it was preferable to have specimens at a variety of over-consolidation ratios (OCR) ranging from an OCR of 6 down to an OCR of 1.6 prior to shearing. To obtain these OCR values, each specimen was isotropically consolidated to an effective confining pressure of 80 psi (552 kPa), which ensured the specimens were in a normally consolidated state and rebounded to an appropriate isotropic stress state at the desired OCR value. Set-up of the consolidation specimens is shown in Figure 6-9.

6.9 Isotropic (Hydrostatic) Consolidation Test

The isotropic consolidation test was performed by doubling the effective chamber pressure every 24 to 96 hours depending on the time to end of primary consolidation. End of primary consolidation was determined based on the dial reading versus logarithm of time relationship in ASTM D 2435. The difference between the constant back pressure and the chamber pressure is defined as the effective chamber pressure and the increments used were 3, 6, 12, 25, 50 and 80 psi (21, 42, 84, 172, 344 and 552 kPa) during loading and then the following unloading steps were used depending on the final confining pressure desired: 80 to 45 to 15 psi (552, 310, 103 kPa), 80 to 55 to 30 psi (552, 379, 207 kPa), and 80 to 50 psi (552, 344 kPa) for the three ending confining pressures. The isotropic consolidation plots for the replicates at each confining pressure can be seen in Figures 6-10, 6-11, and 6-12.

The time for each unloading step varied from 24 to 48 hours depending the condition of each specimen. Axial deflection readings were taken as per ASTM D 2435

for each loading step until 24 hours was reached at which point daily readings were taken until end of primary consolidation.

A goal was that the void ratio after specimen consolidation would be similar for each test replicate to enable a better comparison of resulting stress-strain response. A summary of the void ratio at initial compaction, after backpressure saturation, and finally at the end of consolidation, prior to the initiation of shearing are found in Table 6-2. The lowest standard deviation in the void ratio after consolidation was for the 50 psi confined samples, but those samples exhibited a wide range of coefficient of consolidation and reference void ratio, likely due to an erroneous data point in Series 50-3. The 30 psi confined samples exhibited the most consistent void ratio condition for each stage of consolidation and had the least variation in the consolidation coefficients and reference void ratio parameters.

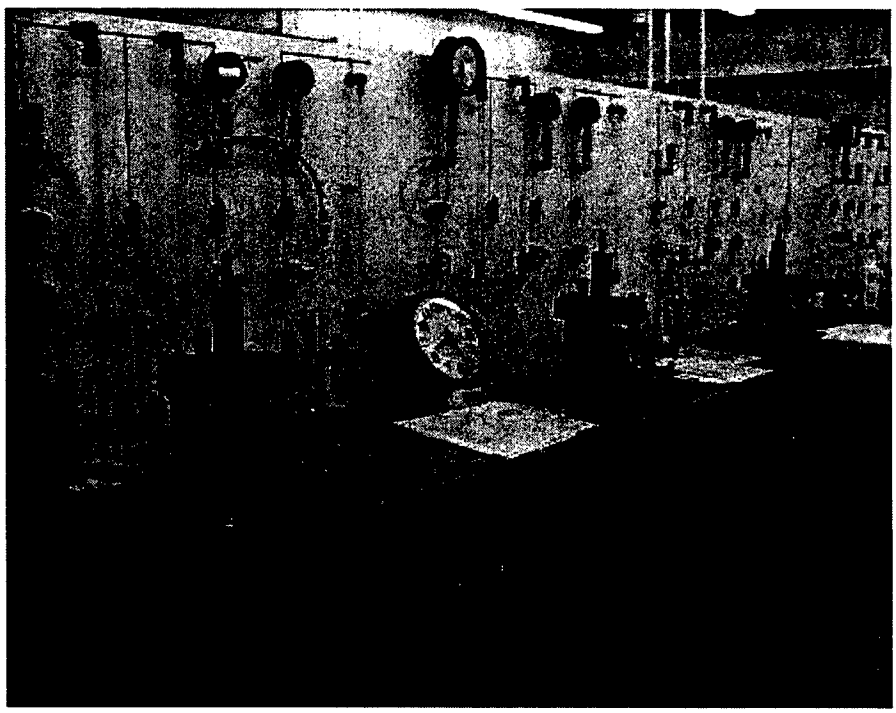

Figure 6-9: Triaxial tests during consolidation phase

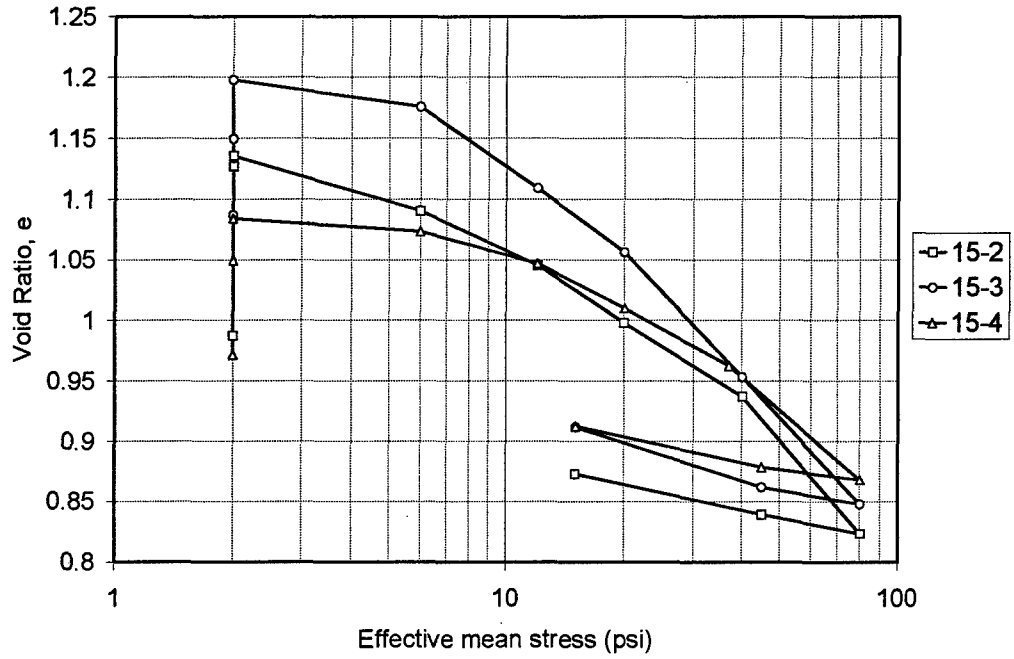

Figure 6-10:Isotropic Consolidation for Buckshot Clay (Series ending in 15 psi confinement)

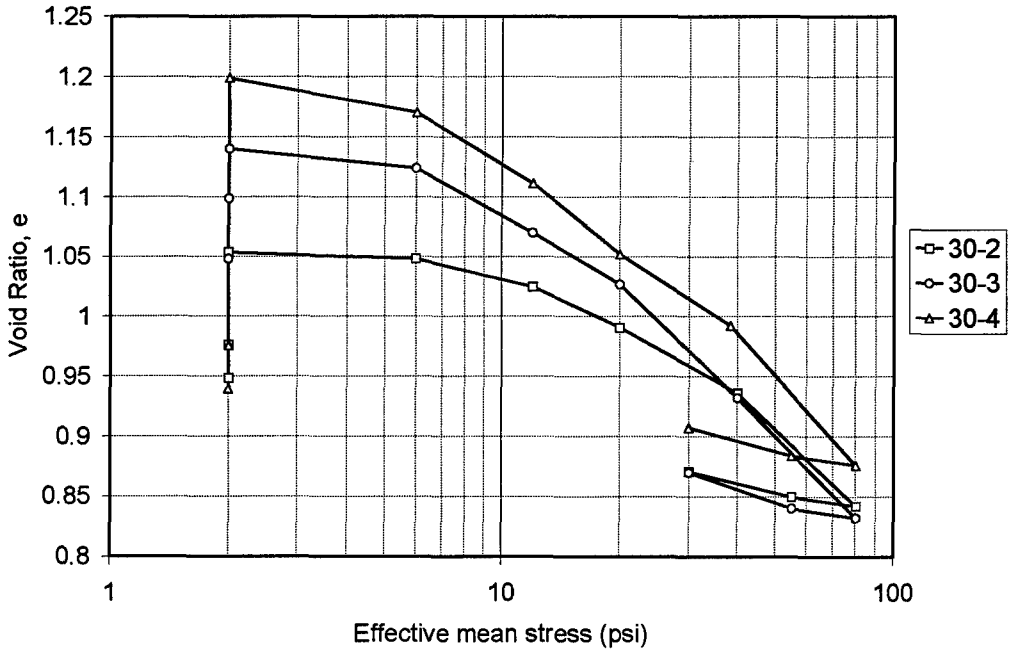

Figure 6-11:Isotropic Consolidation for Buckshot Clay (Series ending in 30 psi confinement)

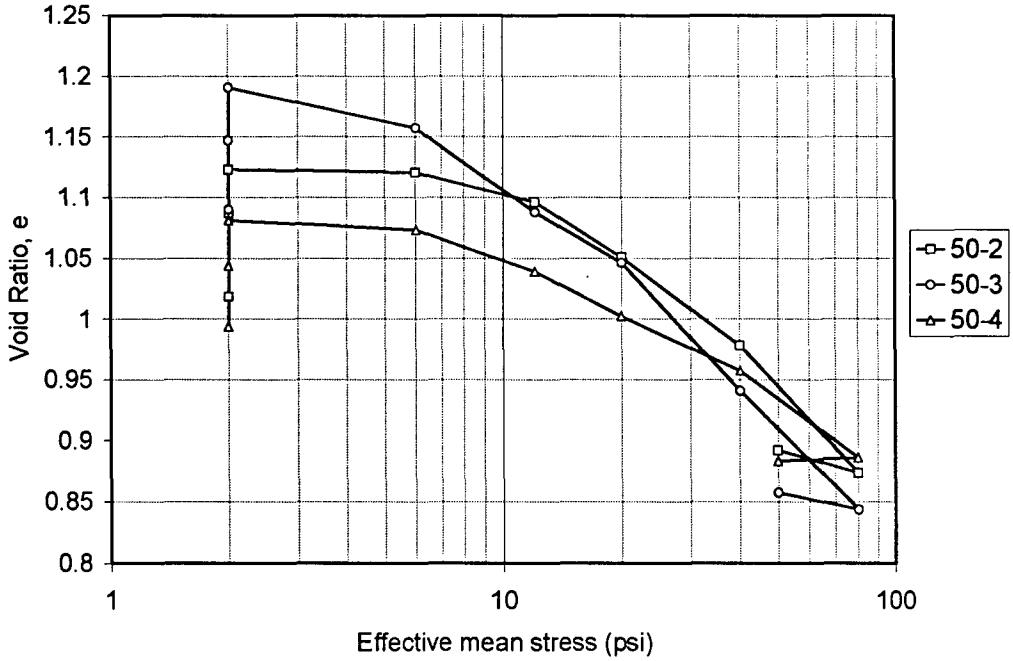

Figure 6-12:Isotropic Consolidation for Buckshot Clay (Series ending in 50 psi confinement)

Table 6-2: Summary of Isotropic Consolidation Data

	Void Ratio					
Specimen	After Compaction	After Back Saturation	After Consolidation	Reference eref	Cc	Cr
15-2	0.9873	1.1355	0.8729	1.550	0.378	0.068
15-3	1.0870	1.1979	0.9118	1.530	0.351	0.088
15-4	0.9717	1.0840	0.9127	1.470	0.283	0.062
Average	1.0153	1.1391	0.8991	1.517	0.337	0.073
Std. Dev.	0.0626	0.0570	0.0227	0.042	0.049	0.014
30-2	0.9484	1.0533	0.8708	1.452	0.312	
30-3	1.0480	1.1401	0.8700	1.480	0.332	
30-4	0.9395	1.1989	0.9072	1.555	0.363	
Average	0.9786	1.1308	0.8827	1.496	0.336	
Std. Dev.	0.0602	0.0732	0.0213	0.053	0.026	
50-2	1.0185	1.1232	0.8922	1.538	0.348	
50-3	1.0900	1.1906	0.8576	1.480	0.323	
50-4	0.9939	1.0813	0.8834	1.330	0.237	
Average	1.0341	1.1317	0.8777	1.449	0.303	
Std. Dev.	0.0499	0.0551	0.0180	0.107	0.058	

6.10 Triaxial Shear

Once final effective chamber pressure was reached, specimens were mounted in a triaxial shearing apparatus that can perform three triaxial compression tests simultaneously shown in Figure 6-13. The loading piston was placed against a load cell with a range of 500 lb (2.22 kN) with an accuracy of +/- 0.1 lb (0.44 N). A vertical deflectometer was placed at the top of the first specimen to measure deflection of all three triaxial specimens. The deflectometer had a travel range of 1 inch (25.4 mm) and an accuracy of 0.001 inches (0.025 mm). An electronic pore pressure transducer with a range of 200 psi (1380 kPa) and an accuracy of +/- 0.1 psi (0.69 kPa) was saturated and then attached to the exit tubing of each specimen to monitor changes in pore pressure during the constant volume shearing. The load cell data, axial deflection and pore pressure readings were stored in a computer which was used to convert and display the information as axial stress (psi), axial strain (%) and pore water pressure (psi).

Triaxial shearing of each specimen was conducted as per ASTM D 4767 at a rate of 0.01 mm/min for a time period of approximately 22 hours at which time an axial strain of 20 percent was achieved and the samples had either failed or reached a critical state response. The specimens were then unloaded and the chambers removed from the mounting apparatus. In this process the chamber pressure and backpressure were removed such that the back pressure never exceeded the chamber pressure. Each chamber was then drained of fluid, and the specimen removed. Figures 6-14 through 6-19 show the resulting shear strain-shear stress-volumetric strain behavior of specimens during the triaxial test. Resulting effective stress path plots are shown and discussed in detail in Chapter VII.

To determine the final moisture content of each specimen, each soil cylinder was trimmed on the top, bottom and sides to remove portions of the specimen with filter paper attached. This was done to minimize the influence of excess water at specimen boundaries due to presence of the filter paper. The interior portion of each specimen was then weighed in a separate pan and dried to obtain final moisture content. The remainder of each specimen and any washings from the membrane, knife and filter paper were

weighed in a separate pan and dried. Weight of solids found from the washings was added to the weight of solids from the core of each specimen to calculate the final weight and volume of solids within each specimen. Using total solids weight and idealized moisture content from the specimen interior allowed calculation of the final weight and volume of water. Table 6-3 summarizes the initial and final volumes, weights and peak shear stress and strain during testing.

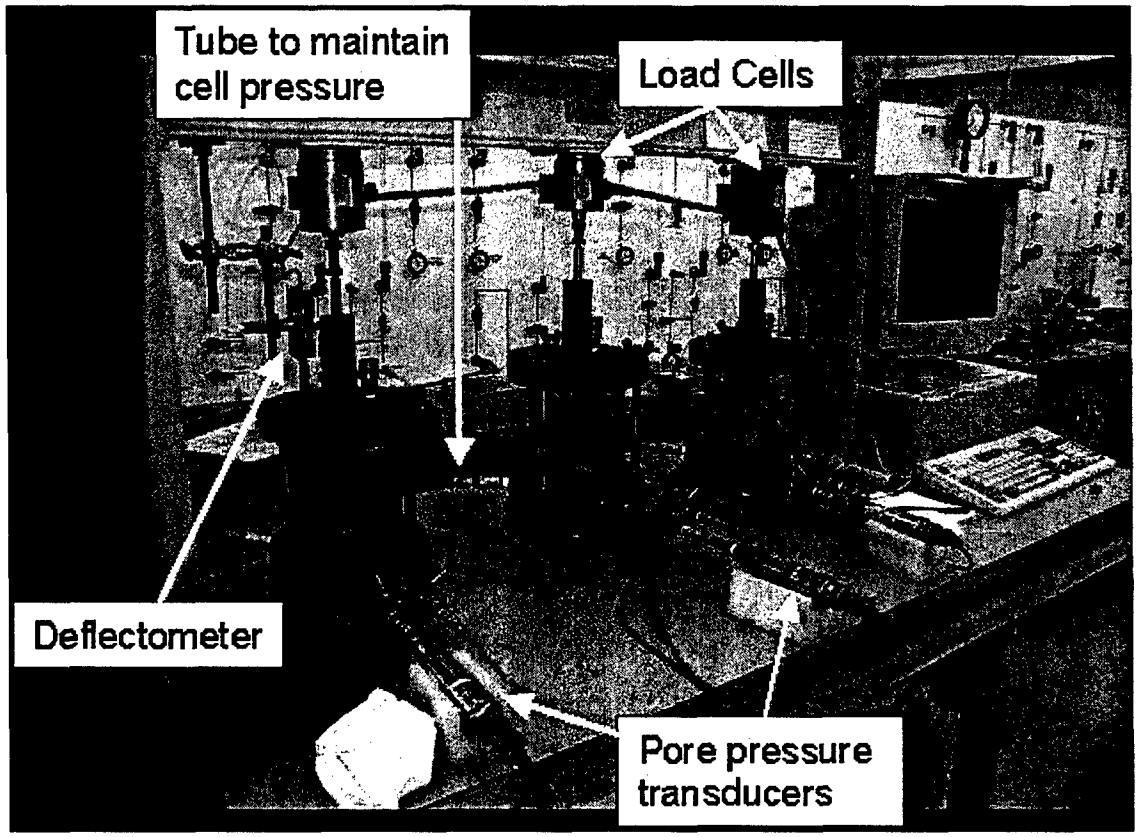

Figure 6-13: Mounting of consolidated triaxial specimens prior to shearing

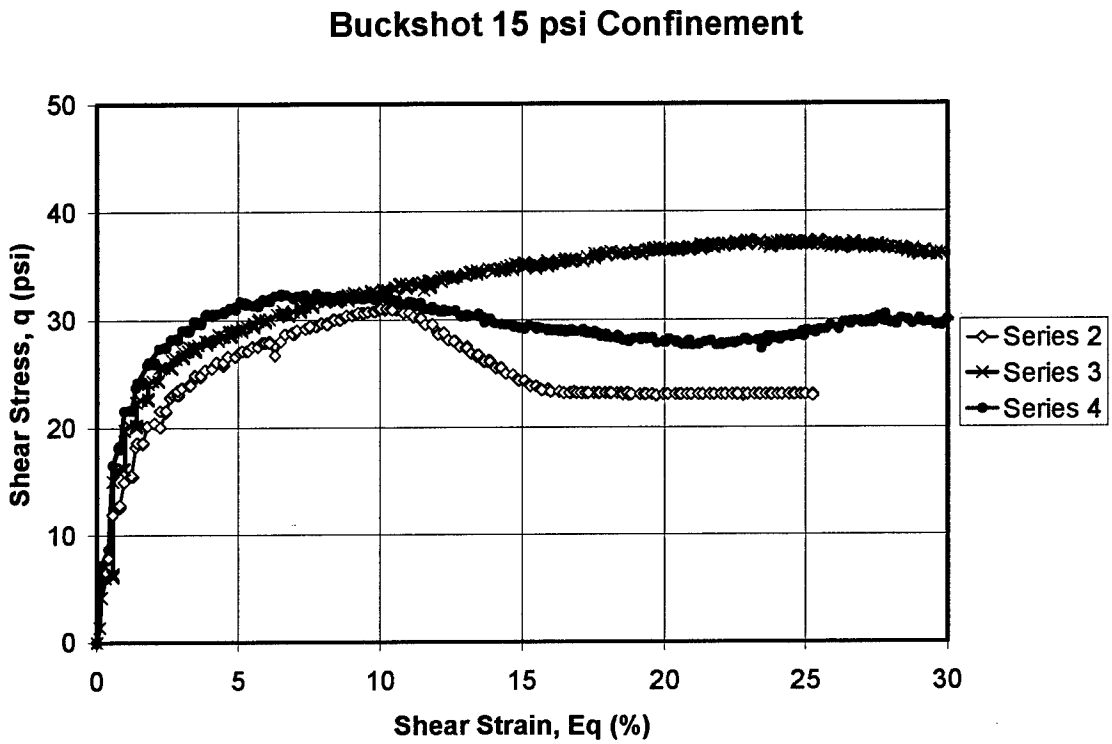

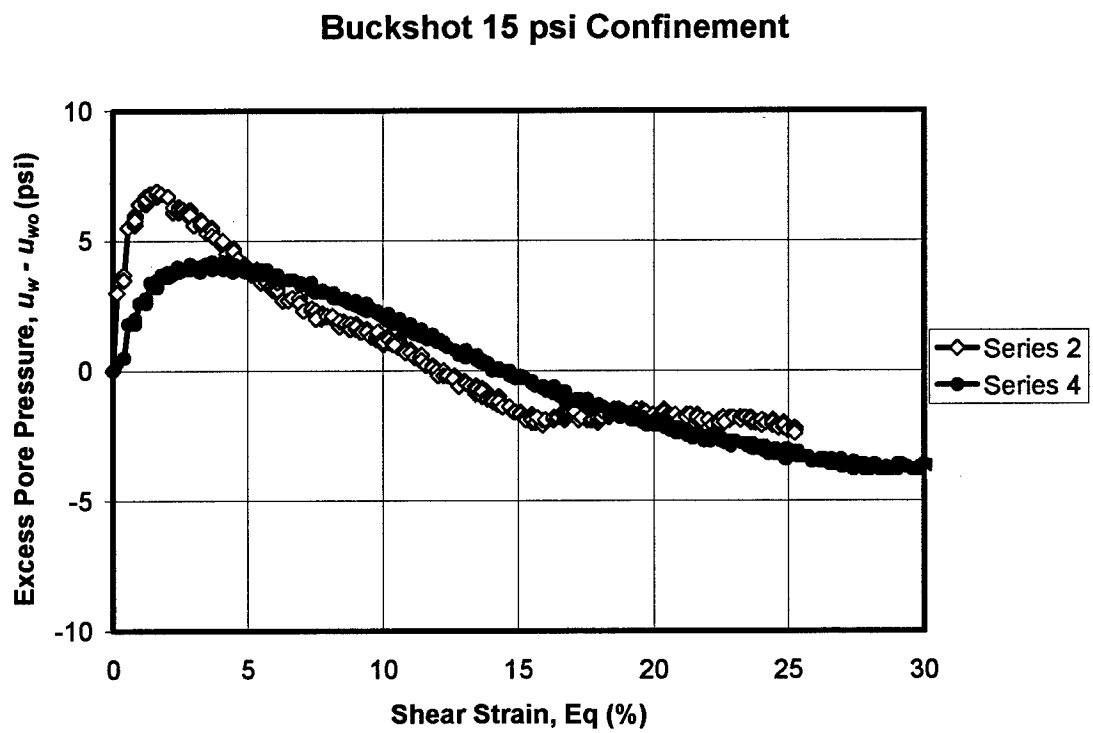

Figures 6-14 and 6-15: Shear Stress and Excess Pore Pressure versus Shear Strain for CU Triaxial Tests conducted at 15 psi confining pressure

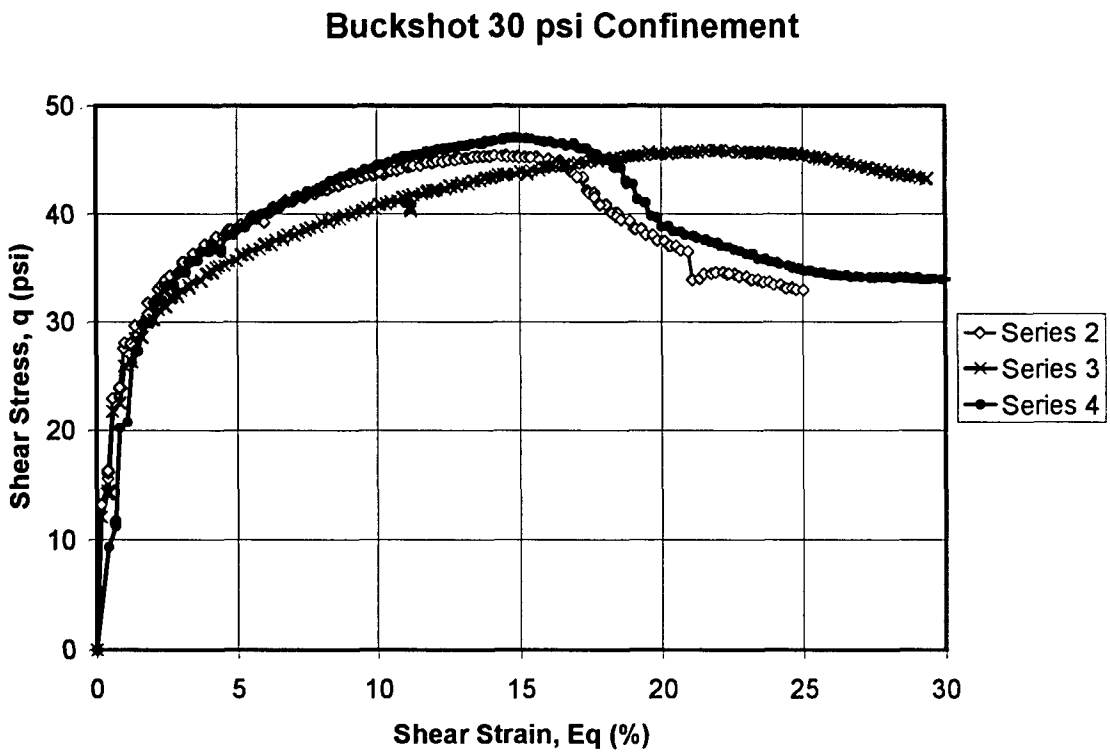

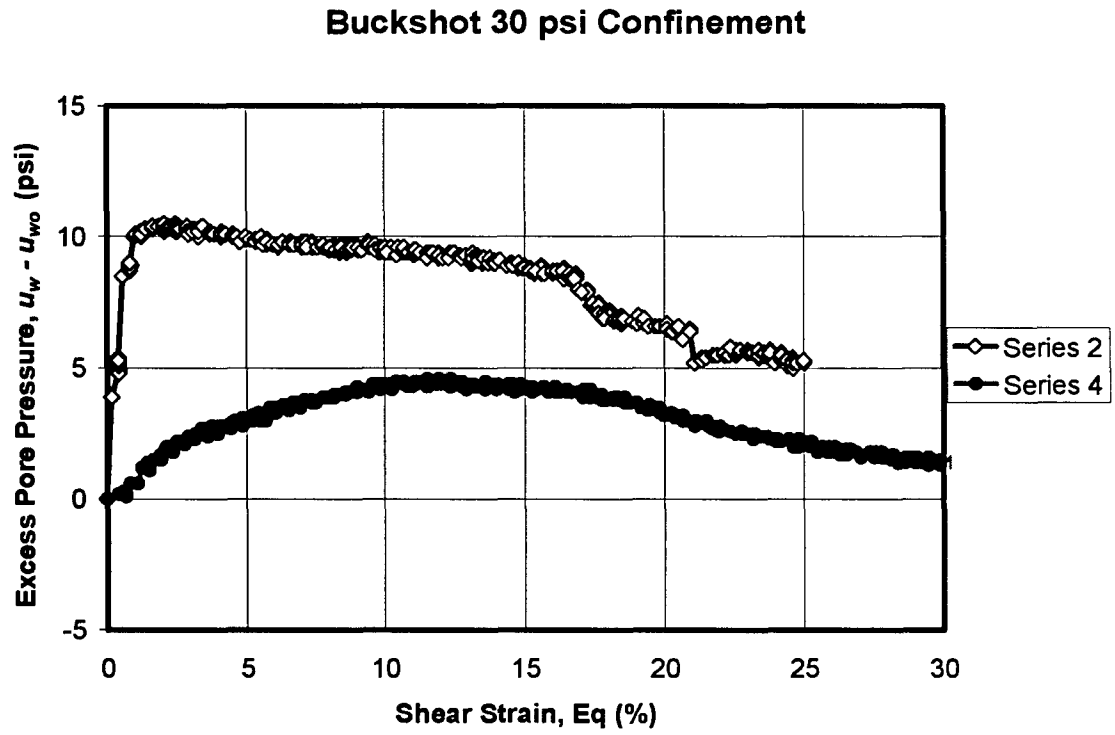

Figures 6-16 and 6-17: Shear Stress and Excess Pore Pressure versus Shear Strain for CU Triaxial Tests conducted at 30 psi confining pressure

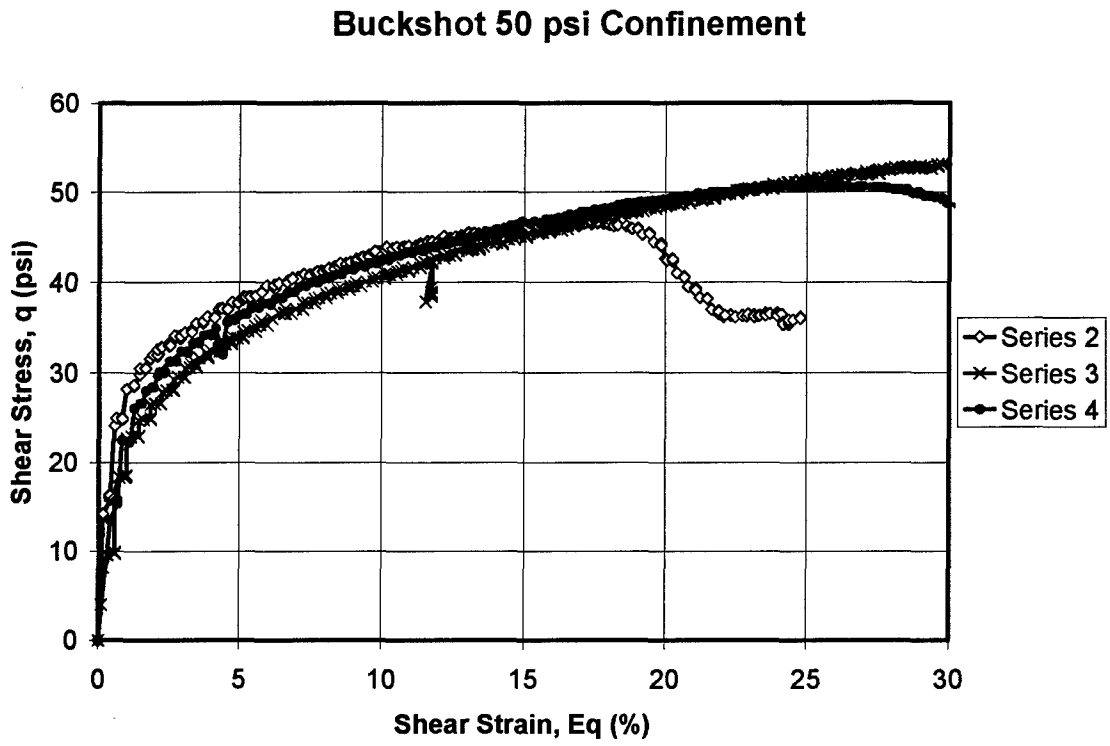

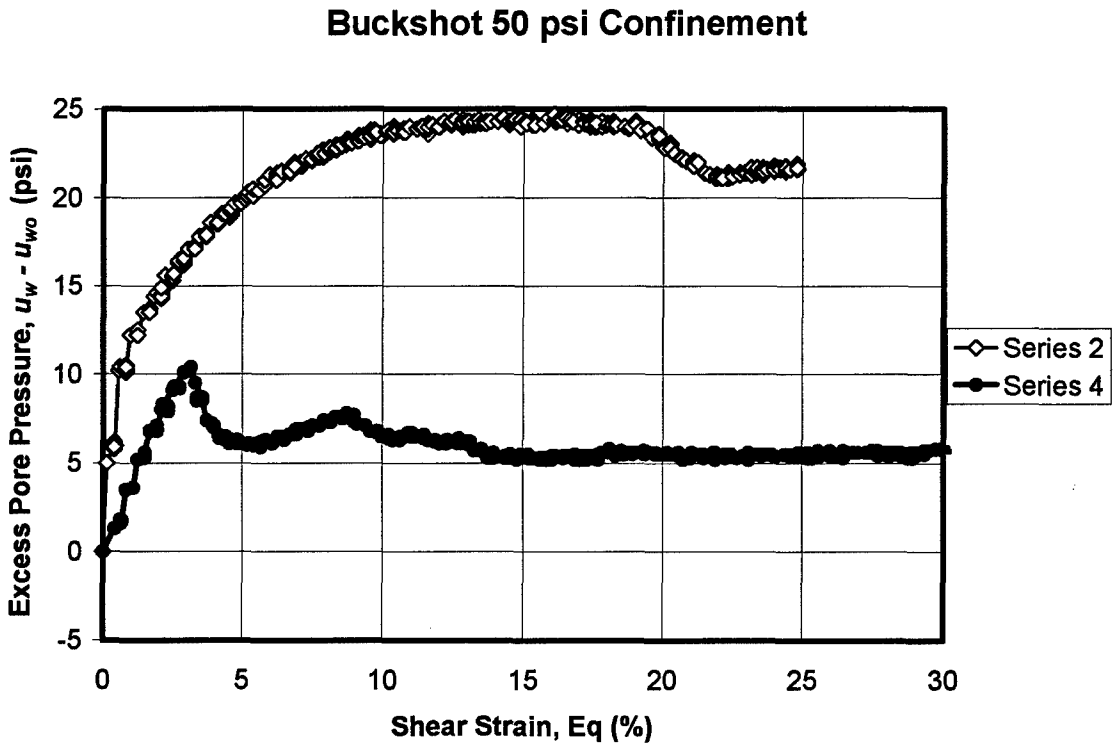

Figures 6-18 and 6-19: Shear Stress and Excess Pore Pressure versus Shear Strain for CU Triaxial Tests conducted at 50 psi confining pressure

6.11 Partially Saturated Triaxial CU Test (Modified Q-test)

Preparation of each specimen occurred in the same order as the saturated CU triaxial test. The only deviation before load was applied to specimens was to leave off the filter paper cage prior to wrapping each specimen in latex membranes and then sealing the chamber. Only filter paper on the top and bottom of each specimen to prevent movement of soil particles was used.

At the beginning of each test, upper and lower drainage valves were opened to the atmosphere so that the air within the specimen could drain freely during the isotropic consolidation phase of the test. The chamber pressure was then increased to one of three different confining pressures: 3, 10 and 30 psi (21, 69 and 207 kPa) in a single increment. The axial deformation of each specimen was measured and the consolidation continued until end of primary consolidation. This took between a few minutes for the driest specimen, at the lowest confining pressure to 48 hours for the wettest specimen, at the highest confining pressure.

At the end of consolidation phase, each chamber was placed in an Unconsolidated-Undrained (UU) shear device which provided a constant rate of axial displacement of 0.06 inches/minute (1.5 mm/minute). This loading rate will produce a 20 percent axial strain in 10 minutes. The drainage valves on each specimen were left open to allow free draining of air within the specimen. Amount of water discharged from specimens was not practical to measure as the rapid shearing of the UU test reduced water flow out of the sample to zero.

A load cell was used to measure the vertical force applied to the specimen and the chamber pressure was held constant providing a measurement of the total major and minor principal stresses.

At the end of each test, chambers were relieved of pressure, drained, filter paper removed from the specimen, and the entire specimen dried and weighed to determine final water content. In almost all tests, there was little to no change in final water content with only a slight change in the specimens tested very wet (40% moisture content).

Table 6-3 provides a summary of initial void ratio, water content and peak deviator or shear strength response for each of the various tests. Figures 6-20 to 6-25 illustrate the shear stress-axial strain curves for each of the five different water content tests conducted. Results are grouped according to confining pressure and series. Further analysis for use of this data to validate the MMM can be found in the following chapter.

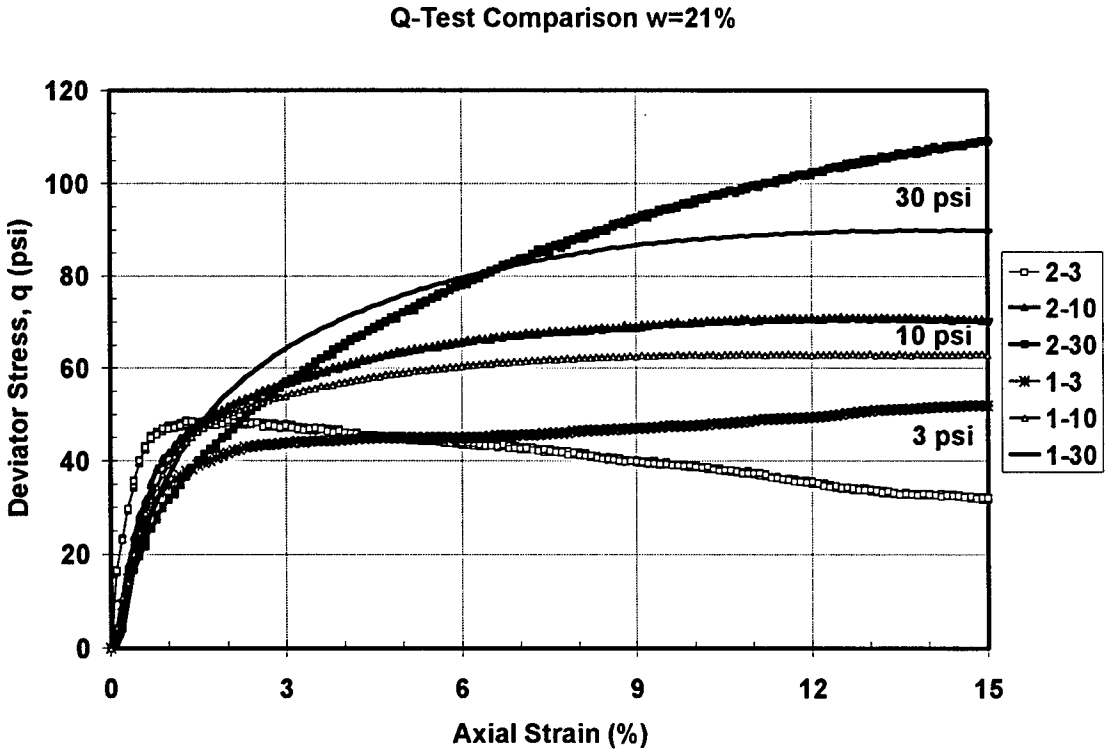

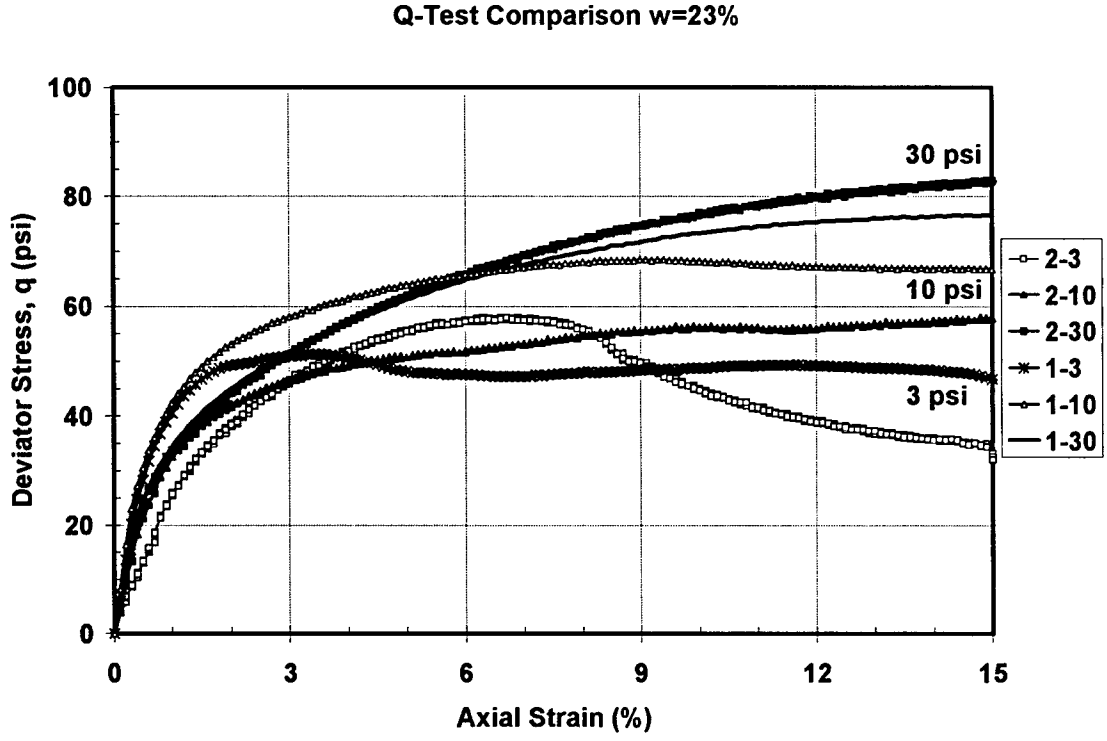

Figures 6-20 and 6-21: Modified Q-Test Shear Stress versus Axial Strain for 21% and 23 % gravimetric water contents

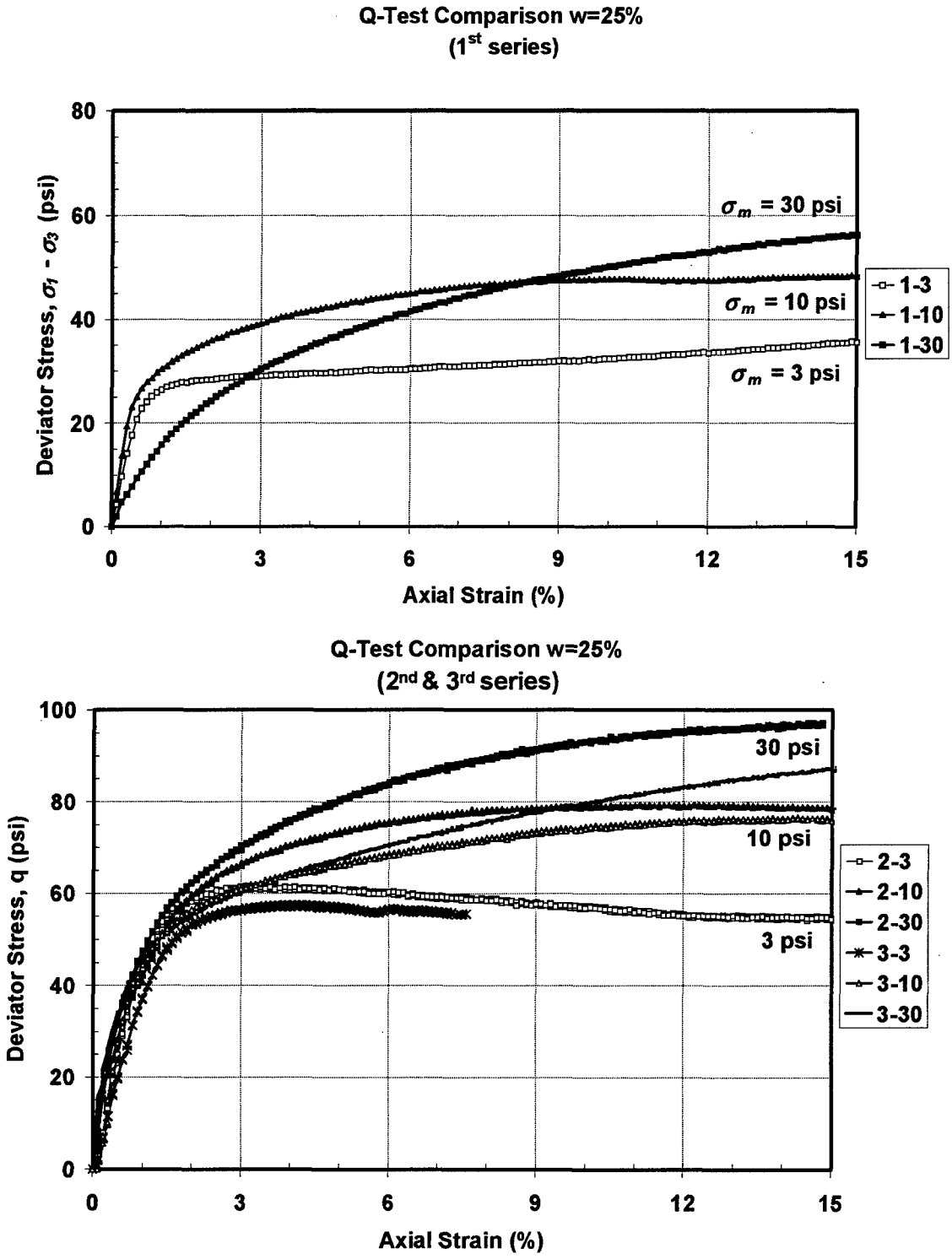

Figures 6-22 and 6-23: Modified Q-Test Shear Stress versus Axial Strain for 25% and gravimetric water contents (Series 1, 2 and 3)

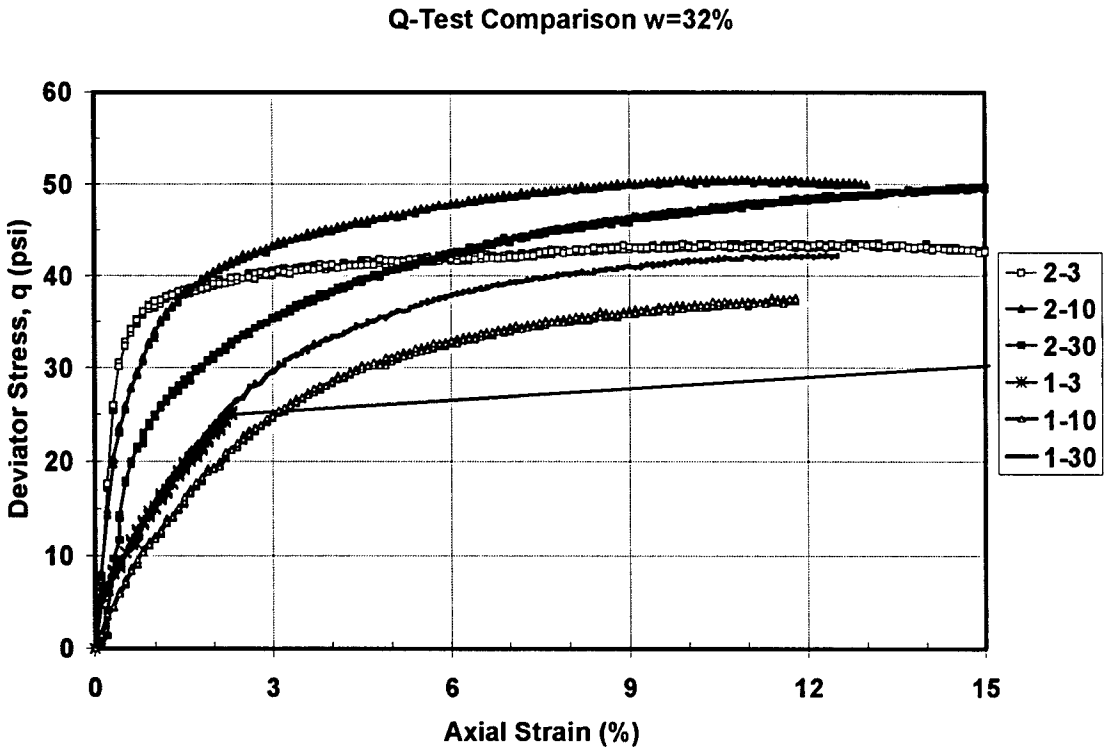

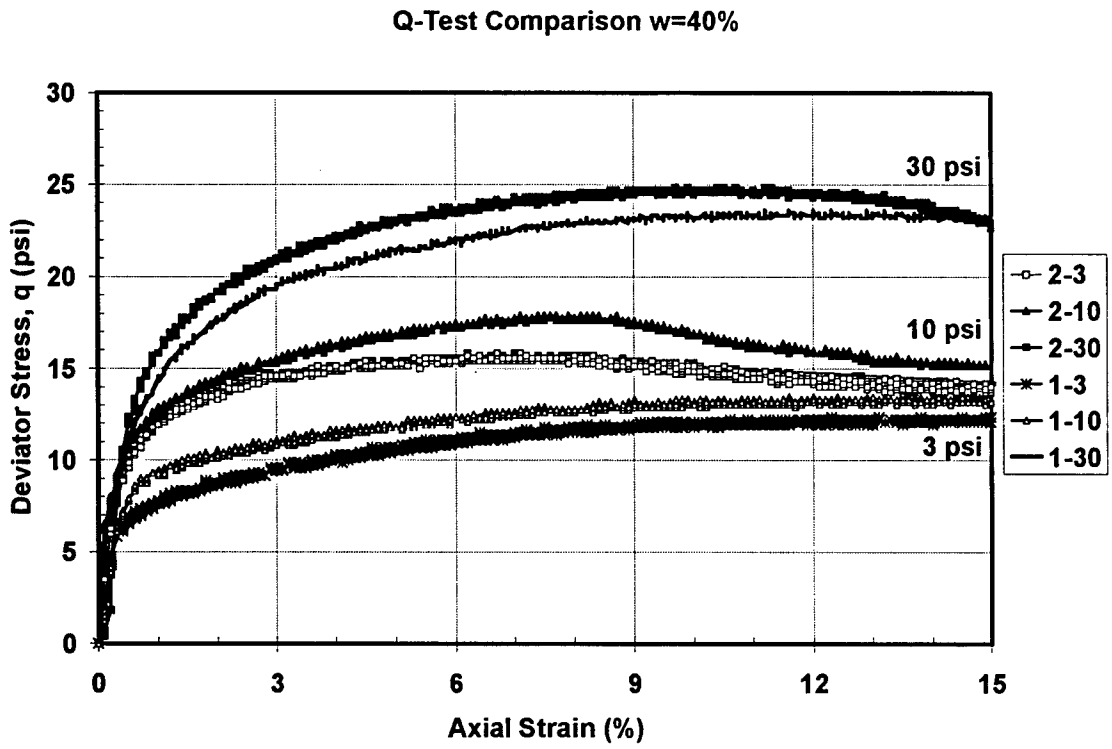

Figures 6-24 and 6-25: Modified Q-Test Shear Stress versus Axial Strain for 32% and 40 % gravimetric water content

Table 6-3: Summary of Modified Q-Test Strength Results

Modified Q-Test Data Summary for Buckshot Clay							
Nominal Water Content %	Series	Void Ratio After Consolidation	Initial Water Content (%)	Dry Density (pcf)	Confining Pressure p, psi	Peak Shear Strength q, psi	q / 2p
21	1	1.0510	20.70	83.36	3	53.8	9.0
	2	1.0000	21.18	85.49	3	48.8	8.1
	Average	1.0255	20.94	84.43	3	51.3	8.5
	1	1.0410	20.90	83.77	10	63.1	3.2
	2	1.0260	20.34	84.39	10	71.3	3.6
	Average	1.0335	20.62	84.08	10	67.2	3.4
	1	0.9865	20.80	86.07	30	90.0	1.5
	2	1.0460	20.18	83.57	30	109.4	1.8
	Average	1.0163	20.49	84.82	30	99.7	1.7
23	1	0.9640	23.30	87.05	3	51.0	8.5
	2	1.0230	22.61	84.52	3	57.9	9.7
	Average	0.9935	22.96	85.79	3	54.5	9.1
	1	0.9260	23.40	88.77	10	68.0	3.4
	2	1.0570	23.16	83.12	10	58.1	2.9
	Average	0.9915	23.28	85.95	10	63.0	3.2
	1	0.9820	23.60	86.26	30	77.0	1.3
	2	1.0160	23.01	84.81	30	82.9	1.4
	Average	0.9990	23.31	85.54	30	80.0	1.3
25	1	0.995	25.95	85.70	3	36.0	6.0
	2	0.9790	24.66	86.40	3	61.7	10.3
	3	0.9299	24.58	88.59	3	57.5	9.6
	Average	0.9680	25.06	86.90	3	51.7	8.6
	1	0.983	25.06	86.22	10	49.85	2.5
	2	0.9540	24.42	87.50	10	79.5	4.0
	3	0.9321	24.92	88.49	10	76.7	3.8
	Average	0.9564	24.80	87.40	10	68.7	3.4
	1	0.923	25.1	88.91	30	61.76	1.0
	2	0.9210	24.48	89.00	30	97.2	1.6
	3	0.9230	25.17	88.91	30	87.9	1.5
	Average	0.9223	24.92	88.94	30	82.3	1.4
32	1	0.9650	30.35	87.01	3	30.0	5.0
	2	0.9813	31.28	86.29	3	43.6	7.3
	Average	0.9732	30.82	86.65	3	36.8	6.1
	1	0.9720	30.32	86.70	10	38.0	1.9
	2	0.9649	31.35	87.02	10	50.6	2.5
	Average	0.9685	30.84	86.86	10	44.3	2.2
	1	0.9420	30.34	88.04	30	42.0	0.7
	2	0.9732	30.94	86.65	30	49.7	0.8
	Average	0.9576	30.64	87.35	30	45.9	0.8
40	1	1.1950	39.90	77.89	3	12.0	2.0
	2	1.1510	39.21	79.49	3	15.8	2.6
	Average	1.1730	39.56	78.69	3	13.9	2.3
	1	1.1830	40.10	78.32	10	14.0	0.7
	2	1.1360	39.06	80.04	10	17.9	0.9
	Average	1.1595	39.58	79.18	10	16.0	0.8
	1	1.1340	40.38	80.12	30	24.0	0.4
	2	1.1110	37.65	80.99	30	24.9	0.4
	Average	1.1225	39.02	80.56	30	24.4	0.4

6.12 Psychrometer Test

In the psychrometer test, soil suction potential is related to condensation and subsequent evaporative response of moisture within a soil enacted by electrical current passed between two nodes of dissimilar metals. Prior work on partially saturated Buckshot clay by Peterson (*1990*) was taken advantage of, since that test program included an extensive thermocouple psychrometer calibration and analysis on Buckshot clay. Details of the test procedure and sample preparation are summarized below. The material characterization is shown in Table 6-1.

Cylindrical specimens of 12, 16, 20, 24, 28 and 32% nominal moisture contents were prepared using a kneading compaction process. The cylindrical molds were 2.8 in (7.1 cm) in diameter by 6 in. (15.2 cm) tall. A 0.35 in (0.9 cm) diameter by 1.3 in (3.3 cm) deep hole was drilled perpendicular to one end of each specimen (Figure 6-26). After mounting the specimens in preparation for conducting triaxial shear tests, a commercial themocouple psychrometer with a ceramic housing equivalent to the size of the drilled hole was inserted into the specimen to ensure a snug fit (Figure 6-27). Filter paper was placed over the end of the housing to protect the psychrometer from soil particles. The triaxial samples were then sealed with filter paper, rubber membranes and silicone and immersed in a temperature controlled water bath to ensure the specimen was isolated from any changes in temperature or humidity effects outside the triaxial chamber. Prior to shearing each specimen, an initial reading of the psychrometer was taken to measure the suction potential within a soil specimen of known gravimetric moisture content and volumetric state (void ratio). These data points are presented in Figure 6-28 in terms of total suction potential and volumetric water content.

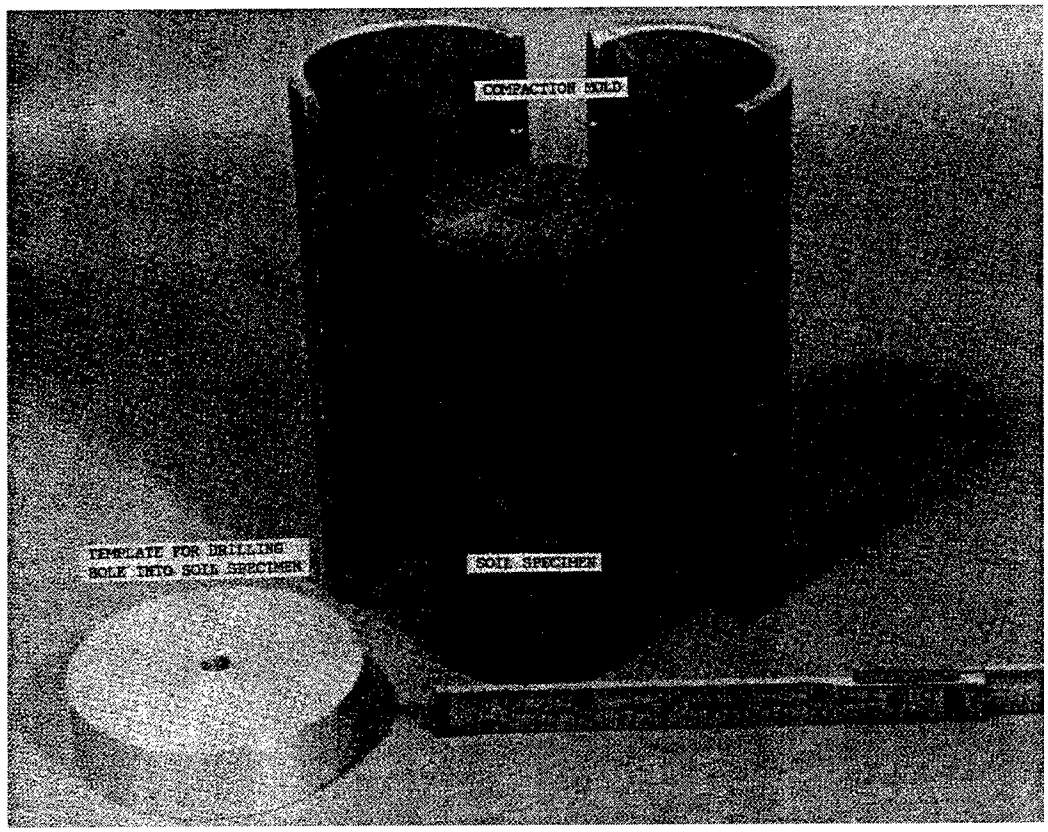

Figure 6-26: Compacted specimen of Buckshot Clay (after Peterson, 1990)

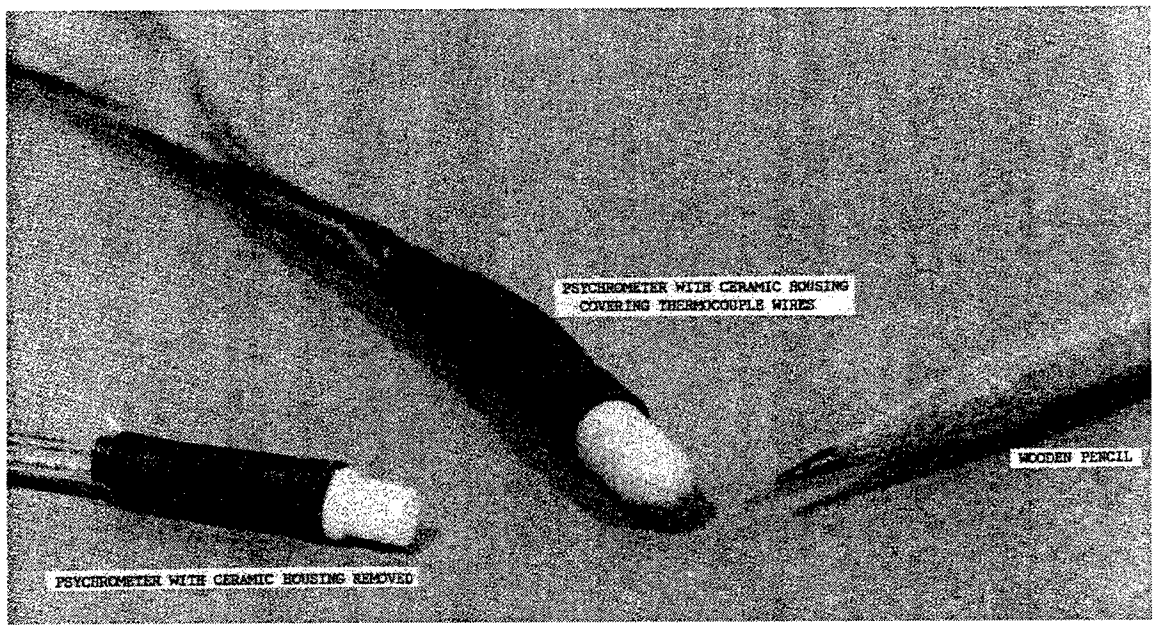

Figure 6-27: Illustration of psychrometers used in triaxial specimens to measure total suction in the Buckshot clay (after Peterson, 1990)

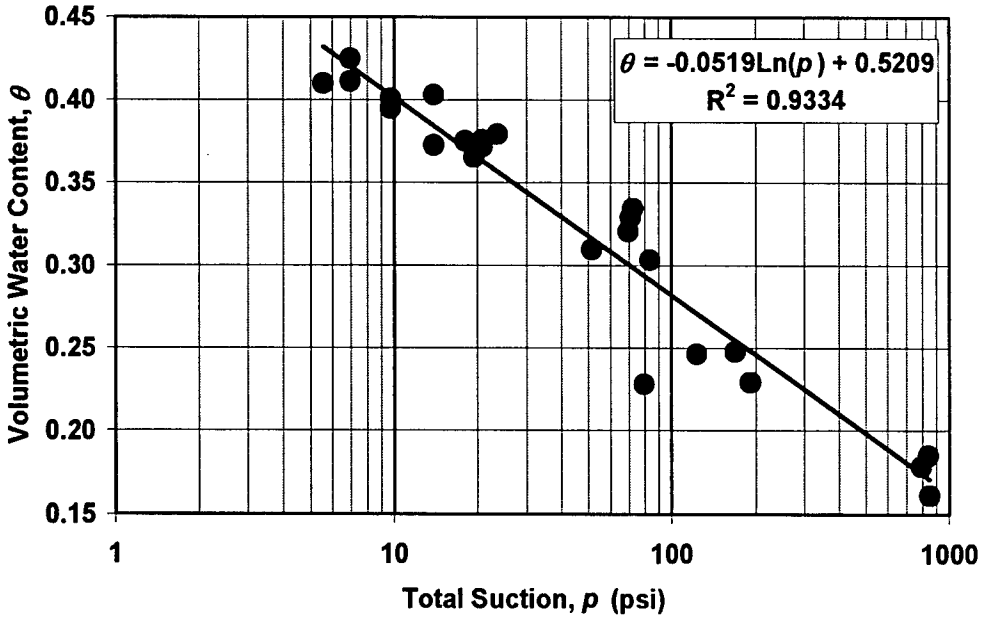

Figure 6-28: Volumetric Water Content versus Total Suction Data (from Peterson, 1990)

6.13 Free Swell and Constant Volume Swell Tests

A series of free swell (FS) and constant volume (CV) swell tests were conducted in order to estimate the role that water content plays in the constitutive response of the CH soil. The FS test would indicate the volume change-water content or similarly strain-suction coupling and the CV test would indicate the stress-water content or similarly the suction-swell pressure coupling.

Tests were based on modifications of ASTM D 4829, developed by Snethen et al., (*1977*) using available electronic consolidation apparatus at ERDC. The purpose of the laboratory tests was not to determine an expansion index or other empirical property, but to document the measured stress and strain responses experienced by the Buckshot clay when wetted from an unsaturated condition.

Each swell specimen tested originated from an extruded 4 inch (101.6 mm) diameter by 4.58 inch (116.4 mm) proctor sample prepared during the compaction process documented earlier. From each proctor specimen, two to three specimens 2.5

inch (63.5 mm) diameter by 0.98 inch (24.9 mm) tall swell were carved to fit within a stainless steel consolidation ring. Specimen shape for swell tests differed from triaxial specimens. Rather than a tall, slender specimen suitable for strength estimation, a short, wide specimen was used for swell tests that would provide ready water access. The test plan called for specimens at three different water contents (15, 19, 23%) at modified proctor energy, two different water contents (23, 25%) at standard energy and a single water content (25%) at light standard energy.

Specimens were trimmed beginning with the top, or alternatively the bottom, of a proctor specimen depending on the orientation in which the sample was sealed and delivered to the tester. Once the first specimen was trimmed, the second was begun at the ending depth of the first specimen. In general, three specimens were obtained from each proctor sample, allowing approximately 0.5 inch of excess to be trimmed for each specimen. For the standard proctor energies, three lifts are used in the compaction process. Therefore one specimen was cut from each lift. For the modified compaction specimens, five lifts are used. As a result, each swell specimen is from a portion of more than one lift. This means some specimen variability due to transitions between lifts.

Figure (6-29) shows dry densities and gravimetric water contents of swell specimens in relation to the proctor density curves. There is wide variation when compared with the proctor density curves due to variability in specimen densities between lifts. Proctor compaction density is very repeatable for a single operator showing much less variability than observed for the swell test specimens. However, it is possible that if each lift in a proctor mold is studied for its own independent density, the outcome would be much more variable, as each compacted lift can vary in thickness which affects the compaction energy absorbed. Lower lifts in the mold receive a higher compactive effort due to residual compaction of higher lifts in the mold causing more energy to be stored allowing density to vary as a function of lift location.

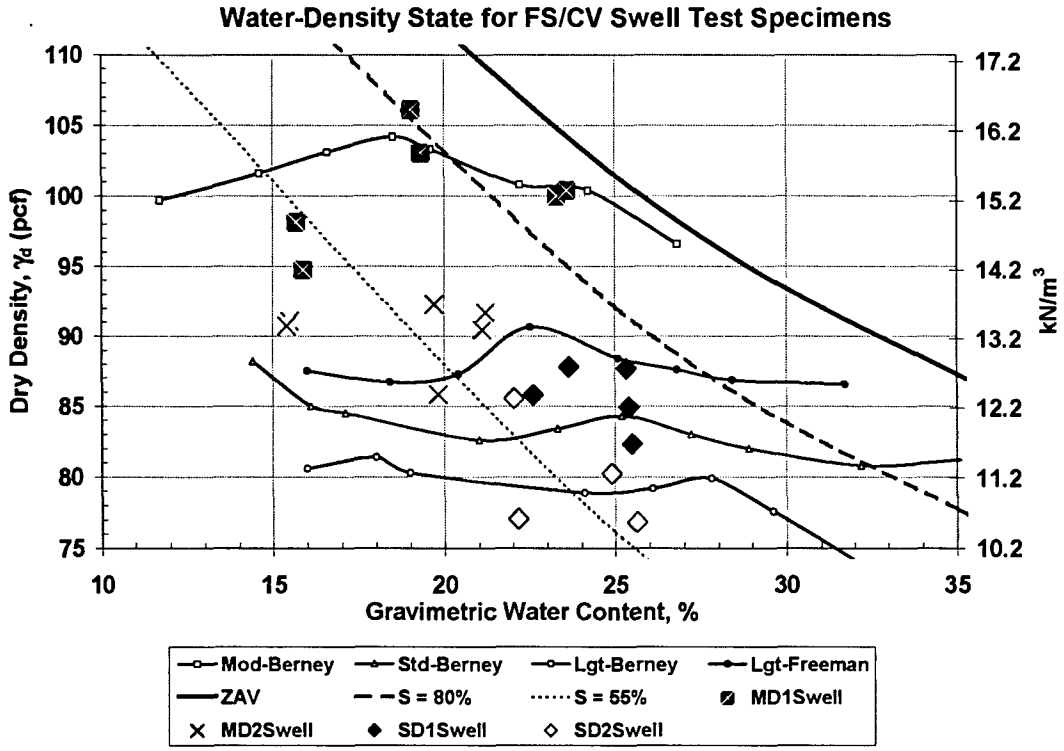

Figure 6-29: Water-Dry Density Conditions for Free Swell and Constant Volume Swell Test Specimens Prior to Inundation

Once the specimens were trimmed, they were weighed and height and diameter were measured. Trimmings were used to estimate initial specimen gravimetric water content. Subsequently filter paper and porous stones were placed on top and bottom of the specimen (Figure 4-9). The consolidation ring, filter paper and porous stones were mounted in a Plexiglas container allowing wetting of the specimen by immersion in a water bath Figure (6-30). The Plexiglas container was then placed in an electronic LoadTrac consolidometer shown in Figure 6-31. After seating, the loading ram was lowered onto the top of the specimen and a small seating pressure of either 0.7 psi or 1.4 psi (4.82 or 9.64 kPa) was applied. This seating load was held constant for approximately 15 to 30 minutes to allow for any axial strain due to the seating load application.

For the CV test, the loading ram was locked into place so no further axial strain could occur during testing. The Plexiglas container was then flooded with distilled water to a level such that the top of the specimen was covered by approximately 0.125 in. (3 mm) of water. This allowed water to infiltrate the soil from both the top and bottom of the specimen. The increase in pressure reacting against the loading ram with time as the specimen began to imbibe water was recorded. The test was allowed to continue for approximately 7 days or until the differential increase in swelling pressure with time reached an asymptotic response.

For the FS test, the loading ram was free to move so piston pressures would not exceed the seating load. The Plexiglas container was then flooded with distilled water as in the CV test. A software program monitored the changes in axial strain as the specimen imbibed water operated a motor controlling the ram location to maintain a constant vertical soil pressure equivalent to the seating pressure on the sample at all times. The test was allowed to continue for approximately 7 days or until the differential axial strain increase with time reached an asymptotic response.

At this point both tests were considered concluded and their containers drained of water prior to unloading so that no additional water would be drawn into the specimens. The specimens were unloaded, removed from the consolidation apparatus, extruded from the consolidation ring and the entire specimen was weighed and dried to determine the end of test (final) water content.

Test results are presented in Tables 6-4 and 6-5. Suction values are estimated from the psychrometer data in Figure 6-28. For the FS test, the axial strain has been converted into a volumetric response reported as void ratio and changes in void ratio referenced as volumetric strain for compatibility with model calculations. For the CV test the equivalent swell pressure represents the differential pressure generated between the final measured pressure due to saturating the specimens and the initial seating pressure. Figures 6-32 and 6-33 illustrate the trend in behavior observed for the key measured values of the FS and CV tests and are summarized by a simple linear regression through the data points. These values will be revisited later in this thesis for the purposes of calibrating the MMM.

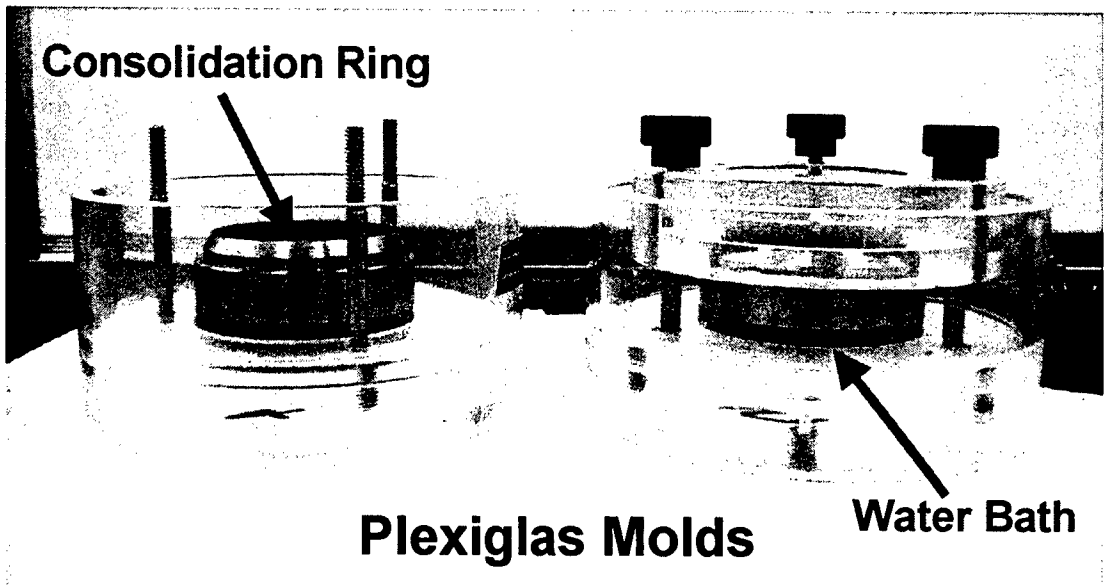

Figure 6-30: Mold set-up for constant volume and free swell tests

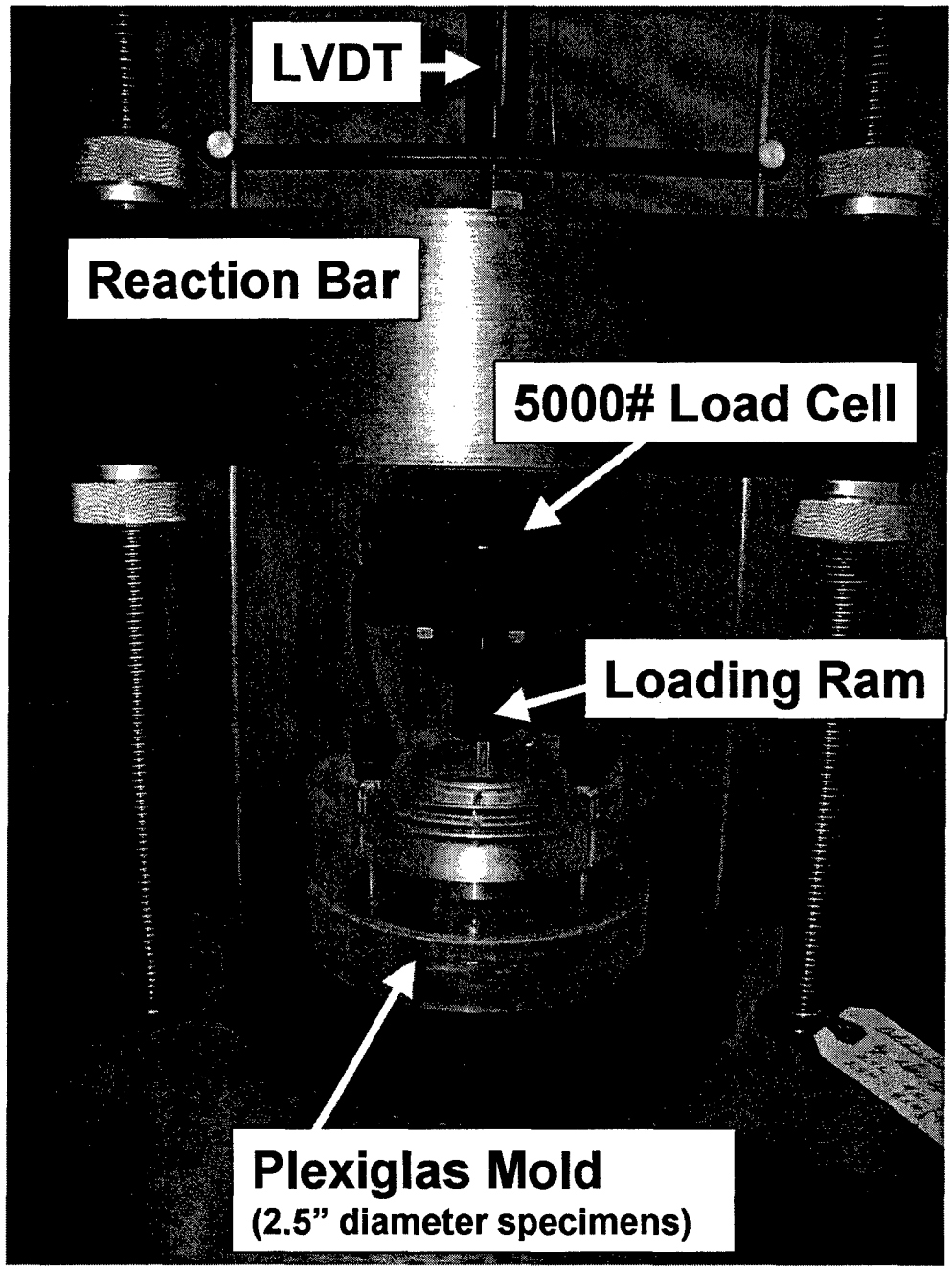

Figure 6-31: Electronic Consolidation Apparatus for Constant Volume and Free Swell Test Specimens

Table 6-4: Summary of Swell Pressure for Constant Volume (CV) Tests and Volumetric Strain for Free Swell (FS) Tests

Series 1	Plot Code	Initial Water Content %	Initial Confinig Pressure psi	Initial Dry Density pcf	Initial Void Ratio eo	Final Void Ratio ef	Change in Void Ratio Ratio	Volumetric Strain %	Measured Swell Pressure psi	Equivalent Swell Pressure psi
MD15CV-1	M15	15.68	1.389	98.13	0.7423				104.40	103.01
MD15FS-1		15.88	1.389	94.76	0.8043	1.0897	0.2854	15.82		
MD19CV-1	M19	19.03	1.389	106.12	0.6112				73.50	72.11
MD19FS-1		19.32	1.389	103.05	0.6592	0.9638	0.3046	18.36		
MD23CV-1	M23	23.27	1.389	100.00	0.7098				41.90	40.51
MD23FS-1		23.57	1.389	100.39	0.7032	0.8257	0.1225	7.19		
SD25CV-1	S25	25.40	0.695	84.94	1.0130				21.11	20.42
SD25FS-1		25.50	1.389	82.34	1.0764	1.1959	0.1195	5.76		
SD25FS-11		25.34	0.695	87.70	0.9496	1.0397	0.0901	4.62		
SD23CV-1	S23	22.58	1.389	85.80	0.9928				13.67	12.28
SD23FS-1		23.64	1.389	87.80	0.9473	1.1701	0.2228	11.44		
LS25CV-1	L25	23.67	0.695	80.15	1.1333				3.11	2.42
LS25FS-1		23.74	1.389	74.32	1.3006	1.4194	0.1188	5.16		
Series 2										
MD15CV-2	M15	15.50	1.389	91.06	0.8776				145.61	144.22
MD15FS-2		15.40	1.389	90.74	0.8843	1.2739	0.3896	20.68		
MD19CV-2	M19	19.80	1.389	85.83	0.9921				73.72	72.33
MD19FS-2		19.70	1.389	92.27	0.8530	1.1475	0.2945	15.89		
MD21CV	M21	21.10	1.389	90.44	0.8905				88.22	86.83
MD21FS		21.20	1.389	91.69	0.8647	1.1477	0.283	15.18		
SD25CV-2	S25	25.64	1.389	76.83	1.2254				18.33	16.94
SD25FS-2		24.91	1.389	80.25	1.1306	1.2981	0.1675	7.86		
SD23CV-2	S23	22.14	1.389	77.08	1.2183				17.01	15.62
SD23FS-2		22.02	1.389	85.57	0.9982	1.1381	0.1399	7.00		

Table 6-5: Summary of Suction, Porosity and VolumetricWater Contents for Free Swell (FS) and Constant Volume (CV) Swell Tests

Series 1	Plot Code	Final Water Content %	Initial Suction psi	Initial Degree of Saturation %	Final Degree of Saturation %	Initial Porosity no	Final Porosity nf	Initial Volumetric Water Content	Final Volumetric Water Content
MD15CV-1	M15	28.38	197.4	57.9	104.7	0.4260	0.4260	0.247	0.446
MD15FS-1		32.10	219.2	54.1	80.7	0.4458	0.5215	0.241	0.421
MD19CV-1	M19	18.52	44.7	85.3	83.0	0.3793	0.3793	0.324	0.315
MD19FS-1		27.31	48.9	80.3	77.6	0.3973	0.4908	0.319	0.381
MD23CV-1	M23	29.09	17.3	89.8	112.3	0.4151	0.4151	0.373	0.466
MD23FS-1		29.12	15.3	91.8	96.6	0.4129	0.4523	0.379	0.437
SD25CV-1	S25	38.00	29.2	68.7	102.8	0.5032	0.5032	0.346	0.517
SD25FS-1		38.16	34.9	64.9	87.4	0.5184	0.5446	0.336	0.476
SD25FS-11		37.00	23.9	73.1	97.5	0.4871	0.5097	0.356	0.497
SD23CV-1	S23	34.64	57.7	62.3	95.6	0.4982	0.4982	0.310	0.476
SD23FS-1		35.98	37.6	68.4	84.3	0.4865	0.5392	0.333	0.454
LS25CV-1	L25	36.33	65.3	57.2	87.8	0.5312	0.5312	0.304	0.467
LS25FS-1		42.86	98.4	50.0	82.7	0.5653	0.5867	0.283	0.485
Series 2									
MD15CV-2	M15	25.00	292.5	48.4	78.1	0.4674	0.4674	0.226	0.365
MD15FS-2		39.00	305.5	47.7	83.9	0.4693	0.5602	0.224	0.470
MD19CV-2	M19	27.60	120.2	54.7	76.2	0.4980	0.4980	0.272	0.380
MD19FS-2		34.50	83.4	63.3	82.4	0.4603	0.5343	0.291	0.440
MD21CV	M21	26.10	63.1	64.9	80.3	0.4710	0.4710	0.306	0.378
MD21FS		34.00	56.5	67.2	81.2	0.4637	0.5344	0.312	0.434
SD25CV-2	S25	34.73	52.1	57.3	77.7	0.5506	0.5506	0.316	0.428
SD25FS-2		36.88	47.7	60.4	77.8	0.5306	0.5649	0.320	0.440
SD23CV-2	S23	32.88	117.6	49.8	73.9	0.5492	0.5492	0.273	0.406
SD23FS-2		32.65	67.9	60.4	78.6	0.4995	0.5323	0.302	0.418

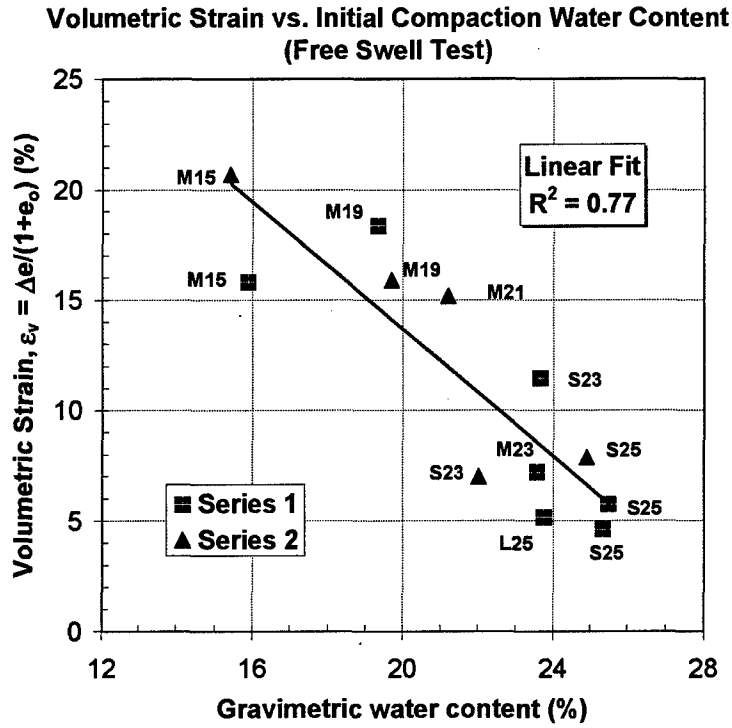

Figure 6-32: Volumetric strain versus Initial Compaction Water Content for Free Swell Test Specimens

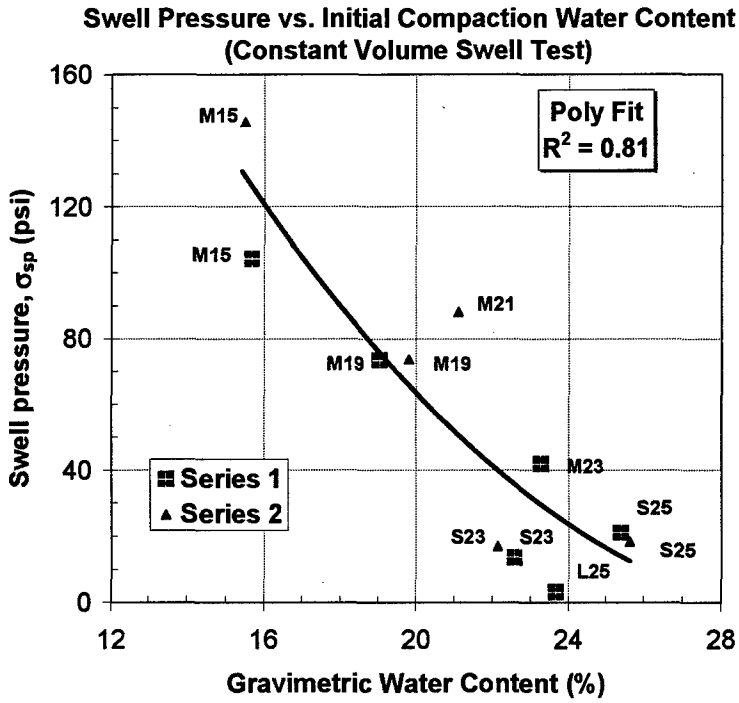

Figure 6-33: Swell Pressure versus Initial Compaction Water Content for Constant Volume Swell Test Specimens

The reversibility assumption between the FS and CV tests in Figure 4-10 suggests that the transfer of free energy from the soil's menisci phase during wetting will be stored elastically within the soil body. This means that a confined specimen of soil under a given swell pressure after wetting should swell to the same axial strain as that of a free swell test. Alternatively, a free swell specimen after reaching its ultimate axial strain after wetting should, when loaded, reach a pressure equivalent to the confined swell pressure when returned to its original volumetric state. In order to determine the reversibility of the free swell-constant volume relationship, the test specimens conducted at 15% water content, modified proctor energy were either consolidated (FS), or allowed to swell (CV) after their respective strain or stress limits had been reached as illustrated in Figure 6-34.

Loading of the FS test was similar to one-dimensional consolidation test and begun after the magnitude of axial swelling was considered complete due to wetting. The test was continued to determine if the consolidation pressure when the sample returned to its initial void ratio matched that of the swell pressure developed during the CV test. As can be seen in Figure 6-34, the pressure reached during consolidation was similar to the swell pressure found in the CV test.

Likewise, the CV test was allowed to swell axially after reaching its ultimate swell pressure to determine if the axial strain upon swelling would equal that of the FS test. It is observed from Figure 6-34 that some hysteresis occurs due to energy losses during the CV test, limiting the magnitude of possible swelling during wetting, as the specimen did not reach the comparable FS axial strain. As an area for future study, this energy loss may be associated with hysteresis in the soil skeleton or accounted for as an additional internal variable associated with volumetric water content. However, this phenomenon will be assumed reversible and linear to simplify calibration of the thermodynamic model.

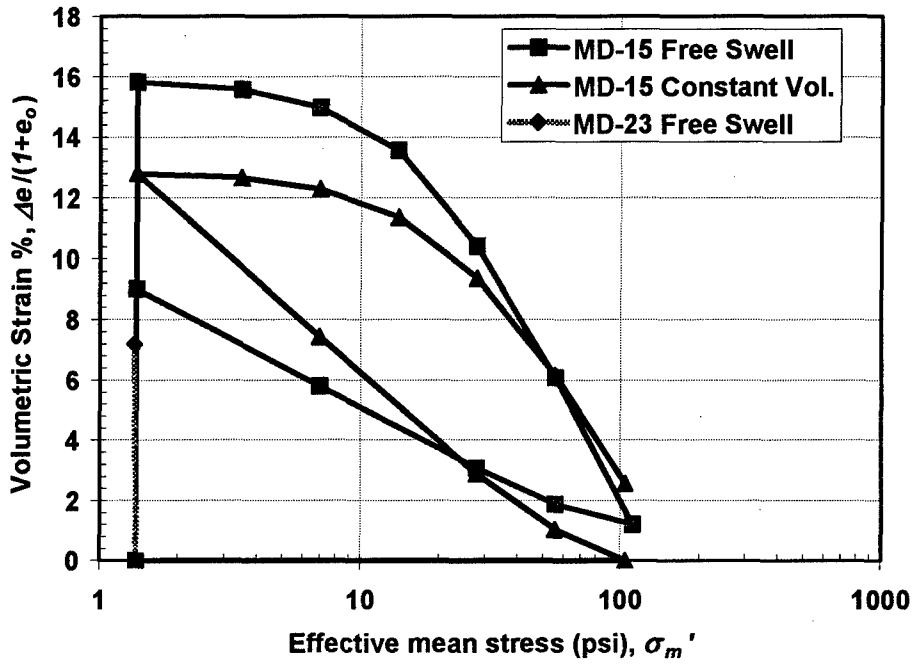

Figure 6-34: Swell and Consolidation of Free Swell and Constant Volume Swell Specimens

CHAPTER VII

Discussion and Analysis of Test Data

The previous chapter described laboratory tests conducted. These tests and data from existing literature provide a broad range of data from which to ascertain the behavior of Buckshot clay. This chapter will address the important features of each group of tests and define the way in which results taken from each test aid in the determining the multi-mechanical model (MMM) parameters.

Calibration of material models requires more skill the more variability present within a material such as a granular or cohesive soil. Materials like metals or polymers have very consistent and well-behaved responses due to the structure of their solids, however soils, while maintaining an inherent consistency in behavior, can produce markedly different responses because of the sensitivity of specimens to their initial prepared condition in the laboratory.

This chapter will also describe the process followed to achieve calibration to fit observed responses of the Buckshot clay. The chapter will also outline the various assumptions made during the interpretation of each set of laboratory data to maintain consistency between laboratory and literature data.

7.1 Index Properties

Data in Table 6-1 was examined to determine if there were any significant differences in Buckshot clay tested and Buckshot clay in the literature. As a first conclusion, the two samples of Buckshot tested and the three samples of Buckshot from literature are deemed fairly consistent by having uniform specific gravity given the changes in borrow pit conditions over a period of twenty years. All the samples exhibit

the same percentage of clay by weight, which is the material most influential in the soil plasticity response. Activity of an illitic clay (such as the Buckshot) has been found to lie between 0.5 and 1.3 (*Holtz, 1981, p. 92*) and an active clay with a tendency to exhibit significant volume change properties as a function of water content is one that has a range of activity between 0.75 to 1. Therefore all the samples exhibit significant levels of activity indicating similar swell/shrink behavior.

Consolidation coefficients are also similar indicating that the Buckshot used in laboratory tests are similar in structural make-up, from one specimen set to another, enabling replication of soil behavior with time. As well, there is similarity in values of compression index, C_c, suggesting that all samples will achieve the same critical state yield response for volumetric stress-strain conditions.

The most noticeable and influential difference in the clay occurs from Peters et al. (*1982*) and Peterson (*1990*) which have a much lower liquid limit and plasticity index than the clay tested. This could potentially reduce the peak shear strength of a triaxial specimen since the lower liquid limit places the clay in a more saturated, weaker condition than a material with a higher liquid limit at identical water content. As well, the magnitude of cohesion is reduced in the lower plasticity samples thus influencing the strength at low confining pressure. The reduced index properties would not adversely affect the suction response since it is primarily a function of moisture, grain size and clay fraction (*Fredlund, 1993*).

Water-density data from Freeman et al. (*2004*) exhibited a larger plasticity range, but was used only to expand the compaction curve ranges shown in Figure 6-3 and are discussed in the following section. However, this data was not used in model parameter calibration.

It is assumed, based on the above discussion, that sufficient evidence exists from these simple index tests, that the data obtained from literature is compatible with date from tested Buckshot clay. As a result, the combined literature and test data are utilized for model calibration.

7.2 Proctor Density

Laboratory compaction curves (Figure 6-2) show that at the varying energies, modified, standard and light, there exists a similar trend in behavior at every level of saturation. There is little difference in densities between standard and light compaction energy. As such, only one test was conducted with a specimen compacted at light energy while the remainder of the laboratory program involved Buckshot clay specimens compacted at either standard or modified energy.

Compaction curves from Freeman (Figure 6-3) illustrate a consistent trend of behavior over intermediate level compaction energies not evaluated in the initial laboratory investigation. There is a close similarity in compaction response at the modified energy where the results of the tested Buckshot (Berney) and that of Freeman coincide showing consistency in the material's moisture-density response. This figure also helps to illustrate the trend in response of the clay as it approaches conditions considerably dry of optimum moisture content and the unique behavior on the wet side of optimum.

Wet of optimum there appears to be a secondary optimum response, which at the present, is a phenomenon not studied for the purposes of this thesis. The reverse trend of increasing density once the sample drops below a critical degree of saturation of approximately 55% was also noted by Toll (*1990*) and is considered in Chapter III as a behavior which is important in the constitutive response of the clay.

7.3 Isotropic Consolidation, 1-D Consolidation

Based on research findings by Peters (*1982*), a good approach to obtaining test specimens whose shear stress-strain response could be replicated was to consolidate each test specimen to a virgin state and then unload and over-consolidate each specimen to a desired initial confining pressure. This technique reduces the influence of non-uniform compaction of replicate specimens

Each specimen was isotropically consolidated to produce specimens that were replicated both in initial state prior to shearing and level of over-consolidation. The isotropic consolidation of each of the triaxial tests enabled the specimens to be brought to very similar void ratios prior to testing. This point is reinforced by the reduced standard deviation between void ratios from an initial compacted state to a final consolidated state shown in Table 6-2. From each of the consolidation plots shown in Figures 6-10 through 6-12, the preconsolidation pressure, σ_p', is approximately 12 to 15 psi. This ensured that all specimens reached a state of virgin consolidation as all the specimens exceeded this pressure prior to shearing. Since each specimen was consolidated to a pressure greater than σ_p', each specimen had an overconsolidation ratio (OCR) (equation 7.1) greater than one.

$$OCR = Maximum\ Past\ Confining\ Pressure/Current\ Confining\ Pressure \quad (7.1)$$

Each specimen was brought to a maximum consolidation pressure of 80 psi and then unloaded to a final confining pressure of 15, 30 or 50 psi producing OCR values of 5.3, 2.67, and 1.6 respectively

The higher the OCR, the greater the specimens tendency to dilate during shear. The lower the OCR, the more the specimen will tend to contract during shear. By producing specimens with a wide range of OCR values, a range of stress-strain response can be demonstrated ranging from contraction to dilation. And greater insight can be provided into Buckshot behavior. This will provide a good test of the MMM's ability to capture the wide range of response possible within this material.

7.4 CU/CD Triaxial Tests

A direct comparison of peak strength behavior in Buckshot clay is difficult because of the tendency for this highly plastic clay to shear-band prior to realizing its ultimate failure state. Shear-banding is the result of a premature failure occurring within the sample during triaxial shear in which a localized plane of weakness or slip plane is generated

(*Skempton, 1964*). A slip plane is a saturated surface passing diagonally through the triaxial specimen that separates it into two angular halves that continue to slide relative to one another without any further change in material behavior with increased loading. This ends the functionality of the test because the strength of the slip plane represents the minimum strength for the specimen under the given confinement. Once generated, no further strength gain, dilatancy or critical state response can be obtained with continued loading. This behavior was exhibited in nearly all the Buckshot triaxial specimens tested and can visually be seen in Figure 7-1. Numerically this is a point where the specimens begin to deviate from the stress path leading to a critical state in Figure 7-2. Shear-banding is evident in the pore pressure response during shearing for the 30 psi and 50 psi confined specimens in Figures 6-17 and 6-19. A large discrepancy between pore-pressure responses and a lack of dilation is a result of premature failure due to shear-banding.

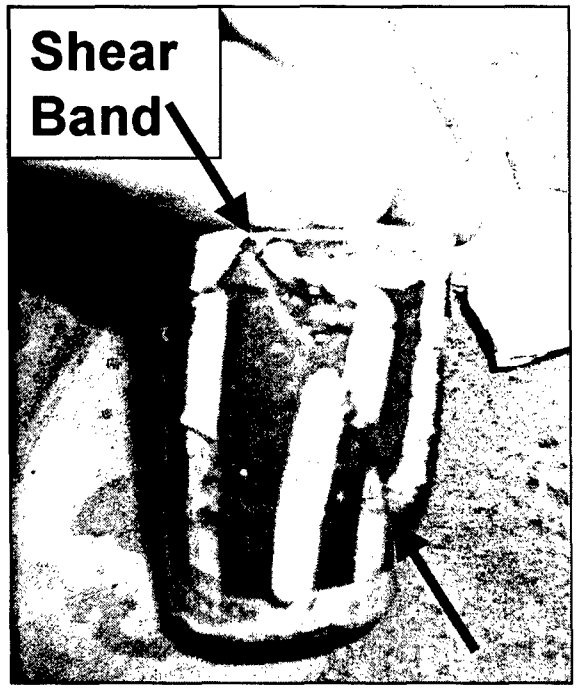

Figure 7-1: Observed shear banding in post-failure Buckshot clay triaxial test specimens

The onset of shear banding dictated the point at which the ultimate shear strength occurred. In Table 7-1 the peak strength data is the maximum value of shear strength obtained in the triaxial test for the points circled in Figure 7-2.

For purposes of calibrating the deviatoric response of the saturated Buckshot clay for the MMM, the 30 psi CU triaxial data (Figure 6-16) was selected as the most representative series to discretize given its reproducible stress-strain response and its proximity to an average confining pressure between all three confining pressures tested. The measured stress-strain, pore pressure, and stress path responses are only valid for conditions prior and up to the onset of shear-banding for calibrating the spring-slider mechanism parameters. Any data obtained beyond the point of shear-banding exhibits a response that relies on unknown mechanisms that interact to produce the localized failure. Since the point at which the shear-banding occurred was similar in terms of peak shear stress and strain for the 30 psi CU triaxial tests and the magnitude of shear strength approaches that of the 30 psi CD triaxial test, this was considered a reliable set of laboratory data to calibrate the Buckshot clay.

The 15 psi tests also provided a consistent set of data for calibration, especially for replicate pore pressure response. However a confining pressure lying between the two extremes was selected as the best representation of the material response. The 15 psi tests will provide a good test set from which to predict response behavior given a calibration using 30 psi data.

By creating specimens with various OCR values, different magnitudes of dilation could be obtained. Assuming that all the specimens begin at the same initial void ratio, those specimens at a lower confining pressure (e.g. higher OCR) will have a greater tendency to dilate or increase in volume during shear inducing a negative change in excess pore pressure. Those specimens at a higher confining pressure (e.g. lower OCR) whose tendency will be to contract will experience a positive change in excess pore pressure. This can be seen in the change in pore pressure with axial strain in Figures 6-15, 6-17 and 6-19. Specimens tested at a high OCR and low, 15 psi, confinement experienced an initial contraction upon loading (positive excess pore pressure change) followed by expansion (negative change in pore pressure) to a final volume greater than

that of the initial specimen. The 30 psi specimens exhibited an initial contraction but at a more gradual rate and then dilated to a slightly lower positive excess pressure than when the test began. And the specimens tested at the lowest OCR at 50 psi confinement, experienced only contraction during shear exhibiting a dilative response only after shear banding occurred.

It is important for the model to capture the changes in strength and volumetric response discussed previously for all the confining pressures exhibited by both the tested data and that by Peters (*1982*). This will lend confidence to the saturated MMM calibration prior to initiating predictions using partially saturated response. Results of these simulations are presented in the Chapter VIII.

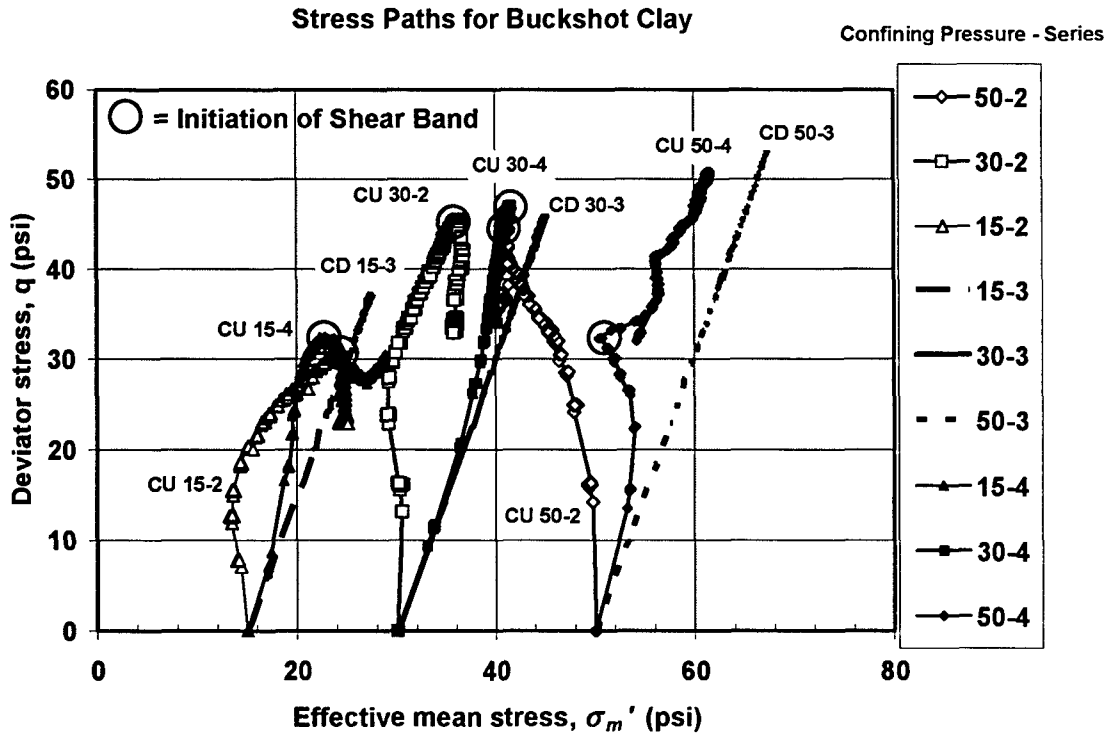

Figure 7-2: CU and CD Triaxial Test Stress Paths and Initiation of Shear Banding

Table 7-1: Summary of CU Triaxial Test Response at Ultimate Strength Conditions

CONDITIONS OF CU TRIAXIAL SPECIMENS AT PEAK STRENGTH

Confining Pressure		Axial Strain	Shear Stress	Mean Stress	Excess Pore Pressure	Shear Strain	Friction Angle	Pe at failure
σ_c'		ε_1	$q = \sigma_1 - \sigma_3$	$p = \sigma_1/3 + 2\sigma_3/3$	u_w	$\varepsilon_q = \varepsilon_1 - \varepsilon_3$	ϕ'	p_e
(psi)	Series	(%)	(psi)	(psi)	(psi)	(%)	(deg.)	(psi)
15	2	6.80	31.06	24.15	-1.20	10.21	31.97	58.78
15	3	15.29	37.32	27.54	0.00	22.93	33.56	55.68
15	4	5.17	32.49	22.83	-3.00	7.75	35.11	58.65
Average		5.98	33.62	24.84	-2.10	8.98	33.55	57.70
St. Dev			3.28	2.43			1.57	1.75
30	2	9.68	45.50	36.17	-9.00	14.52	31.33	73.04
30	3	14.32	45.87	45.29	0.00	21.47	25.68	65.97
30	4	9.71	47.03	41.38	-4.40	14.57	28.54	60.82
Average		9.70	46.13	40.95	-6.70	14.55	28.52	66.61
St. Dev			0.80	4.58		4.00	2.83	6.14
50	2	11.85	46.84	41.51	-24.10	17.77	28.35	71.74
50	3	20.00	53.24	67.45	0.00	30.10	20.41	95.68
50	4	24.05	50.81	61.54	-5.40	24.05	21.28	77.13
Average		17.95	50.29	56.83	-14.75	20.91	23.35	81.52
St. Dev			3.23	13.59			4.35	12.56

7.5 CU/CD Triaxial Tests with Peters data

Figure 7-3 provides a graphical comparison of the Mohr-circle peak shear strengths achieved from the tested Buckshot clay and that by Peters (*1982*). Visually, the Peters sample appears to be stronger than the current research (Berney) by virtue of the greater friction angle, β. This is primarily due in part to the sample preparation prior to conducting the triaxial tests. Peters used a slurry consolidation technique to minimize inhomogeneities within the specimens while Berney used a compaction technique that introduced more heterogeneity to each specimen. Both techniques produce specimens requiring a one-dimensional compaction process. The result of these two different material preparations is that the Peters sample shear banded at higher shear stresses giving the appearance of a stronger material as seen in Figure 7-3. In this figure, the Mohr-circle shear strength envelope of the Peters soil passes above that of Berney. However, the strength of a material is also a function of its density (state) and in the case of Peters, the initial void ratio of each specimen was greater for each specimen, thereby creating a higher strength.

To best compare the general behavior of the Buckshot clay, a plot of normalized stress path that accounts for the current state as well as the strength of the material is shown in Figure 7-4. This plot encompasses the six CU triaxial tests, the three CD triaxial tests (represented as points since no data prior to the end condition was recorded) and the CD and CU triaxial tests from Peters. Normalizing their response with respect to their reference pressure, p_e, (equation 4.105) reveals general trends in behavior that begin to show the global response of the Buckshot clay.

In Figure 7-4, only triaxial shear response prior to the initiation of shear banding is included and therefore the stress paths all fall short of meeting at a singular critical state point. However, all the stress paths tend toward a singular value representing the critical state, M_c. The range of M_c is shown as the oval shape highlighting the end points of the various tests with values ranging from between 0.77 to 1.27 with an average of 1.02. For the purposes of the model, this provides a reasonable bound to the behavior as it represents the point at which the critical state line (dotted) naturally tends through the data.

Therefore, given the comparison of the tested Buckshot clay to the Peters' data whose material exhibits slightly different plasticity characteristics, there seems to be a good general trend in material response on these normalized plots that will enable a sound calibration of the MMM for prediction purposes. The intent of the MMM and its calibration is to obtain model simulations that can predict the trends in behavior that match those of a soil of interest. Since the soil has inherent variability as evidenced by the data, then this should test the ability of the model to simulate response based on calibration from a variety of data sets.

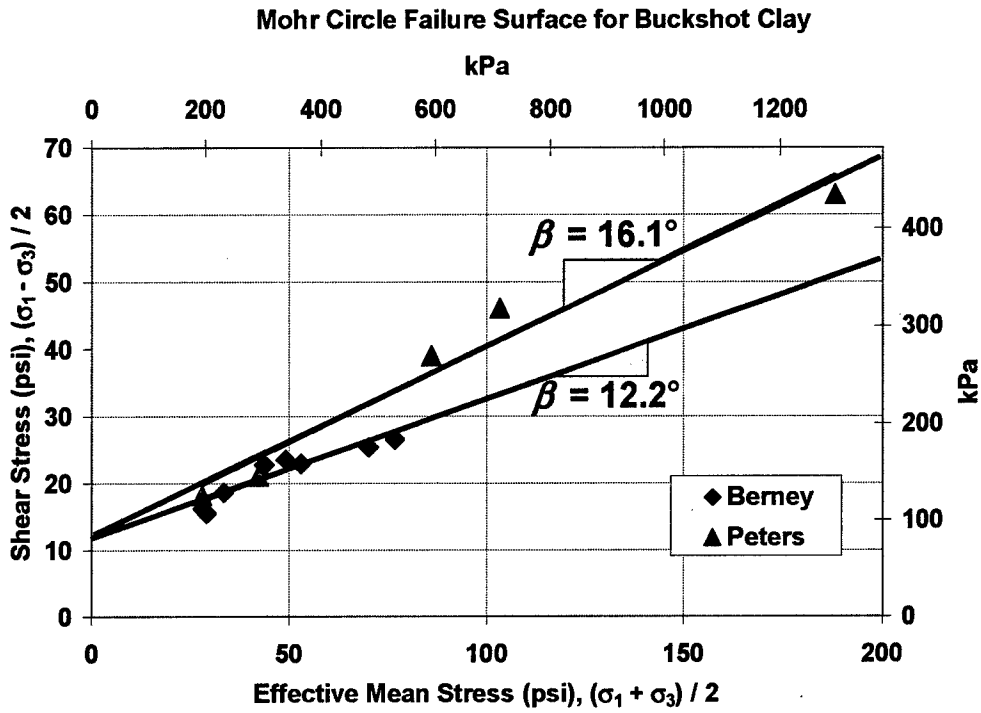

Figure 7-3: Mohr Circle Envelopes for Peak Shear Strength for Peters and Berney Buckshot Clay Specimens

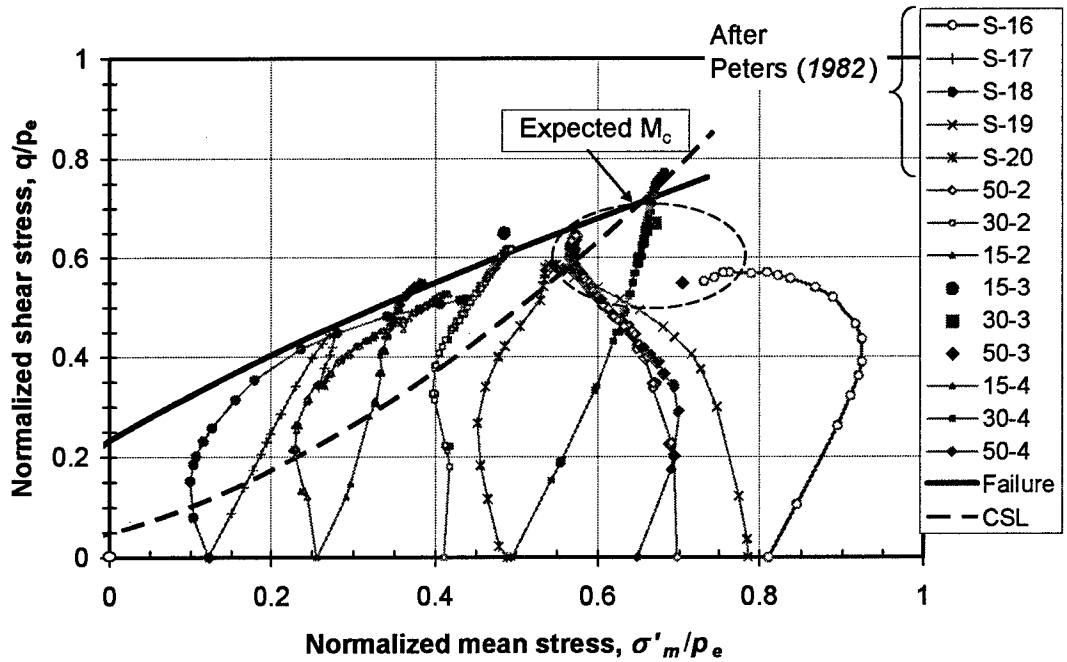

Figure 7-4: Normalized Stress Path with Overlain Failure Surface and Critical State Line used in MMM Calibration

7.6 Psychrometer Test

Analysis of data obtained from Peterson (*1990*) indicates there is a strong correlation between volumetric water content of the soil and magnitude of suction potential present within the Buckshot clay (Figure 7-5). This figure shows a regression of the logarithm of suction versus the arithmetic value of volumetric water content, θ. A very high coefficient of determination, R^2, is obtained indicating that the correlation between the two variables is strong enough to consider for modeling purposes.

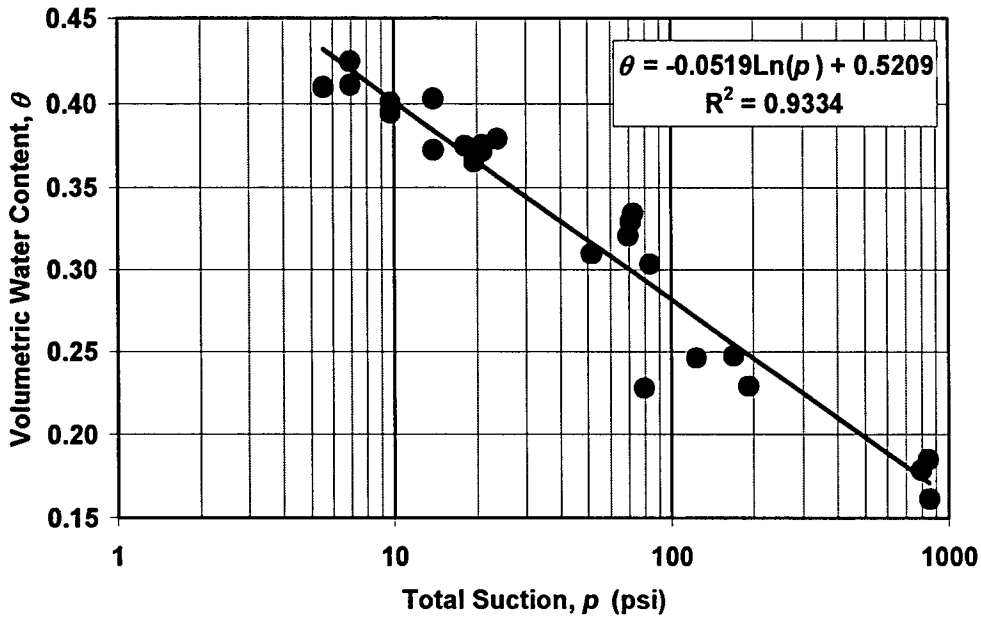

Figure 7-5: Volumetric water content versus suction with log-linear regression

7.7 Free Swell (FS) and Constant Volume (CV) Swell Tests

The Constant volume swell tests were conducted on light (L), standard (S) and modified (M) proctor energy compacted specimens to evaluate the swell potential over a large range of densities and water contents. Results of the CV tests shown in Figure 6-32 reveal a linear trend whereby the swell pressure increases as the gravimetric water content decreases. Scatter in the data found in Figure 6-32 is a result of the sensitivity of

volumetric water content in estimating suction potential. Any discrepancy in the measure of total specimen volume will affect θ. This will result in a magnification of the error seen in the suction estimate taken from the semi-logarithmic plot given in Figure 7-5.

The linear observation was used in development of the thermodynamic model, i.e. that volumetric water content and swell pressure should be inversely related. As seen from the psychrometer test data in Figure 7-5, suction potential increases as water content decreases, and by setting the water content as a constant between the FS and CV tests, there exists a relationship between the swell pressure and the suction potential as described in Chapter IV. This relationship is further observed in the plot relating the suction potential to swell pressure reduced by a square root factor shown in Figure 7-6. The square root factor is used to evaluate the K modulus ratios derived in the equality expressions presented in Chapter IV.

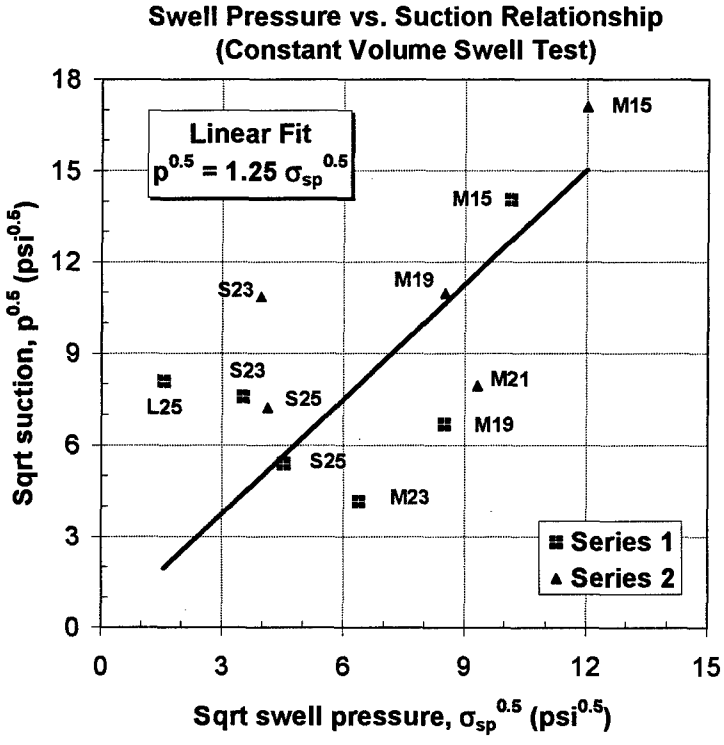

Figure 7-6: Constant volume swell pressure relationship visualized from laboratory data

Linearity of the relationships were applied by using the simplifying assumption that the suction potential versus swell pressure is a reversible process. As long as volumetric water content is defined within the soil, a suction or swell pressure can be defined independent of past history and the change of either variable with water content will obey the derived relationships. The limitation to this assumption is that the definition of suction will always be defined by the drying curve given in Figure 7-5, which represents an upper bound. Hysteresis in the drying and wetting cycles will reduce suction, thereby altering the strength and volume change response. It is therefore possible that the constitutive model may over-predict the potential strength and volume change associated with volumetric water content with cyclic wetting and drying. However, the internal variables are coupled in the constitutive response and may account for any observed hysteresis.

The Free swell tests were conducted on light (L), standard (S) and modified (M) proctor energy compacted specimens to evaluate the swell potential over a large range of densities and water contents. Figure 6-32 shows the results of two replicate tests conducted at various water contents for the three proctor energies. The first trend noted is that as the gravimetric water content decreased, the magnitude of volumetric swell increased for each compaction level. Of interest, is that almost independent of compaction level, the volumetric strain is related to the water content of the specimen. This is shown by the similar magnitudes of volumetric strain for each modified/standard energy pair of data for specimens both wet and dry of optimum moisture content. For example, at 23% water content, the standard test is dry of optimum (25%) and the modified test is wet of optimum (19%) but both yield similar volumetric swelling strain. A similar result is found between the standard and light energy specimens at 25% water content. In neither case is the magnitude of swell significantly different, given their relation to the compaction curves shown in Figure 6-29. This suggests that the use of water content as an independent variable controlling constitutive response of a soil is a valid assumption based on the observed behavior.

7.8 Modified Q Tests

From 2 to 3 series of 15 different permutations of Modified Q-tests as defined in Section 6.11, were conducted covering three confining pressures, 3, 10, and 30 psi and five water contents, 21, 23, 25, 32, and 40%. All specimens were trimmed from Buckshot clay samples compacted at standard proctor energy. For each of the specimens, peak shear strength was recorded and a plot of the average shear strengths in relation to the confining pressure and water content are shown along with the dry density of the specimens in Figure 7-7.

The shear strength beginning on the wet side of optimum ($w > 25\%$) gradually increases with a combination of decreasing water content and increasing dry density until optimum ($w = 25\%$) is reached. After optimum, as the dry density begins to decrease with a further reduction in water content, the strength declines and has a magnitude dependent on the confining stress. Lastly, for the two higher confined specimens a second increasing strength trend is observed once the specimens reach a point where dry density once again increases with a reduction in water content. Work by Seed, et al., (*1959a*) on shear strength of cohesive soils demonstrated trends in shear strength for Q-tests conducted at a zero confining pressure that are very similar to the one observed for the 3 psi confined specimens.

Of interest is the trend of the secondary strength increase at very low water contents for the higher confined specimens. It is supposed that the strength gained from suction potential at lower water contents due to an internal confinement on the grain structure is offset by the more granular texture clays exhibit when dried below optimum moisture and (*Brackley, 1975*). It has been noted that at saturations less than 55%, suction no longer acts uniformly in the soil reducing its strength potential. However, because of the tendency of dry clay to behave as a granular, sand-like material, the confining pressure can have a greater effect on the frictional strength response and provide the secondary strength increase observed in the 10 and 30 psi confined specimens. What this suggests is that in a partially saturated soil, when the water content of the specimen is such that it no longer hinders compaction on the dry side of optimum

(a local minimum in the density), the structure becomes granular and strength is principally derived from the frictional capacity of the soil (*Berney, et al., 2003*).

To compare replicate behavior for the various Q tests, Figures 6-20 to 6-25 show the axial strain-shear stress response for all of the test configurations. All the specimens for the first series were prepared with the first sample of Buckshot clay. The second and third series of specimens were prepared from the second sample of Buckshot clay. All specimens show good consistency between replicates in that for each configuration, a similar pattern of constitutive response is observed. For each water content tested, the higher the confining pressure, the higher the ultimate shear strength. This result was expected because of a similar trend observed with an increase in shear strength with confining pressure found in the CU triaxial tests. Lastly, strain-softening behavior was observed at the lowest confining pressure for water contents equal to or less than optimum (25%), similar to that of the saturated CU tests.

Of importance to note is that for the 21 and 23% moisture content specimens, little difference exists in the constitutive behavior between series suggesting a good repeatability. However, both the 25 and 32% water content tests experience a dramatic increase in peak strength from the first series to the second and third. The liquid limit and plasticity index are lower for the second Buckshot sample, indicating potential for a higher strength even given the similar classification and swell behavior (*Mitchell, 1976*). This is typical of the behavior of soils, where one sample can exhibit properties slightly different from another. For the Buckshot, since no saturated triaxial tests were conducted on the second sample, the indication of improved strength could not be estimated from merely changes in Atterberg limits.

The importance of these strength differences will be discussed in further detail concerning the model simulations in the Chapter VIII. The Q-tests are the validation tests for the constitutive model based on calibration efforts from laboratory tests discussed previously. Ability of the model to capture stress-strain behavior of the Buckshot clay given varying moisture contents and confining pressures without using tests of that nature to calibrate the material will provide a means to evaluate the robustness of the model. As

well, the ability to discern between two samples of clay to show the model sensitivity to its initial calibration will be illustrated.

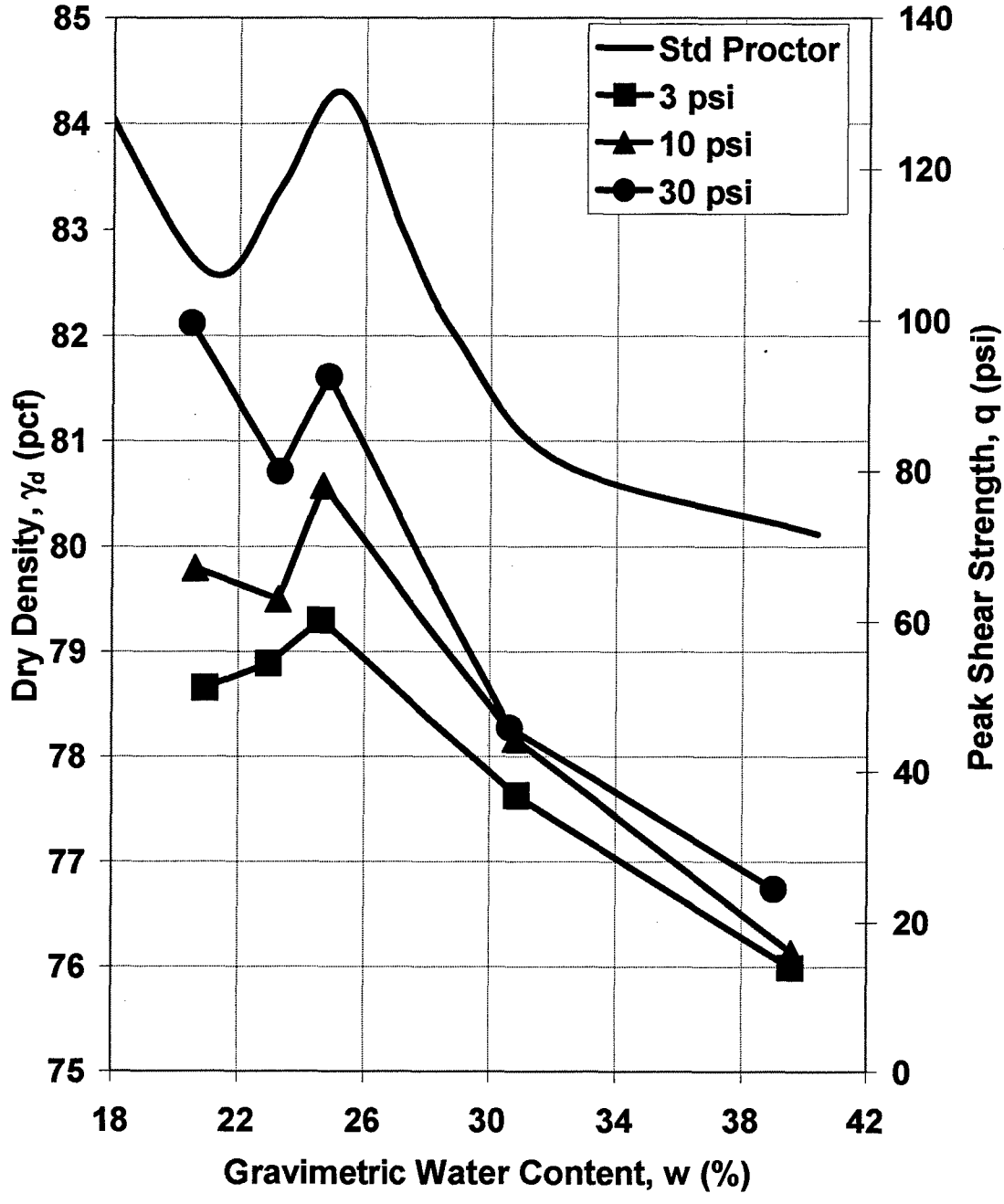

Figure 7-7: Comparison of average Q-Test shear strengths with relation to the standard proctor compaction curve

CHAPTER VIII
Calibration and Verification

8.1 Approach

In Chapter V the global and mechanism parameters for the PS-MMM were introduced that must be calibrated in order to perform simulations using the constitutive driver. Chapter VI outlines were provided of the test plan and acquisition of laboratory data to be used in the calibration and analysis. In Chapter VII, data reduction required to determine the calibration parameters were described. This chapter is divided into two parts. The first half uses the information and parameter definitions given in the previous chapters to determine the magnitude of the global and mechanism parameters that define the Buckshot clay in the PS-MMM. The second part presents the simulations on saturated CU and CD triaxial tests, followed by simulations of partially saturated FS and CV tests, and verification tests on partially saturated CU triaxial tests.

This chapter brings together the knowledge and formulation from the previous chapters, applies them through a constitutive model simulations that are directly compared to their laboratory counterparts. The success of the model formulation will be discussed along a discussion of preliminary conclusions.

8.2 Calibration of Global Parameters

There are eighteen global parameters required for the calibration of the PS-MMM. These parameters are listed in Table 5.1 and described in detail in section 5.4.3. A summary of the values obtained for use in the thesis simulations is provided in Table 8.1. Following is a detailed discussion for the determination of each global parameter.

Table 8.1: Summary of input values for global MMM properties

POISSON	0.25	EREF	1.454
CR	0.011	BETA	3.154
PHILIM	42	GAMMA	0.25
PHIRATIO	0.619	BETAS	0.75
DECAY	1.5	BETAH	0.4
PSIMAX	60	Pr	22000
PSIMIN	1	Kappa	-0.0519
DECAY V	0.5	Alpha	0.25
a	0.2	Lambda	0.3

8.2.1 Yield Limits

PHIMAX, PHILIM, *a*, and DECAY

To determine the Buckshot clay yield conditions, a concave downward yield surface has to be defined based on the max/min friction angles, a parabolic curvature parameter Decay and the normalized cohesion intercept, *a*. Figure 8-1 presents all the normalized triaxial stress paths for both the tested Buckshot (Berney) and those from Peters (*1982*). The solid line represents the failure envelope as calculated from the parameters given in Table 8.2:

Table 8.2: Yield Limit Parameter Values

Code Name	Symbol	Value
PHIMAX	ϕ_{max}	42°
	ϕ_{min}	26°
PHIRATIO	ϕ_{min}/ϕ_{max}	0.619
DECAY	Decay	1.5
a	*a*	0.2

The purpose of selecting these values was to describe an envelope that provided an upper bound to all normalized stress paths ensuring that they were encompassed within the yield surface and that its shape followed the curvature dictated by the stress paths.

To compare the friction angles determined from the yield surface to those determined from a linear Mohr circle envelope, Figure 8-2 shows that average friction angles at the peak strength are 16.8 and 12.5 degrees for data by Peters (*1982*) and Berney respectively. These values fall far short of the max/min limits imposed on the model. This is most likely due to the shear banding effects whose response falls outside the bounds of the stress-strain relationship as described in Chapter VII. The friction angle measured at the ultimate state for each sample was premature due to the effects of shear banding and early collapse of the soil. Therefore, the maximum friction angle should exceed that of the measured value. This is accounted for by ensuring that the failure envelope at least encompasses and possibly exceeds the strength given by the stress paths that have not yet reached a critical state.

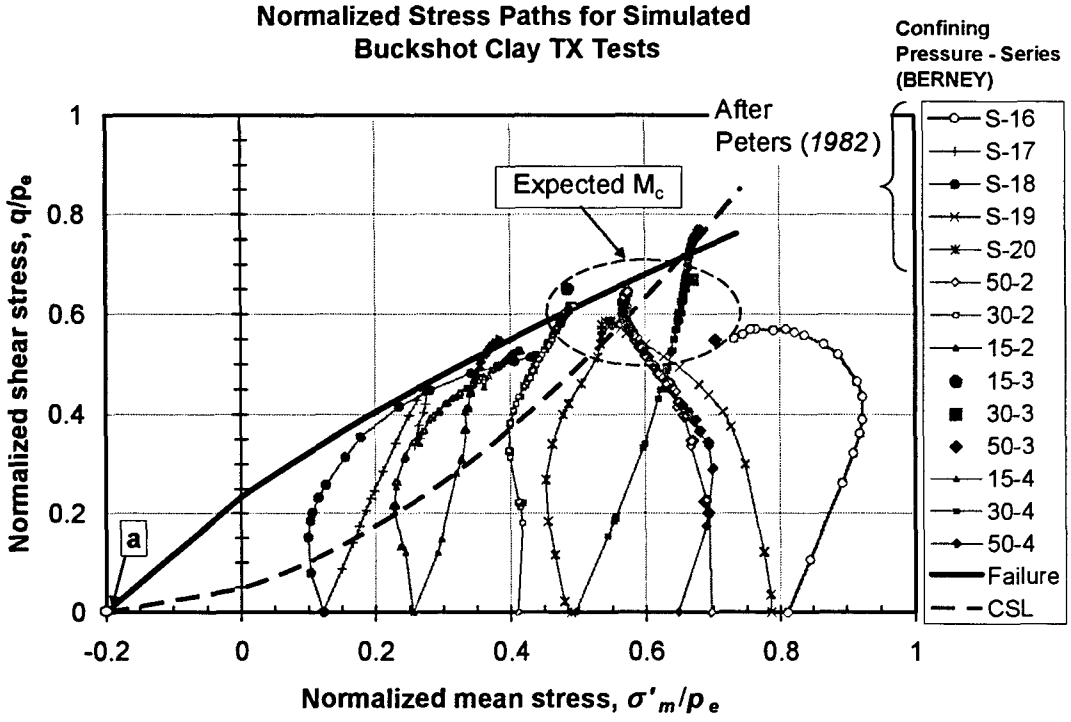

Figure 8-1: Normalized Stress Paths and Failure Envelope from Calibration Data

The normalized cohesion, a, represents the mean stress offset that shifts the failure surface to a tensile limit which produces a traditional cohesive intercept at a condition of zero mean stress, which is found along the normalized shear stress axis, q/p_e. Influence of cohesion on soil shear strength is most noticeable during the early shear strain response of the loading cycle. By varying the normalized cohesion to aid in fitting the early stress-strain response, a value of $a = 0.20$ was found to provide the best fit for the data from the tested Buckshot and Peters. The value of a is coupled with the failure surface and the value of 0.2 was found to best shape the triaxial yield surface in Figure 8-1 with the friction and decay values found in Table 8.2.

It can be seen from Figure 8-1 that the cohesive intercept for a condition of zero normalized shear stress, q/p_e, is equal to a value of about 0.22. To verify that this value is reasonable from an analysis of triaxial data from the tested Buckshot and Peters, the cohesive intercept found at zero normal stress from a linear regression of the Mohr circle strength envelope from Peters and the tested Buckshot was found to be 12.2 psi and 11.6 psi, respectively in Figure 8-2.

Based on the void ratio of the tested Buckshot, the average reference pressure, p_e (equation 4.105), was equal to 68.6 psi. Taking the ratio between the cohesive intercept and the reference pressure, a normalized cohesion value equal to 0.17 was found. This value is comparable to the 0.22 measured from the normalized stress path plot in Figure 8-1 considering that the ultimate strength of the Buckshot was likely not fully realized due to the occurrence of shear-banding. If this strength was realized it likely would shift the cohesive intercept to a value higher than that measured in the laboratory program bringing the value close to that found in Figure 8-1. Therefore calibrating the PS-MMM to match small stress-strain response using a normalized cohesion made the appropriate correction for the laboratory data which showed a lower strength due to shear-banding.

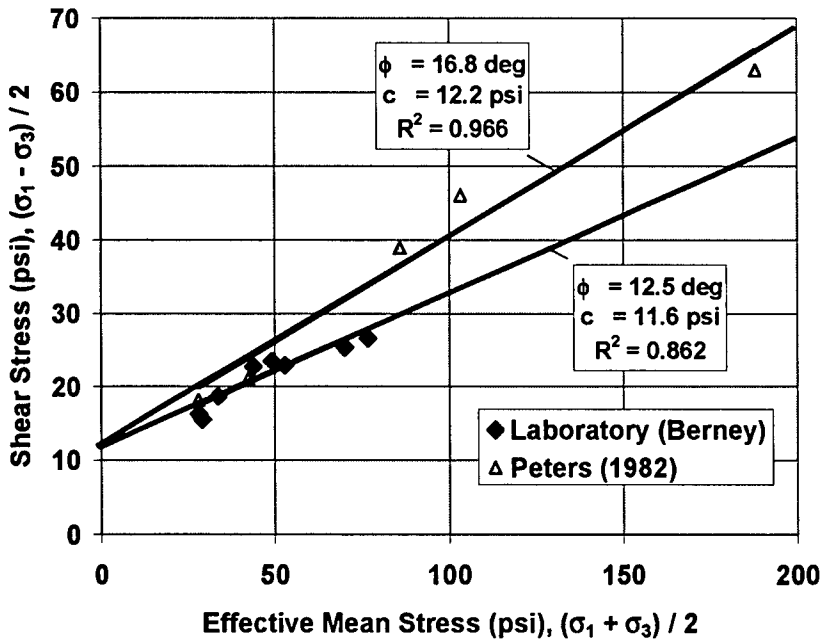

Figure 8-2: Mohr Circle Failure Envelope for Buckshot Clay

8.2.2 Critical State Line

PSIMAX, PSIMIN, and DecayV

In order to represent the critical state line (CSL) for the Buckshot clay, the curvature of the normalized triaxial stress paths given in Figure 8-1 were analyzed. The dotted line represents the concave upward fit of the CSL which must begin at the origin (*a*) and follow through the critical state point, M_c. The trace must pass through the points along individual stress paths at which there is no tendency to dilate or contract. If contraction occurs, the slope of the stress paths tend towards a σ_m/p_e approaching 0 with increase in shear stress. If dilation occurs the stress paths tend in the opposite direction. At the point when neither is occurring, the normalized stress path appears vertical or as a reversal in slope. Therefore these slope reversals represent the change in behavior of the volumetric response which must be approximated by the trace of the critical state line. The parameters that best fit this parabolic shape determined with the software program CModeler (Appendix A), adjusted by DecayV, are given in Table 8.3.

Table 8.3: Critical State Calibration Parameters

Code Name	Symbol	Value
PSIMAX	φ_{max}	60°
PSIMIN	φ_{min}	1°
DecayV	DecayV	0.5

8.2.3 Volumetric Limits

BETA, C_r, EREF and GAMMA

Data taken from the isotropic or one-dimensional consolidation tests provided the necessary parameters to evaluate the volumetric behavior of the Buckshot clay. Considering all the isotropic compression tests conducted during the consolidation phase of the CU triaxial tests given in Table 6-2, an average slope on a semi-logarithmic plot of void ratio versus effective mean stress was 0.325 for the compression index, C_c. Since the data by Peters was also included in the analysis, the compression indices for both the tested Buckshot and Peters were averaged from Table 6-1 to arrive at a more general value of 0.317. This is well within the standard deviation of the mean value from the tested Buckshot. The parameter BETA is defined as the inverse of the compression index and equals 3.154.

The reconsolidation index, C_r, is intended to produce the elastic volumetric response of the soil and is typically found from the unloading response of a saturated one-dimensional consolidation test. However, estimating this parameter during an isotropic or one-dimensional consolidation test proved difficult. For most practical analyses, the value of C_r taken from these plots is satisfactory in estimating volume change since its value is always estimated too high predicting greater volume change and therefore a more conservative value. However, to properly obtain C_r to estimate the elastic bulk modulus, K, stress-strain response taken at a very small reductions in stress beginning at the initiation of unloading the consolidation specimen is necessary. This necessity was discovered over the course of the research since a value of C_r of 0.011 was required to obtain a satisfactory predictive response in both triaxial shear and hydrostatic

behavior. The value is considerably smaller than the value of 0.07 taken from the actual plotted data in Figures 6-10 through 6-12.

The reference void ratio, EREF, is defined as the intercept of the normal consolidation line (NCL) with slope C_c, at a mean stress of 1 psi. Table 6-2 lists all values of EREF taken from isotropic consolidation plots. An average value of 1.454 was selected based on an average of the tested Buckshot and that from Peters.

8.2.4 Partially Saturated Parameters

κ, α, p_r and λ

Calibration of partially saturated parameters is presented via two different means, considering that psychrometer data is or is not available. To determine the calibration tests necessary to account for effects of suction, a combination of tests were used to determine interchangeability of the two approaches.

The modulus K_3^o can be determined directly from a plot of suction versus volumetric water content if such data is available as in Figure 8-4. In some instances, this type of information may not be available as the psychrometer test is not a common test. Therefore, the Constant Volume (CV) and Free Swell (FS) tests coupled with the consolidation test can be used to back out K_3^o by finding K_1^o and K_2^o first and then equating them to K_3^o as described in Chapter IV.

Figure 8-3 shows data taken from Peterson (*1990*) and regressed for purposes of determining K_3^o. From this plot, the reference suction, p_r, defined as the linear intercept on the suction axis, is equal to approximately 22,000 psi. This provides an upper bound to the suction potential. It has been stated, however, that the limitation of the model is that when volumetric water content drops to values below 0.3 (or approximately 55% saturation) the moisture available is no longer uniformly distributed amongst the intergranluar particles, but is contained within a very few tight packets of soil with high suction potential. These packets no longer contribute to the overall strength of the global material.

The slope of the log-linear trend line is known as κ and its inverse is related to K_3^o by equation 4.103:

$$K_3^o = -\frac{1}{\kappa(1-\alpha)}$$

The value of κ from Figure 8-3 is found to be –0.0519.

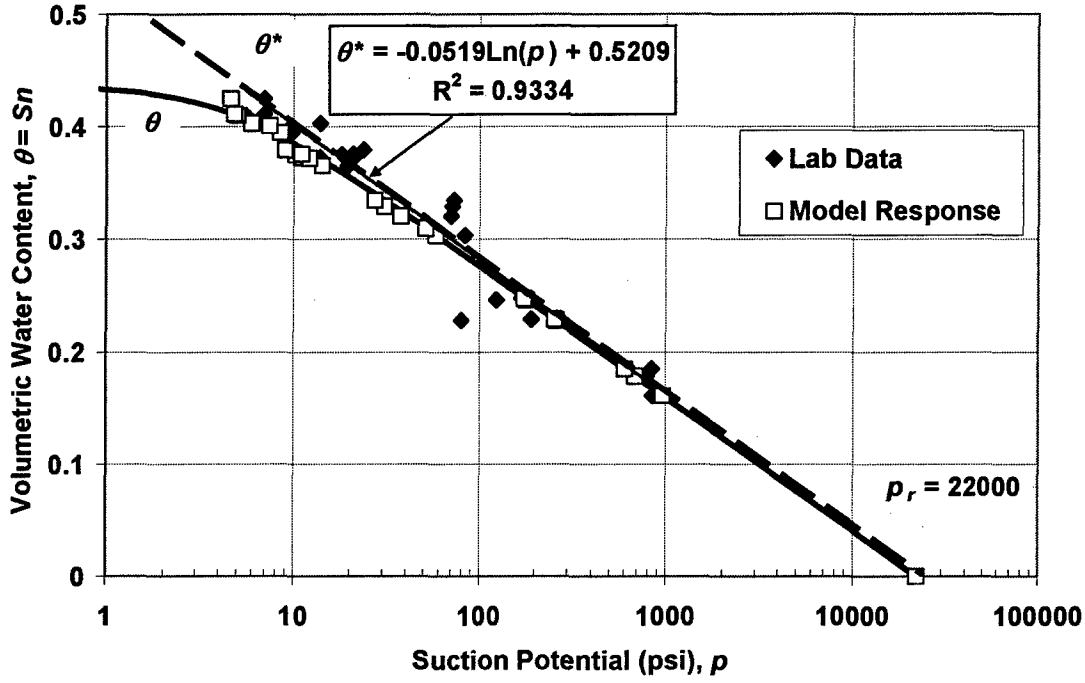

Figure 8-3: Volumetric Water Content versus Suction to determine calibration parameters

The value of α is determined from the relationship between the free swell and constant volume swell test developed in Chapter IV using equation 4.96 below:

$$\alpha = \frac{\exp\left(\frac{2.303}{C^*}\left(e_{sw} - e_f\right)\right) - 0.5}{\exp\left(\frac{2.303}{C^*}\left(e_{sw} - e_f\right)\right) - 1.0}$$

Table 8.4 shows computed values of α obtained by taking swell pressure and volumetric strain data from the series of FS and CV laboratory experiments described in Chapter VI.

Table 8.4: Summary of Free Swell and Constant Volume Swell tests and resulting model parameters

Proctor Energy	Gravimetric Water Content (%)	Q_{sw} (psi)	e_{sw}	e_f	K_1	alpha
MOD	15	104.4	0.8043	1.0897	25.3	0.42
MOD	19	73.5	0.6592	0.9638	23.3	0.43
MOD	23	41.9	0.7032	0.8257	23.9	0.13
STD	25	21.8	1.0764	1.1959	29.2	0.12
STD	25	21.1	0.9496	1.0397	27.4	-0.07
STD	23	13.7	0.9473	1.1701	27.3	0.37
LOW	25	3.8	1.3006	1.4194	32.3	0.12
MOD	15	145.6	0.8843	1.2739	26.5	0.47
MOD	19	73.7	0.853	1.1475	26.0	0.43
MOD	21	88.2	0.8647	1.1477	26.2	0.42
STD	25	18.3	1.1306	1.2981	29.9	0.28
STD	23	17.0	0.9982	1.1381	28.1	0.20
				Average =	27.1	0.28
				Standard Deviation =	2.5	0.17

Data in Table 8.4 shows that all the test sets produce α values that lie within the bounds dictated by the consistency assumption of reversibility between the swell pressure and swell strain such that α is less than or equal to 0.5. However, there exists one data point (STD-25) with a value of α less than zero, which is possible because the assumptions made about the elastic reversibility of the system are made only for model calibration and in actuality the response is likely non-linear owing to the presence of internal variables.

A value of $\alpha = 0.25$ was found to produce the best predicted partially saturated response based on trial and error model experimentation. This value is very close to the average value given in Table 8.4 and falls well within the standard deviation of the observed test results.

Assuming that pyschrometer data is unavailable the value of α can still be obtained from equation 4.96, however κ and p_{ref} must be estimated solely from data obtained from the FS and CV tests.

From equations 4.92 and 4.84 we have that:

$$K_2^2 = \alpha K_1 K_3 \qquad \text{and} \qquad \sqrt{p_{sw}} = \frac{1}{2}\frac{K_3^o}{K_2^o}\sqrt{Q_{sw}}$$

These relationships were arrived at by the condition that there must be a coupling between the volume change and the swell pressure, σ_{sw} response of a material. The governing assumption is that this behavior is recoverable and therefore linear. In actuality, there is an irreversibility between the swell and swell pressure due to the presence of internal variables within the water phase of the material.

The slope κ must be determined from the log-linear relationship between volumetric water content and swell pressure, σ_{sw}, in the same manner as was determined from psychrometer data in Figure 8-4. This is possible because of the equality between suction and swell pressure governed by the constant volume swell relationship (equation 4.84). Only the data pairs which fit along the straight line portion of the response were used to determine the slope κ, since κ ignores the curved response found at low suctions/swell pressures illustrated by the lighter data points.

By this technique, a value of $\kappa = -0.0592$ is found that is similar to the value of $\kappa = -0.0519$ using the psychrometer data. The reference swell pressure, σ_{spref}, was found to be 10,250. The value of K_1^o can be computed from the consolidation test and K_3^o can now be computed knowing κ and α. The compatibility expression:

$$K_2^o = \sqrt{\alpha K_1^o K_3^o}$$

allows a solution to K_2^o.

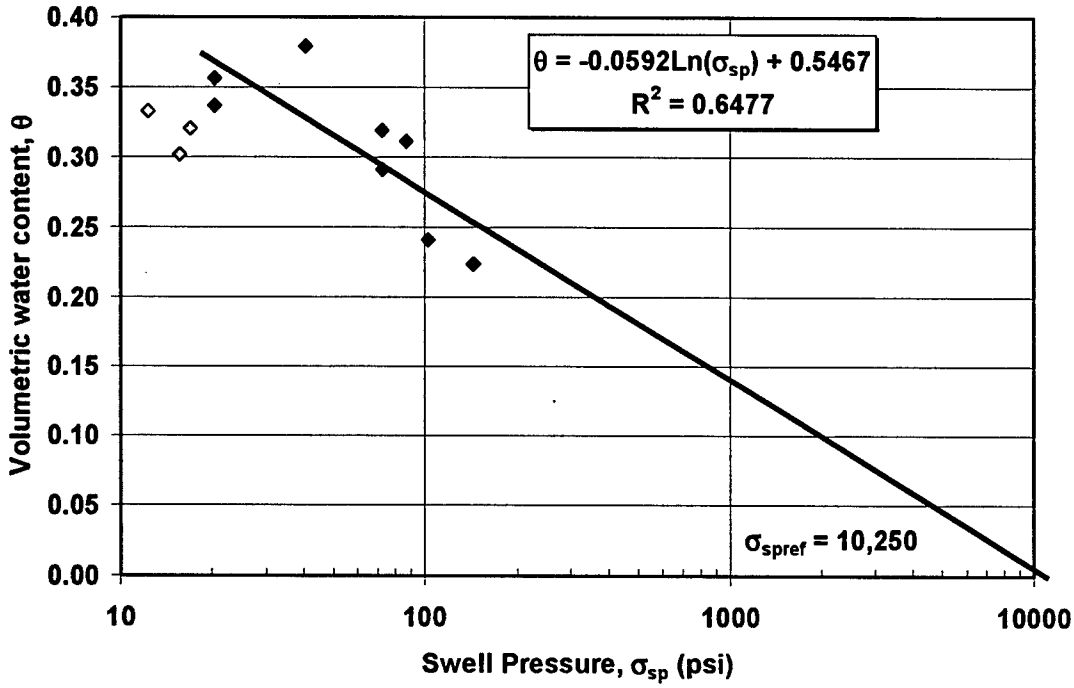

Figure 8-4: Log-linear relationship between Swell Pressure and Volumetric Water Content

Using the relationship between K_3^o and K_2^o from the CV test the reference swell pressure can be converted to a suction reference pressure by substituting in K_3^o and K_2^o and σ_{spref} into equation 4.84. Based on these calculations for $\alpha = 0.25$, a reference suction of approximately 9000 psi is found. Using the $0.5*(K_3^o/K_2^o)$ ratio value of 1.25 obtained from the constant volume swell test (Figure 7-5) a reference suction pressure, p_r, of 16,000 can be estimated. This compares to the reference suction of 22,000 psi found using the psychrometer data. This variability is seen as the greatest limitation of not having psychrometer or some direct suction data because of the error in extrapolating the data on a logarithmic axis. However, since the reference suction far exceeds suction magnitudes typical in compacted fills and the slope, κ, dictates the response, the error in estimating the reference suction should not greatly influence the model response.

Using the standard and modified proctor compaction test data described in Figure 6-2, Figure 8-5 shows the approximation of λ by the technique described in Section 4.5. A straight-line tangent to the dry side compaction curve was taken for both the modified and standard proctor data. Points occurring below a critical degree of saturation (approximately 55%) were discounted in selecting the range of data to draw the tangent because this is the point at which the distribution of suction within the specimen begins to act locally. The value of λ has a range from 0.2 for the modified curve to 0.36 for the standard curve. An average value of 0.3 was chosen for the simulations of both modified and standard proctor swell and triaxial specimens.

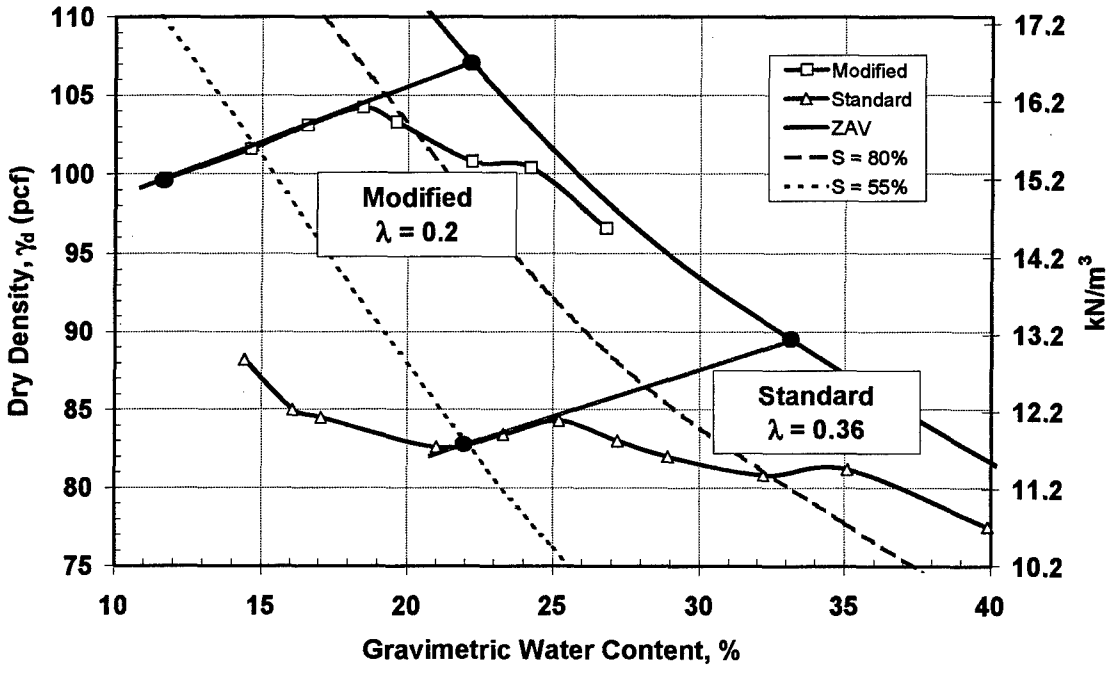

Figure 8-5: Illustration of Lambda coefficients determined from slopes of dry-side Standard and Modified Compaction Curves

8.3 Calibration of Mechanism Parameters

A software program titled CModeler, described in Appendix A, was used to produce a set of mechanism calibration parameters based on the response of a single saturated triaxial test and a single one-dimensional (isotropic) consolidation test. There are 20 distributed material parameters required for calibration of the PS-MMM and are listed in Table 5.2. A summary of the values used in the thesis simulations is provided in Table 8.5.

Table 8.5. Summary of Mechanism property values used in MMM

	PHIFRAC	SHEARRATIO	HLIMIT	BULKRATIO	PFACT
1	0.3418	0.3761	0.1377	0.3094	0.5438
2	0.5776	0.1560	0.4623	0.4785	0.2566
3	0.8129	0.1217	0.9201	0.2102	0.2527
4	1.0000	0.0379	0.9518	0.0013	0.1025

8.3.1 Deviatoric Mechanism Parameters

To calibrate the deviatoric mechanism parameters, the shear stress-shear strain, q-ε_q response of a triaxial curve (Figure 8-6a) is discretized into four distinct shear stress-shear strain points. These points are in addition to the origin as shown in Figure 8-6b for a specific confining pressure.

From these four points, the differential stress, strain and modulus are calculated for each element in a series representation of the MMM as shown in Figure 5-4. These values are then converted into a parallel distribution of shear modulus (SHEARRATIO), friction angle (PHIFRAC) and proportion of mean stress (PFACT) that describe the behavior of the parallel spring-slider assembly. For this thesis, the 30 psi confined CU triaxial test was discretized for the calibration to produce the relevant mechanism parameters given in Table 8.5.

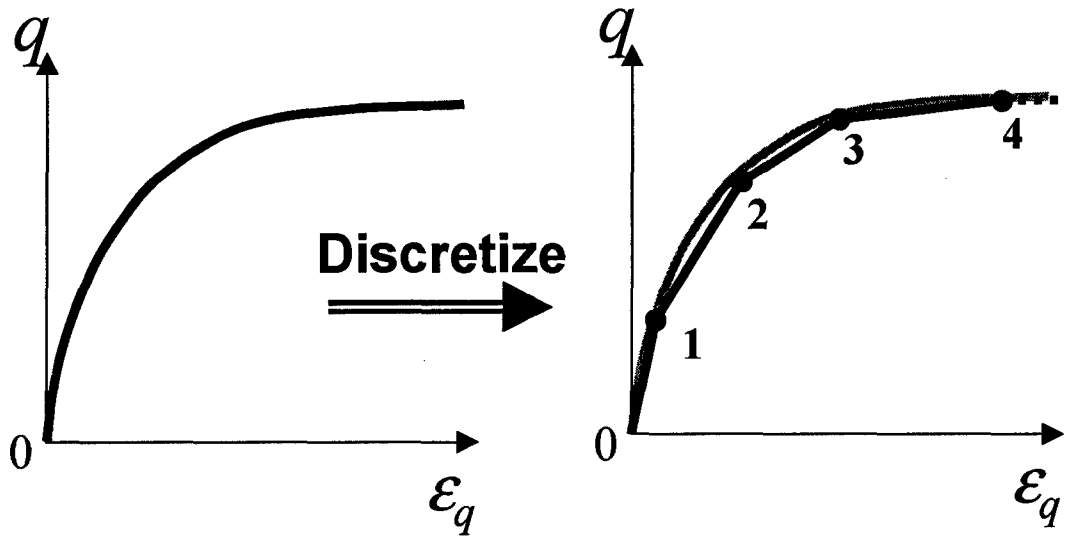

Figure 8-6 a,b: Typical shear strain, ε_q versus shear stress, q for triaxial calibration test and discretized for MMM analysis

8.3.2 Hydrostatic Mechanism Parameters

To calibrate the hydrostatic mechanism parameters, data from the isotropic consolidation tests in Chapter VI were plotted in a void ratio-logarithm of mean stress space. Four discrete points are selected along the curve (Figure 8-7a) that represent points along a normalized mean stress-volumetric strain path (Figure 8-7b) which produces a similar calibration routine as the deviatoric process.

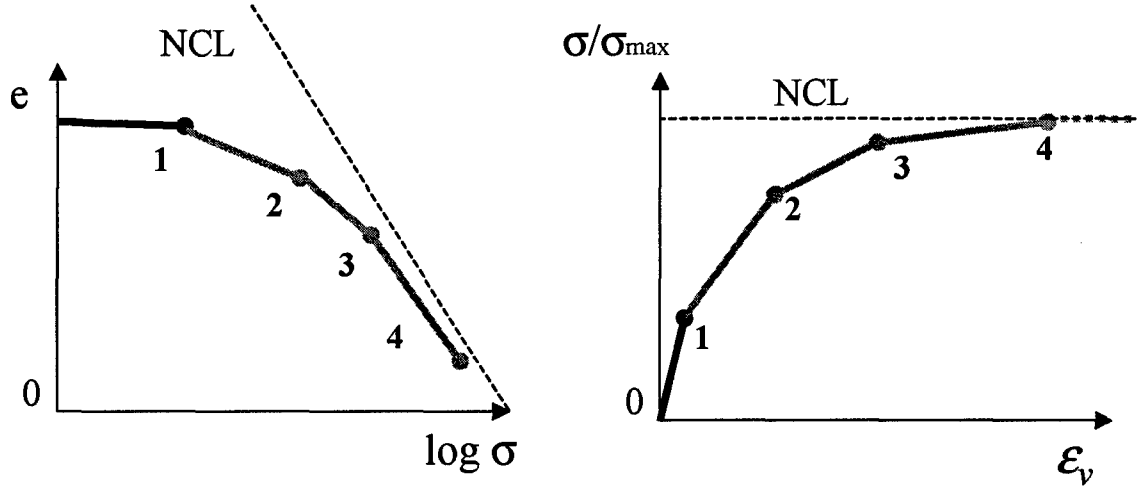

Figure 8-7 a,b: Illustration of e-log σ_m and the converted stress-strain response for calibration

From these four points, the differential strength and modulus of the hydrostatic response is assigned to the elements in a series representation of the spring-slider assembly of the PS-MMM. Those values are then converted into a parallel distribution of bulk modulus (BULKRATIO) and yield strength (HLIMIT) values given in Table 8.5 based on the formulations in Appendix A. Appendix A describes the behavior of the parallel spring-slider assembly.

8.3.3 Beta Factors and Poisson Ratio

The final step in the mechanism calibration is the use of the BetaS, BetaH and Poisson's ratio which act as adjustment parameters to the model fit. As these parameters are changed, the modulus distribution amongst the elements for deviatoric (BetaS), hydrostatic (BetaH) response is adjusted. The Poisson's ratio (POISSON) adjusts the dependency of shear modulus on bulk modulus to allow a better fit of the constitutive response.

The benefit of these adjustment factors comes into play when simulating the response of several triaxial tests at varying confining pressures. Initially, the stress paths for specimens that deviate from the calibrated confinement may not be predicted as desired, with the variation arising from confining pressure. Since calibration is made with only one confining pressure, the adjustment of the Beta factors and Poisson's ratio allows for a better approximation of the entire soil response creating the best average constitutive fits for the range of data on hand. The values for BetaS, BetaH and Poisson's ratio that best captured the behavior of the Buckshot Clay are found in Table 8.1

8.4 Saturated Simulations

Prior to testing the model for partially saturated conditions, it was necessary to verify the predictive capabilities of the PS-MMM with the inclusion of the dual constitutive relationships, the new definitions of intergranular stress and pore pressures and stress dependent bulk and shear moduli. The following series of figures illustrates

the ability of the saturated model to accurately capture the strength-deformation relationships for the Buckshot clay over a very wide range of confining pressures using both tested laboratory data and data from Peters. Of interest is that only the shear stress-shear strain curve for the 30 psi confining pressure was used in calibrating the mechanism parameters to accompany the critical state parameters. These calibrations alone provide the model's ability to capture all other manner of strain, strength and dilation.

Figure 8-8 demonstrates the predicted effective stress paths for the three different confining pressures (15, 30 and 50 psi) of the CU triaxial tests performed by Berney. Figures 8-9, 8-11, and 8-13 present the shear stress-shear strain predictions for the three confining pressures tested by Berney, paired with figures 8-10, 8-12, and 8-14 showing the predicted changes in pore water pressure/dilatancy of the material with shear strain.

Figures 8-15 and 8-17 present the shear stress-shear strain predictions for the two different confining pressures (32 and 200 psi) of the CU triaxial tests performed by Peters, paired with figures 8-16 and 8-18 showing the predicted changes in pore water pressure/dilatancy of the material with shear strain. The 32 psi test is shown because it was prepared with a lower initial void ratio that the 30 psi test in the Berney data. This allows a comparison between predicted response for changes in void ratio at a constant confining pressure.

Figures 8-19 and 8-21 present the shear stress-shear strain predictions for the two different confining pressures (32 and 432 psi) of the consolidated drained (CD) triaxial tests performed by Peters, paired with figures 8-20 and 8-22 showing the predicted changes in volumetric strain/dilatancy of the material with shear strain.

These plots reveal a good agreement between the model predictions and the laboratory data. The plots show an ability to capture the saturated peak strength, dilative properties, modulus softening and overall constitutive response for a wide range of confining pressures and initial conditions. This agreement is for data from both the thesis (Berney) and Peters and for drained and undrained conditions. This suggests that the model calibration and assumptions in its formulation are valid for a saturated material.

The next section deals with predictions of swell tests and partially saturated CU triaxial test results using the partially saturated calibration parameters.

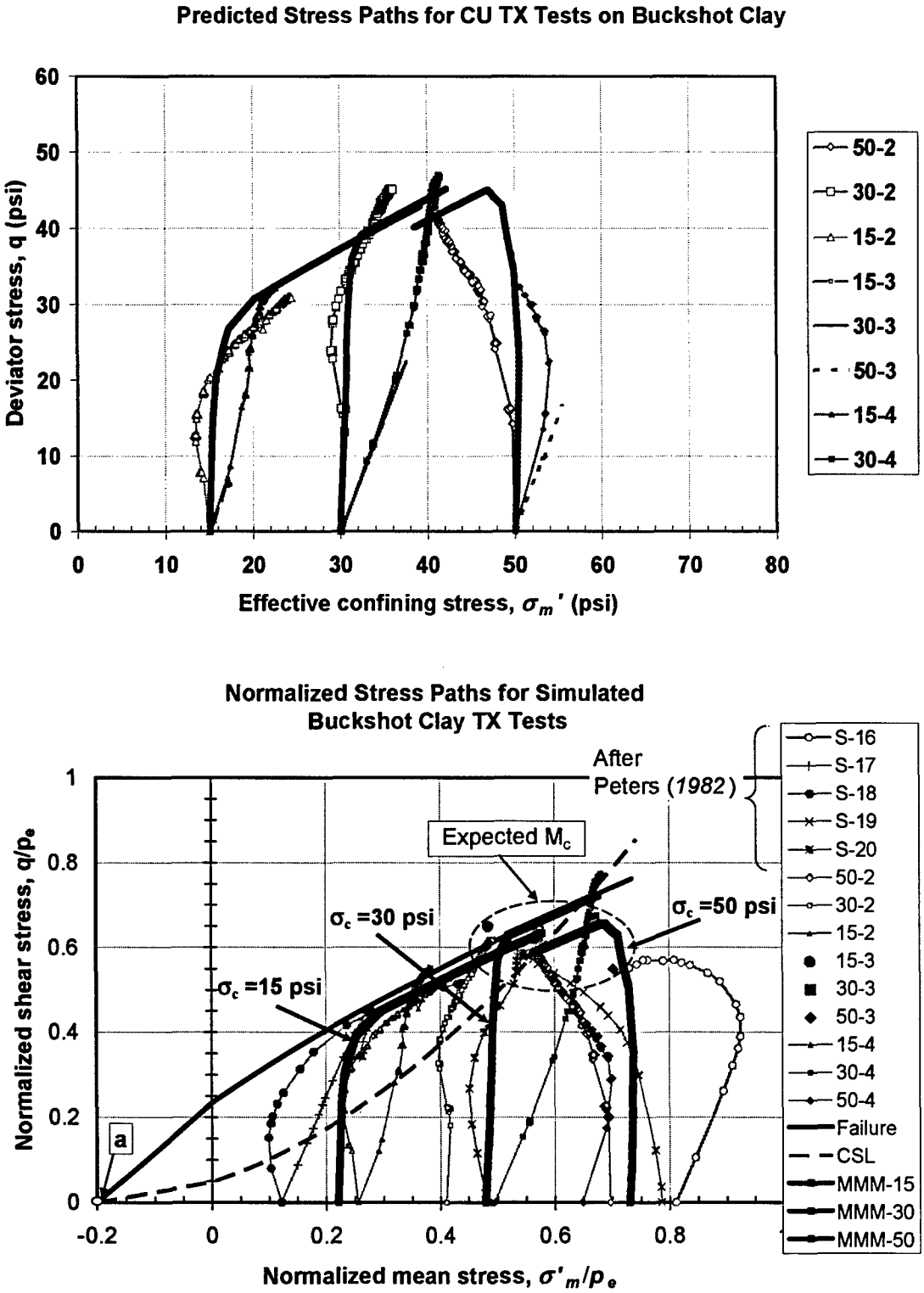

Figure 8-8: Predicted CU Stress Paths for Saturated Buckshot Clay

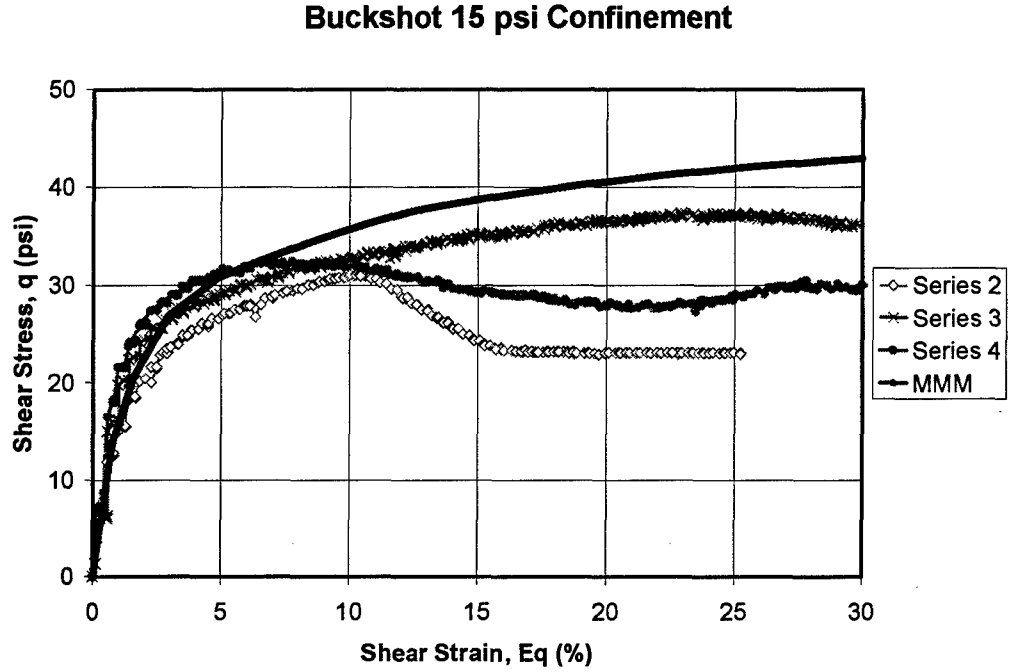

Figure 8-9: MMM simulation of shear stress-shear strain response of 15 psi confined CU triaxial test

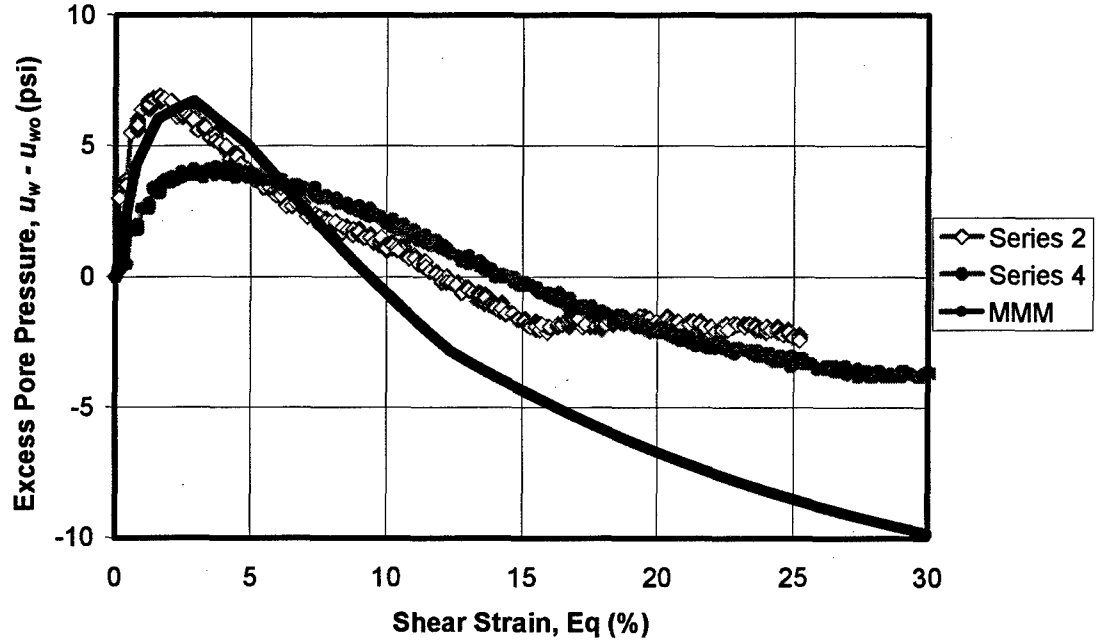

Figure 8-10: MMM simulation of pore pressure response of 15 psi confined CU triaxial specimen

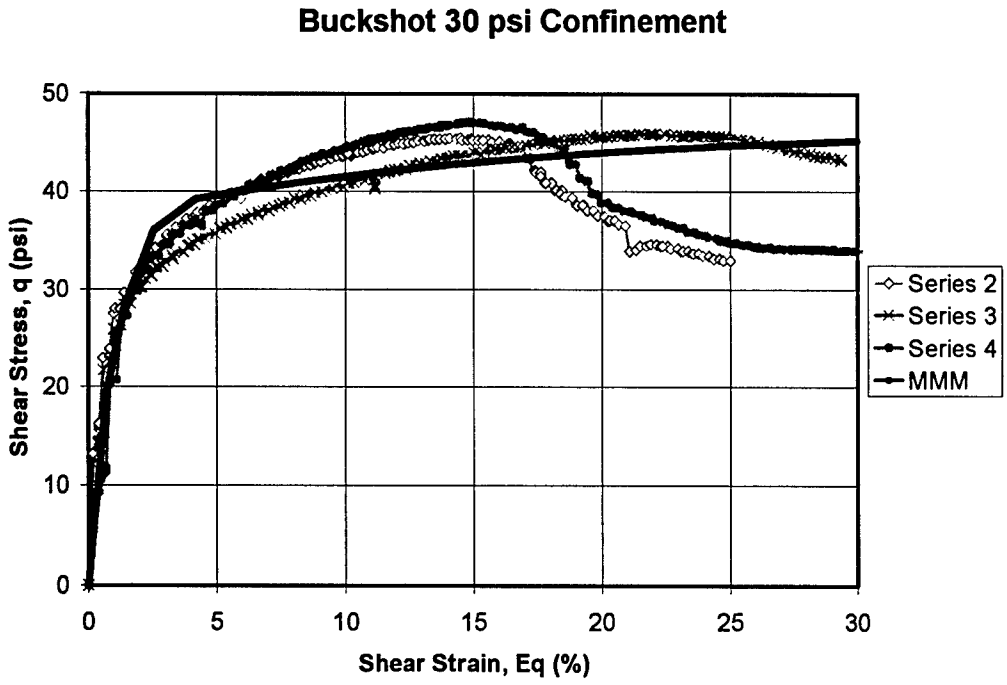

Figure 8-11: MMM simulation of shear stress-shear strain response of 30 psi confined CU triaxial specimen

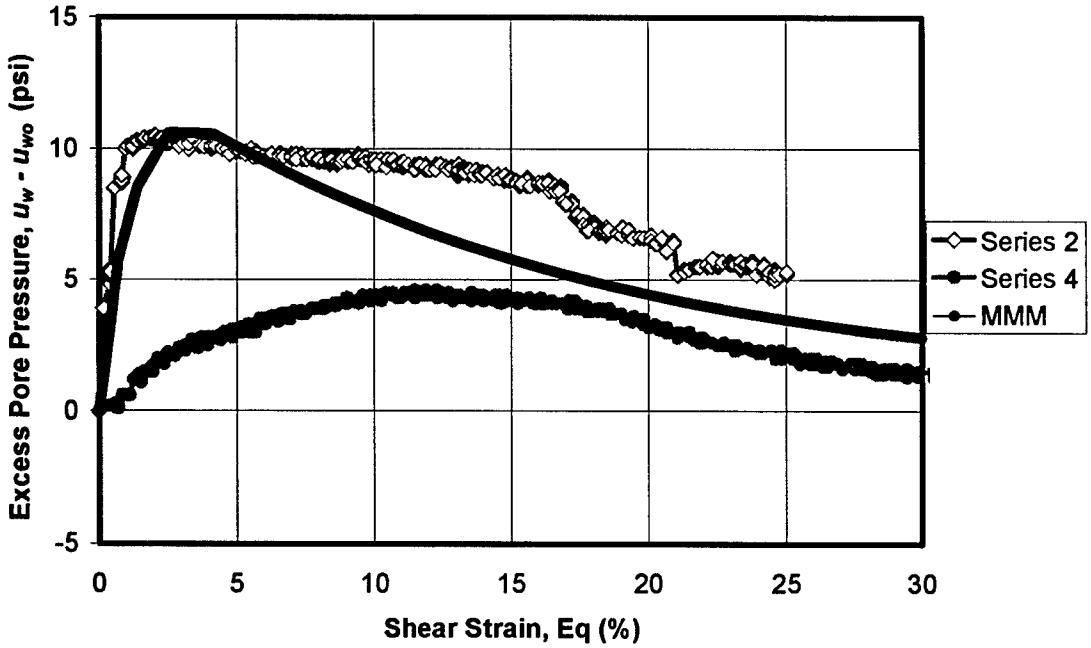

Figure 8-12: MMM simulation of pore pressure response of 30 psi confined CU triaxial specimen

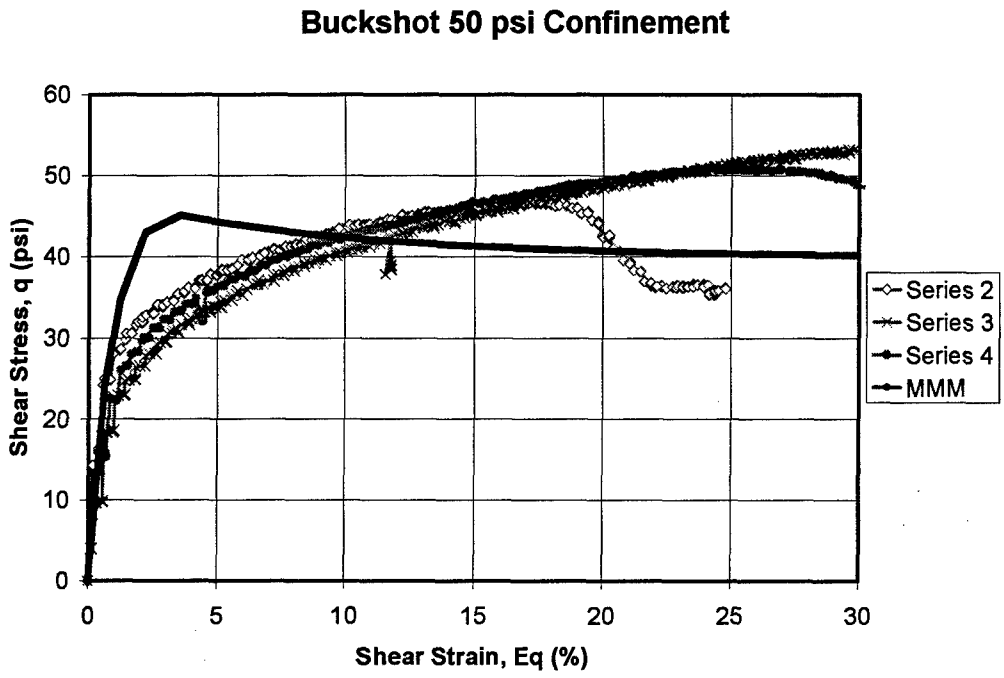

Figure 8-13: MMM simulation of shear stress-shear strain response of 50 psi confined CU triaxial specimen

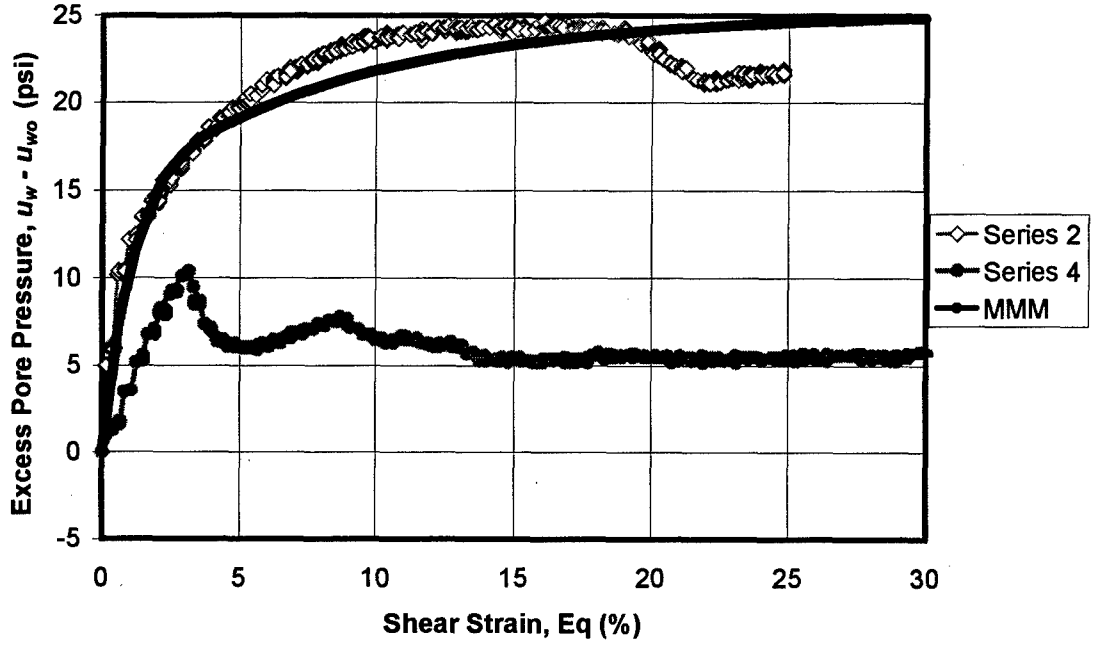

Figure 8-14: MMM simulation of pore pressure response of 50 psi confined CU triaxial specimen

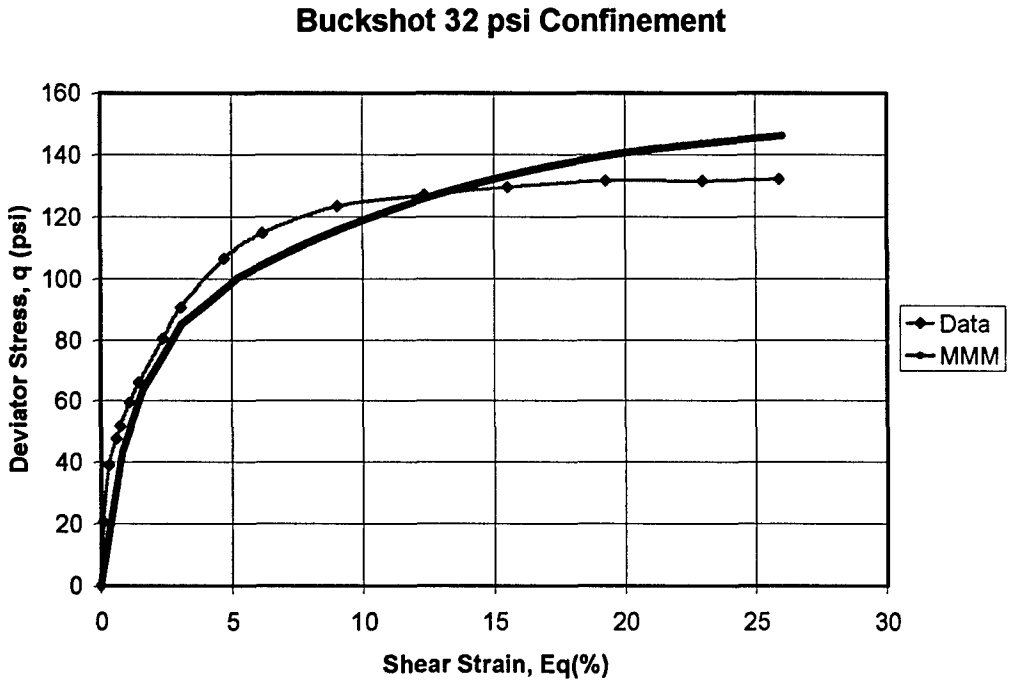

Figure 8-15: MMM simulation of shear stress-shear strain response of 32 psi confined CU triaxial specimen (from Peters)

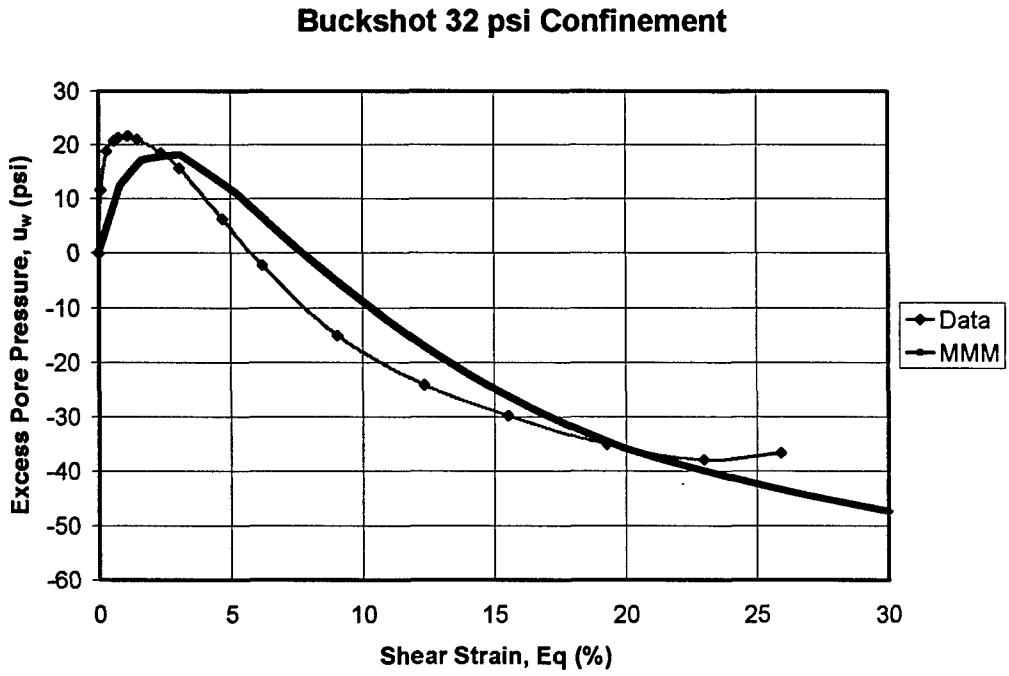

Figure 8-16: MMM simulation of pore pressure response of 32 psi confined CU triaxial specimen (from Peters)

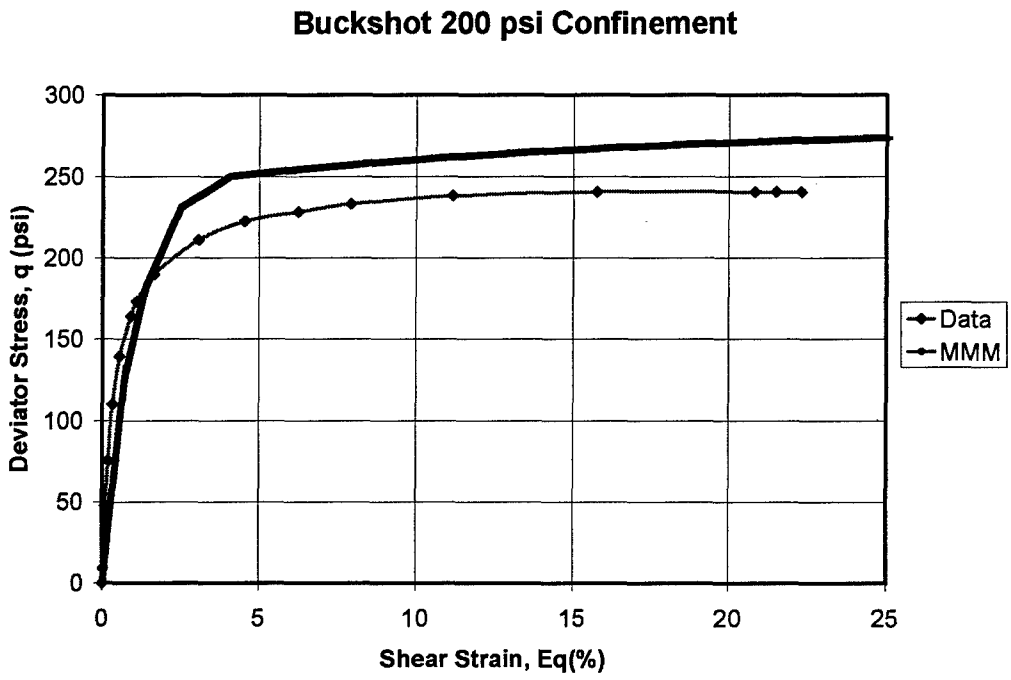

Figure 8-17: MMM simulation of shear stress-shear strain response of 200 psi confined CU triaxial specimen (from Peters)

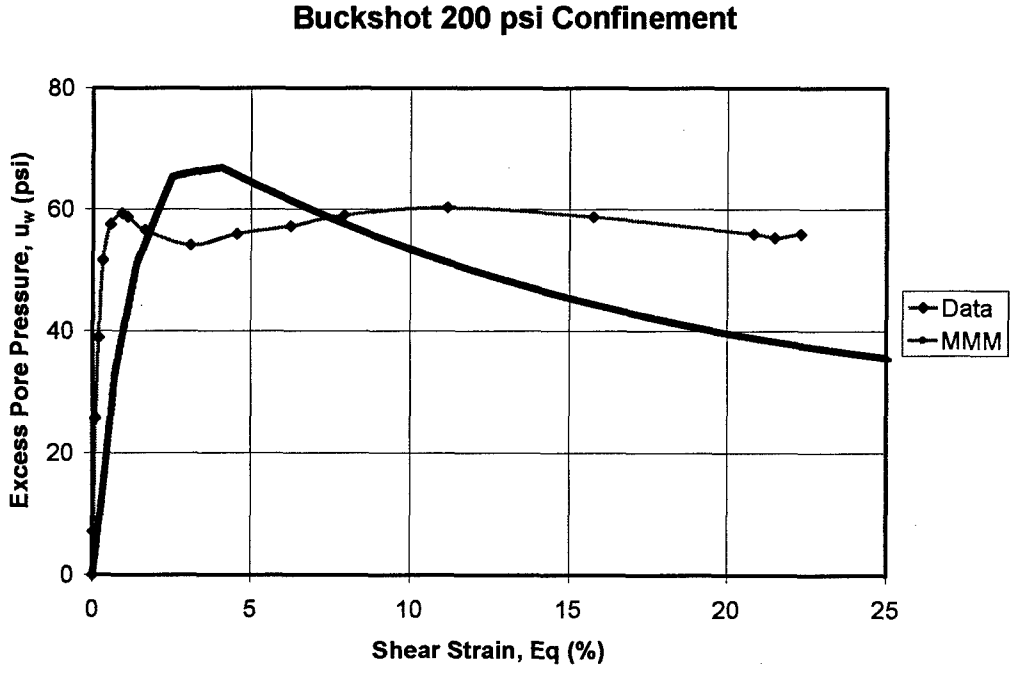

Figure 8-18: MMM simulation of pore pressure response of 200 psi confined CU triaxial specimen (from Peters)

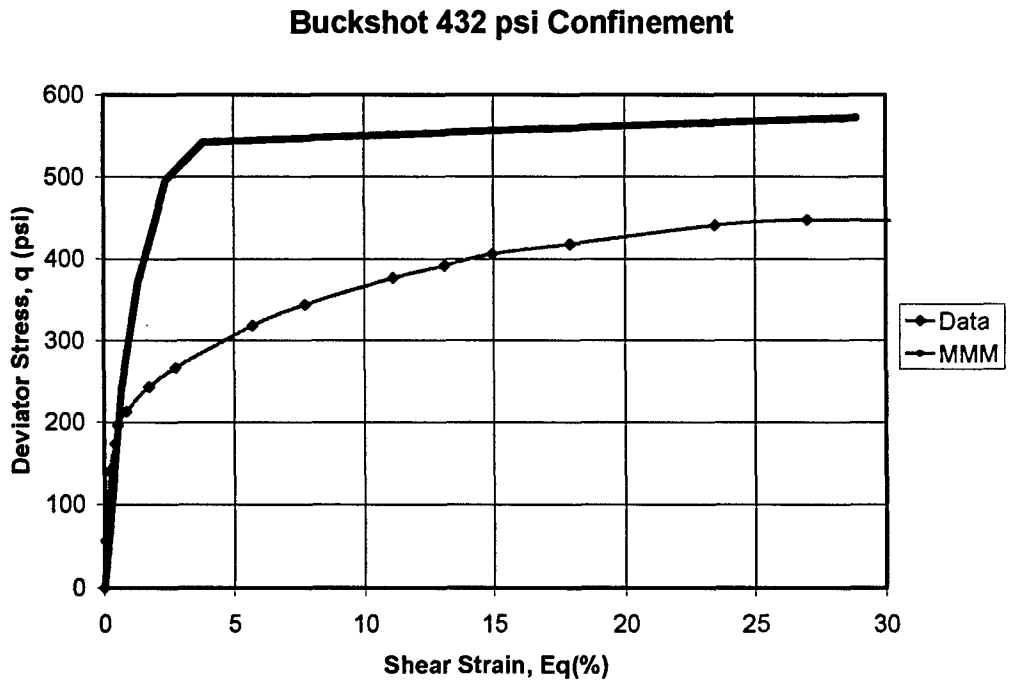

Figure 8-19: MMM simulation of shear stress-shear strain response of 432 psi confined CD triaxial specimen

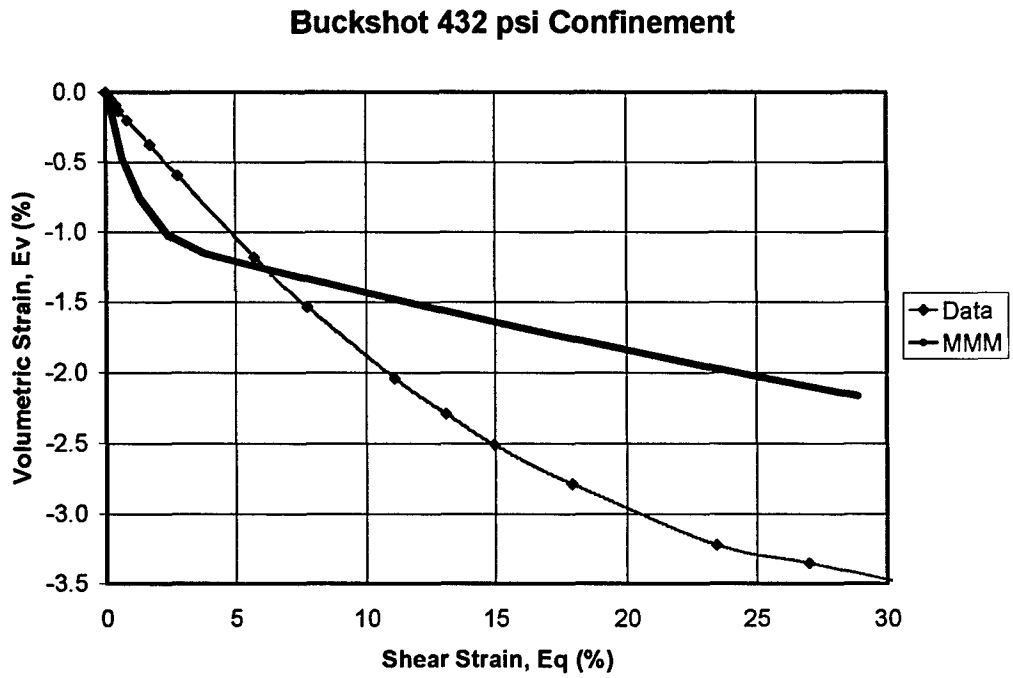

Figure 8-20: MMM simulation of volumetric strain response of 432 psi confined CD triaxial specimen (from Peters)

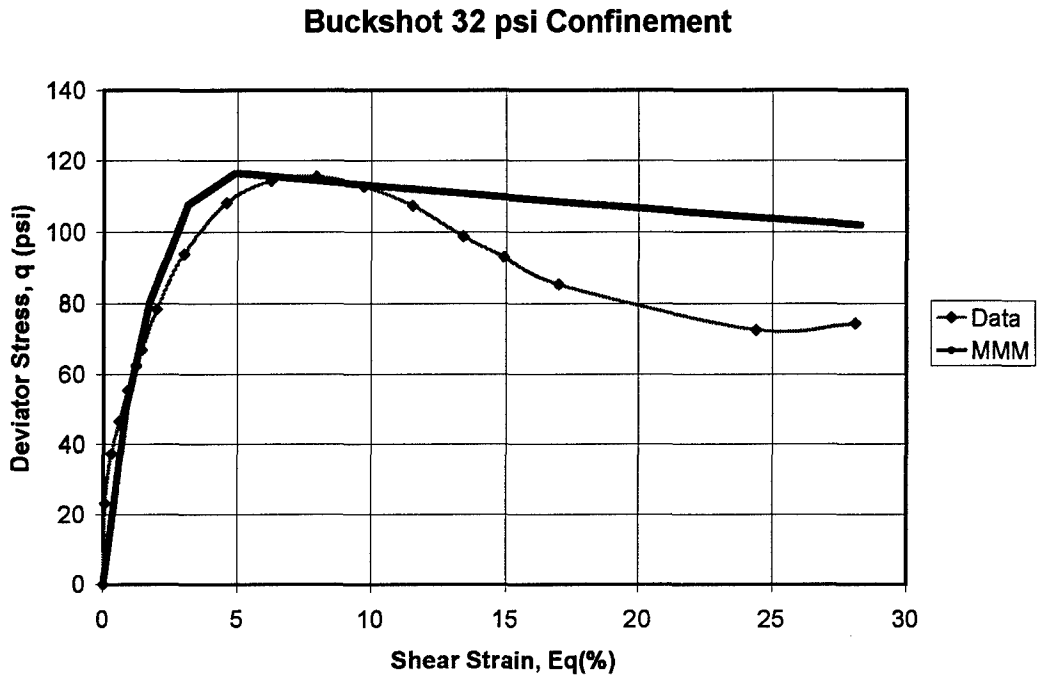

Figure 8-21: MMM simulation of shear stress-shear strain response of 32 psi confined CD triaxial specimen

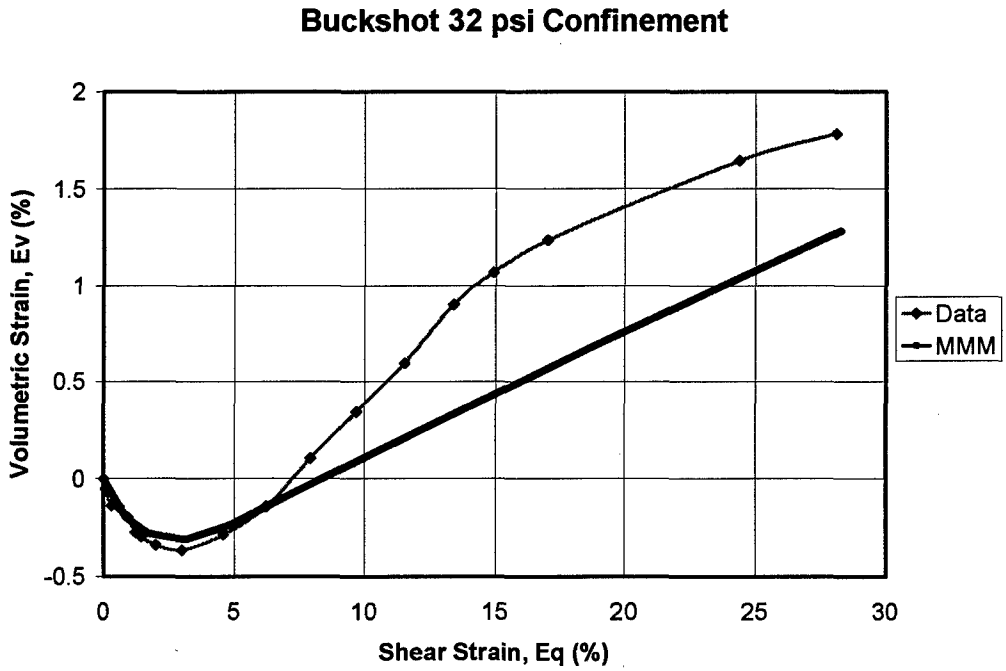

Figure 8-22: MMM simulation of volumetric strain response of 32 psi confined CD triaxial specimen (from Peters)

8.5 Partially Saturated Swell Simulations

To evaluate effectiveness of the partially saturated calibration and model formulation to capture the response of a plastic, expansive clay, simulations were performed under conditions of free swell, constant volume swell and consolidated undrained triaxial loading. The results of these simulations are plotted alongside laboratory data to allow a visual comparison as to the model capabilities. This exercise is not to intended to determine the level of accuracy of the model, but to provide assurance that a partially saturated model developed from the principles of free energy, with the assumptions discussed earlier, can predict complex partially saturated soil response. As well, the definition of intergranular stress can be incorporated into an effective stress model (PS-MMM) and provide the capability of obtaining swelling and strengthening associated with partial saturation.

8.5.1 Numerical Compaction

The behavior of the MMM is strongly influenced by the stress-strain history of the material. This is due to the fact that the system of springs and sliders acts as a built in memory of past loading. Loading can vary the spring moduli and therefore the strain resulting from future changes in stress. This became an important issue when predicting the soil swelling response.

All past research conducted on the modeling of mechanical response for saturated conditions using the MMM had only considered initializing the spring slider mechanisms for the isotropic load applied in a triaxial chamber prior to sample shearing. When the partially saturated model was first implemented to determine the swelling magnitudes of strain and stress, only an average hydrostatic intergranular stresses, Q_h, was applied as a confining pressure. This resulted in only initializing the hydrostatic stresses leaving the residual shear strain in the system zero at the onset of swelling. Three-dimensional volumetric strain is not the same phenomena seen in the initialization of a true one-dimensional swell test, which is more accurately an anisotropic loading of the piston on

the laterally confined sample. By taking this approach to initializing the stresses, the model severely under-predicted magnitudes of free swell volume and swell pressure.

In order to better model a remolded soil as used in the laboratory program, and to simulate the sample swelling in a one-dimensional consolidation ring, it was decided to apply a measure of over-consolidation to the specimens in one-dimensional loading to lock in shear and mean stresses. This established an initial reservoir of potential energy within the soil that could be released as the degree of saturation was increased during wetting. This allowed the model to better predict magnitudes of free swell strain and constant volume swell stress.

As detailed in the specimen construction section of Chapter VI, the Buckshot was compacted dynamically in a standard, cylindrical metal Proctor mold. The dynamic effects of loading are ignored in this thesis for reasons of complexity outside the bounds of this topic. A static, drained loading in one-dimension was implemented in the PS-MMM to approximate the magnitude of stress imposed by the proctor hammer in the following five loading/unloading steps:

1) The soil was assigned a very high void ratio near the reference void ratio and an initial saturation from which a suction could be determined. This suction potential was then converted into a hydrostatic intergranular stress that was applied to the hydrostatic sliders to provide some initial modulus within the system to resist loading. This mimics preparation of the soil prior to compaction, where it is placed in a mixing container and allowed to absorb water to equilibrium water content prior to compaction.
2) The soil was then maintained at a constant suction and water content, allowing saturation to vary while the specimens were first loaded to an estimated magnitude of Proctor stress by allowing the vertical strain to change, while the lateral strain remains zero. This induces additional hydrostatic as well as shear stresses into the system. The simulation represents application of a static load to the soil, densifying the soil, which reduces the air voids and increases the degree of saturation for a constant gravimetric water content.

3) The specimen is then allowed to unload to a condition of near zero vertical stress in a one-dimensional process where only the vertical strain is allowed to change. This simulates piston release after it has contacted the soil. This also is conducted under a constant suction/water content condition.
4) The specimen is then allowed to relaxed to a near zero lateral stress by allowing lateral strain without further vertical strain. This simulates removal of the soil from the steel Proctor mold and storage in an unconfined state where the stresses relax.
5) At this point the water content-dry density magnitude was determined to compare with the compaction curves and sample state obtained from the laboratory. If the systems matched, the test continued to provide the CV, FS and CU predicted data. If water content-dry density data existed far from the desired compaction curves, the applied Proctor stress was changed manually until a sufficient match occurred. A trial and error process was performed until a consistent set of Proctor stresses was found as shown in Table 8.8.

Residual shear and hydrostatic stresses locked into the slider mechanisms prior to conducting the swell tests resulted in a good approximation of the swell response as will be discussed in the next section.

8.5.2 Free Swell Test Simulation

Modeling free swell was selected as the initial test of the PS- MMM. For the free swell test, four simulations were conducted spanning the range of initial water content and densities tested in the laboratory. Since these tests were used in the model calibration, it follows that they would predict the laboratory behavior well. A series of four specimens were numerically simulated at varying gravimetric water contents. Their volumetric strain due to free swell was compared to that measured in the laboratory specimens (Figure 8-23). It was difficult to create an exact match to the water content and density for each laboratory specimen due to the necessity of first compacting the

specimen within the model as described earlier. Therefore, the comparisons shown in Figure 8-23 illustrate that the model predicts along the same trend line of response as was found during laboratory investigation.

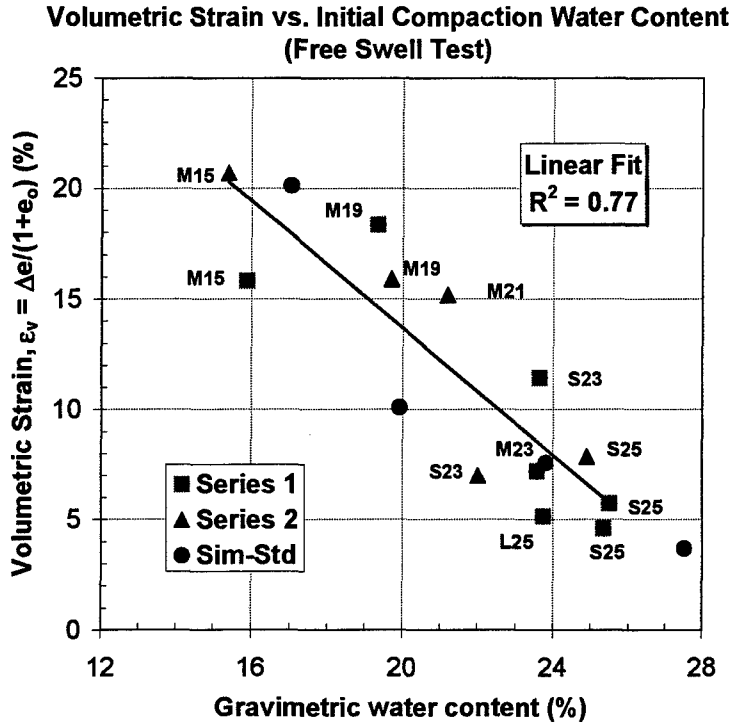

Figure 8-23: Free Swell Test Simulations Plotted over existing laboratory data for Volumetric Strain versus Water Content

The trend line shown in Figure 8-23 serves as a reference by which to judge the model predictive capability. What is noticeable is the model predictions experience some variability about the trend line. This is likely because the model, when incorporating internal variables, behaves non-linearly in a fashion more indicative of actual soil behavior presented in the figure.

It is necessary to perform numerical compactions at varying stresses and water contents to obtain an initial stored energy within each specimen. This stored energy should also occur at a magnitude of suction comparable to that used within the laboratory specimens. Release of this energy during swelling produces a volumetric strain both in the laboratory and in the model whose magnitude is defined in Table 8.6. Numerically,

as this energy is released, it enacts a swelling stress that causes a tensile yield within the sliders. As the level of saturation increases due to wetting, the partially saturated reference void ratio, e_{refU}, and pressure, p_{ew}, decrease and approach the saturated reference void ratio, e_{refS}, and pressure, p_e. In order for there to be continued swelling, the soil must retain a swelling potential strong enough to overcome the ever decreasing yield strength of the sliders as the soil wets. Eventually a limit is reached where the pull of the soil and the strength of the sliders reach an impasse and no further volumetric strain or saturation can occur.

This behavior was observed in the laboratory data shown in Tables 6.4 and 6.5, at lower initial soil saturation levels, the lower the final saturation upon completion of the test. This behavior is not specified in the PS-MMM, but is captured. Therefore, the final simulation levels of saturation below 100%, detailed in Table 8.7 for the FS series, is a numerical representation of the physical laboratory behavior.

This phenomenon is best observed with the driest specimen, FS-4, which at its limit volumetric strain only achieved a saturation of 71%. Based on the bounds of the hydrostatic model, the maximum saturated void ratio sustainable by a specimen under 1.4 psi confinement is 1.407 based on equation (4.105). The maximum partially saturated void ratio at the limit of test FS-4 is 1.494 according to equation (4.106). At a void ratio of 1.398 for test FS-4, only another 1% volumetric strain was possible before the numerical bounds of the model prevented further swell suggesting within the model, this represented a completed test. This indicates a tendency for the partially saturated model to continue swelling to a potentially higher void ratio. However, swell is restricted by the saturated bound on state resulting in a limiting saturation. There is no oscillation within the PS-MMM, such as might be assumed where a partially saturated soil could swell beyond e_{refS} towards e_{refU} and then collapse back to the e_{refS} when saturation approaches 100%. Therefore, the limit saturation defined by the MMM at the end of the test indicates a condition at which the majority of the free energy in the specimen has been transferred to swell. Beyond this point, little additional swell is possible with continued wetting because there is a lack of energy to further yield additional sliders. From a

constitutive standpoint, only a reduction in strength would then be possible with further wetting as p_{ew} approached p_e.

Table 8.6: Simulation Summary of Swell Pressure for Constant Volume (CV) Tests and Volumetric Strain for Free Swell (FS) Tests

Simulations		Initial Water Content %	Initial Confinig Pressure psi	Initial Dry Density pcf	Initial Void Ratio eo	Final Void Ratio ef	Change in Void Ratio Ratio	Volumetric Strain %	Measured Swell Pressure psi	Equivalent Swell Pressure psi
CV-1		27.51	1.40	87.17	0.9614	0.9614			13.50	12.10
FS-1		27.51	1.40	87.17	0.9614	1.0339	0.0725	3.70		
CV-2		23.81	1.40	89.70	0.9060	0.9060			26.87	25.47
FS-2		23.81	1.40	89.70	0.9060	1.0504	0.1444	7.58		
CV-3		19.92	1.40	92.22	0.8541	0.8541			54.09	52.69
FS-3		19.92	1.40	92.22	0.8541	1.0412	0.1871	10.09		
CV-4		17.03	1.40	86.16	0.9843	0.9843			141.03	139.63
FS-4		17.03	1.40	86.16	0.9843	1.3836	0.3993	20.12		

Table 8.7: Simulation Summary of Suction, Porosity and VolumetricWater Contents for Free Swell (FS) and Constant Volume (CV) Swell Tests

Simulations		Final Water Content %	Initial Suction psi	Initial Degree of Saturation %	Final Degree of Saturation %	Initial Porosity no	Final Porosity nf	Initial Volumetric Water Content	Final Volumetric Water Content
CV-1		34.81	13.3	78.4	99.2	0.4902	0.4902	0.384	0.486
FS-1		37.28	13.3	78.4	98.8	0.4902	0.5083	0.384	0.502
CV-2		32.87	30.0	72.0	99.4	0.4753	0.4753	0.342	0.472
FS-2		37.88	30.0	72.0	98.8	0.4753	0.5123	0.342	0.506
CV-3		30.89	75.4	63.9	99.1	0.4607	0.4607	0.294	0.457
FS-3		35.04	75.4	63.9	92.2	0.4607	0.5101	0.294	0.470
CV-4		35.56	236.4	47.4	99.0	0.4960	0.4960	0.235	0.491
FS-4		35.85	236.4	47.4	71.0	0.4960	0.5805	0.235	0.412

8.5.3 Constant Volume Test Simulation

For the constant volume swell (CV) test, four simulations were conducted spanning the range of initial water contents and densities tested in the laboratory. Two comparisons of the data were made: square root of suction, $p^{0.5}$ versus square root of swell pressure, $\sigma_{sp}{}^{0.5}$, (Figure 8-24) and swell pressure, σ_{sp}, versus gravimetric water content, w (Figure 8-25). As was the case for the free swell test, it was difficult to create an exact match to the water content and density found in the lab due to the necessity of first compacting the specimen within the model as described earlier. Therefore, the

comparisons shown in Figures 8-24 and 8-25 illustrate that the model predicts along the same trend line of response as was found during laboratory investigation.

The purpose of providing a trend line symbolizes the linear behavior assumed in the model development and calibration. The line also serves as a reference by which to judge the model predictive capability. The laboratory data scatter in Figure 8-24 suggests that a linear trend may not be the best measure of response. However, it was assumed as a simplification for initial model trials and calibration. Since this relationship is tied to the relevant K moduli and α, these parameters can be modified to account for non-linearities observed. This non-linearity becomes more apparent when the swell pressure is viewed with respect to gravimetric water content in Figure 8-25, where an exponential response is observed. Data in Figure 8-25 represent a better approximation of the physical behavior than Figure 8-24. What is noticeable is the model predictions exhibit very little variability about the trend line suggesting that the model reproduces the response for which it is calibrated. And what variability there is, is likely because the variability in stored energy due to numerical compaction. Therefore the PS-MMM is able to capture soil swell pressure behavior.

Release of initial stored compaction energy during swelling produces a swelling pressure both in the laboratory and in the model. Swell pressure magnitude is given in Table 8.6. Numerically, as this energy is released, a swelling stress develops. As the level of saturation increases due to wetting, the partially saturated reference pressure, p_{ew}, decreases and approaches the saturated reference pressure, p_e. Since the constant volume test is a suction driven test with no strain allowed, the PS-MMM reached saturations near 100% at the end of each test because changes in swell pressure and suction can occur without yielding to the sliders. Therefore the limiting saturation behavior of the free swell test is not evident here, as swell pressure will increase up to the value determined by the CV swell pressure relationship.

This behavior was observed in the first series of laboratory data shown in Tables 6.4 and 6.5, where CV tests of the first sample approached saturation. In the second CV series, the specimens were removed as soon as a peak swell pressure was reached and not allowed to continue absorbing water to a limiting saturation. This behavior is not

specified in the PS-MMM, but is captured as a result of assumptions made during model development. Therefore, ability of the model simulations to achieve full saturation as shown in Table 8.7 for the CV series, is a numerical representation of the laboratory behavior.

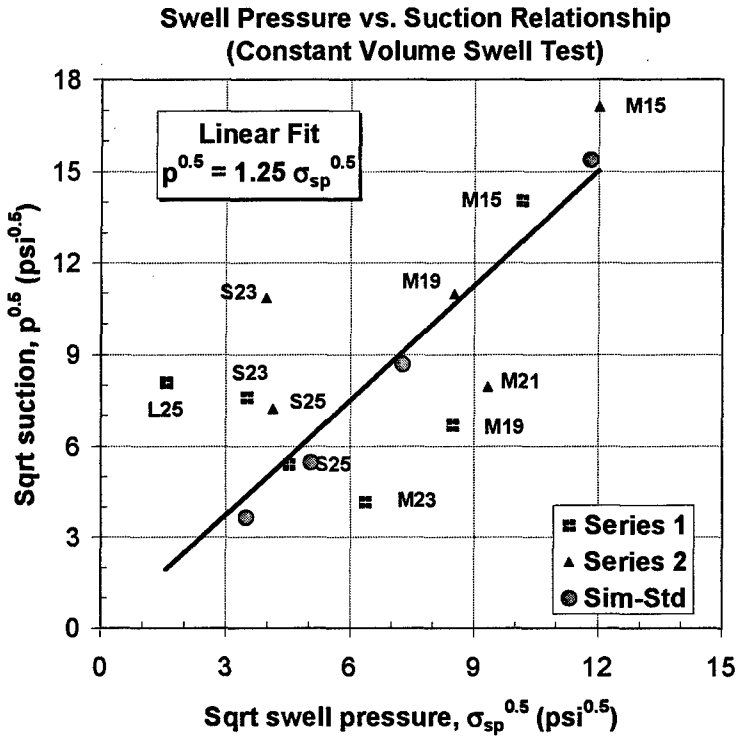

Figure 8-24: Constant Volume Swell Test Simulations Plotted over existing laboratory data for Suction-Swell Pressure Comparison

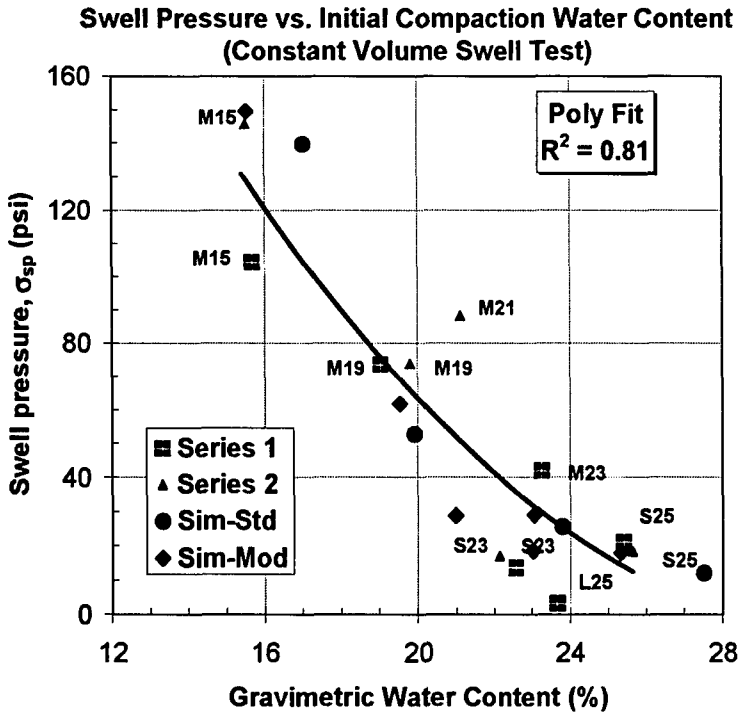

Figure 8-25: Constant Volume Swell Test Simulations Plotted over existing laboratory data for Swell Pressure versus Water Content

8.5.4 Summary of Swelling Response

Based on data and figures discussed in the previous sections, the model predicts the trends in response used during the model development. As well, the model behavior captured intricacies of the differing saturation behavior between the FS and CV without any modifications to the system. These results, coupled with those of the saturated predictions, are evidence the partially saturated MMM is capable of reproducing the spectrum of soil response required of a partially saturated soil. In the next section, data not used in the calibration will predicted.

8.6 Partially Saturated Modified Q-Test Simulations

Results of modified Q-tests given in Chapter VI were used exclusively as the final test of the theoretical formulation to indicate if the model could predict the effects of mechanical compaction, differing density and saturation and a triaxial stress path for a partially saturated soil.

The PS-MMM predicts an ideal soil response under a given set of state conditions as the model itself has no capacity for shear banding or premature failure due to deficiencies in the laboratory specimen or eccentricity in the vertical loading of a specimen in the triaxial chamber. Therefore the model will predict an average soil response based on broad range of data obtained from various sources to produce the calibration. The goal of this exercise was not to judge the model on whether it could provide exact response, but rather capture the general trend in shape and peak strength exhibited in the laboratory such that the governing assumptions made in the model formulation account for the known behaviors of partially saturated soils.

8.6.1 Simulation Data

Figures 8-26 through 8-31 show PS-MMM simulations for the Buckshot clay soil specimens compacted at gravimetric water contents of 21, 23, 25, and 32% for three confining pressures of 3, 10 and 30 psi. The black line is the model simulation and the gray lines are the laboratory response. Table 8.8 shows the initial state and water content of each simulated specimen prior to numerical compaction and then immediately preceding shear for comparison to the laboratory conditions given in Table 6.3. Figure 8-32 shows a summary of the peak strength data normalized by the confining pressures used in the model and laboratory. Figures 8-33 through 8-36 illustrate the changing failure surfaces based on moisture contents of laboratory and model simulations. Lastly, Figures 8-37 and 8-38 show the independent response of friction angle and cohesion at peak shear response for all four water contents tested.

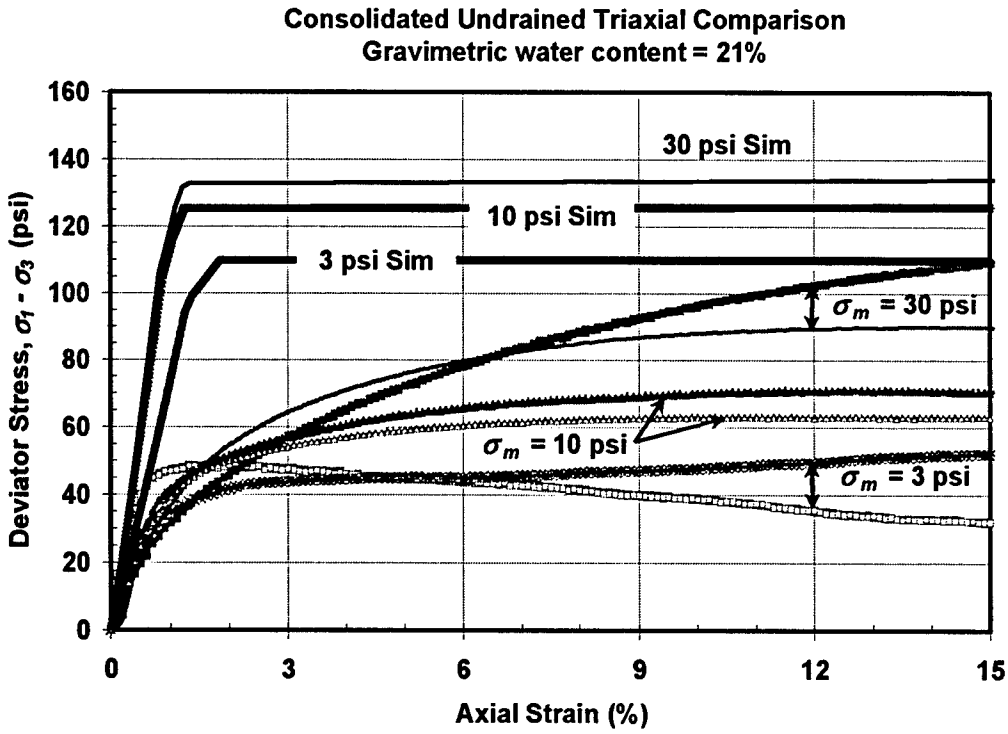

Figure 8-26: Simulations of Q-test for 21% water content samples

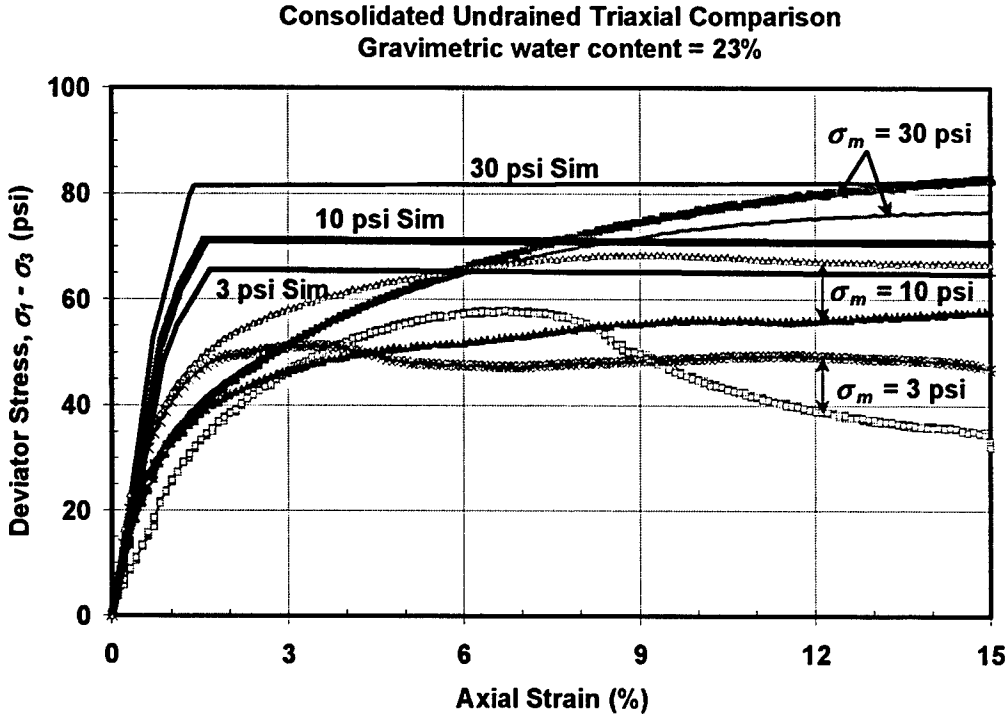

Figure 8-27: Simulations of Q-test for 23% water content samples

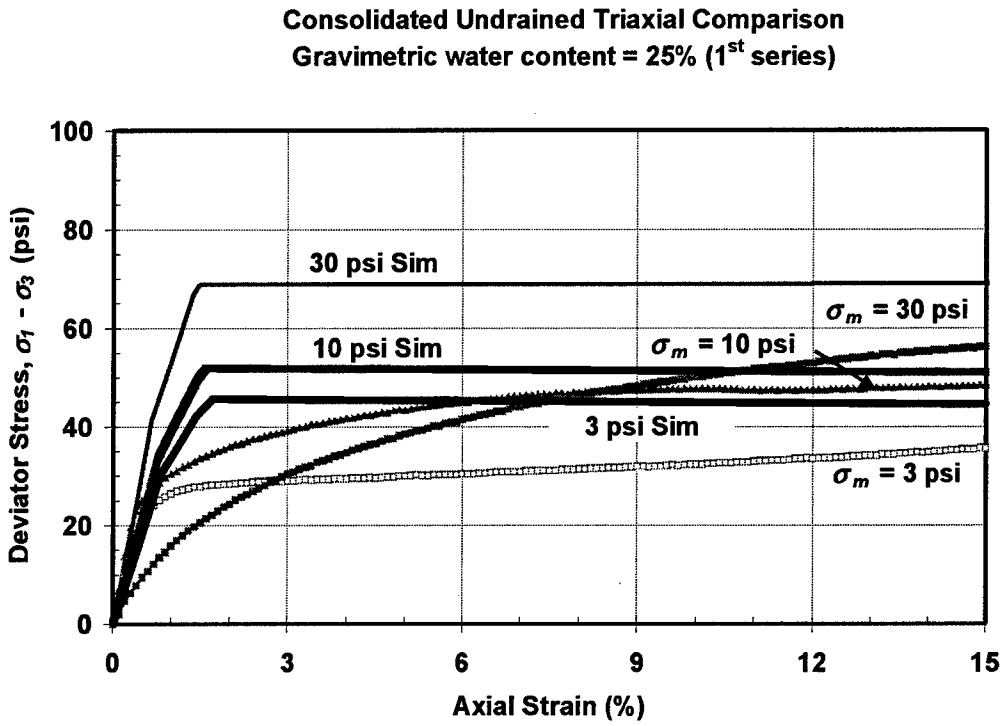

Figure 8-28: Simulations of Q-test for 25% water content (1st series)

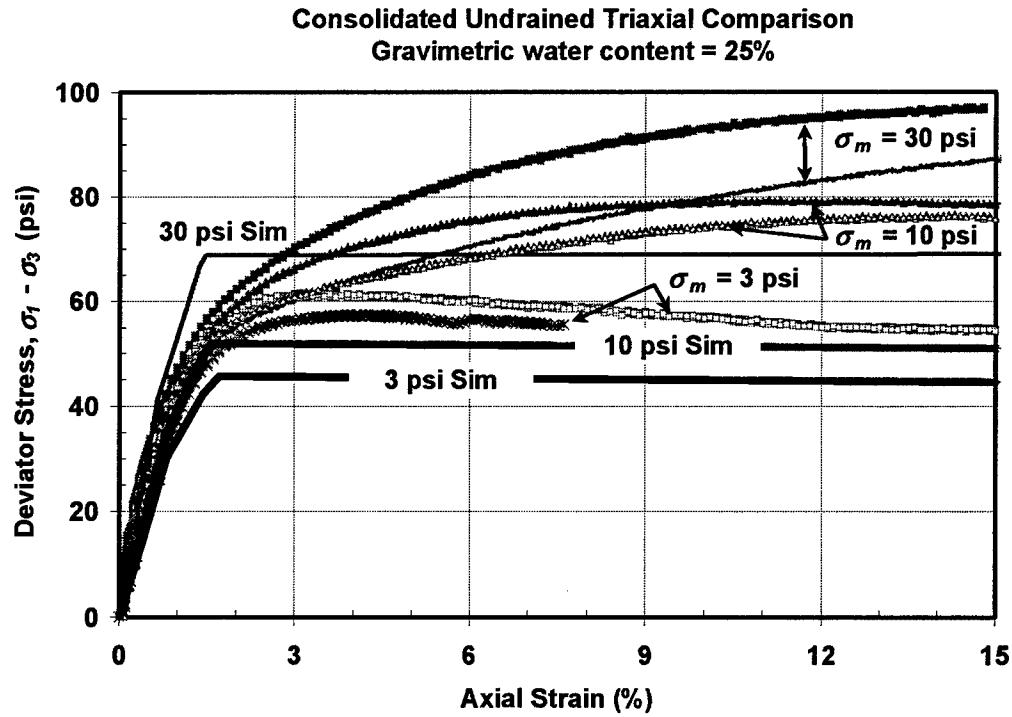

Figure 8-29: Simulations of Q-test for 25% water content (2nd & 3rd series)

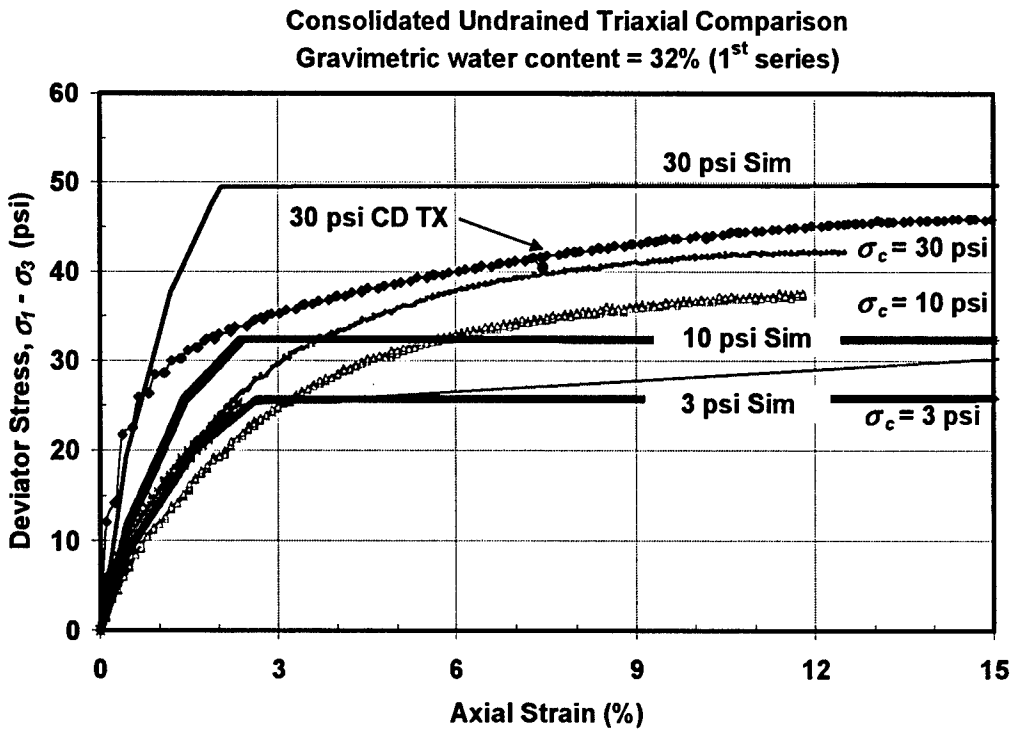

Figure 8-30: Simulations of Q-test for 32% water content (1st series) with CD Saturated TX Test for reference

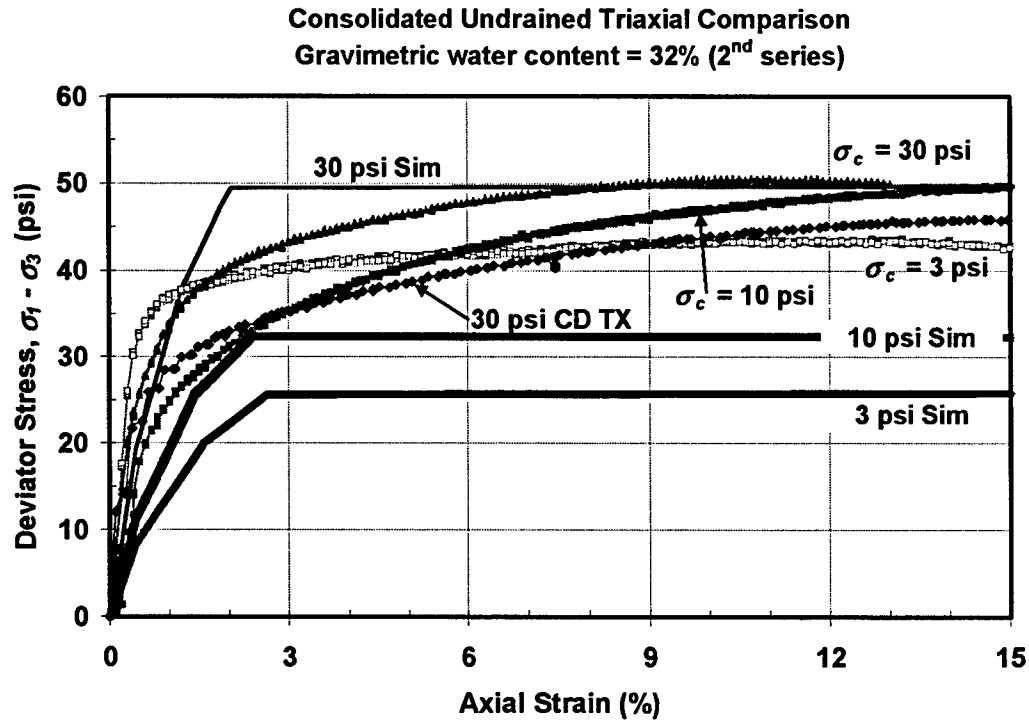

Figure 8-31: Simulations of Q-test for 32% water content (2nd series) with CD Saturated TX Test for reference

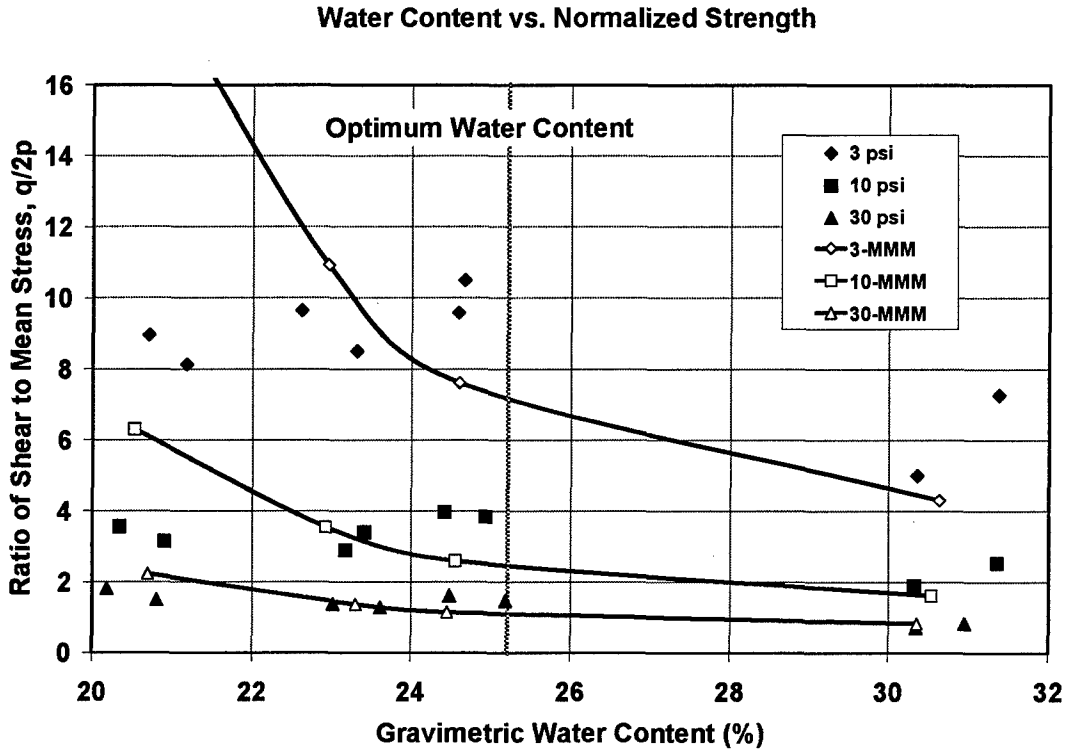

Figure 8-32: Summary of Shear Strength to Water Content for MMM Simulations of Undrained Confined (Q) Compression Tests

Table 8.8: Summary of Q-Test MMM Simulations

Q-Test SIMULATIONS										
		Lambda = 0.3			Initial	Initial	Initial		Peak	
Nominal w%	Condition	Proctor Load (psi)	Model Void Ratio	Initial Saturation	Void Ratio	Water Content (%)	Dry Density (pcf)	Confining Pressure σ_c, (psi)	Shear Strength q, (psi)	$q/2\sigma_c$
21	Proctor	300	1.06	0.55	1.0268	20.93	84.36			
	Consol				1.0258	20.92	84.40	3	110.7	18.5
	Proctor	300	1.06	0.54	1.0257	20.54	84.40			
	Consol				1.0235	20.52	84.50	10	126.05	6.3
	Proctor	300	1.05	0.55	1.0177	20.75	84.74			
	Consol				1.0120	20.69	84.98	30	134.4	2.2
23	Proctor	300	1	0.63	0.9975	23.4	85.59			
	Consol				0.9963	23.29	85.65	3	65.59	10.9
	Proctor	300	1	0.63	0.9975	22.96	85.59			
	Consol				0.9939	22.92	85.75	10	71.23	3.6
	Proctor	300	1	0.64	1.0040	22.96	85.32			
	Consol				0.9938	22.92	85.75	30	82.35	1.4
25	Proctor	300	0.95	0.7	0.9780	24.62	86.44			
	Consol				0.9762	24.6	86.52	3	45.69	7.6
	Proctor	300	0.95	0.7	0.9780	24.62	86.44			
	Consol				0.9726	24.55	86.68	10	51.98	2.6
	Proctor	300	0.95	0.7	0.9780	24.62	86.44			
	Consol				0.9647	24.45	87.02	30	69.09	1.2
32	Proctor	300	0.9	0.9	0.9722	30.69	86.69			
	Consol				0.9687	30.63	86.85	3	25.85	4.3
	Proctor	300	0.9	0.9	0.9722	30.69	86.69			
	Consol				0.9625	30.53	87.12	10	32.37	1.6
	Proctor	300	0.9	0.9	0.9722	30.69	86.69			
	Consol				0.9507	30.35	87.65	30	49.75	0.8

8.6.2 Shear Stress-Axial Strain Response

Figure 8-32 shows a plot of normalized shear strength versus water content for predicted model and laboratory test results. Laboratory test results, as noted in Chapter VII, experience a peak at a water content just slightly less than optimum and decrease on both the wet and dry sides of that peak. The only exception to this behavior occurred for the highest confined sample (30 psi) at the driest condition as seen in Figure 7-7. The model response experiences only an increasing strength with decreasing water content. For an ideal soil, this indicates that the model behaves appropriately, showing an increase in strength with increasing suction potential. This behavior occurs because of the increase in mean stress provided by the suction potential which increases the slider strength and leading to a higher peak strength. The discrepancy from the laboratory data occurs because the model represents the soil as a continuum and as such cannot capture the packetization effect that occurs with the laboratory specimens once the water content

approaches saturation near 55%. As was discussed in earlier chapters, at water contents dry of optimum, the distribution of suction potential no longer fully contributes to the macro behavior of the soil specimen. Although this represents a limitation of the model, it stands as an area for future research to identify a means to reduce the contribution of suction as a function of water content at peak strength.

As a result of this continuum effect, the strength and resulting modulus are over predicted in the 21% content specimens shown in Figures 8-26. The 23% specimen represents a better approximation of the strength by capturing the 10 and 30 psi magnitudes well and over predicts the strength of the 3 psi sample by about 15%. A softening of the initial stiffness can be noted going from the 21 to 23% specimens, better representing the constitutive response and a trend that will be noticed in wetter specimens as well.

For the 25% specimens, the model over predicts the strength for each confinement in the first series. There is reasonable agreement at the intermediate, 10 psi stress. Shear strengths for the second series are under predicted for each confinement level. However, on average the peak strength is approximated well, as shown in Figure 8-32. Of the two series tests, the constitutive behavior is captured best for the second series, where the initial softening of the modulus occurs very near that of the laboratory data. This is especially evident for the 3 and 10 psi specimens.

For the 32% simulation, the model over predicted strengths of the first series which is the softer of the two series relative to the standard 30 psi CD triaxial test. The model under predicted strengths for the second series with the exception of the 30 psi confined test. The modulus softening and constitutive response are represented best at this water content showing that as the model saturates, the effect of the stiffness and strength is reduced.

There are two criteria at issue. First, strengths at lower saturations are too high and second, this strength is a result of a much higher stiffness than observed in the laboratory. Recognizing the model behaves as in a continuum, a means to reduce the suction contribution at low saturations would account for both of these discrepancies as the stiffness, and similarly strength, derive their magnitudes from the mean stress

contribution of both the boundary and suction stresses. However, the practical limit of the model response for airfield construction is at saturations above this limit where the distribution of moisture can be assumed uniform throughout the soil. The study of response at low saturation is left to future research in the next generation of this constitutive model.

8.6.3 Failure Surface Behavior

The model can also be examined by comparing the Mohr circle failure envelope for both model and laboratory response and to compare changes in friction and cohesion experienced by both. The failure envelope is a means to combine the influence of all three confining pressures into one behavior. Figure 8-37 shows the friction angle from Figures 8-33 to 8-36 varies considerably with water content for the laboratory specimens versus a steady but slight decline in the model simulations. If this figure is compared to Figure 7-7, a very similar trend in behavior is observed owing to the direct correlation between strength and friction angle in these specimens. Since this type of behavior cannot be accounted for in the present PS-MMM, this plot serves to show that it is a behavior that will need to be accounted for.

The idea that cohesion increases with suction has been proposed by Fredlund (*1993*) in the form of a friction angle associated with the suction potential of a soil as given in equation 3.4. This same behavior is exhibited within the PS-MMM according to Figure 8-38 which shows an increasing cohesion with decrease in water content or conversely an increase in suction. It should be noted that cohesion in the sense of the PS-MMM formulation, is an offset of the hydrostatic intergranular stress that allows an increase in strength which is directly correlated with the aforementioned cohesive intercept. However, this effect is captured without the definition of a friction parameter associated with suction as suggested by Fredlund. Furthermore, identification of this friction parameter would require an extensive test series nearly identical to the one performed simply to define it. As well, since the friction parameter is non-linear (*Escario, et al., 1987*) this makes it more difficult to capture, using standard sets of

laboratory tests for calibration. Also, additional parameters would be required to capture the non-linearity. Therefore, it is considered a very positive effect of the model to still be able to capture the increase in strength consistent with the concepts of Fredlund merely by using suction potential as an influence on the intergranular stress as defined in the model formulation.

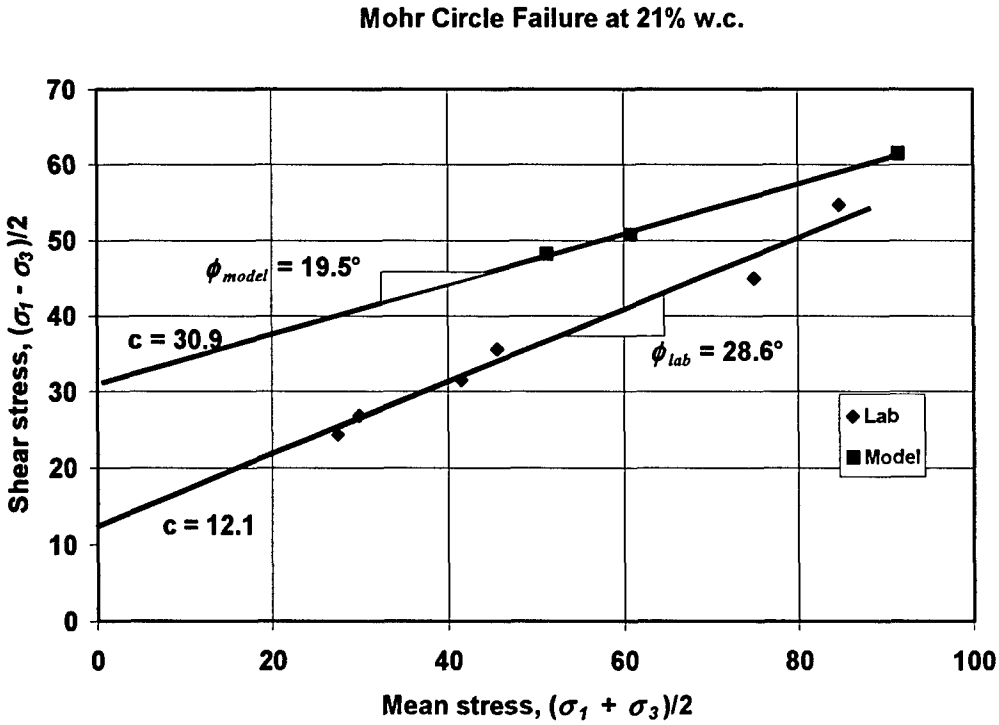

Figure 8-33: Comparison of Laboratory Mohr circle failure envelope with PS-MMM at 21% water content

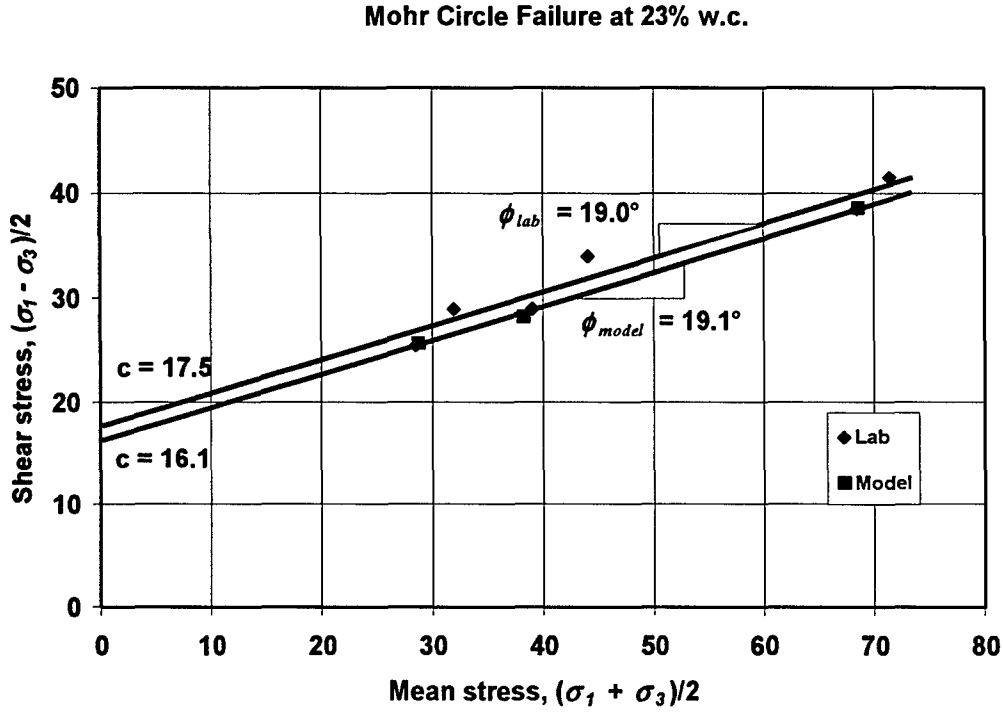

Figure 8-34: Comparison of Laboratory Mohr circle failure envelope with PS-MMM at 23% water content

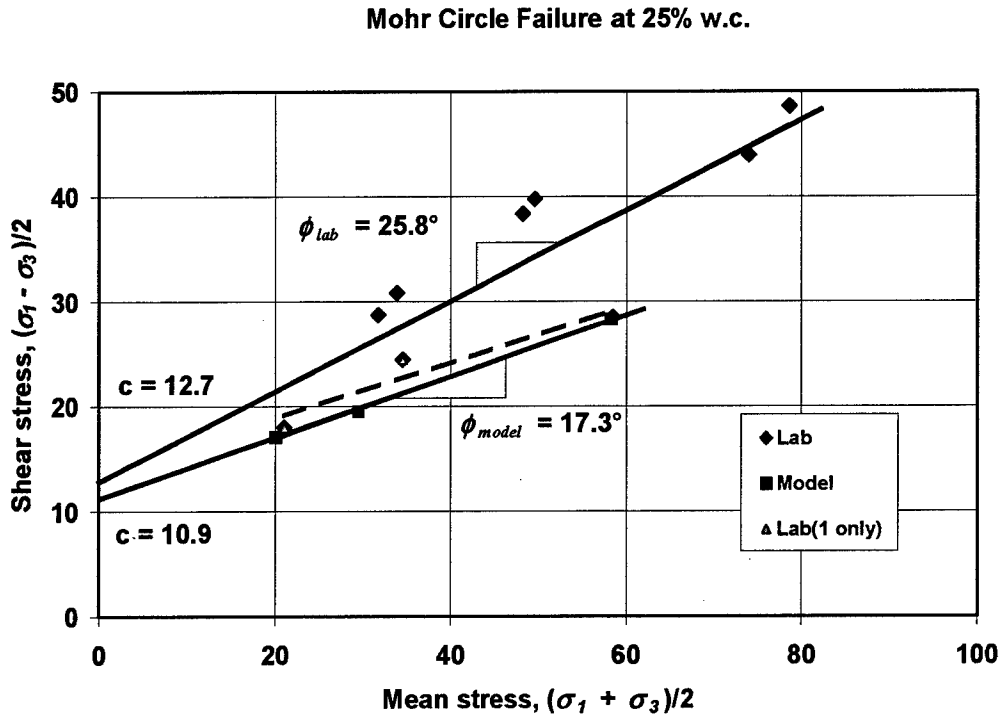

Figure 8-35: Comparison of Laboratory Mohr circle failure envelope with PS-MMM at 25% water content

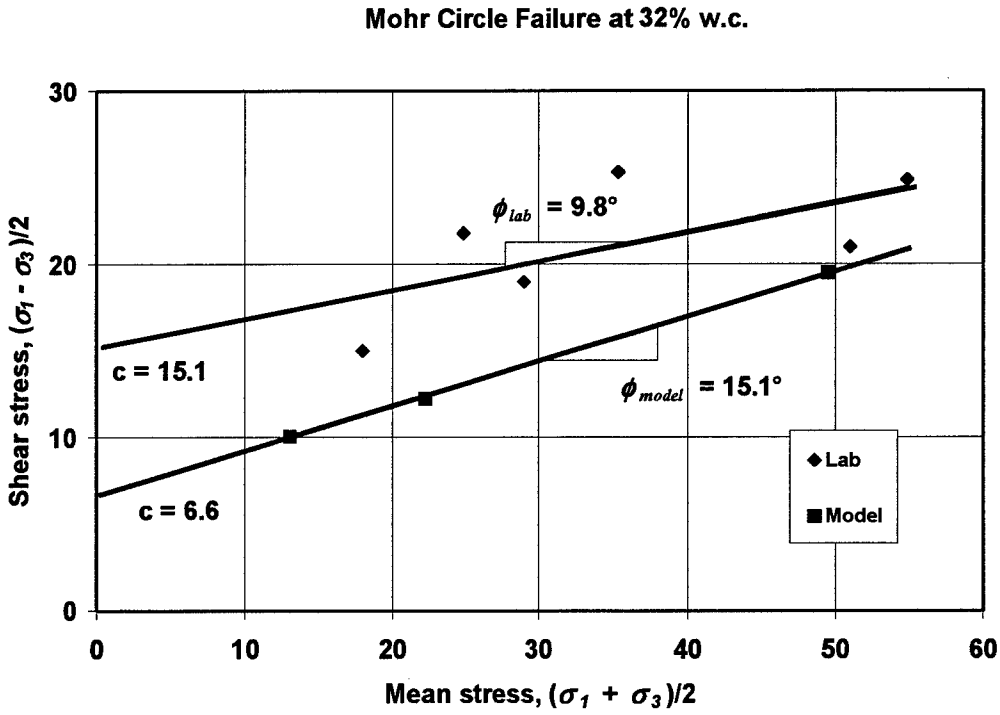

Figure 8-36: Comparison of Laboratory Mohr circle failure envelope with PS-MMM at 32% water content

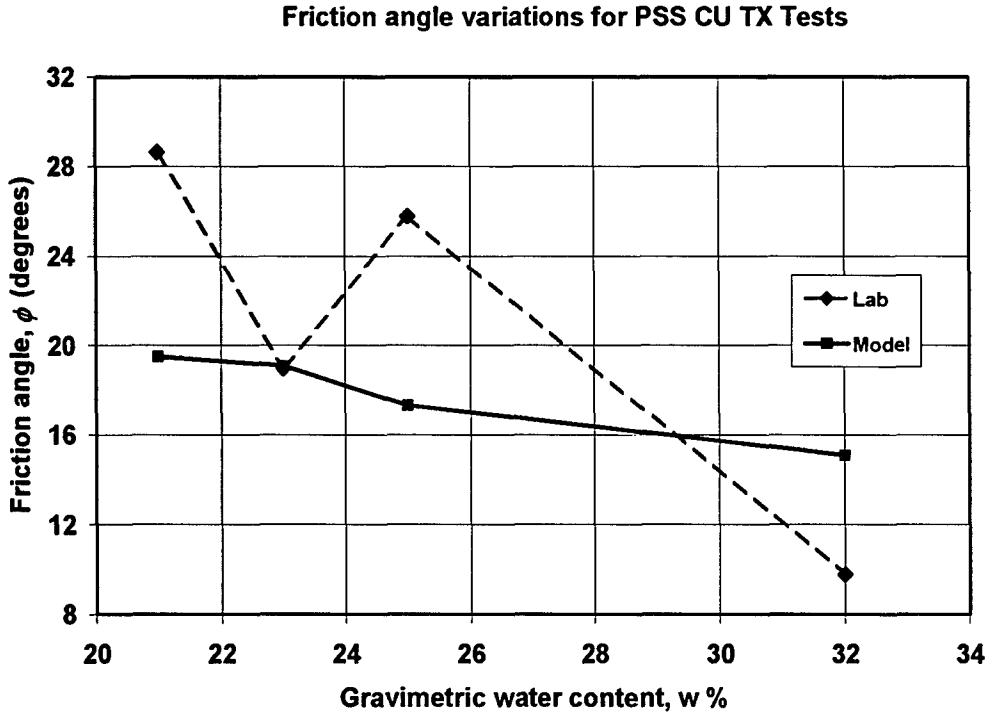

Figure 8-37: Comparison of Laboratory and PS-MMM Friction Angles

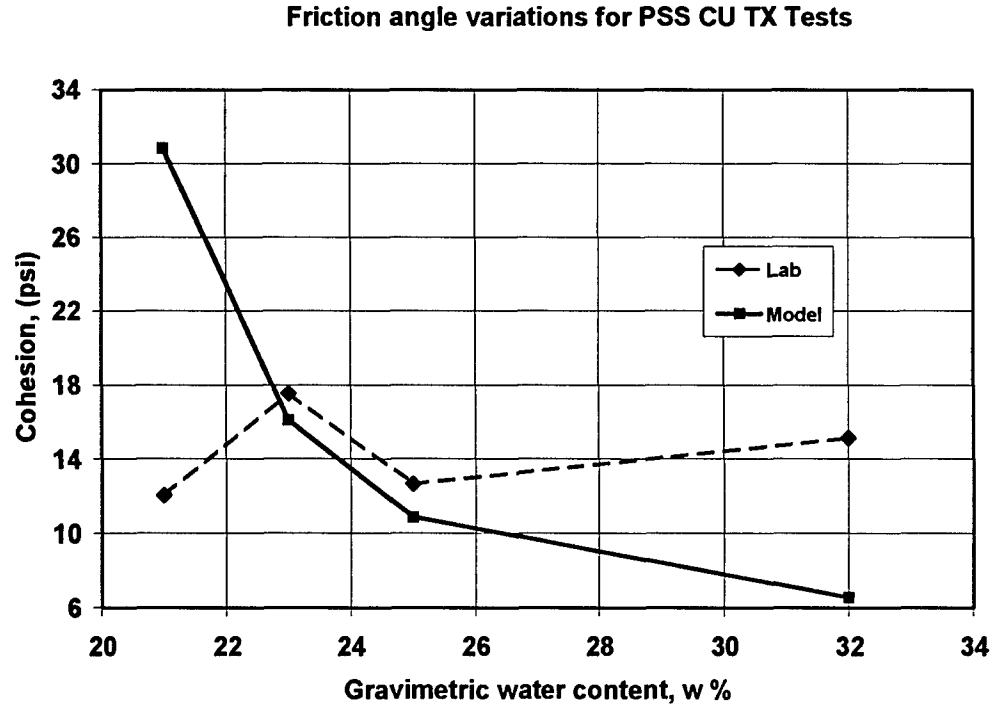

Figure 8-38: Comparison of Laboratory and PS-MMM Cohesion Intercepts

8.6.4 General Predictive Capability

Figure 8-39 compares all predicted and measured data. Overall, the model tends to capture the peak shear ratio at higher water contents (small $q/2\sigma_c$) and generally under predicting the ratio as the sample dries until reaching the lowest water contents (high $q/2\sigma_c$) at which point it tends to over predict the ratio. At these lower water contents, the large stiffness of the model behavior dominates the strength response, much more so than the laboratory specimens. As well, for the higher confined specimens, a better approximation of strength occurs.

Overall, because of the continuum assumption, the model best predicts response within a range of water contents lying just below optimum to anything wet of optimum. Relating that range to most practical applications, it is rare that a compacted fill would be compacted at differential water contents drier that those given in the best fit ranges of the model. The necessity of determining the factors that reduce the influence of suction in the model at low water contents becomes apparent for model predictions in arid environments where the drying of compacted fills can create brittle soils with a tendency to fracture upon loading rather than deform plastically. The estimation of these effects is to be considered for future research and incorporated into the next generation of the model.

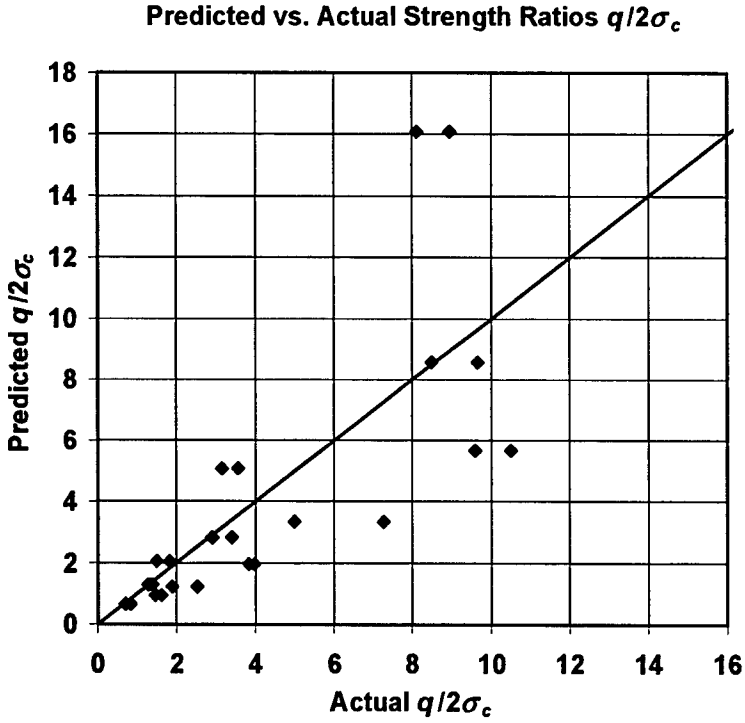

Figure 8-39: Comparison of Laboratory and PS-MMM Cohesion

CHAPTER IX
Conclusions

The most common soil encountered in construction is that of a partially saturated soil and more specifically compacted fills. A partially saturated soil (PSS) is a complex multi-phase system consisting of air, water and solid material whose response is a function of not only the external and internal stress state but as well the moisture condition present within the soil. In traditional soil mechanics, this moisture effect has largely been ignored to produce a conservative design that always assumes the worst-case scenario whereby a fully saturated soil is present. Prediction of performance assuming in-situ conditions within a soil structure is much too conservative. A soil in a saturated state is typically at its weakest strength condition and is the least susceptible to volume change due to changes in its water content. Therefore there is a need to understand the mechanics of the partially saturated system as a step forward in the knowledge base of material responses. This thesis provides a partially saturated constitutive model to account for the influence of partial saturation to advance the state of practice in predicting performance of structures containing compacted fill.

Soils placed and compacted for airfield pavement foundations are known as compacted fill. In order to increase the soil strength, the compacted fill is almost always placed in a partially saturated condition. A PSS is stronger than saturated soil owing to an influence of suction on the intergranular stresses within the soil skeleton. Partially saturated soils are also susceptible to volume changes such as swelling and collapse resulting from not only external loadings but also from changing moisture conditions. Therefore, there is a need to model the unique constitutive responses of PSS to advance model development in the area of compacted fill design and analysis.

A theoretical formulation of thermodynamic behavior of partially saturated soils based on the first two laws of thermodynamics has been developed. It assumed a coupling in the free energy between the suction and soil skeleton stress. This led to the definition of an intergranular stress that is coupled to the suction and is conjugate to the internal variables in the system. This coupling further defines a conjugate variable associated with the suction potential of the soil as volumetric water content. From this formulation was derived a set of incremental constitutive relationships that interrelate behavior of suction, strain, stress and volumetric water content. These relationships allow definition of an soil skeleton stress as a function of intergranular stress. The intergranular stress accounts for the actual transfer of stress between grains of soil due not just to boundary stresses but also internal stresses derived from suction. This coupling of stresses in an incremental relationship can be incorporated into any effective stress model capable of identifying suction and volumetric water content as variables within the system.

A simplifying idea within the formulation is the assumption that suction acts only as a hydrostatic stress, therefore not influencing the shear response directly. As well, since the model assumes a continuum behavior, the suction is distributed equally throughout a soil specimen. Of importance is that suction is not considered a cohesive effect, but a confining pressure exerted on the normal grain to grain contacts within the soil matrix. Out of this comes the behavior of strength and swelling.

A log-linear relationship was assumed between suction and volumetric water content similar to the log-linear relationship between mean intergranular stress and volumetric strain. Internal variables were incorporated to account for hysteresis in the stress-strain response. However, the suction-water content behavior was assumed reversible. And, based on this assumption, the definition of the coefficients that define the behavior of the incremental relationships can be determined from common geotechnical laboratory tests that isolate certain modulus coefficients.

Laboratory investigation has shown that magnitude of suction potential is proportional to increase in strength of the soil up to a limiting suction or degree of saturation. At this point no more strength increase and indeed a strength loss is observed.

This strength loss is due to packetization of the soil whereby packets of soil grains, bound tightly by suction, act independent of the macro structure of the soil specimen resulting in soil strength no longer proportional to the magnitude of suction. A parameter was used to account for increase in volumetric stiffness due to suction. This parameter shifts the normally consolidated line as a function of the degree of saturation which led to the definition of a new partially saturated reference pressure. This concept proved to be the key link in allowing a model that was capable of normalizing the constitutive behavior of soil with not only density (state) but also degree of saturation.

Implementation of the partially saturated thermodynamic formulation was made through use of the modular Multi-Mechanical Model (MMM) program. This program incorporated the incremental relationships and definitions for suction and volumetric water content. The MMM is an effective stress constitutive driver that is a simplification of the endochronic theory. In application it is a rheologic model containing a parallel series of elastic-plastic elements divided into an elastic spring and a plastic slider. The MMM has the ability to distinguish the mechanisms of response in a partially saturated soil because of its ability to separate out the fundamental mechanisms of response through its modular construction and rheologic spring-slider assemblages. Definitions of strength and dilatant behavior in the MMM are based on Critical State Soil Mechanics, which is widely used and understood. The framework of the MMM allowed the development of a direct, linear calibration technique that would expedite its use and lay the foundation for transitioning the model's usage to engineering practice.

A comprehensive laboratory testing program was conducted on a highly plastic, cohesive Buckshot clay. Additional data was obtained from several researchers that had tests on the same material. Laboratory test results provided data required to calibrate and validate the original saturated MMM and the newly developed partially saturated MMM (PS-MMM). Free swell and constant volume swell tests were introduced as essential laboratory tests for predicting perfomance of partially saturated soils. A series of undrained triaxial tests conducted on the Buckshot clay at varying water contents verified the correlation between suction and strength. And, represented a set of test data not used in the model calibration from which to verify the capabilities of the MMM.

From the laboratory investigation, it was found that the constant volume swell test (CV) and the free swell test (FS) provide linear relationships that are proportional to the water content and volumetric water content of the soil. These linear relationships were the basis for an assumption of reversibility within the swelling behavior. It is noted that hysteresis does exist within the swelling response. Also hysteresis is noted in the wetting-drying behavior of the suction-water content response. This suggests that there is a need for additional internal variables within the water phase to improve upon model predictions.

Examples of model calibration were presented throughout the thesis and are shown to be simple in concept and application. Calibration of stress dependent moduli emerging from the thermodynamic formulation of the partially saturated model is presented using common soil laboratory tests. A consistent calibration is shown for the partial saturated parameters for various levels of data available.

Simulations were performed on all saturated triaxial tests used in the calibration of the critical state parameters and saturated response. Model simulations proved very good over a wide range of confining pressures and initial densities. The saturated PS-MMM was able to match modulus behavior, strain softening, dilatancy and peak strength response, all essential to ensure proper model behavior. As such, these results gave confidence that the model's operation is fundamentally sound.

Simulations were performed on partially saturated samples to identify the volumetric strain and swell pressure occurring during wetting of an expansive cohesive soil with an initial suction. Given the mechanical behavior of the PS-MMM it became necessary to numerically compact the soil specimens to induce a certain amount of residual strain or energy associated with suction capable of inducing swell. Swell test simulations proved good at matching the linear trends assumed during model development and represented by the laboratory data. As well, the unique behavior of a limiting saturation during free swell and a full saturation during constant volume swell were capture by the model, a feature that was not specifically accounted for, but produced as a result of the model formulation.

Validation simulations were performed on a series of partially saturated triaxial tests compacted at varying water contents to provide a range of suction potential for the model to simulate. The simulations revealed that the PS-MMM was capable of predicting trends in behavior whereby strength increased with decreasing water content and increased confinement. In general, the model tended to over estimate peak strength and modulus response at very low saturation. However, as the saturation of specimens increased, both constitutive behavior and peak strength were better represented, with the best simulated response occurring at water contents slightly dry of optimum through to saturation; a range of water contents commonly encountered in compacted fills.

The model severely over predicted the strength and modulus response of the driest water content specimens. This phenomenon was explained by the fact that the PS-MMM is a continuum and therefore assumes a uniform distribution and full association of suction potential throughout the soil. In actual compacted soils, when saturation drops below a critical value around 55%, the suction is no longer distributed throughout the soil specimen and the failure mechanisms begins to obey those of fracture mechanics rather than plastic flow. Therefore, within the limits of the model bounds its predictive response for strength is consistent with the formulation and assumptions made within the model.

Overall the model captures the essential elements of constitutive response for partially saturated soil. For all simulations, the model predicted the desired trend in response and for the validation tests not used in the model development, the model was able to predict behavior for which it was not conditioned. The model, through a thermodynamic formulation accounts for swelling, has the potential for collapse and predicts increased strength with suction. Development of a straightforward calibration sets the stage for the inherent simplicity of the model's design. The model represents a step forward in the design of constitutive models for partially saturated soil reducing the number of parameters necessary to capture behavior. Further, the necessary parameters are linked to definite physical properties of the soil. This allowed for a much improved prediction of soil response.

The ideal application of this work is for performance predictions of airfields and compacted fills subjected to changes in environmental and loading conditions. The rigorous development of a thermodynamic model holds the potential to advance the art of pavement design and evaluation. The improved partially saturation capability will enable better modeling of the actual soil conditions providing the best possible estimate of response to loading. This will benefit significantly researchers and designers tasked with predicting performance of current and future pavement structures requiring a detailed knowledge of the in-situ conditions of the compacted fill foundation material.

CHAPTER X

Recommendations for Future Research

Development of the thermodynamic constitutive theory for partially saturated soils has demonstrated that coupling of the free energies within the soil skeleton and the water menisci can reproduce strength and deformation characteristics observed in PSS. The model predictions however show that there is still room for improvement. Based on the assumptions made to simplify the model calibration during model development, the following are areas for future:

1) The quadratic coupling between the free energy of the soil skeleton and air-water interface is one of only many functional possibilities. A third order or higher relationship could be introduced that weights the energies according to their relative influence on the partially saturated response. Formulation of the coupling would appear simple, but its introduction into the constitutive model would present a real challenge as a complex mixture of coefficients would be present and new techniques to calibrate them would be necessary.

2) The assumption of reversibility of the volumetric water content-suction relationship is certainly one made only for model convenience. True behavior of a soil is a non-linear response where reversal of the wetting, drying cycle induces hysteresis. This suggests a log-linear relationship

$$\ln\left(\frac{p}{p_r}\right) = -\frac{1}{\kappa}\theta$$

should actually include internal variables terms, q_θ, in the water content (strain) term that accounts for the cyclic response of moisture change.

$$\ln\left(\frac{p}{p_r}\right) = -\sum \frac{1}{\kappa^i}\left(\theta - q_\theta^i\right) \tag{10.1}$$

Application of this function would be similar to the development and calibration of the spring-slider elements in the MMM. The wetting-drying curves would be discretized and assigned an internal variable representing a loss term to reduce the potential saturation within the soil. This is an important issue and one that will enhance future predictions of cyclic wetting-drying of the soil in addition to the cyclic loading capabilities already present.

3) Comparison of the model to triaxial test data that included pore air and water pressures to evaluate the pore pressure features of the model. This comparison would determine if assumptions of the stiffness coefficients for water and air are valid.

4) Investigation into the role of the stress dependent moduli to determine if suction has a lower influence on stiffness than external forces transferred through the skeleton as discussed in Chapter VIII.

5) Consideration of the reduced suction potential influence on strength response as the degree of saturation falls below a critical threshold. This would entail development of a non-linear volumetric water content-suction function that may look something like Figure 10-1.

This is only one possibility, where a function exists to non-linearize the portion of suction potential contributing to the total intergranular stress as saturation drops below a threshold value. This would begin to capture the softening of soils even as suction continues to increase as seen in the laboratory data in Figure 7-5.

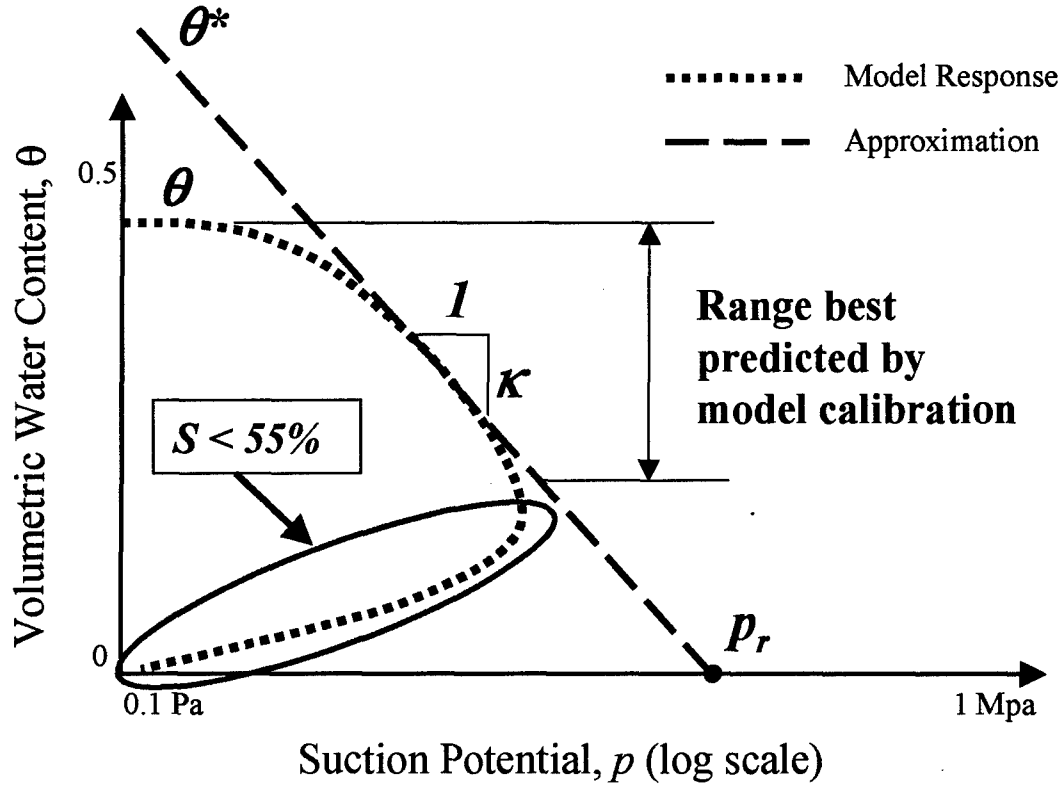

Figure 10-1: Potential non-linearity of θ-p relationship at critical degrees of saturation

6) Lastly, to evaluate the model's capability to capture the collapse phenomenon, calibration and simulation of soils such as sand or non-cohesive silt that are subject to collapse when partially saturated should be investigated. The quasi-stable volumetric states at low degrees of saturation can be established within the model, and the modulus, κ, of the suction-water content response would be quite small such that small changes in water content would initiate large changes in suction. This would provide a rapid decrease in strength as the specimens become saturated. Ideally this will translate into a rapid decrease in volume of the soil and indicate a collapse behavior as the suction derived mean stress becomes very small creating an effective stress within the model no longer capable of sustaining the volumetric states under the boundary loading conditions.

While the means to evaluate this behavior are present in the model, laboratory tests to evaluate it in the Buckshot clay were not conducted given the magnitude of

collapsing volume change is small with such a cohesive soil and difficult to separate out from the swelling response inherent in the material.

LIST OF REFERENCES

LIST OF REFERENCES

Aitchison, G. D. (**1960**). "Relationships of Moisture Stress and Effective Stress Functions in Unsaturated Soils," *Pore Pressure and Suction in Soils, Conference* by British Nat. Soc. of the Int. Soc. of Soil Mech. and Found. Eng., London, England: Butterworths, March, 1960, pp.47-52.

Alonso, E. E., Gens, A. and Josa, A., (**1990**). "A constitutive model for partially saturated soils," *Geotechnique,* Vol. 40, No. 3 pp. 405-430.

Barden, L., A. O. Madedor, and G. R. Sides (**1969**). "Volume Change Characteristics of Unsaturated Clay," *Journal of the Soil Mechanics and Foundations Division,* ASCE, Vol. 95, No. SM1, Jan, 1969, pp. 33-50.

Barden L, A. McGown, and K. Collins (**1973**). "The Collapse Mechanism in Partly Saturated Soil," *Engineering Geology,* Vol. 7, pp. 49-60.

Barker, W. R. and Gonzalez, C. R. (**1991**). "Pavement Design by Elastic Layer Theory," *Proceedings of the ASCE Conference on Aircraft/Pavement Interaction,* Kansas City, MO.

Berney, E. S., Peters, J. F., Newman, J. K., and Smith, D. M., (**2003**). "Effect of Surfactant on Dry-side Compaction of Silty-Sand," *Proceedings 8th Intl. Conf. on Low Volume Roads,* Transportation Research Record, No. 1819, Vol. 2. pp. 57-62.

Biot, M. A. (**1941**). "General Theory of Three-Dimensional Consolidation," *Journal of Applied Physics,* Vol. 12, no. 2, Feb. 1941, pp. 155-164.

Biot, M. A. (**1977**). "Variational Lagrangian-thermodynamics of non isothermal finite strain. Mechanics of porous solid and thermo-molecular diffusion," *International Journal of Solids and Structures,* Vol. 13, 579-597.

Bishop, A. W., Alpan, I., Blight, G. E. and Donald, I. B. (**1960**). "Factors Controlling the Strength of Partially Saturated Soils," *Research Conference on Shear Strength of Cohesive Soils,* ASCE, pp. 503-532.

Bishop, A. W., and Garga, V. K., (**1969**). "Draind Tension Tests in London Clay," *Geotechnique,* Vol. 19, No. 2, pp. 309-313.

Blight, G. E. (**1965**). "A Study of Effective Stresses for Volume Change," *Proceedings of the Symposium on Moisture Equilibria and Moisture Changes in Soils Beneath Covered Areas*, Sydney Australia, Buttersworth: London, 1965, pp. 259-269.

Bolt, G. H. and R. D. Miller (**1958**). "Calculation of Total and Component Potentials of Water in Soil," *American Geophysics Union Transportation*, Vol. 39, pp. 917-928, 1958.

Brackley, I.J.A. (**1975**). "A model of unsaturated clay structure and its application to swell behaviour," *Sixth Regional Conference for Africa for Soil Mechanics and Foundation Engineering*, Durban, South Africa, Sept. 1975, pp. 71-79.

Buckingham, E. (**1907**). *Studies of the movement of Soil Suctino*, U.S. Dept. of Agriculture, Bureau of Soils, Bull. No. 10.

Burland, J. B. (**1965**). "Some Aspects of the Mechanical Behavior of Partially Saturated Soils," *Proceedings of the Symposium on Moisture Equilibria and Moisture Changes in Soils Beneath Covered Areas*, Sydney Australia, Buttersworth: London, 1965, pp. 270-278.

Briggs, Lyman J. (**1897**). "The Mechanics of Soil Moisture," *Bulletin No. 10*, U.S. Dept. of Agriculture, Division of Soils, Washington: Government Printing Office, 1897.

Coleman, Bernard D. and Morton E. Gurtin, (**1967**), "Thermodynamics with Internal State Variables," *The Journal of Chemical Physics*, Vol. 47, No. 2, pp. 597-613.

Colman, B. and Gurtin, M. (**1967**). "Thermodynamics of Internal State Variables," *Journal of Chemistry and Physics*, Vol 47, pp 597-613.

Coussy, O. (**1989**). "A general theory of thermoporoelasticity for saturated porous materials," *Transport in porous media*, Vol. 4, pp. 281-293.

Coussy, O. (**1995**). *Mechanics of Porous Continua*, John Wiley & Sons; New York, New York, 1995.

Cox, D. W. (**1978**). "Volume Change of Compacted Clay Fill," *Proceedings of the Conference on Clay Fills*, Institution of Civil Engineers, London, U.K., pp. 79-87.

Croney, D., and J. D. Coleman (**1948**). "Soil Thermodynamics Applied to the Movement of Moisture in Road Foundations," *Proceedings of the 7th International Congress of Applied Mechanics*, Vol. 3, 1948, pp. 163-177.

Croney, D. and J. D. Coleman (**1961**). "Pore Pressure and Suction in Soil," *Pore Pressure and Suction in Soils*, Buttersworth; London, 1961.

Cundal, P. A. (**2002**). "A discrete future for numerical modeling," *Discrete Element Methods: Numerical Modeling of Discontinua*, ASCE Geotechnical Special Publication No. 117, 3-4.

Dudley, J. H. (**1970**). "Review of Collapsing Soils," *Journal of the Soil Mechanics and Foundations Division*, ASCE, Vol. 96, No. SM3, pp. 925-947.

Escario, V. and J. Saez (**1986**). "The Shear Strength of Partly Saturated Soils," *Geotechnique*, Vol. 36, No. 3, pp. 453-456.

Escario, V. and J. Saez (**1987**). "Shear Strength of Partly Saturated Soils Versus Suction," *Proceedings of the 6th International Conference on Expansive Soils*, Delhi, India, Vol. 2, pp. 602-604.

Fenwick, W. B. (**1968**). "Gyratory compaction of soil. Report 3, Crushed limestone data report," *TR S-68-6 Rept. 3*, U.S. Army Corps of Engineers, Waterways Experiment Station, Vicksburg, MS.

Fredlund, D. G., and N. R. Morgenstern (**1977**). "Stress State Variables for Unsaturated Soils," *Journal of the Soil Mechanics and Foundations Division*, ASCE, Vol. 103, 1977, pp. 447-466.

Fredlund, D. G., and H. Rahardjo (**1993**). *Soil Mechanics for Unsaturated Soils*, New York, New York: John Wiley and Sons, 517 pp. 1993.

Freeman, R.B., Velez, E., Mason, L., and Carr, H. (**2004**). "Airfield Pavement Test Section with High Repetition Traffic," *draft technical report*, Geotechnical and Structures Laboratory, Engineer Research and Development Center, U.S. Army Corps of Engineers.

Gens, A. and Alonso, E. E., (**1992**). "A framework for the behaviour of unsaturated expansive clays," *Canadian Geotechnical Journal*, Vol. 29, pp. 1013-1032.

Herman, W. and Bertholf, L. D. (**1983**) "Explicit Lagrangian Finite-Difference Methods," *Computational Methods for Transient Analysis*, Ed. T. Belytschko and T. J. R. Hughes, Elsevier Science Publishers,B. V. pp 361-416.

Hilf, J. W. (**1956**). "An Investigation of Pore-Water Pressure in compacted Cohesive Soils," Ph.D. Dissertation, Technical Memorandum No. 654, U.S. Dept. of the Interior, Bureau of Reclamation, Design and Construction Division, Denver, Colorado.

Holtz, R. D. and Kovacs, W. D. (**1981**). *An Introduction to Geotechnical Engineering*, N. M. Newmark and W. J. Hall Eds., Prentice-Hall, Inc.; Englewood Cliffs, New Jersey.

Houlsby, G. T. **(1997)**. "The work input to an unsaturated granular media," *Geotechnique*, Vol. 47, No. 1, pp. 193-196.

Houlsby, G. T. and Puzrin, A. M. **(2000)** "A thermodynamic framework for constitutive models for rate-independent dissipative materials," *International Journal of Plasticity*, Vol 16, pp 1017-1047.

Jaky, J. **(1948)**. "Pressure in silos," *Proceedings of the 2nd International Conference on Soil Mechanics and Foundation Engineering*, Vol. 1, pp. 103-107.

Jennings, J. E. B., and J. B. Burland **(1962)**. "Limitations to the Use of Effective Stress in Partly Saturated Soils," *Geotechnique*, Vol. 12, No. 2, pp. 125-144.

Josa, A., **(1988)**. "Un modelo elastoplastico para suelos no saturados," *Tesis Doctorae*, Universitat Politecnica de Catalunya, Barcelons, Spain.

Lawton, E. C. **(1986)**. "Wetting Induced Collapse on Compacted Soil," *Ph.D. Thesis*, Washington State Univeristy, Pullman, Washington.

Lawton, E. C., R. J. Fragaszy, and J. H. Hardcastle, **(1989)**. "Collapse of Compacted Clayey Sand," *Journal of Geotechnical Engineering*, ASCE, Vol. 115, No. 9, pp. 1252-1267.

Leavell, D. A. and Peters, J. F. **(1987)**. "Uniaxial Tensile Test for Soil," *TR GL-87-10*, U.S. Army Corps of Engineers, Waterways Experiment Station, Vicksburg, MS.

Lee, E. H. **(1962)**, "Viscoelasticity," *Handbook of Engineering Mechanics.* McGraw-Hill, New York, pp. 53-1 to 53-21.

Lee, I. K. and Ingles, O. G., **(1968)**. "Strength and Deformation of Soil and Rock," in *Soil Mechanics Selected Topics*, I. K. Lee, Ed., Elsevier, New York, pp. 268-283.

Leonards, G. A. **(1952)**. Discussion to "Effect of Compaction on Soil Properties", by S. D. Wilson, *Proceedings , Conference on Soil Stabilization*, M.I.T., June, pp. 159-161.

Leonards, G. A. **(1955)**. "Strength Characteristics of Compacted Clays," *Transactions of the American Society of Civil Engineers*, Vol. 120, paper no. 2780, pp. 1420-1454.

Li, X. S. **(2003)**. "Effective stress in unsaturated soil: a microstructural analysis," *Geotechnique*, Vol. 53, No. 2, pp. 273-277.

Lubliner, J. (1990). *Plasticity Theory*, Macmillan Publ. Co.; New York, New York.

Matsuoka, H. (**1974**). "Stress-strain relationships on sand based on the spatial mobilized plane," *Soils and Foundations*, Vol. 16, No. 2, pp. 47-61.

Matyas, E. L. and H. S. Radakrishna (**1968**). "Volume Change Characteristics of Patially Saturated Soils," *Goetechnique*, Vol. 18, No.4, Dec. 1968, pp. 432-448.

Meade, R. B. (**1988**). "Regarding the Development of a Micromechanically-based Elastic-Plastic Constitutive Model for Soils," *Internal Memorandum,* Soils and Rock Mechanics Division, Geotechincal Laboratory, U.S. Army Corps of Engineers, ERDC, Vicksburg, MS.

Mitchell, J. K. (**1976**). *Fundamentals of soil behavior*, John Wiley and Sons; New York, New York.

Molenkamp, F. and A. H. Nazemi (**2003**). "Interactions between two rough spheres, water bridge and water vapour," *Geotechnique*, Vol. 53, No. 2, pp. 255-264.

Peters, John F., Dan A. Leavell, Lawrence D. Johnson (**1982**). *Analysis of Strain Softening Behavior of Soil*, US Army Corps of Engineers, Waterways Experiment Station, Vicksburg, MS.

Peters, J. F. and Leavell, D. A., (**1988**). "Relationship Between Tensile and Compressive Strengths of Compacted Soils," *Advanced Triaxial Testing of Soil and Rock, ASTM STP 977,* Robert T. Donaghe, Ronald C. Chaney, and Marshall L. Silver, Eds., American Society for Testing and Materials, Philadelphia, 1988, pp. 169-188.

Peters, J. F. (**1988**). "Regarding Implementation of a Micromechanically-based Elastic-Plastic Constitutive Model for Soils," *Internal Memorandum,* Soils and Rock Mechanics Division, Geotechincal Laboratory, U.S. Army Corps of Engineers, ERDC, Vicksburg, MS.

Peters, J. F. (**1991**). "Computational Aspects of Endochronic Plasticity," *Proceedings of Computer Methods and Advances in Geomechanics*, Eds. G. Beer, J. R. Booker, and J. P. Carter, A. A. Balkema, pp. 1197-1202.

Peterson, R. W., (**1990**). "The Influence of Soil Suction on the Shear Strength of Unsaturated Soil," *Miscellaneous Paper GL-90-17*, Dept. of the Army, US Army Corps of Engineers, Waterways Experiment Station, Vicksburg, MS.

Porter, O. J. (**1942**). *Lecture Course on the California Method of Determining the Relative Bearing Value of Soils and Application to Design of Highways and Runways*, War Dept., US Engineer Office, Sacramento, CA, Apr. 6-10, 1942.

Proctor, R. R. (**1933**). "Fundamental Principles of Soil Compaction," *Engineering News Record,* Aug. 31, Sept. 7, 21, 28, 1933.

Radakrishna, H. S. (**1967**). "Compressiblity of Partially Saturated Soils," *Ph.D. Thesis*, University of Waterloo, Canada.

Schofield, A. and Wroth, P. (**1968**). *Critical State Soil Mechanics*, McGraw Hill; New York, New York.

Seed, H. B., Chan, C. K. (**1959a**). "Structure and Strength Characteristics of Compacted Clays," *Journal of the Soil Mechanics and Foundations Division*, ASCE, Vol. SM5 Part I, Oct. 1959, pp. 87-128.

Seed, H. B. and C. K. Chan (**1959b**). "Undrained Strength of Compacted Clays After Soaking," *Journal of the Soil Mechanics and Foundations Division,* ASCE, Vol. 85, No. SM6 Part I, Dec. 1959, pp. 31-47.

Seed, H. B., J. K. Mitchell, and C. K. Chan (**1960**). "The Strength of Compacted Cohesive Soils," *Research Conference on Shear Strength of Cohesive Soils*, ASCE, pp. 877-964.

Seed, H. B., R. J. Woodward, and R. Lundgren (**1962**). "Prediction of Swelling Potential for Compacted Clays," *Journal of the Soil Mechanics and Foundations Division*, ASCE, Vol. 88, No. SM3, pp. 53-87.

Sivakumar, V. (**1993**). "A Critical State Framework for Unsaturated Soil," *Ph.D. Thesis*, University of Sheffield, England.

Skempton, A.W. (**1964**). "Long term stability of clay slopes," *Géotechnique*, Vol. 14, No. 2, pp. 77-101.

Smith, D. M. (**2000**). *Response of Granular Layers in Flexible Pavements Subjected to Aircraft Loads*, Ph.D. Dissertation, Louisiana State University, Baton Rouge, LA.

Smith, D. M., Peters, J. F., and Rollings, R. S. (**2001**). "Development of a Granular Media for Finite Element Analysis," *ERDC/GSL TR-01-3*, U.S. Army Engineering Research and Development Center, Vicksburg, MS.

Snethen, D. R., L. D. Johnson, and D. M. Patrick (**1977**). "An Investigation Of The Natural Microscale Mechanisms That Cause Volume Change In Expansive Clays," *Report No. FHWA-RD-77-75*, Office of Research and Development, Federal Highway Administration; Washington, D. C.

Subba Rao, K. S. (**2000**). "Swell-Shrink Behavior of Expansive Soils – Geotechnical Challenges," *Indian Geotechnical Journal*, Vol. 30, No. 1, Jan. 2000.

Terzaghi, Karl (**1943**). *Theoretical Soil Mechanics*, New York, New York: Wiley, 1943.

Timoshenko, S. P., and J. N. Goodier, (**1937, 1987**). *Theory of Elasticity*, McGraw Hill Inc.; St. Louis, MS, pp. 244-249.

Toll, D. G. (**1988**). "The Behavior of Unsaturated Compacted Naturally Occurring Gravel," *Ph.D. Thesis*, University of London, England.

Tordesillas, A. and S. Walsh (**2002**). "Incorporating roling resistance and contact anisotropy in micromechanical models of granular media," *Powder Technology*, 124:106-111.

Valanis, K. C. (**1968**). "Unified theory of thermomechanical behavior of viscoelastic materials," *Mechanical Behavior of Materials under Dynamic Loads,* ed. U.. Lindholm, Springer-Verlag, New York, pp 343-364.

Valanis, K. C. (**1971**) "A theory of viscoplasticity without a yield surface, Part I: General theory; Part II: Applications to mechanical of metals," Archives of Mechanics, Vol 23, pp 517-551.

Valanis, K.C., (**1980**), "Fundamental consequences of a new intrinsic time measure. Plasticity as a limit of the endochronic theory," *Archives of Mechanics*, Vol. 32, pp. 171-191.

Valanis, K. C. and Lee, C. F. (**1984**). "Endochronic Plasticity: Physical Basis and Applications," *Mechanics of Engineering Materials*, ed. C. S. Desai and R. H. Gallagher, John Wiley & Sons Ltd. pp 591-609.

Valanis K. C. and Reed, H. E. (**1986**). "An endochronic plasticity theory for concrete," *Mechanics of Materials*, Vol 5, pp 277-295.

Valanis, K. C. and Peters, J. F. (**1991**). "An Endochronic Plasticity Theory with Shear-Volumetric Coupling," *International Journal for Numerical and Analytical Methods in Geomechanics*, Vol. 15, pp. 77-102.

Wilson, S. D. (**1952**). "Effect of Compaction on Soil Properties," *Proceedings , Conference on Soil Stabilization*, M.I.T., June, pp. 148-158.

Wheeler, S. J. and Sivakumar, V., (**1995**). "An elasto-plastic critical state framework for unsaturated soil," *Geotechnique*, Vol. 45, No. 1, pp. 35-53.

APPENDICES

Appendix A
The Use of CModeler for Calibration of the MMM

A.1 Introduction to CModeler

A stand-alone version of the Multi-Mechanical Model called CModeler (Constitutive Model Calibrator) was written to aid in determining the global and distributed parameters required for the saturated calibration of the MMM program. CModeler is a Visual Basic program that provides the user a simple PC compatible platform to readily simulate triaxial laboratory tests to establish viability of model calibration parameters shown in Section A.2.

CModeler consists of a graphical front end for visual calibration of the global model parameters (Section A.3) coupled with a FORTRAN program titled Calibrator.f90 (Section A.5) that takes discretized stress-strain data input from CModeler and generates the distributed calibration parameters (Section A.4). The description of the global parameters in Table 5.1 is well documented in section 5.4.3 and CModeler allows a graphical means to obtain each parameter through analysis of various stress spaces shown in the following figures. The distributed calibration parameters are obtained through CModeler by graphically approximating a stress-strain curve by dividing it into four segments as described in Chapter 8.3, inserting the stress-strain magnitude of each discrete point into a series spring-slider assembly and then through algebra converting the linear system into a parallel spring-slider assemblage.

As discussed in Chapter 5 and 8, selection of stress-strain pairs in deviatoric or hydrostatic stress space represents the behavior of the spring sliders in a series assemblage (Figure 5-4). Calibrator.f90 converts this series arrangement to parallel through the use of algebraic relationships that convert between Kelvin and Maxwell elements. A detailed discussion of this conversion process and its method in the code is examined here.

A.2 Operation of CModeler Software

To begin work in CModeler, a database file must be either opened or created from the default screen as shown in Figure A-1:

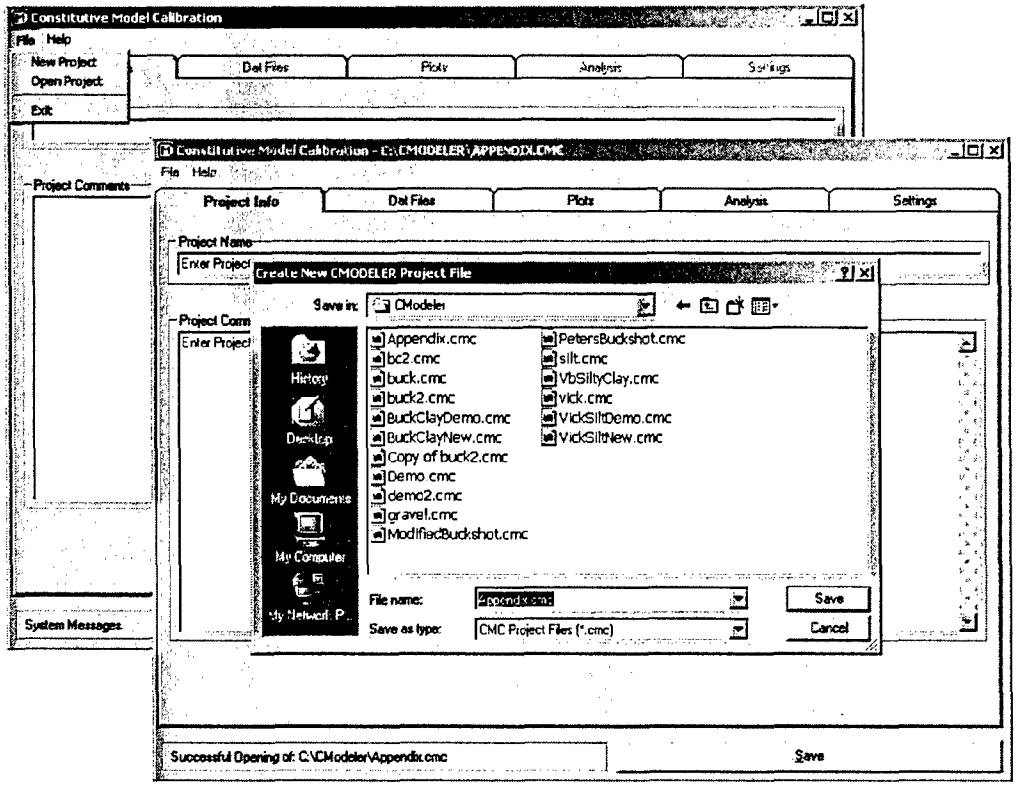

Figure A-1: Opening default screen to CModeler

Once a file has been created or opened, a series of data files must be input containing laboratory data taken from either drained or undrained triaxial tests or isotropic/one-dimensional consolidation tests as shown in Figure A-2. The Dat Files tab and the ADD or DELETE buttons allow selection of data files in a digitized format. The data file formats necessary for proper assimilation of laboratory test data by CModeler are given in Figure A-3.

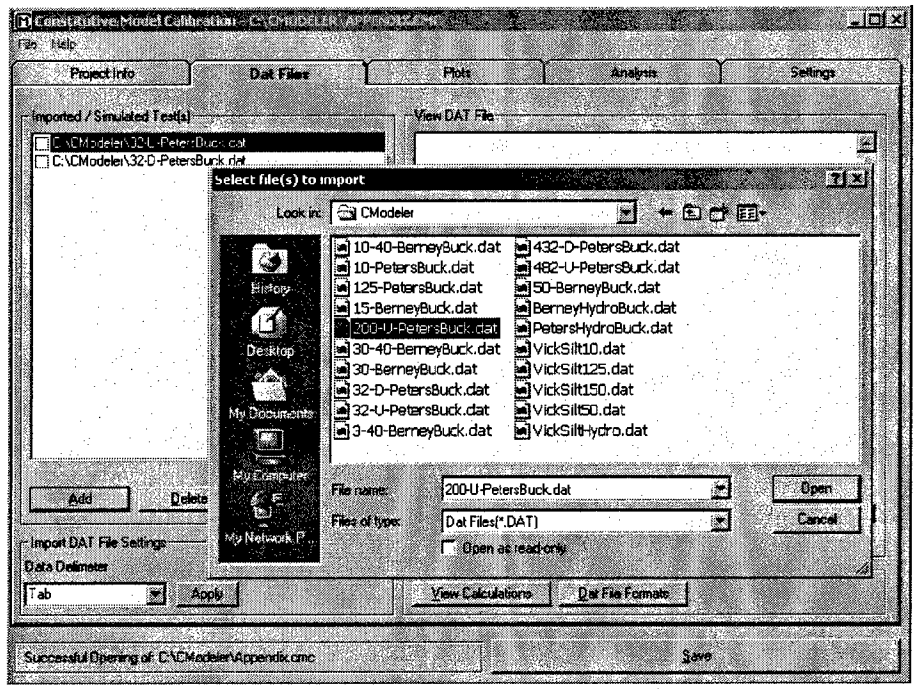

Figure A-2: Opening and incorporation of data files into CModeler

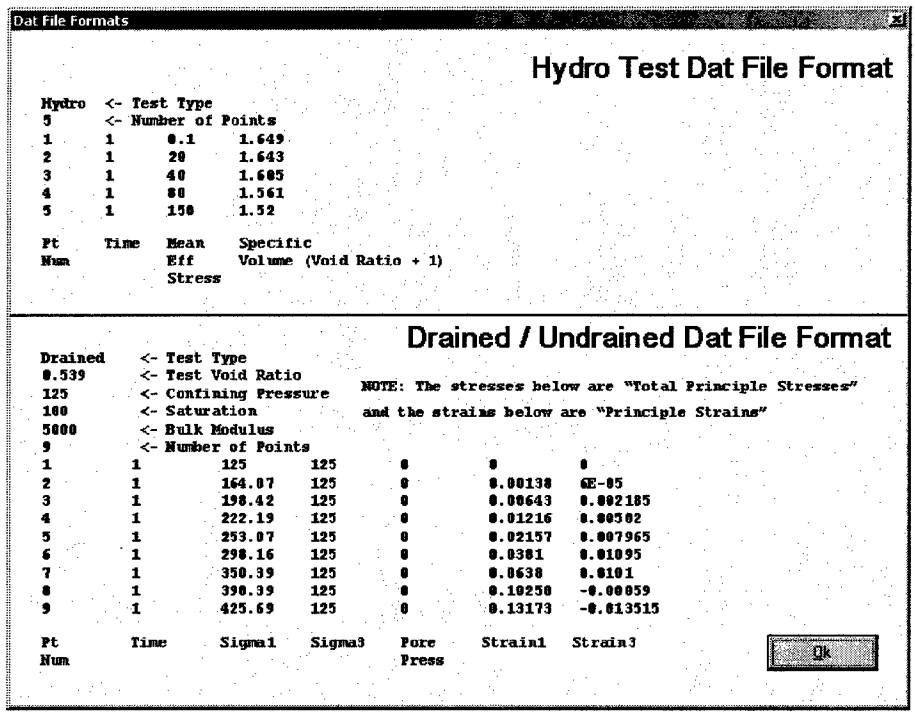

Dat File Formats

Hydro Test Dat File Format

```
Hydro   <- Test Type
5       <- Number of Points
1       1       0.1     1.649
2       1       20      1.643
3       1       40      1.605
4       1       80      1.561
5       1       150     1.52

Pt      Time    Mean    Specific
Num             Eff     Volume (Void Ratio + 1)
                Stress
```

Drained / Undrained Dat File Format

```
Drained     <- Test Type
0.539       <- Test Void Ratio
125         <- Confining Pressure
100         <- Saturation
5000        <- Bulk Modulus
9           <- Number of Points
```

NOTE: The stresses below are "Total Principle Stresses" and the strains below are "Principle Strains"

Pt Num	Time	Sigma1	Sigma3	Pore Press	Strain1	Strain3
1	1	125	125	0	0	0
2	1	164.07	125	0	0.00138	6E-05
3	1	198.42	125	0	0.00643	0.002185
4	1	222.19	125	0	0.01216	0.00502
5	1	253.07	125	0	0.02157	0.007965
6	1	298.16	125	0	0.0381	0.01095
7	1	350.39	125	0	0.0638	0.0101
8	1	390.39	125	0	0.10250	-0.00059
9	1	425.69	125	0	0.13173	-0.013515

Ok

Figure A-3: Hydrostatic (consolidation) and Triaxial (Drained/Undrained) File Formats for CModeler

A.3 Calibration of Global Parameters using CModeler

To begin using the software, the Analysis screen (*Figure A-4*) shows the user the necessary input parameters for calibrating the model and the drop down window shown illustrates the types of calibration techniques available within the package. Yield/Dilatancy allows selection of the friction and dilation angles to fit the strength and critical state envelopes in a normalized stress space. Shear calibration allows selection of four points on a specific triaxial shear stress-strain plot to define the relative shear modulus and strength for the deviatoric spring-slider mechanisms. The Mean calibration function allows selection of four points from a consolidation data set in semi-logarithmic space to calibrate the bulk modulus and strength for the hydrostatic spring-slider mechanisms. Bulk modulus is no longer applicable, where K in the above illustration is now for the input of Poisson's ratio. Shear modulus is no longer input, but calculated from bulk modulus and Poisson's ratio and is a dead cell in the Figures.

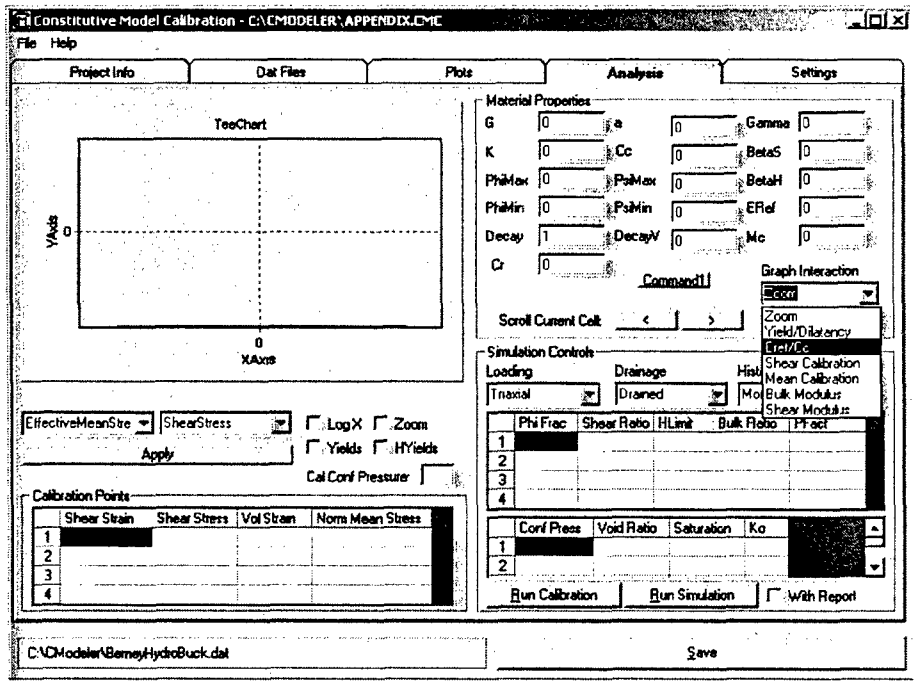

Figure A-4: Blank analysis screen for CModeler illustrating the necessary calibration inputs

To perform the calibration for both the hydrostatic mechanisms and to define the reference void ratio and compression indices, a consolidation test of the format in Figure A-3 must be selected from the database of laboratory tests as shown in Figure A-5.

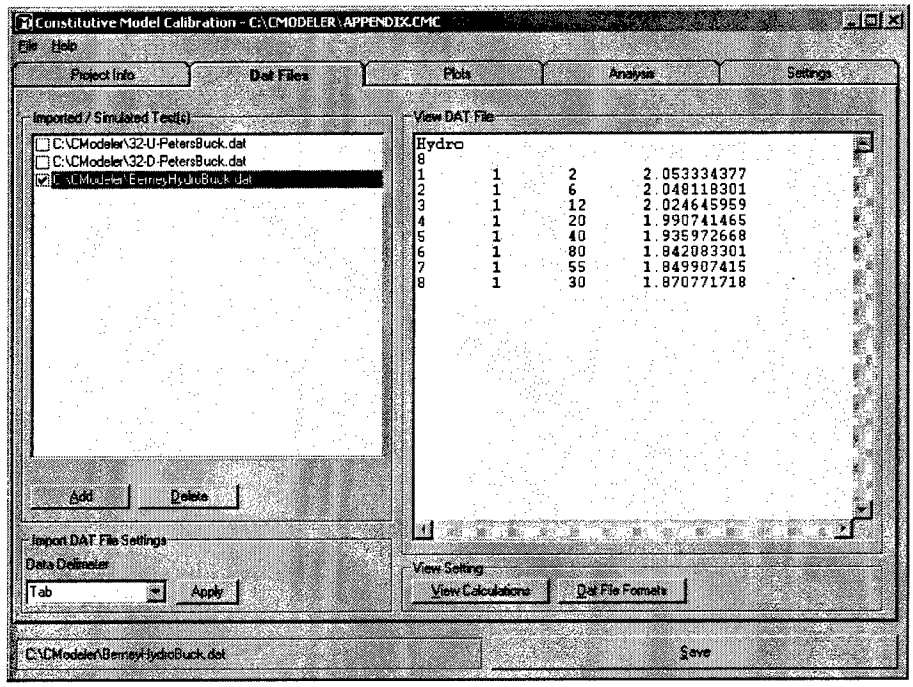

Figure A-5: Selecting a consolidation test for Mean calibration

Once the data sets are selected from the available list, using the Analysis tab, both the Eref/Cc and the Mean calibration options plot the data in the proper void ratio-log mean stress space. The Eref/Cc option provides 3 points which can be graphically aligned along the normal and reconsolidation planes of the data as shown in Figure A-6 to determine the reference void ratio, e_{ref}, compression index, C_c and the recompression index, C_r. The Mean calibration option provides 4 points which can be graphically arranged to trace the compression loading stress path of the consolidation test to define the modulus and strength limits of the hydrostatic spring-slider mechanisms as shown in Figure A-7.

To begin calibration of the shear response, a specific triaxial data set must be selected at a given confining pressure of the proper format shown in Figure A-8. The Analysis tab is next selected when the Shear calibration option is selected, the triaxial

data is automatically plotted in a shear strain-shear stress space along with four points that can be moved graphically to depict the modulus and strength limits of the deviatoric spring-slider mechanisms as shown in Figure A-9.

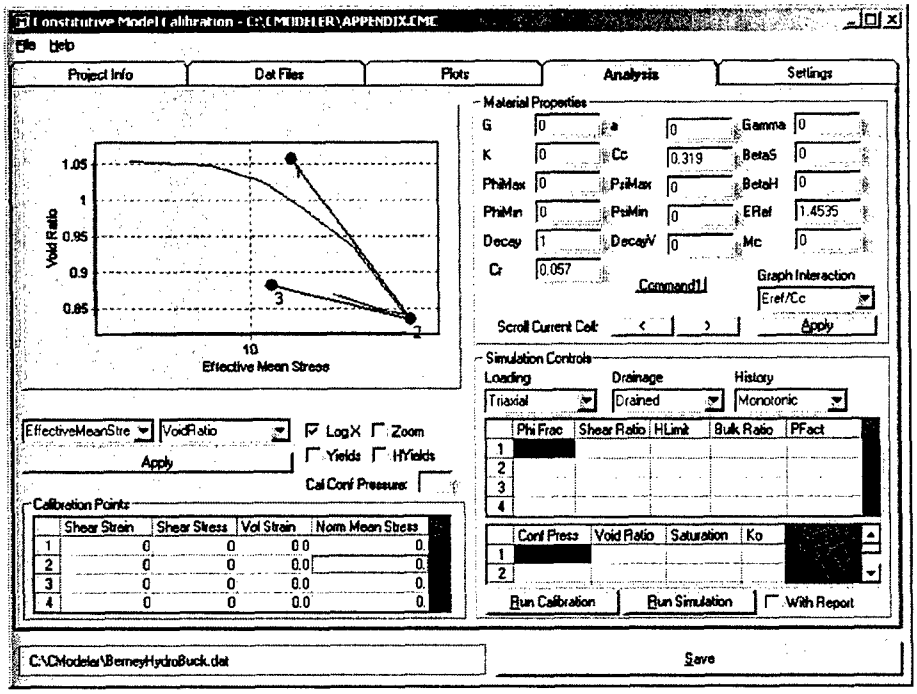

Figure A-6: Determination of the reference void ratio and compression indices

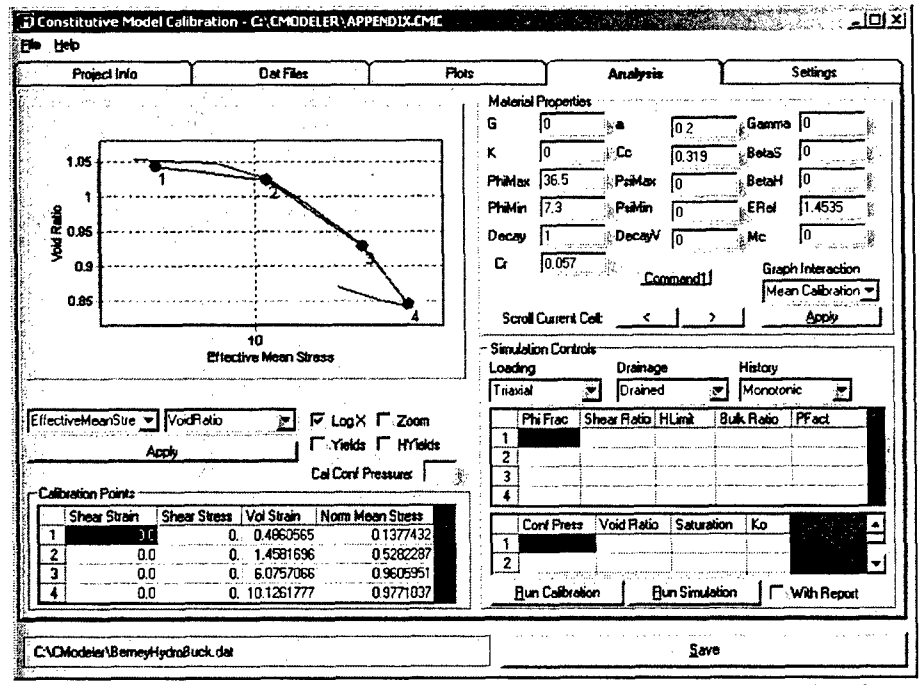

Figure A-7: Calibration of the hydrostatic mechanisms through Mean Calibration option

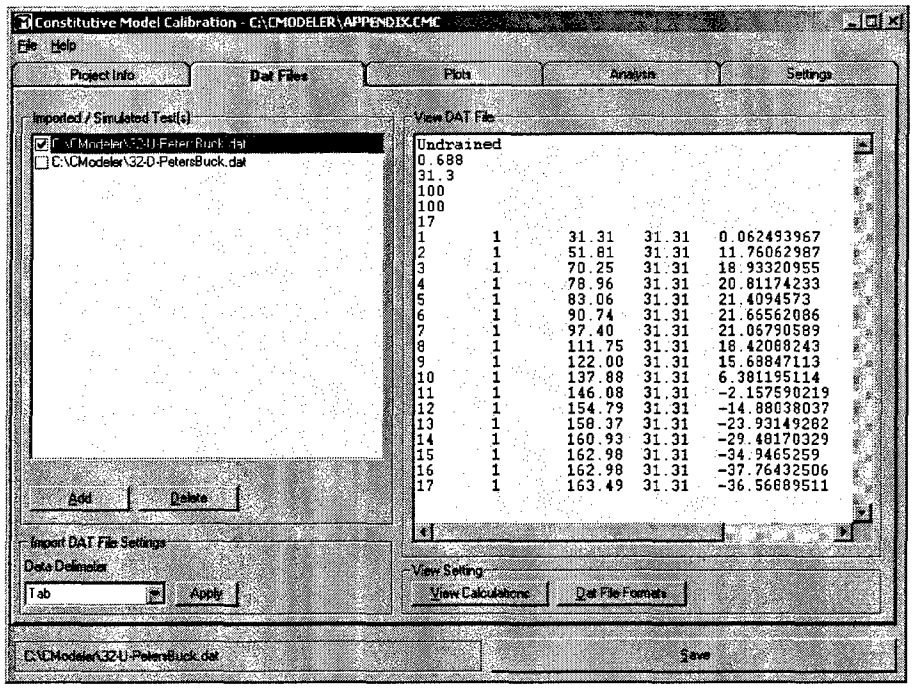

Figure A-8: Selecting a triaxial test for Shear calibration

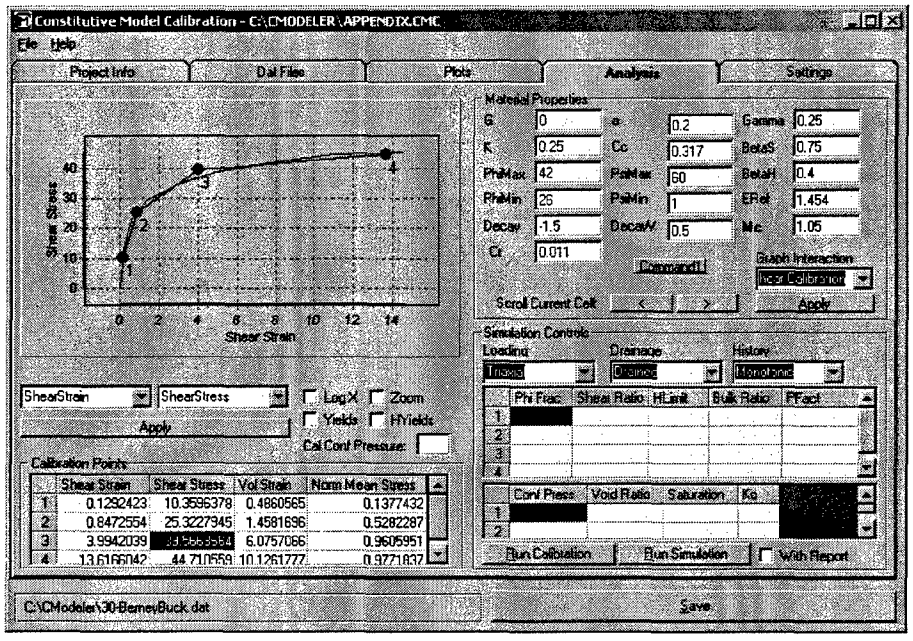

Figure A-9: Calibration of deviatoric mechanisms through Shear Calibration option

To calibrate the maximum and minimum friction and dilatant angles, Phi and Psi, as many triaxial tests as possible should be selected from the database and under the Analysis tab, the Yield/Dilatancy option will plot them all in the proper normalized shear-mean stress space along with four points which can be graphically moved to provide the limits to the friction and dilatancy angles, the normalized cohesion value, *a* found along the mean stress axis and the critical state parameter, M_c shown in Figure A-10. In addition to the four points, a pair of curved lines representing the failure and critical state envelopes appears to help the user visually interpolate the location of the surfaces. Three points define the curvature of the failure and critical state envelopes: the position of PhiMax, M_c and the value of Decay for failure and PsiMin, M_c and DecayV for the critical state. The values of Decay and DecayV are manually input by the user.

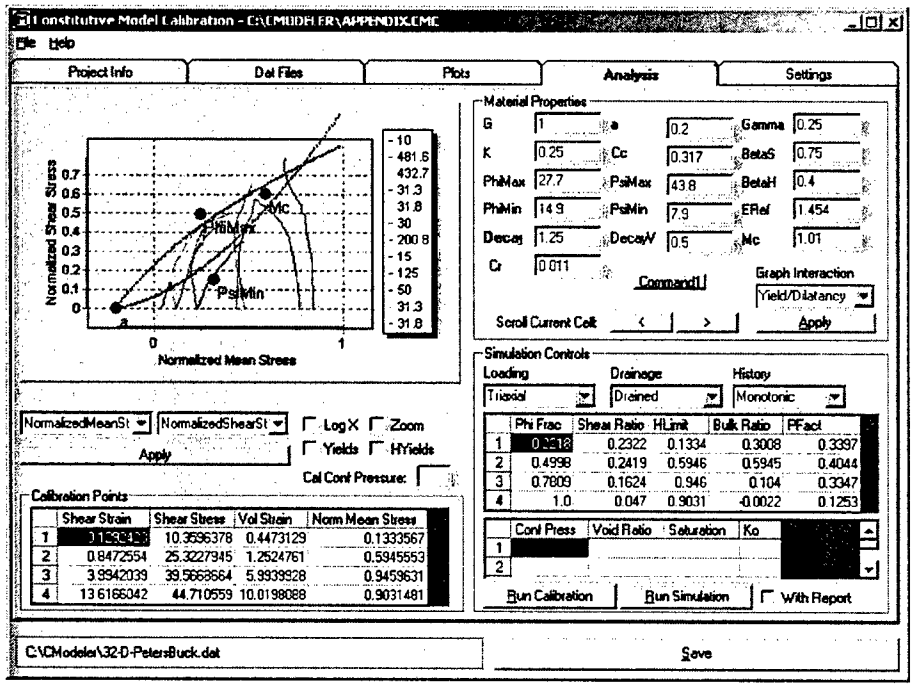

Figure A-10: Yield and Dilatancy Calibration using CModeler

This procedure represents the final set of values to be determined graphically. BetaS and BetaH must be input manually within their ranges of 0 to 1 and Gamma is typically input manually. Given the proper data, it is possible to determine Gamma

graphically and/or statistically by solving equation 5.12 for each triaxial test shown in equation A.1.

$$\frac{d\varepsilon_v^p}{d\varepsilon_q^p} = \gamma\left(M_c - \frac{q_i}{p_i}\right) \tag{A.1}$$

CModeler allows the user to calculate this relationship and provides the visual means to observe its relationship.

Once all the Calibration points and Material Properties are inserted, a confining pressure associated with the Shear calibration (Figure 9) must be input into the Cal Conf Pressure box. Once this is done, the distributed parameters PhiFrac, ShearRatio, HLimit, BulkRatio and PFact can be determined by simply pressing the Run Calibration button. These 20 numbers represent the modulus, strength and relative distribution of these factors for both the deviatoric and hydrostatic parallel arrangement of spring-slider mechanisms used by the MMM shown in Figure A-11.

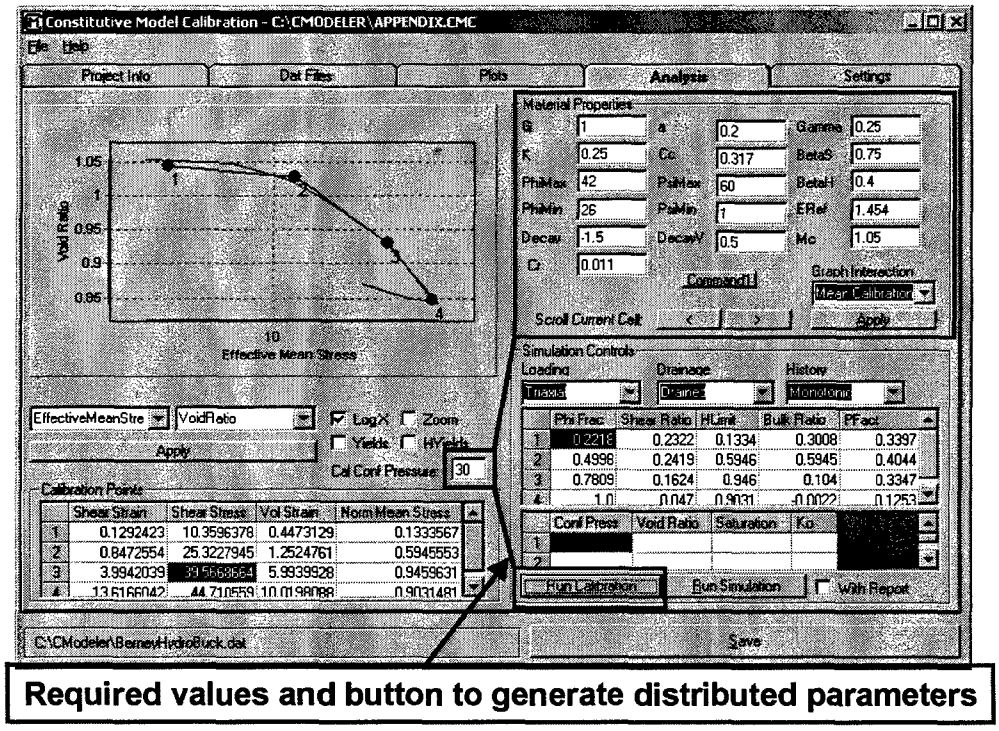

Figure A-11: Procedure to determine distributed parameters for operation of MMM

Combining these with the Material Properties, simulations of saturated triaxial tests at any confining pressure and initial void ratio can be performed and the results plotted separate or in tandem with existing laboratory data shown in Figure A-12.

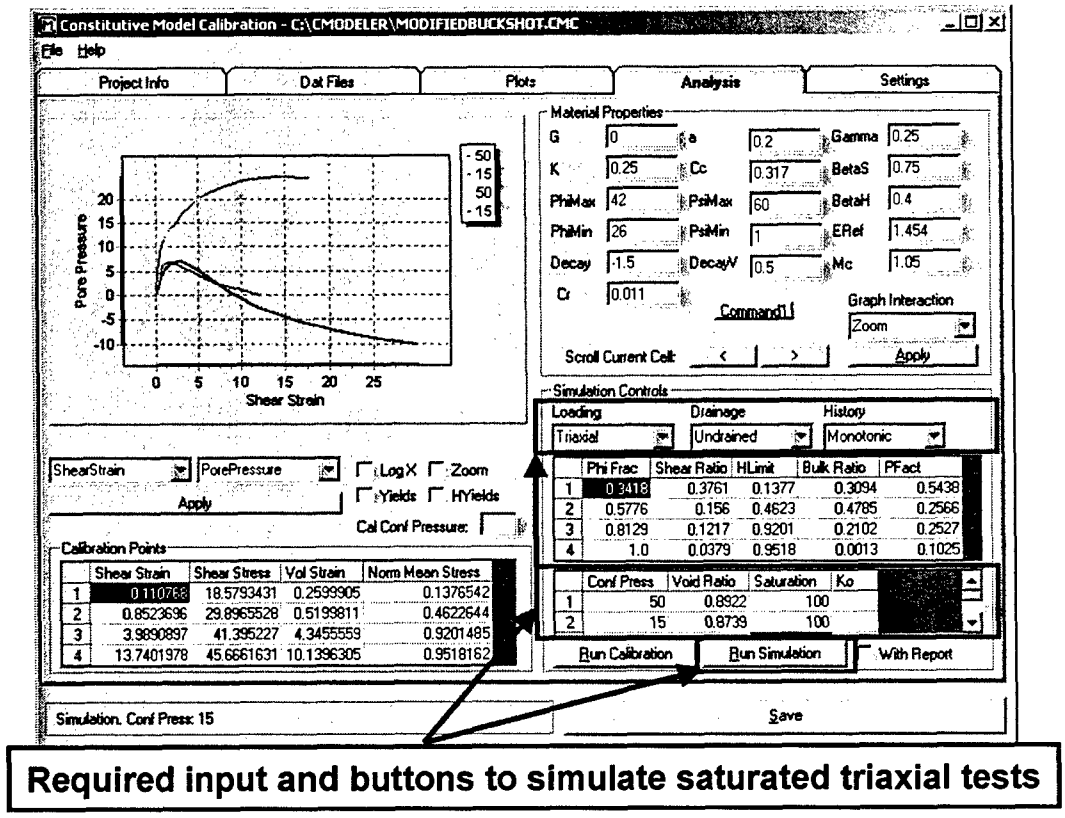

Figure A-12: Procedure to simulate saturated triaxial tests for any void ratio/mean stress condition

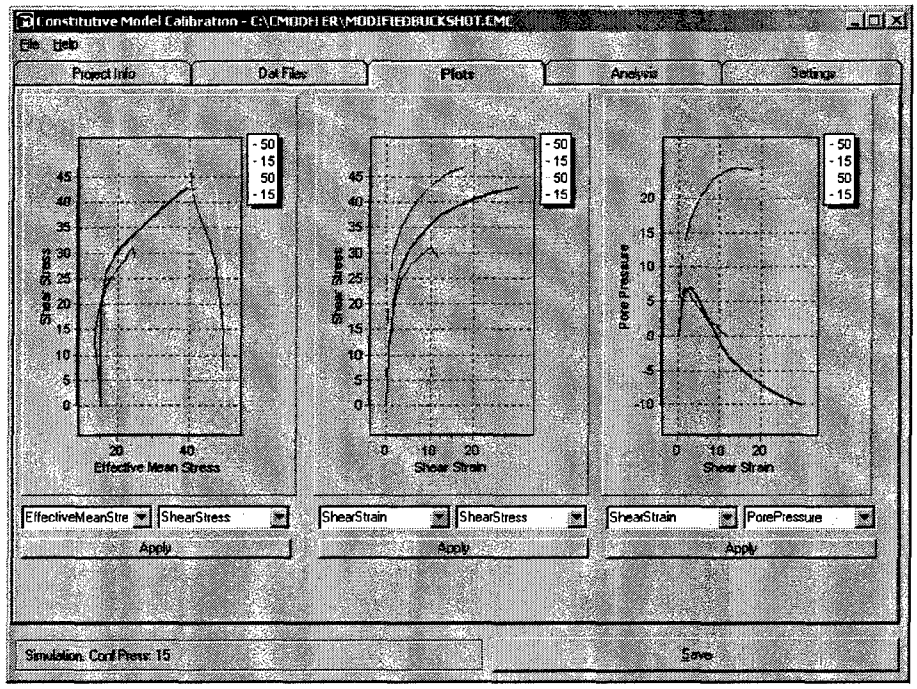

Figure A-13: Use of Plots tab to display multiple variables for model comparison

A.4 Calibration of the Distributed Parameters

In order to calibrate the distributed parameters in the MMM, CModeler requires the selection of four points (not including the origin) in a shear strain-shear stress space as shown in Figure A-9 and four points along the void ratio-effective mean stress space as shown in Figure A-7. These 8 data points are then passed to Calibrator.f90 along with the initial confining pressure of the sheared triaxial specimen, the maximum and minimum friction angles along the failure envelope of all the triaxial specimens, the fitting parameter β_s and β_h and an estimate of the maximum bulk and shear modulus. These last two modulus parameters are now obsolete as they are divided out during the computation of the distributed parameters and as such are no longer necessary. As well, the magnitudes of the maximum moduli are based on the methods described in section 5.4.3 and no longer are fitted to any unique triaxial curve.

The following steps will provide the reader an overview of the operation of Calibrator.f90 along with a reiteration of the common stress definitions used:

A.4.1 Initialize the Data Set

Begin by taking the shear stress-strain response data and reduce by graphically selecting 4 distinct data points that best fit the response. This data will be used to generate the deviatoric calibration curve in the series system. As well, select 4 distinct points along the void ratio-mean stress curve using a consolidation data set that best fits the hydrostatic response.

The definition of shear stress passed to the program is:

$$q = \sigma_1 - \sigma_3 \tag{A.2}$$

σ_1 = major principal stress (largest)

σ_3 = minor principal stress (smallest)

The definition of mean stress is:

$$p = (\sigma_1 + 2\sigma_3)/3 \tag{A.3}$$

The definition of the reference stress, p_{ei} is :

$$p_{ei} = p_{eo} * 10 \wedge [(e_o - e_i)/C_c] \tag{A.4}$$

where e_o is the value of void ratio at the stress p_{eo} defined as 1 psi in the present formulation, and p_{ei} is reference stress along the normally consolidated line (NCL) for any void ratio, e selected to define the consolidation curve as shown in Figure A-14.

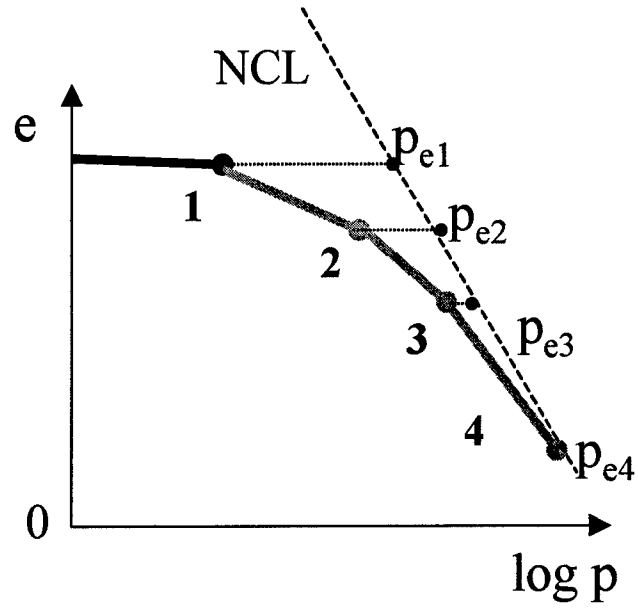

Figure A-14: Definition of p_{ei} for points selected from consolidation data

The definition of shear strain is:

$$\varepsilon_q = \varepsilon_1 - \varepsilon_3 \tag{A.5}$$

ε_1 = major principal strain

ε_3 = minor principal strain

The definition of volumetric strain is:

$$\varepsilon_v = \varepsilon_1 + 2\varepsilon_3 \tag{A.6}$$

which is calculated from void ratio within CModeler as:

$$\varepsilon_{vi} = \frac{e_o - e_i}{1 + e_o} \tag{A.7}$$

A.4.2 Data Insertion

Once the 4 shear stress-shear strain data points are determined in CModeler, they are then passed including the value of p_e at $q = 0$, $p = p_o$ into the Calibrator.f90 program. Because only shear stress is passed, a value of mean stress must be determined for each point in order to define the strength in terms of a friction angle. Because the test is defined as triaxial, the effective stress path for the behavior is defined, allowing calculation of the mean stress for each shear stress point:

$$p_i = p_o + q_i/3 \tag{A.8}$$

where p_o is the initial confining pressure of the specimen [Cal Conf Pressure], σ_3 for the chosen triaxial test. The strength can then be expressed as a normalized frictional strength as follows:

$$\eta_i = q_i/p_i \tag{A.9}$$

CModeler is designed to automatically determine the normalized mean strength as a value passed to the Calibrator.f90 program. For each void ratio-mean stress point selected from a consolidation response, the normalized mean strength is calculated p_i/p_{ei} along with the volumetric strain based on the differential void ratio, ε_v.

A.4.3 Calculation of Secant Modulus

Calibrator.f90 assumes there exists a relationship between the normalized shear strength ratio, η_i/η_{max} vs. the normalized shear modulus ratio, $1 - G_i/G_{max}$ and the normalized mean stress, p_i/p_{eo} versus the normalized bulk modulus ratio $1 - K_i/K_{max}$ shown in Figure A-15.

$$\frac{\eta_i}{\eta_{\max}} = 1 - \left(1 - \frac{G_{si}}{G_{\max}}\right)^{\beta s} \qquad \frac{p_i}{p_{eo}} = 1 - \left(1 - \frac{K_{si}}{K_{\max}}\right)^{\beta h}$$

However, the know quantities of this expression that are passed to the program are the strength ratios and the fitting parameters. Therefore to interpolate the modulus response between each pair of shear strength points, the expressions are rearranged and solved as follows:

$$1 - \frac{G_{si}}{G_{\max}} = 1 - \left(1 - \frac{\eta_i}{\eta_{\max}}\right)^{1/\beta s} \qquad G_{si} = (1 - G_{si}/G_{max}) * G_{max} \tag{A.10}$$

$$1 - \frac{K_{si}}{K_{\max}} = 1 - \left(1 - \frac{p_i}{p_{eo}}\right)^{1/\beta h} \qquad K_{si} = (1 - K_{si}/K_{max}) * K_{max} \tag{A.11}$$

The values β_s and β_h are empirical fitting factors which are designed to allow the computation of the secant shear and bulk moduli, G_{si} and K_{si} for any value of shear stress and material confinement, η_i.

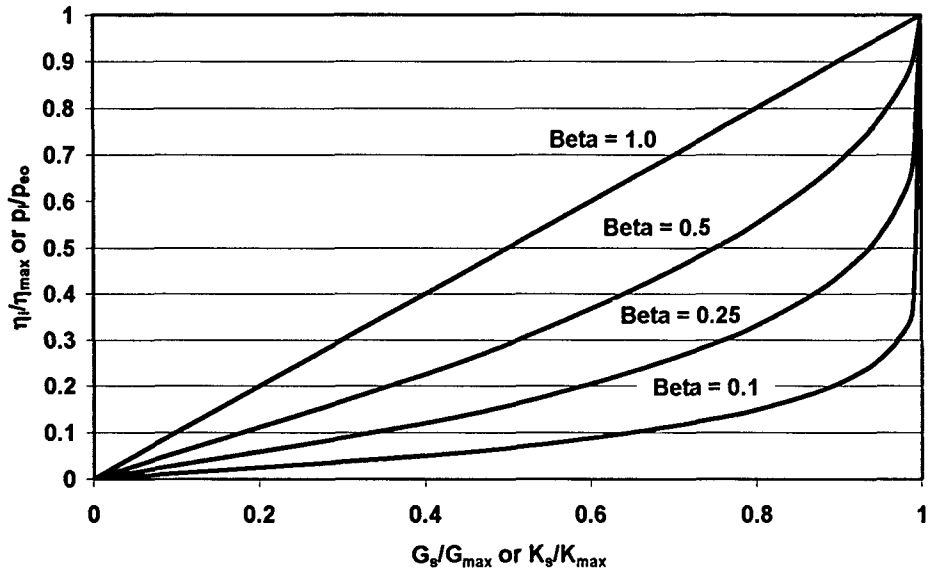

Figure A-15: Influence of Beta factors on normalized shear/mean stress strength ratio versus normalized shear/bulk modulus ratio

The rheological representation of the strength and modulus ratio distributions into a series spring-slider assemblage for the deviatoric and hydrostatic response is illustrated in Figure A-16.

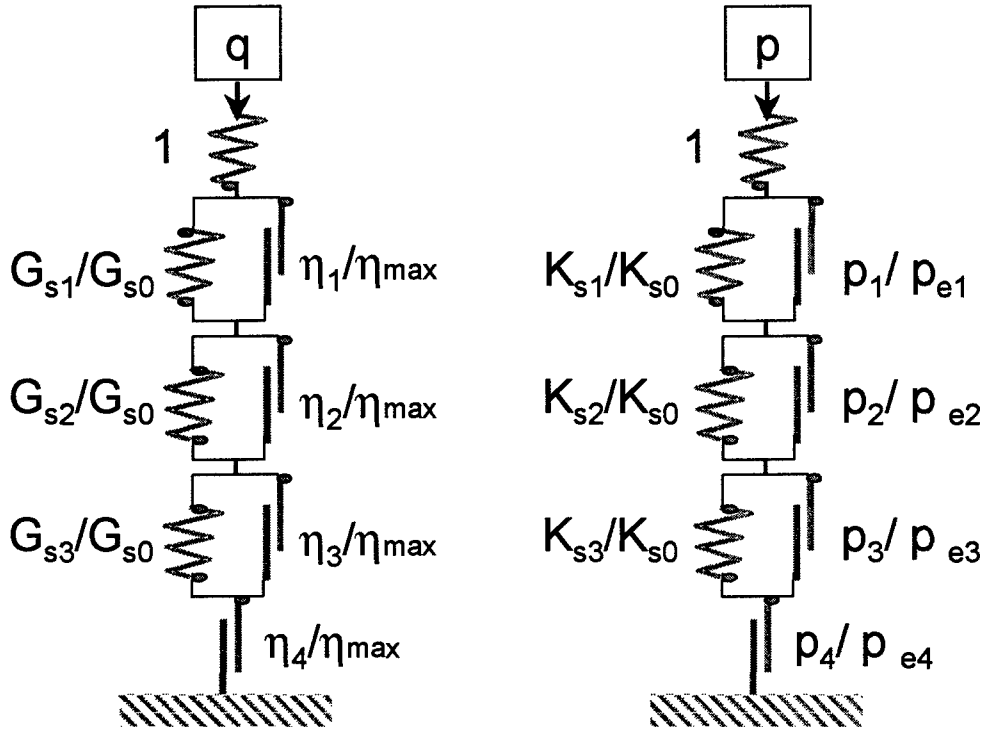

Figure A-16: Series spring-slider assemblage for deviatoric (q) and hydrostatic (p) mechanisms

A.4.4 Converting Series to Parallel for ShearRatio & BulkRatio

The following will describe the equations used to convert the discretized data obtained above into the system of parallel spring-slider inputs necessary for operation of the MMM. For each value of the secant shear and bulk modulus, G_{si} and K_{si} the magnitude of the secant moduli in a parallel assembly is computed based on the inverted sum of the reciprocal secant spring moduli as can be seen in the FORTRAN code given in section A.5.

Once the parallel secant moduli magnitudes are defined, the equivalent parallel transformation requires only a differential modulus to be computed between secant magnitudes to calculate the actual moduli, G_{pi} and K_{pi} between individual stress points.

$$\text{ShearRatio(i)} = G_{pi}/G_{max} \tag{A.12}$$

$G_{max,parallel} = G_{max\ (series)}$ and

$G_{pi} = \Sigma_i\ (G_{si} - G_{si-1})$ from i = 1 to 4

$$BulkRatio(i) = K_{pi}/K_{max} \tag{A.13}$$

$K_{max,parallel} = K_{max\ (series)}$

$K_{pi} = \Sigma_i\ (K_{si} - K_{si-1})$ from i = 1 to 4

The values of the hydrostatic stress limit are taken directly from the inputted points in CModeler:

$$Hlimit\ (i) = p_i/p_{ei} \tag{A.14}$$

A.4.5 Computation of PhiFrac and Pfact Variables

To compute the distribution of friction angle to each element:

$$PhiFrac\ (i) = \phi_i/\phi_{max} = \mu_i \tag{A.15}$$

expand the definition of the slider stress as follows:

$$s^{\alpha} = \eta_i\ \theta p = F_i.$$

θp represents the correction for $p_e(\theta)$ for the mean stress, p_i applied to each slider. In the following computations, θp will cancel out of the expression so it is a parameter of convenience only and is a constant between both the parallel and series systems.

η_i represents the frictional resistance, where $\eta = f(\phi)$ as derived in the series model. η will take on two values, one for compression, η_i^c and one for extension, η_i^e where:

$$\eta_i^e = 3\eta_i^c / (3 + \eta_i^c) \tag{A.16}$$

We also separate

$$\eta_i = \mu_i p_i^f \tag{A.17}$$

p_i^f = PFrac (i) and is independent of stress path. It is the fraction of mean stress distributed to each slider controlling the yield strength of the element.
μ_i = PhiFrac (i), the partial friction angle that adjusts the resistance of each slider to match the Mohr yield criterion.

For reference, the FORTRAN code using the following convenience:

$$H_{bar,i} = G_i' \text{ as } Gp_i / \Sigma G_r \text{ where } r = i \text{ to } n \tag{A.18}$$

The following expressions show the expansion of the slider stresses in compression (η^c), or for a similar expansion for extension (η^e) :

$$F_1 = \mu_1 p_1^f \theta p = \eta_i \theta p = s_a G_1' \tag{A.19}$$
$$F_2 = \mu_2 p_2^f \theta p = [s_b - s_a G_1'] G_2'$$
$$F_3 = \mu_3 p_3^f \theta p = [s_c - s_a G_1'(1 - G_2') - s_b G_2'] G_3'$$
$$F_4 = \mu_4 p_4^f \theta p = [s_d - s_a G_1'(1 - G_2' - G_3' + G_2' G_3') - s_b G_2'(1 - G_3') - s_c G_3'] G_4'$$

To solve for the friction angles of the sliders in the parallel system we take the ratio:

$$\text{UPRatio (i)} = F_i^e / F_i^c \tag{A.20}$$

where the value of UPRatio is not permitted to be less than 0.5.
This leads to:

$$\sin \phi_i = 3 (1 - \text{UPRatio(i)})/(1 + \text{UPRatio(i)}) \quad \text{(A.21)}$$

From which the definition of PhiFrac can be obtained for each parallel slider.

At this point, it should be noted that the value of friction angle determined from this process represents the strength in a parallel assemblage and will not be equal to frictional strength found in a series representation. Knowing the value of ϕ_i from the calculation above, we can compute PFrac by the following:

$$\mu_i^c = 6 \sin \phi_i / (3 - \sin \phi_i) \quad \text{(A.22)}$$

$$\text{Pfrac (i)} = \mu_i^c p_i^f / \mu_i^c \quad \text{(A.23)}$$

The four values for each of the five distributed parameters is passed back into CModeler and displayed as shown in Figure 11. The magnitudes of the β factors can be adjusted to better fit the response of the desired triaxial data. CModeler does permit the manual adjustment of each of the 20 parameters to suit the calibration but this technique is not recommended as the consistency between the parallel and series representation will be lost for the given global parameters.

A.5 FORTRAN Code for Cablibrator.f90

Following is the complete FORTRAN code for the Calibrator.f90 program linked to CModeler for calculation of the distributed parameters. All attempts to match variables in the previous discussion to the coded variables were made.

```
!   Last change:  ESB  6 Dec 2001    1:26 pm
!   Subroutine Calibrator which takes the basic inputs derived from an analysis
!   of the approximated data curve and computes the parallel model parameters
!    PROGRAM main
```

```
      SUBROUTINE Calibrator(RealArr, PhiFrac, ShearRatio, PFact, BulkRatio, Hlimit, Phi)
      dll_export calibrator
!
!     IMPLICIT NONE

!*  ****************************** Properties ***********************************
      REAL (KIND=8) :: ConfinningPressure
      REAL (KIND=8) :: Pe                       ! Parameters defining volumetric state
      REAL (KIND=8) :: PhiFrac(4)               ! Fraction of PhiLim for each shear mechanism
      REAL (KIND=8) :: Pfact(4)                 ! factor to apportion mean stress to mechanism
      REAL (KIND=8) :: ShearRatio(4)            ! Shear modulus for internal mechanism
      REAL (KIND=8) :: Hlimit(4)                ! Limit of internal hydrostatic mechanism
      REAL (KIND=8) :: BulkRatio(4)             ! Bulk modulus for internal mechanism


      REAL (KIND=8) :: PhiMin, Cc, Cr, eref
      REAL (KIND=8) :: BetaS, BetaH             ! hyperbolic fitting parameter
      REAL (KIND=8) :: Phimax, sinphimax        ! maximum friction angle for the material
      REAL (KIND=8) :: etamax                    ! maximum eta value for phimax
      REAL (KIND=8) :: Gmax, Kmax                ! Maximum modulus values
      REAL (KIND=8) :: ModfacS(4), ModfacH(4)  ! 1 - Gs/Go values from hyperbolic plot
      REAL (KIND=8) :: Gs(4), Ks(4)              ! Secant shear modulus for series model
      REAL (KIND=8) :: G(4), K(4)                ! Shear modulus for each spring in series
      REAL (KIND=8) :: Gp(4), Kp(4)              ! Shear modulus for each spring in parallel
      REAL (KIND=8) :: etac(4), etae(4)          ! Eta values in compression and extension
      REAL (KIND=8) :: ModShrStrs(4), ModShrStr(4)
      REAL (KIND=8) :: ModNorStrs(4), ModVolStr(4)
!*  ***************************************************************************

      INTEGER  :: n=4                            ! number of elements in the series model
      REAL (KIND=8) ::RealArr(40)

!     Incremental columns from spreadsheet to aid in computation
      REAL (KIND=8) :: UPRatio(4), Sinphi(4), Phi(4), uic(4), upc(4), upe(4)
      REAL (KIND=8) :: Ginv(4), Kinv(4), Hsum(4), Hbar(4), Hstar(4)

!     Counters
      INTEGER  :: i, j, r

      OPEN (13, FILE = 'c:\CModeler\CalibRun.txt',STATUS = 'UNKNOWN')
      WRITE (13,*)  'Initializing Calibrator'

!     Read in problem specification and parameters
!      OPEN (16, FILE = 'Vickssilt50.dat')
!      READ(16,*) ConfinningPressure
!      READ(16,*) Phimin, Phimax
!      READ(16,*) BetaS, BetaH
```

```
!     READ(16,*) Kmax, Gmax
!     READ(16,*) (ModShrStrs(r), r=1,4)
!     READ(16,*) (ModShrStr(r), r=1,4)
!     READ(16,*) (ModNorStrs(r), r=1,4)
!     READ(16,*) (ModVolStr(r), r=1,4)
!     CLOSE(16)
!
!    Load the input data from Real arrays passed.
      ConfinningPressure = RealArr(1)
      Phimin = RealArr(2)
      Phimax = RealArr(3)
      BetaS = RealArr(4)
      BetaH = RealArr(5)
      Kmax = RealArr(6)
      Gmax = RealArr(7)

      DO I = 8,11
         ModShrStrs(I-7) = RealArr(I)
      END DO

      DO I = 12,15
         ModShrStr(I-11) = RealArr(I)
      END DO

      DO I = 16,19
         ModNorStrs(I-15) = RealArr(I)
      END DO

      DO I = 20,23
         ModVolStr(I-19) = RealArr(I)
      END DO

      WRITE (13,*) 'Confinning Pressure = ',ConfinningPressure
      WRITE (13,*) 'PhiMax = ', Phimax
      WRITE (13,*) 'PhiMin = ', Phimin
      WRITE (13,*) 'BetaS, BetaH = ',BetaS, BetaH
      WRITE (13,*) 'Kmax = ', Kmax
      WRITE (13,*) 'Gmax = ', Gmax
      WRITE (13,*) 'Shear Stress  = ', (ModShrStrs(r), r=1,4)
      WRITE (13,*) 'Shear Strains = ', (ModShrStr(r), r=1,4)
      WRITE (13,*) 'Normal Stress = ', (ModNorStrs(r), r=1,4)
      WRITE (13,*) 'Normal Strain = ', (ModVolStr(r), r=1,4)

!    Determine the table values for eta and secant shear G modulus
      sinphimax = SIN(Phimax*3.14156/180)
      etamax = (6*sinphimax)/(3-sinphimax)
      WRITE (13,*) 'Etamax =', etamax
      i = 0
      do i=1,n
```

```
      etac(i) = ModShrStrs(i)/(ModShrStrs(i)/3 + ConfinningPressure)
      if (etac(i) > etamax) then
          WRITE (13,*) 'Program failed at point ',i,' at value ',etac(i)
          STOP
      end if
      ModfacS(i) = 1 - (1 - etac(i)/etamax)**(1 / BetaS)
      ModfacH(i) = 1 - (1 - ModNorStrs(i))**(1 / BetaH)
      Gs(i) = (1 - ModfacS(i))*Gmax
      Ks(i) = (1 - ModfacH(i))*Kmax
      etae(i) = 3*etac(i)/(3+etac(i))
    END do

    WRITE (13,*) 'Etac(i) = ', (etac(r), r=1,4)
    WRITE (13,*) 'ModfacS = ', (ModfacS(r), r=1,4)
    WRITE (13,*) 'Gs(i)   = ', (ModfacS(r), r=1,4)
    WRITE (13,*) 'ModfacH = ', (ModfacH(r), r=1,4)
    WRITE (13,*) 'Ks(i)   = ', (ModfacS(r), r=1,4)

!   Create Modulus block
    Ginv(1) = 1/Gmax
    G(1)    = 1/(1/Gs(1) - Ginv(1))
    Kinv(1) = 1/Kmax
    K(1)    = 1/(1/Ks(1) - Kinv(1))
    IF (G(1) < 0) THEN
      WRITE (13,*) 'Program failed at point 1 value of G(1) of: ',G(1)
      STOP
    END IF
    IF (K(1) < 0) THEN
      WRITE (13,*) 'Program failed at point 1 value of K(1) of: ',G(1)
      STOP
    END IF

    i = 0
    Do i = 2,n
     Ginv(i) = 1/G(i-1) + Ginv(i-1)
     G(i)    = 1/(1/Gs(i) - Ginv(i))
     IF (G(i) < 0) THEN
      WRITE (13,*) 'Program failed at point ',i,' value of G of: ',G(i)
      STOP
     END IF
     Kinv(i) = 1/K(i-1) + Kinv(i-1)
     K(i)    = 1/(1/Ks(i) - Kinv(i))
     IF (K(i) < 0) THEN
      WRITE (13,*) 'Program failed at point ',i,' value of K of: ',K(i)
      STOP
     END IF
    END do

!   Calculate Gp and Kp
```

```
      Gp(1) = Gmax - Gs(1)
      Kp(1) = Kmax - Ks(1)
      i = 0
      do i=2,n
       Gp(i) = Gs(i-1) - Gs(i)
       Kp(i) = Ks(i-1) - Ks(i)
      END do

!     Calculate Hsum, Hbar and Hstar
      i = 0
      j = 0
      do i=1,n
       Hsum(i) = 0
       do j=n,i,-1
         Hsum(i) = Gp(j) + Hsum(i)
       END do
      END do
!     ---------------------------------
      i = 0
      do i=1,n
       Hbar(i) = Gp(i)/Hsum(i)
      END do
!     ---------------------------------
      i = 0
      do i=2,n
       Hstar(i) = Hbar(i-1)*Hbar(i)/Gp(i)
      END do

!     Calculate upc and upe for 4 elements

      upc(1) = etac(1)*Hbar(1)
      upe(1) = etae(1)*Hbar(1)

      upc(2) = (etac(2)-upc(1))*Hbar(2)
      upe(2) = (etae(2)-upe(1))*Hbar(2)

      upc(3) = (etac(3)-Hsum(3)*etac(1)*Hstar(2)-etac(2)*Hbar(2))*Hbar(3)
      upe(3) = (etae(3)-Hsum(3)*etae(1)*Hstar(2)-etae(2)*Hbar(2))*Hbar(3)

      upc(4) = (etac(4)-Hsum(4)*(etac(1)*Hstar(2)+etac(2)*Hstar(3))-etac(3)*Hbar(3))*Hbar(4)
      upe(4) = (etae(4)-Hsum(4)*(etae(1)*Hstar(2)+etae(2)*Hstar(3))-etae(3)*Hbar(3))*Hbar(4)

      i=0
      do i=1,n
       UPRatio(i) = upe(i)/upc(i)
      END do

      WRITE (13,*) 'UPRatio = ', (UPRatio(r), r=1,4)
```

```
!   Check to see if parallel peak friction angle is greater than 90 deg.
    if (UPRatio(4) < 0.5) THEN
     UPRatio(4) = 0.5
    end if

!   Generate additional data columns for generating ratios
    i = 0
    do i=1,n
     Sinphi(i) = 3*(1-UPRatio(i))/(1+UPRatio(i))
     Phi(i)    = asin(Sinphi(i))*180/3.14156
     uic(i)    = 6*Sinphi(i)/(3-Sinphi(i))
    END do

    WRITE (13,*) 'Phi(i) = ', (Phi(r), r=1,4)
!   Check peak friction angle and scale back if necessary

    if (Phi(n) > 90) then
     Phi(n)=90
    end if
    WRITE (13,*) 'Final Phi= ', Phi(n)
!   Determine the parallel parameters
    i=0
    do i=1,n
     PhiFrac(i) = Phi(i)/Phi(n)
     ShearRatio(i)  = Gp(i)/Gmax
     BulkRatio(i)  = Kp(i)/Kmax
     Hlimit(i)    = 1-(1-ModfacH(i))**BetaH
     PFact(i)   = upc(i)/uic(i)
    END do

!   Write parameters out
20    FORMAT (5(F7.5,2x))
    write (13,*) 'Phimax = ', Phi(n)
    write (13,*) ' '
    write (13,*) 'PhiFrac ',' Gratio ',' PFact ',' Bratio ',' Hlimit'
    do i=1,n
     WRITE (13,20) PhiFrac(i), ShearRatio(i), PFact(i), BulkRatio(i), Hlimit(i)
    END do
    CLOSE (13)
!    END PROGRAM main
    END SUBROUTINE Calibrator
```

APPENDIX B

Partially Saturated Multi-Mechanical Model (PS-MMM) FORTRAN Code

Following is the complete FORTRAN code for the Multi-Mechanical Model (MMM) for a saturated and a partially saturated soil. The CModeler program described in Appendix A passes its calibration parameters to MMM which then performs either a drained triaxial (CD), an undrained triaxial (CU) or a free swell (FS) or a constant volume (CV) swell test on the material depending on the users desire. The CD and CU tests can be run from CModeler for the saturated condition, but FS, CV and any partially saturated triaxial tests require manual operation of the program from a user generated input file.

The FORTRAN code is given in its entirety and most variable names are represented as defined in the body of the thesis. A description of each variable is given at the beginning of the main program body and any supporting variables at the beginning of each individual subroutine.

```
!   Last change:  ESB  23 Oct 2003   10:02 am

!     SUBROUTINE multimech(RealArr,IntArr,Step,Strain1,Strain3,Sig11,Sig22,Sig33,PorePress,&
!         Y1,Y2,Y3,Length,LCount)
!     dll_export multimech
!
   !MS$ATTRIBUTES DLLEXPORT :: multimech
   !MS$ATTRIBUTES ALIAS :'multimech' :: multimech
!
     PROGRAM MAIN

     IMPLICIT NONE

     CHARACTER (LEN=1) :: Drainage
     CHARACTER (LEN=2) :: SwellType
```

```
      LOGICAL :: DRAINED

      LOGICAL :: Sflag(4)
      LOGICAL :: Hflag(4)
      LOGICAL :: Tflag(4)

      LOGICAL :: SflagSave(4)
      LOGICAL :: HflagSave(4)
      LOGICAL :: TflagSave(4)

      LOGICAL :: idump

!     Input Data
      REAL (KIND=8) ::RealArr(60)
      INTEGER :: IntArr(10)

!     Output Data
      INTEGER :: Length
      PARAMETER (Length=10000)
      INTEGER :: Step(Length),Y1(Length),Y2(Length),Y3(Length)
      REAL (KIND=8) :: Strain(Length),Vratio(Length),PorePress(Length)
      REAL (KIND=8) :: Strain1(Length),Strain2(Length),Strain3(Length)
      REAL (KIND=8) :: Sig11(Length),Sig22(Length),Sig33(Length)
      REAL (KIND=8) :: Eps11(Length),Eps22(Length),Eps33(Length), NTimes

      INTEGER :: iprint, Numout, im, iter, siter, liter

      INTEGER :: icode, smech, hmech, tmech

      INTEGER :: r,I,LCount              ! Index for mechanism

      INTEGER :: Manual, CFlag, SwFlag, PoiFlag, BCheck

      INTEGER :: QhFlag(4)
      INTEGER :: QhFSum

      REAL (KIND=8) :: DsInc             ! Variables used in iteration
      REAL (KIND=8) :: SigError
      REAL (KIND=8) :: Dir, DirInit
      REAL (KIND=8) :: TStress

      REAL (KIND=8) :: Sparms(60)        ! Parameters
      REAL (KIND=8) :: State             ! Void ratio
      REAL (KIND=8) :: InitState         ! Void ratio after confinning pressure applied
      REAL (KIND=8) :: Qs(6,4)           ! Internal shear forces
      REAL (KIND=8) :: Qh(4)             ! Internal hydrostatic forces

      REAL (KIND=8) :: StateSave         ! Void ratio
      REAL (KIND=8) :: QsSave(6,4)       ! Internal shear forces
      REAL (KIND=8) :: QhSave(4)         ! Internal hydrostatic forces

      REAL (KIND=8) :: D(3,3)            ! Strain Increment tensor
      REAL (KIND=8) :: Eps(3,3)          ! Strain
      REAL (KIND=8) :: Ds(6)             ! Strain increment vector

      REAL (KIND=8) :: Sigma(3,3)        ! Stress tensor
      REAL (KIND=8) :: Stress(6)         ! Stress vector
      REAL (KIND=8) :: Sigc              ! Confinning stress

      REAL (KIND=8) :: DeltaEps          ! Strain increment
```

```
      REAL (KIND=8) :: TotalEps                    ! Total strain
      REAL (KIND=8) :: VolStrainEps, VolStrainE ! Computational Variables

      REAL (KIND=8) :: Fh, beta, Pe, Cr            ! Parameters defining Saturated volumetric state
      REAL (KIND=8) :: Mc                          ! Shear-volume coupling parameter
      REAL (KIND=8) :: Cohesion                    ! Cohesion parameter in stress units
      REAL (KIND=8) :: C                           ! Normalized Cohesive Intercept Parameter
      REAL (KIND=8) :: Gamma                       ! Dilatancy factor
      REAL (KIND=8) :: Decay                       ! Defines rate that PhiLim falls with OCR
      REAL (KIND=8) :: PhiRatio                    ! Ratio of maximum and minimum PhiLim
      REAL (KIND=8) :: PhiLim                      ! Mohr-Coulomb friction angle
      REAL (KIND=8) :: PhiR                        ! Friction angle in radians
      REAL (KIND=8) :: PsiMax                      ! Friction angle for Dilatant Surface at Mc
      REAL (KIND=8) :: PsiMin                      ! Friction angle for low stress Dilatancy Surface
      REAL (KIND=8) :: DecayV                      ! Defines rate that Psi increases with pe
      REAL (KIND=8) :: BulkMod                     ! Elastic Bulk Modulus
      REAL (KIND=8) :: ShearMod                    ! Elastic Shear Modulus
      REAL (KIND=8) :: Poisson                     ! Poisson's Ratio
      REAL (KIND=8) :: PhiFrac(4)                  ! Fraction of PhiLim for each shear mechanism
      REAL (KIND=8) :: Pfact(4)                    ! factor to apportion mean stress to mechanism
      REAL (KIND=8) :: ShearRatio(4)               ! Shear modulus for internal mechanism
      REAL (KIND=8) :: Hlimit(4)                   ! Limit of internal hydrostatic mechanism
      REAL (KIND=8) :: BulkRatio(4)                ! Bulk modulus for internal mechanism
!*
      REAL (KIND=8) :: Qe, Pew                     ! Normalization for Intergranular Stress
      REAL (KIND=8) :: K(3), Ksave(3)              ! PSS Moduli Array
      REAL (KIND=8) :: K1o, K2o                    ! K1, K2 Calculated Moduli
      REAL (KIND=8) :: Kappa, K3o                  ! K3 and Kappa Modulus from swell test data
      REAL (KIND=8) :: Sat, SatSave                ! Degree of Saturation (%)
      REAL (KIND=8) :: SucSave                     ! Temporary suction during iteration
      REAL (KIND=8) :: Theta, ThetaStar            ! Volumetric Water content
      REAL (KIND=8) :: SucInit, Suc, dSuc          ! Initial Suction of sample
      REAL (KIND=8) :: Qsp                         ! Initial Sample Swell Pressure
      REAL (KIND=8) :: Lambda                      ! Modifier for Volumetric Stiffness with Saturation
      REAL (KIND=8) :: Pr                          ! Reference Suction for 0 Vol. water content
      REAL (KIND=8) :: SigInit                     ! Temporary cauchy stress during iteration
      REAL (KIND=8) :: CStress(3), CStressSave(3)  ! Cauchy stresses
      REAL (KIND=8) :: Ua, Uw                      ! Air and Water Pore Pressures
      REAL (KIND=8) :: dQ(4)                       ! Differential intergranular stresses for iteration
      REAL (KIND=8) :: CSig                        ! Mean Cauchy stress from Iterations
      REAL (KIND=8) :: CrBar                       ! C* parameter in thesis to determine alpha
      REAL (KIND=8) :: Alpha                       ! Relates K3,K1 to K2 like a Poisson's ratio
      REAL (KIND=8) :: fSat                        ! Computes Saturation as a function
      REAL (KIND=8) :: Poros, Temp
!*
      REAL (KIND=8) :: Sigma1,Sigma3,PoreP         ! Printing Variables to check beahvior
      REAL (KIND=8) :: TestState                   ! State of material after intialization
      REAL (KIND=8) :: Qhtemp, Qstemp              ! Temporary intergranular stresses during iteration
      REAL (KIND=8) :: Proctor                     ! Determines if sample is partially saturated
      REAL (KIND=8) :: dumstress, StateInit, SigInitSave, TempState

      REAL (KIND=8) :: QhDiff
      REAL (KIND=8) :: BRatioSum
      REAL (KIND=8) :: BRNorm(4)
      REAL (KIND=8) :: CsigSave
      REAL (KIND=8) :: UaApp, UwApp, UwSave, UaSave  ! Pore water pressure variables

!*  Cyclic Loading Conditions
      LOGICAL :: Cyclic,Strs_Mode,Strn_Mode,Cycle_Mode,Combination
      REAL (KIND=8) :: UBound,LBound
```

```
      INTEGER :: Num_Cycles,Max_Cycles

      idump = .false.
!     Open file to put debug data
      OPEN (23, FILE = 'c:\MultiMech2001\SuctionCModeler\MMDump.txt',STATUS = 'UNKNOWN')
      OPEN (13, FILE = 'c:\MultiMech2001\SuctionCModeler\Dump.out',STATUS = 'UNKNOWN')
      OPEN (33, FILE = 'c:\MultiMech2001\SuctionCModeler\Stresses.out', STATUS ='UNKNOWN')

!     Open file to put results
      OPEN (14, FILE = 'c:\MultiMech2001\SuctionCModeler\Results.out')
      OPEN (24, FILE = 'c:\MultiMech2001\SuctionCModeler\QTX.out')

!     Subroutine to open file in RealArray from Datafile
      Manual = 1
      IF (Manual .EQ. 1) THEN

!      Read in problem specification and parameters
      OPEN (17, FILE = 'c:\MultiMech2001\SuctionCModeler\BuckDemo.txt')
!      OPEN (16, FILE = InputFile)
       READ(17,*) DeltaEps, TotalEps, Numout, Drainage, SwellType
       READ(17,*) Sigc, State, Sat, Proctor
       READ(17,*) beta, Fh, Cr, Lambda
       READ(17,*) C, Mc, Gamma
       READ(17,*) PhiLim, Decay, PhiRatio
       READ(17,*) Kappa, ShearMod, Pr, Alpha, Poisson
       READ(17,*) PsiMax, PsiMin, DecayV
       READ(17,*) IntArr(3), IntArr(4)
       READ(17,*) (PhiFrac(r), r=1,4)
       READ(17,*) (Pfact(r),   r=1,4)
       READ(17,*) (ShearRatio(r), r=1,4)
       READ(17,*) (Hlimit(r), r=1,4)
       READ(17,*) (BulkRatio(r),   r=1,4)

      CLOSE(17)
      WRITE(*,*) 'Program has successfully read the input data'

!      Check loading type
       IF(Drainage .EQ. 'U' .OR. Drainage .EQ. 'u')THEN
         DRAINED = .TRUE.
       ELSE
         DRAINED = .FALSE.
       END IF
      END IF
!
      IF (Manual .EQ. 0) THEN

!      Load the input data from Integer arrays passed.
       IF (IntArr(1) .EQ. 1) THEN
        DRAINED = .FALSE.
       ELSE
        DRAINED = .TRUE.
       END IF

       NumOut = IntArr(2)

!      Load the input data from Real arrays passed.
       DeltaEps = RealArr(1)
       TotalEps = RealArr(2)
       Sigc = RealArr(3)
       State = RealArr(4)
```

```
beta = RealArr(5)
Fh = RealArr(6)
C = RealArr(7)
Mc = RealArr(8)
Gamma = RealArr(9)
PhiLim = RealArr(10)
Decay = RealArr(11)
PhiRatio = RealArr(12)
Kappa = RealArr(13)
IF (PoiFlag .EQ. 1) THEN
 Poisson = RealArr(14)
ELSE
 ShearMod = RealArr(14)
END IF
DO I = 15,18
 PhiFrac(I-14) = RealArr(I)      ! PhiFrac 15 - 18
END DO

DO I = 19,22
 ShearRatio(I-18) = RealArr(I)   ! Shear Ratio 19 - 22
END DO

DO I = 23,26
 Hlimit(I-22) = RealArr(I)       ! HLimit 23 - 26
END DO

DO I = 27,30
 BulkRatio(I-26) = RealArr(I)    ! Bulk Ratio 27 - 30
END DO

DO I = 31,34
 Pfact(I-30) = RealArr(I)        ! PFact 30 - 33
END DO

Cr    = RealArr(37)
PsiMax = RealArr(38)
PsiMin = RealArr(39)
DecayV = RealArr(40)
Lambda = RealArr(41)
Pr    = RealArr(42)

END IF
WRITE(*,*) 'Program has successfully input data to Variable Names'
WRITE(23,'(A11,F10.3)') 'DeltaEps = ', DeltaEps
WRITE(23,'(A11,F10.3)') 'TotalEps = ', TotalEps
WRITE(23,'(A11,F10.3)') 'Sigc = ', SigC
WRITE(23,'(A11,F10.3)') 'State = ', State
WRITE(23,'(A11,F10.3)') 'Sat = ', Sat
WRITE(23,'(A11,F10.3)') 'Beta = ', Beta
WRITE(23,'(A11,F10.3)') 'Fh = ', Fh
WRITE(23,'(A11,F10.3)') 'C = ', C
WRITE(23,'(A11,F10.3)') 'Mc = ', Mc
WRITE(23,'(A11,F10.3)') 'Gamma = ', Gamma
WRITE(23,'(A11,F10.3)') 'PhiLim = ', PhiLim
WRITE(23,'(A11,F10.3)') 'Decay = ', Decay
WRITE(23,'(A11,F10.3)') 'PhiRatio = ', PhiRatio
WRITE(23,'(A11,F10.3)') 'Kappa = ', Kappa
!  WRITE(23,'(A11,F10.3)') 'ShearMod = ', ShearMod
WRITE(23,'(A11,F10.3)') 'Poisson Ratio = ', Poisson
WRITE(23,'(A11,F10.3)') 'Cr = ', Cr
```

```
      WRITE(23,'(A11,F10.3)') 'Psimax = ', PsiMax
      WRITE(23,'(A11,F10.3)') 'Psimin = ', PsiMin
      WRITE(23,'(A11,F10.3)') 'DecayV = ', DecayV
      WRITE(23,'(A11,F10.3)') 'Lambda = ', Lambda
      WRITE(23,'(A11,F10.3)') 'Pr = ', Pr
      WRITE(23,'(A11,F10.3)') 'Alpha = ', Alpha
      WRITE(23,'(5(A10))') 'PhiFrac: ','ShearRatio: ','HLimit: ','BulkRatio: ','PFact: '
!
      DO I = 1,4
        WRITE(23,'(5(F10.4))') PhiFrac(I), ShearRatio(I), HLimit(I), BulkRatio(I), PFact(I)
      END DO

!     End Loaded Array Data

!     Check the cyclic loading conditions
      Cyclic = .FALSE.
      Strs_Mode = .false.
      Strn_Mode = .false.
      Cycle_Mode = .false.
      Combination = .false.

      if (INTARR(3) .EQ. 1) THEN
       Cyclic = .true.
       Strs_Mode = .true.
       UBound = RealArr(35)
      else if (INTARR(3) .EQ. 2) THEN
       Cyclic = .true.
       UBound = RealArr(35)
       Strn_Mode = .true.
      else if (INTARR(3) .EQ. 3) THEN
       Cyclic = .true.
       UBound = RealArr(35)
       Combination = .true.
!       write(67,*)'This is a combo problem'
      else
!       write(67,*)'Current Mode = ',IntArr(3)
      end if
      if (Cyclic) THEN
       LBound = RealArr(36)
       Max_Cycles  = IntArr(4)
       Num_Cycles = 0
      end if

!     Set number of computation steps
      Ntimes = (TotalEps/DeltaEps) - 1

!     Convert all to tension-positive convention
      DeltaEps = -DeltaEps
      TotalEps = -TotalEps
      Sigc     = -Sigc

!     Include Lambda factor for increased volumetric stiffness with Saturation
      Pe  = 10**((Fh - State)*beta)
      fSat = Sat*(1.0+0.005/(1-Sat))
      Pew  = -Pe*10**(Lambda*(1-Sat)*beta)
!     Convert cohesion to a hydrostatic offset

      PhiR = PhiLim * 3.141592/180.
!     Cohesion is only a function of saturated response (note must remain a positive value)
      Cohesion = -C * Pe
```

```
!   Define Shear Modulus Behavior
    PoiFlag = 1

!   Define Parms
    SParms( 1) = beta
    SParms( 2) = Fh
    SParms( 3) = C
!   C is passed instead of Cohesion because it is no longer a constant
!   Cohesion is recalculated in SandDriver according to updated State and Pe
    SParms( 4) = PhiFrac(1) * PhiLim
    SParms( 5) = PhiFrac(2) * PhiLim
    SParms( 6) = PhiFrac(3) * PhiLim
    SParms( 7) = PhiFrac(4) * PhiLim
    IF (PoiFlag .eq. 1) THEN
      Sparms( 8) = ShearRatio(1)
      SParms( 9) = ShearRatio(2)
      SParms(10) = ShearRatio(3)
      Sparms(11) = ShearRatio(4)
    ELSE
      Sparms( 8) = ShearRatio(1) * ShearMod
      SParms( 9) = ShearRatio(2) * ShearMod
      SParms(10) = ShearRatio(3) * ShearMod
      Sparms(11) = ShearRatio(4) * ShearMod
    END IF
    SParms(12) = Pfact(1)
    SParms(13) = Pfact(2)
    SParms(14) = Pfact(3)
    SParms(15) = Pfact(4)
    SParms(16) = Hlimit(1)
    SParms(17) = Hlimit(2)
    SParms(18) = Hlimit(3)
    SParms(19) = Hlimit(4)
    Sparms(20) = BulkRatio(1)
    SParms(21) = BulkRatio(2)
    SParms(22) = BulkRatio(3)
    Sparms(23) = BulkRatio(4)
    Sparms(24) = Mc
    Sparms(25) = Decay
    Sparms(26) = PhiRatio
    Sparms(27) = Gamma
    Sparms(28) = Cr
    Sparms(29) = PsiMax
    Sparms(30) = PsiMin
    Sparms(31) = DecayV
    Sparms(32) = Lambda
    Sparms(33) = Pr
    Sparms(37) = Alpha
    Sparms(38) = Poisson
! ***** Distribute K1, K2 moduli amongst mechanisms as above, K2 is positive
    CrBar = 0.5*(Cr + 1.0/beta)
    K1o   = 2.303 * (1.0 + State) / CrBar
    K3o   = -(1.0 / Kappa) / (1-Alpha)
    K2o   = 1.0*SQRT(ABS(Alpha*K1o*K3o))

    WRITE(23,'(A11,F10.3)') 'CrBar = ', CrBar
    WRITE(23,'(A11,F10.3)') 'Alpha = ', Alpha

! ***** Create K Moduli array
    SParms(34) = K1o
```

```
    SParms(35) = K2o
    SParms(36) = K3o

    WRITE(23,'(A11,F10.3)') 'K1o = ', SParms(34)
    WRITE(23,'(A11,F10.3)') 'K2o = ', SParms(35)
    WRITE(23,'(A11,F10.3)') 'K3o = ', SParms(36)

! ***** Initialize Suction, Swell Pressure and Q reference pressure
    ThetaStar = fSat * State / (1+State)
    SucInit  = -Pr * EXP(-K3o * (1-Alpha) * ThetaStar)
    Qsp      = 4.0 * (K2o / K3o)**2.0 * SucInit
    Qe       = Qsp + Pew
    Theta    = Sat * State / (1+State)
    WRITE(*,*) 'Program has Initialized the Input Variables'
    WRITE(23,'(A11,F10.3)') 'ThetaInit = ', Theta
    WRITE(23,'(A11,F10.3)') 'SucInit  = ', SucInit
    WRITE(23,'(A11,F10.3)') 'Pe       = ', Pe
    WRITE(23,'(A11,F10.3)') 'Qsp      = ', Qsp
    WRITE(23,'(A11,F10.3)') 'Qe       = ', Qe
    WRITE(33,*) 'CStress1  CStress3  Stress1  Stress3  Theta  State   Sat   dSigma',&
      'SigInit  Suc'

!**** INITIALIZE THE SAMPLE ASSUMING NO CONFINING
PRESSURE************************************

    IF (ABS(Proctor) .EQ. 0) THEN
      BulkMod = ABS(SigC / Cr)
    ELSE
      BulkMod = ABS(Qsp / Cr)
    END IF

    IF (PoiFlag .EQ. 1) THEN
       ShearMod = 3.0 * BulkMod * (1.0 - 2.0*Poisson)/(1.0 + 2.0*Poisson)
    END IF

    IF (ABS(Proctor) .GT. 0) THEN

      QhFlag = 0
      QhDiff = 0
      QhFSum = 0
      BRatioSum = 0.0

!   Distribute initial suction pressure to hydrostatic mechanisms based on Qsp
      DO r=1,4
        Qh(r) = BulkRatio(r) * Qsp
        WRITE(23,*) 'Qh(',r,') for Qsp = ',Qh(r)
        IF(Qh(r) .LT. Qe * Hlimit(r)) THEN
          Qh(r) = Qe * Hlimit(r)
          Qhflag(r) = 1
          WRITE(23,*) 'Qh(',r,') for Qsp = ',Qh(r)
        END IF
      END DO

      QhDiff = Qsp - (Qh(1) + Qh(2) + Qh(3) + Qh(4))
      QhFSum = QhFlag(1) + QhFlag(2) + QhFlag(3) + QhFlag(4)

!   Iterate on stress distribution on all sliders are in equilibrium
      DO WHILE ( ABS ( Qsp - (Qh(1) + Qh(2) + Qh(3) + Qh(4))) .GT. 1.e-7)

        IF (QhFSum .EQ. 0) THEN
```

```
            EXIT
          ELSE IF (QhFSum .EQ. 1) THEN
            BRatioSum = BulkRatio(2) + BulkRatio(3) + BulkRatio(4)
            DO r = 2,4
              BRNorm(r) = BulkRatio(r)/BRatioSum
              WRITE(*,*) BRNorm(r)
              Qh(r) = BRNorm(r) * QhDiff + Qh(r)
              IF (Qh(r) .LT. Qe * Hlimit(r)) THEN
                Qh(r) = Qe * Hlimit(r)
                Qhflag(r) = 1
              END IF
            END DO
          ELSE IF (QhFSum .EQ. 2) THEN
            BRatioSum = BulkRatio(3) + BulkRatio(4)
            DO r = 3,4
              BRNorm(r) = BulkRatio(r)/BRatioSum
              Qh(r) = BRNorm(r) * QhDiff + Qh(r)
              IF (Qh(r) .LT. Qe * Hlimit(r)) THEN
                Qh(r) = Qe * Hlimit(r)
                Qhflag(r) = 1
              END IF
            END DO
          ELSE IF (QhFSum .EQ. 3) THEN
              Qh(4) = QhDiff + Qh(4)
              IF (Qh(4) .LT. Qe * Hlimit(4)) THEN
                WRITE(*,*) 'Void Ratio is Invalid for System'
                STOP
              END IF
        END IF

          QhDiff = Qsp - (Qh(1) + Qh(2) + Qh(3) + Qh(4))
          QhFSum = QhFlag(1) + QhFlag(2) + QhFlag(3) + QhFlag(4)

          END DO
          WRITE(*,*) 'Program has Initialized the Suction'
          WRITE(23,*) 'State after suction =',State
          WRITE(23,*) 'Saturation after suction =',Sat
          WRITE(23,*)
          WRITE(23,*) 'Major Principal Stress =',CStress(1)
          WRITE(23,*) 'Minor Principal Stress =',CStress(3)
      END IF

        Qstemp = ( Stress(1) - Stress(3) )
        Qhtemp = ( Qh(1) + Qh(2) + Qh(3) + Qh(4) )
        WRITE(23,*) 'Qh and Qs =', Qhtemp, Qstemp
        WRITE(23,*) 'Saturation =', Sat

!   Initialize internal shear mechanisms
      Qs = 0.0
     WRITE(13,*) 'CStress1    CStress3    Strain1    Strain3'

!*****************************PROCTOR TEST DEFINED*****************************
      Proctor = -Proctor
      IF (ABS(Proctor) .GT. 0) THEN

!******************************************************************************

      SigInit = 0.0

!     Calculate the Initial BulkModulus
```

```
      IF (PoiFlag .EQ. 1) THEN
        ShearMod = 3.0 * BulkMod * (1.0 - 2.0*Poisson)/(1.0 + 2.0*Poisson)
      END IF
      WRITE(23,'(A11,F10.3)') 'BulkMod    = ', BulkMod
      WRITE(23,'(A11,F10.3)') 'Proctor    = ', Proctor
      WRITE(23,'(A11,F10.3)') 'Proctor+Qsp = ', Proctor + Qsp

!     Load the specimen in 1-D compression for Proctor test (100 psi = Standard)
      QsSave   = Qs
      QhSave   = Qh
      StateSave = State
      SflagSave = Sflag
      HflagSave = Hflag
      TflagSave = Tflag
      SatSave  = Sat
      CFlag    = 1
      CSig     = SigC
      iter = 0
      WRITE(33,*) '----------Beginning Load----------'
      WRITE(33,*) 'CStress1  CStress3 Stress1  Stress3 Theta  State    Sat',&
        '   dSigma   SigInit   Suc'
      DO WHILE (CStress(1) .GT. Proctor)
        Ds(1) = -0.001
        Ds(2) = 0
        Ds(3) = 0

!       Reset state to intial values
        Sat = SatSave
        Suc = SucInit
        dSuc  = 0.0
        dQ   = 0.0
        idump = .false.
        SwFlag = 2

        CALL Sand_Driver(Sat, Suc, Ds, State, Qs, Qh, CStress, Stress, Sparms, &
                         Swflag, Sflag, Hflag, Tflag, idump)
          dQ = Qh - QhSave
          QhSave = Qh
        Swflag = 0

        Sat = (1.0 + State)/State * Theta
        IF (Sat .GT. 0.99999) THEN
          Sat = 0.999999
          Theta = Sat * State / (1 + State)
        END IF

        CALL EffStress(dQ,Qh,SigInit,CStress,Stress,Suc,dSuc,State,Sat,SwFlag,SParms)
        SigInit = (CStress(1)+CStress(2)+CStress(3))/3
        SatSave = Sat

        Qstemp = ( Stress(1) - Stress(3) )
        Qhtemp = ( Qh(1) + Qh(2) + Qh(3) + Qh(4) )

        WRITE(13,'(2(F9.2,1x),1x,2(F8.5,1x))') CStress(1), CStress(3), Ds(1), Ds(3)

      END DO
!     Print out conditions after proctor loading for compaction curve and note yielded sliders

      WRITE(*,*) 'Program has Applied the Proctor Loading'
```

```
      WRITE(33,*) '----------------------------END of LOADING----------------------'
      WRITE(13,*) '----------------------------END of LOADING----------------------'
      WRITE(23,*) 'State after loading =',State
      WRITE(23,*) 'Saturation after loading =',Sat
      WRITE(23,*) 'Suction after loading =',Suc
      WRITE(23,*)
      WRITE(23,*) 'Major Principal Stress =',CStress(1)
      WRITE(23,*) 'Minor Principal Stress =',CStress(3)
      WRITE(23,*)
      WRITE(23,*) 'Qh(1) =',Qh(1) ,HFlag(1)
      WRITE(23,*) 'Qh(2) =',Qh(2) ,HFlag(2)
      WRITE(23,*) 'Qh(3) =', Qh(3),HFlag(3)
      WRITE(23,*) 'Qh(4) =',Qh(4) ,HFlag(4)

!     Reset SigC to the Seating Load specified in the input file

      WRITE(*,*) '*****************************************************'
      WRITE(*,*)
      WRITE(*,*) 'Water Content =', Sat*State/2.74*100
      WRITE(*,*) 'Dry Density   =', 2.74*62.4/(1+State)
      WRITE(33,*) '------------------------ BEGIN UNLOADING ----------------------'
      WRITE(33,*) 'CStress1  CStress3  Stress1  Stress3  Theta  State    Sat',&
      '   dSigma    SigInit   Suc'
      WRITE(23,*) 'SigC    =', SigC

!******************** Unload the compacted specimen to Zero stress ****************************

!     Use small increments of vertical strain to unload specimen
      DO WHILE (Cstress(1) .LT. -1.0)

        Ds(1) = 0.00001
        Ds(2) = 0
        Ds(3) = 0

!       Reset state to intial values
        Sat = SatSave
        Suc = SucInit
        dSuc  = 0.0
        dQ    = 0.0
        idump = .false.
        SwFlag = 2

        CALL Sand_Driver(Sat, Suc, Ds, State, Qs, Qh, CStress, Stress, Sparms, &
                         Swflag, Sflag, Hflag, Tflag, idump)
          dQ = Qh - QhSave
        QhSave = Qh

        Swflag = 1
        Sat = (1 + State)/State * Theta

!       For numerical consistency, when Sat approaches 1 do not allow it to exceed 1
        IF (Sat .GT. 0.99999) THEN
          Sat = 0.999999
          Theta = Sat * State / (1 + State)
        END IF

        SatSave = Sat
        CALL EffStress(dQ,Qh,SigInit,CStress,Stress,Suc,dSuc,State,Sat,SwFlag,SParms)
        WRITE(13,'(2(F9.2,1x),1x,2(F8.5,1x))') CStress(1), CStress(3), Ds(1), Ds(3)
        SatSave = Sat
```

```
      SigInit = (CStress(1)+CStress(2)+CStress(3))/3
      Qstemp = ( Stress(1) - Stress(3) )
      Qhtemp = ( Qh(1) + Qh(2) + Qh(3) + Qh(4) )

    END DO
    WRITE(*,*) 'Program has Unloaded the Proctor Stress'
    WRITE(33,*) '---------------------- END of VERTICAL UNLOADING ----------------'
    WRITE(13,*) '---------------------- END of VERTICAL UNLOADING ----------------'
    WRITE(33,*)
    WRITE (23,*) 'Prior to the lateral adjustment'
    WRITE(23,*) '-----------------------------'
    WRITE (23,*) 'CSig =', SigInit
    WRITE (23,*) 'CStress(1) and Cstress(3) =', Cstress(1),CStress(3)
    WRITE (23,*)
    WRITE(23,*) 'State after unloading =',State
    WRITE(23,*) 'Saturation after un loading =',Sat
    WRITE(23,*) 'Suction after unloading =', Suc
    WRITE(23,*)

!********************************** LATERAL STRESS ADJUSTMENT
*******************************

!   Through several steps the lateral and vertical effective stresses are reduced to a zero
!   using small strain increments

!   Reduce lateral stress first with no vertical strain allowed
    liter = 0
    DsInc = 0.00001
     DO liter=1,10

     IF (CStress(2) .GT. 0) THEN
       Dir = -DsInc
       DO WHILE (CStress(2) .GT. 0.0)

        Ds(1) = 0
        Ds(2) = Dir
        Ds(3) = Ds(2)

!       Reset state to intial values
        Sat = SatSave
        Suc = SucInit
        dSuc  = 0.0
        dQ   = 0.0
        idump = .false.
        SwFlag = 2

        CALL Sand_Driver(Sat, Suc, Ds, State, Qs, Qh, CStress, Stress, Sparms, &
                         Swflag, Sflag, Hflag, Tflag, idump)
          dQ = Qh - QhSave
          QhSave = Qh
        Swflag = 0
        Sat = (1 + State)/State * Theta
        IF (Sat .GT. 0.999999) THEN
          Sat = 0.999999
          Theta = Sat * State / (1 + State)
        END IF

        SatSave = Sat
        CALL EffStress(dQ,Qh,SigInit,CStress,Stress,Suc,dSuc,State,Sat,SwFlag,SParms)
        SatSave = Sat
```

```
        WRITE(13,'(2(F9.2,1x),1x,2(F8.5,1x))') CStress(1), CStress(3), Ds(1), Ds(3)
        SigInit = (CStress(1)+CStress(2)+CStress(3))/3
        END DO

      ELSE
!     Fine adjustment loop for lateral stress relaxation to
!      correct for excessive strain increment
        Dir = DsInc
        DO WHILE (CStress(2) .LT. -0.01)
        Ds(1) = 0
        Ds(2) = Dir
        Ds(3) = Ds(2)

!       Reset state to intial values
        Sat = SatSave
        Suc = SucInit
        dSuc  = 0.0
        dQ    = 0.0
        idump = .false.
        SwFlag = 2

        CALL Sand_Driver(Sat, Suc, Ds, State, Qs, Qh, CStress, Stress, Sparms, &
                         Swflag, Sflag, Hflag, Tflag, idump)
          dQ = Qh - QhSave
          QhSave = Qh
        Swflag = 0
        Sat = (1 + State)/State * Theta
        IF (Sat .GT. 0.99999) THEN
          Sat = 0.999999
          Theta = Sat * State / (1 + State)
        END IF
        SatSave = Sat
        CALL EffStress(dQ,Qh,SigInit,CStress,Stress,Suc,dSuc,State,Sat,SwFlag,SParms)
!       SatSave = Sat
        WRITE(13,'(2(F9.2,1x),1x,2(F8.5,1x))') CStress(1), CStress(3), Ds(1), Ds(3)
        SigInit = (CStress(1)+CStress(2)+CStress(3))/3
        END DO
      END IF

! ------------------------------------------------------------------------

!     Reduce any remaining vertical stress accrued during lateral unloading
      IF (CStress(1) .GT. 0) THEN
        Dir = -DsInc
        DO WHILE (CStress(1) .GT. 0.0)
        Ds(1) = Dir
        Ds(2) = 0
        Ds(3) = 0

!       Reset state to intial values
        Sat = SatSave
        Suc = SucInit
        dSuc  = 0.0
        dQ    = 0.0
        idump = .false.
        SwFlag = 2

        CALL Sand_Driver(Sat, Suc, Ds, State, Qs, Qh, CStress, Stress, Sparms, &
                         Swflag, Sflag, Hflag, Tflag, idump)
          dQ = Qh - QhSave
```

```
        QhSave = Qh
      Swflag = 0

      Sat = (1.0 + State)/State * Theta
      IF (Sat .GT. 0.99999) THEN
        Sat = 0.999999
        Theta = Sat * State / (1 + State)
      END IF
      SatSave = Sat
      WRITE(13,'(2(F9.2,1x),1x,2(F8.5,1x))') CStress(1), CStress(3), Ds(1), Ds(3)
      CALL EffStress(dQ,Qh,SigInit,CStress,Stress,Suc,dSuc,State,Sat,SwFlag,SParms)
      SigInit = (CStress(1)+CStress(2)+CStress(3))/3
     END DO

!    Fine adjustment loop for lateral stress relaxation to correct
!     for excessive strain increment
     ELSE
      Dir = DsInc
      DO WHILE (CStress(1) .LT. -0.01)
       Ds(1) = Dir
       Ds(2) = 0
       Ds(3) = 0

!      Reset state to intial values
       Sat = SatSave
       Suc = SucInit
       dSuc  = 0.0
       dQ   = 0.0
       idump = .false.
       SwFlag = 2

       CALL Sand_Driver(Sat, Suc, Ds, State, Qs, Qh, CStress, Stress, Sparms, &
                        Swflag, Sflag, Hflag, Tflag, idump)
         dQ = Qh - QhSave
         QhSave = Qh
       Swflag = 0

       Sat = (1.0 + State)/State * Theta
       IF (Sat .GT. 0.99999) THEN
         Sat = 0.999999
         Theta = Sat * State / (1 + State)
       END IF
       SatSave = Sat
       WRITE(13,'(2(F9.2,1x),1x,2(F8.5,1x))') CStress(1), CStress(3), Ds(1), Ds(3)
       CALL EffStress(dQ,Qh,SigInit,CStress,Stress,Suc,dSuc,State,Sat,SwFlag,SParms)
       SigInit = (CStress(1)+CStress(2)+CStress(3))/3
!       SatSave = Sat
      END DO
     END IF
     END DO   ! End of adjustment loop

     DO WHILE (Cstress(1) .LT. -0.5)

       Ds(1) = 0.0001
       Ds(2) = 0
       Ds(3) = 0

!      Reset state to intial values
       Sat = SatSave
       Suc = SucInit
```

```
      dSuc  = 0.0
      dQ    = 0.0
      idump = .false.
      SwFlag = 2

      CALL Sand_Driver(Sat, Suc, Ds, State, Qs, Qh, CStress, Stress, Sparms, &
                       Swflag, Sflag, Hflag, Tflag, idump)
        dQ = Qh - QhSave
        QhSave = Qh
      Swflag = 0
      Sat = (1 + State)/State * Theta
      IF (Sat .GT. 0.99999) THEN
        Sat = 0.999999
        Theta = Sat * State / (1 + State)
      END IF
      SatSave = Sat
      CALL EffStress(dQ,Qh,SigInit,CStress,Stress,Suc,dSuc,State,Sat,SwFlag,SParms)
      Eps(1,1) = Eps(1,1) + Ds(1)
      Eps(2,2) = Eps(2,2) + Ds(2)
      WRITE(13,'(2(F9.2,1x),1x,2(F8.5,1x))') CStress(1), CStress(3), Ds(1), Ds(3)

      SigInit = (CStress(1)+CStress(2)+CStress(3))/3

      Qstemp = ( Stress(1) - Stress(3) )
      Qhtemp = ( Qh(1) + Qh(2) + Qh(3) + Qh(4) )

    END DO

    WRITE(*,*) 'Program has Finished the lateral unloading'
    WRITE(33,*) '---------------------- END of LATERAL UNLOADING ----------------'
    WRITE(13,*) '---------------------- END of LATERAL UNLOADING ----------------'
    WRITE(33,*)
    WRITE(23,*) 'Prior to applying the seating load'
    WRITE(23,*)'-----------------------------'
    WRITE(23,*) 'Csig =',SigInit
    WRITE(23,*) 'CStress(1) and Cstress(3) =', Cstress(1),CStress(3)
    WRITE(23,*)
    WRITE(23,*) 'State after unloading =',State
    WRITE(23,*) 'Saturation after un loading =',Sat
    WRITE(23,*)
    WRITE(*,*) '*****************************************************'
    WRITE(*,*)
    WRITE(*,*) 'Water Content =', Sat*State/2.74*100
    WRITE(*,*) 'Dry Density   =', 2.74*62.4/(1+State)


!*****************************************END LATERAL STRESS
ADJUSTMENT************************

!   Completes the Proctor loading behavior (if Proctor = 0) then the above is not run.
    END IF

!******* Ignore this loop if test has proctor loading added ***************!

   IF (Proctor .EQ. 0) THEN
   WRITE(*,*) 'Water Content =', Sat*State/2.74*100
   WRITE(*,*) 'Dry Density   =', 2.74*62.4/(1+State)
   WRITE(*,*) 'Saturation    =', Sat
   WRITE(*,*) 'State =',State
```

```
!  Distribute suction and seating stresses evenly among mechanisms
   WRITE(*,*) 'Program is Running the Initialization of non-Proctor sliders'
   WRITE (23,*) 'Pe, Qe=', Pe, Qe
   DO r=1,4
     Qh(r) = BulkRatio(r) * (Sigc + Qsp)
    WRITE(23,*) 'Qh(',r,') = ',Qh(r)
     IF(Qh(r) .LT. Qe * Hlimit(r)) Qh(r) = Qe * Hlimit(r)
    WRITE(23,*) 'Qh(',r,') = ',Qh(r)
   END DO
    WRITE(23,*)

   iter = 0
   DsInc = ABS((Qh(1) + Qh(2) + Qh(3) + Qh(4) - (Sigc +Qsp))/BulkMod)
   Dir= -1.0 * DsInc
   WRITE(13,*) '----------------------------'
   Ds=0.0
   Ds(1) = Dir
   QsSave   = Qs
   QhSave   = Qh
   StateSave = State
   SflagSave = Sflag
   HflagSave = Hflag
   TflagSave = Tflag
   SatSave  = Sat
   SigError  = 0.0
   CFlag    = 1
   SigInitSave  = Qh(1) + Qh(2) + Qh(3) + Qh(4) - Qsp
   CStressSave = CStress

   DO WHILE(ABS(Qh(1)+Qh(2)+Qh(3)+Qh(4)-(SigC + Qsp)) .GT. 1.E-7 .and. iter .LT. 100)
     Ds(1) = Ds(1) - Dir
     Ds(2) = Ds(1)
     Ds(3) = Ds(1)

!    Reset state to intial values
     Qs   = QsSave
     Qh   = QhSave
     Suc  = SucInit
     Sat  = SatSave
     State = StateSave
     Sflag = SflagSave
     Hflag = HflagSave
     Tflag = TflagSave
     dSuc  = 0.0
     dQ   = 0.0
     idump = .false.
     SigInit  = SigInitSave
     CStress  = CStressSave
     SwFlag = 8
     CALL Sand_Driver(Sat, Suc, Ds, State, Qs, Qh, CStress, Stress, Sparms, &
                      Swflag, Sflag, Hflag, Tflag, idump)
     dQ = Qh - QhSave

     CALL EffStress(dQ,Qh,SigInit,CStress,Stress,Suc,dSuc,State,Sat,SwFlag,SParms)

!    Check for change in sign of error. If changed, modify increment size

     IF(Dir*(Qh(1)+Qh(2)+Qh(3)+Qh(4)-(Sigc + Qsp)) .LT. 0)THEN

       DsInc = DsInc * ABS( (CStress(2)-Sigc)/(SigError-(CStress(2)-Sigc)) )
```

```
      END IF

!     Compute error correction increment

      SigError =  Qh(1) + Qh(2) + Qh(3) + Qh(4) - (Sigc + Qsp)
      Dir=SIGN(DsInc, SigError)

     iter = iter + 1
    END DO
   END IF
   WRITE(*,*) 'State =',State
   WRITE(23,*) 'CStress =',CStress

!****************************** RE-APPLY SEATING LOAD ************************************

   IF (SwellType .EQ. 'FS' .or. SwellType .EQ. 'CV') THEN


    DO WHILE (CStress(1) .GT. SigC)

      Ds(1) = -0.0000005
      Ds(2) = 0
      Ds(3) = 0

!     Reset state to intial values
      Sat = SatSave
      Suc = SucInit
      dSuc  = 0.0
      dQ   = 0.0
      idump = .false.
      SwFlag = 2

      CALL Sand_Driver(Sat, Suc, Ds, State, Qs, Qh, CStress, Stress, Sparms, &
                  Swflag, Sflag, Hflag, Tflag, idump)
        dQ = Qh - QhSave
        QhSave = Qh
      Swflag = 0

      Sat = (1.0 + State)/State * Theta
      IF (Sat .GT. 0.99999) THEN
        Sat = 0.999999
        Theta = Sat * State / (1 + State)
      END IF

      CALL EffStress(dQ,Qh,SigInit,CStress,Stress,Suc,dSuc,State,Sat,SwFlag,SParms)
      SigInit = (CStress(1)+CStress(2)+CStress(3))/3
      SatSave = Sat

      Qstemp = ( Stress(1) - Stress(3) )
      Qhtemp = ( Qh(1) + Qh(2) + Qh(3) + Qh(4) )

      IF (SwellType .EQ. 'FS') THEN
        WRITE(13,'(4(f9.4,1x))') CStress(1), CStress(3), Eps(1,1), State
      END IF

    END DO
    WRITE(33,*) '---------------- END OF SEATING LOAD APPLICATION ----------------'
    WRITE(13,*) '---------------- END OF SEATING LOAD APPLICATION ----------------'
```

```
      END IF
      WRITE(23,*) 'After applying the seating load'
      WRITE(23,*) '----------------------'
      WRITE (23,*) 'CSig =', SigInit
      WRITE (23,*) 'CStress(1) and Cstress(3) =', Cstress(1),CStress(3)
      WRITE (23,*)
      WRITE(23,*) 'State after unloading =',State
      WRITE(23,*) 'Saturation after un loading =',Sat
      WRITE(23,*) 'Suction after unloading =',Suc
      WRITE(23,*)
      WRITE(23,*)
      WRITE(23,*) 'Qh(1) =',Qh(1) ,HFlag(1)
      WRITE(23,*) 'Qh(2) =',Qh(2) ,HFlag(2)
      WRITE(23,*) 'Qh(3) =', Qh(3),HFlag(3)
      WRITE(23,*) 'Qh(4) =',Qh(4) ,HFlag(4)
      WRITE(23,*) 'Qhdiff =',Qh(1)+Qh(2)+Qh(3)+Qh(4)-Qsp

        do r=1,4
          WRITE(23,*) r
          WRITE(23,'(3(f8.4,2x))') Qs(1,r), Qs(4,r), Qs(5,r)
          WRITE(23,'(3(f8.4,2x))') Qs(4,r), Qs(2,r), Qs(6,r)
          WRITE(23,'(3(f8.4,2x))') Qs(5,r), Qs(6,r), Qs(3,r)
        end do
      WRITE(33,*) '----------------------TEST BEGINS----------------------'
      WRITE(33,*) 'CStress1  CStress3  Stress1  Stress3  Theta  State   Sat',&
      '   dSigma   SigInit   Suc'

     PoiFlag = 1

!**********************END of INITIALIZATION OF THE SYSTEM*********************************!

      SwFlag = 0

!     Print out the stress-state conditions of the soil after suction and proctor loading

      WRITE(23,*) '*****************************************'
      WRITE(23,*) '*                                       *'
      WRITE(23,*) '* The state after conf press = ', State
      WRITE(23,*) '*                                       *'
      WRITE(23,*) '*****************************************'
      WRITE(23,*)
      WRITE(23,*) 'Qh(1) =',Qh(1)
      WRITE(23,*) 'Qh(2) =',Qh(2)
      WRITE(23,*) 'Qh(3) =', Qh(3)
      WRITE(23,*) 'Qh(4) =',Qh(4)

      WRITE(23,*) 'Eps (1,1)= ', Ds(1)
      WRITE(23,*) 'Eps (2,2)= ', Ds(2)
      VolStrainEps = (Ds(1) + 2.0 * Ds(2)) * 100.0
      VolStrainE   = (State - StateSave)/(1.0 + StateSave) * 100.0
      WRITE(23,*) 'VolStrainEps= ', VolstrainEps
      WRITE(23,*) 'VolStrainE=   ', VolstrainE
      WRITE(23,*)
      WRITE(23,*) '*********************************************************************************'
      InitState = State

!     STOP !---Used to stop program for Proctor test analysis

!*****************************************************************************************************
!*
```

```
!*
!*                                  Constant Volume Swell TEST
!*
!*************************************************************************************************

    TestState = State

    SucInit = Suc
    SigInit = (CStress(1) + CStress(2) + CStress(3))/3.0
    WRITE(13,*) 'iter =0 and SigInit =', SigInit, 'Suc = ',Suc, 'State =',State
    WRITE(23,*) 'SwellType =',SwellType


    IF (SwellType .EQ. 'CV' .OR. SwellType .EQ. 'cv') THEN
    WRITE(13,*) 'CStress(1)   Suc     Sat    Theta    State'
    WRITE(13,'(5(f8.4,2x))') CStress(1), Suc, Sat, Theta, State
     QhSave = Qh
     QsSave = Qs
     StateSave = State
     SwFlag = 1
      DO WHILE (Suc .LT. -0.001)
       dQ = 0.0

!       Standard constant volume test, no strain is allowed
       Ds = 0.0
       State  = StateSave
       Stress  =0.0
       Qh = QhSave
       Qs = QsSave
       dSuc = 0.005

       CALL Sand_Driver(Sat, Suc, Ds, State, Qs, Qh, CStress, Stress, Sparms, &
                  SwFlag, Sflag, Hflag, Tflag, idump)
        dQ = Qh - QhSave

       CALL EffStress(dQ,Qh,SigInit,CStress,Stress,Suc,dSuc,State,Sat,SwFlag,SParms)

       SigInit = (CStress(1) + CStress(2) + CStress(3))/3.0
       QhSave = Qh
       QsSave = Qs
      icode = 1
      smech=0
      hmech=0
      tmech=0
      ! Record number of yielded sliders due to swell pressure
      do r=1,4

        IF(sflag(r)) smech=smech + icode
        IF(hflag(r)) hmech=hmech + icode
        IF(tflag(r)) tmech=tmech + icode

        icode = 10*icode

      end do
      Qstemp =  Stress(1) - Stress(3)
      Qhtemp =  Qh(1) + Qh(2) + Qh(3) + Qh(4)
      WRITE(13,'(3(f9.2,1x),3(i4,1x))')  Qhtemp, Qstemp, CSTress(1), smech, hmech, tmech
     END DO
    WRITE(23,*) 'Final Saturation =', Sat
    WRITE(23,*) 'Final Suction    =', Suc
```

```
      WRITE(23,*) 'Final Void Ratio =', State
      WRITE(23,*) 'Final Mean Stress=', SigInit
     END IF
!    END OF CV TEST

!*****************************************************************************************************
!*
!*
!*                                                Free Swell TEST
!*
!*
!*****************************************************************************************************

     IF (SwellType .EQ. 'FS' .or. SwellType .EQ. 'fs') THEN
     WRITE(24,*) ' SumQh     Q1-Q3'
     WRITE(24,*) '---------------'
      Ds(1) = D(1,1)
      Ds(2) = D(2,2)
      Ds(3) = D(3,3)
      Ds(4) = D(1,2)
      Ds(5) = D(1,3)
      Ds(6) = D(2,3)

!    Set the current axial stress to the start of the test
      Sigc  = CStress(1)

      WRITE(13,*)
      WRITE(13,*) 'CStress1   CStress3  AxStrain   VoidRatio'

!    Assume constant confinning stress. Save state data

      iter    = 0
      Suc     = SucInit
      SigError = CStress(1)-Sigc
      CSig    = SigInit
      StateInit = State

!    Increment the Suction

      DO WHILE (Suc .LT. -0.01)

        QsSave   = Qs
        QhSave   = Qh
        StateSave = State
        SflagSave = Sflag
        HflagSave = Hflag
        TflagSave = Tflag
        SucSave  = Suc
        SatSave  = Sat
        SwFlag   = 1
        CSigSave = CSig
        dQ = 0.0
        siter = 0

!    Possible looping structures for difficult swelling soils
!       IF (Suc .LT. -10.0) THEN
!         dSuc = 0.001
!       ELSE IF (Suc .LT. -5.0) THEN
!         dSuc = 0.00001
!       ELSE
```

```
!       dSuc = 0.000001

!       END IF

        dSuc = 0.005

!       Zero strain is the initial guess.
        Ds(1) = 0
        Ds(2) = 0
        Ds(3) = Ds(2)

        CALL Sand_Driver(Sat, Suc, Ds, State, Qs, Qh, Cstress, Stress, Sparms, &
                         SwFlag, Sflag, Hflag, Tflag, idump)
         dQ = Qh - QhSave

       CALL EffStress(dQ,Qh,SigInit,CStress,Stress,Suc,dSuc,State,Sat,SwFlag,SParms)

!       Compute Error and iterate on confinning stress

        DsInc   = 0.0001 * ABS( (CStress(1)-Sigc)/(SigError-(CStress(1)-Sigc)))
       Dir= SIGN(DsInc, CStress(1)-Sigc)

      DO WHILE(ABS(CStress(1) - SigC) .GT. 1.E-3 ) !.and. siter .LT. 5000)

!        Correct axial strain
         Ds(1) = Ds(1) - Dir
         Ds(2) = 0
         Ds(3) = 0

!        Reset state to intial values
         Qs    = QsSave
         Qh    = QhSave
         State = StateSave
         Sflag = SflagSave
         Hflag = HflagSave
         Tflag = TflagSave
         Sat   = SatSave
         Suc   = SucSave
         CSig  = CSigSave

!        Compute new stress
         CALL Sand_Driver(Sat, Suc, Ds, State, Qs, Qh, Cstress, Stress, Sparms, &
                          SwFlag, Sflag, Hflag, Tflag, idump)
           dQ = Qh - QhSave

         CALL EffStress(dQ,Qh,SigInit,CStress,Stress,Suc,dSuc,State,Sat,SwFlag,SParms)

!        Check for convergence
         IF(ABS(CStress(1)-Sigc) .LT. 1.e-07) THEN
           EXIT
         END IF

!        Check for change in sign of error. If changed, modify increment size
        IF(Dir*(CStress(1)-Sigc) .LT. 0)THEN

!          Looping structure for difficult swelling soils
!           DsInc = DsInc * ABS( (CStress(1)-Sigc)/(SigError-(CStress(1)-Sigc)) )
!           IF (Sat .GT. 0.87) THEN
!             DsInc = DsInc * 0.001
!           ELSE
```

```
            DsInc = DsInc * 0.05
!           END IF

          END IF

!         Compute error correction increment
          SigError =  CStress(1)-Sigc
          Dir=SIGN(DsInc, SigError)
          siter = siter + 1

        END DO

!       IF (iter .EQ. 5) THEN
!         STOP
!       END IF

        icode = 1
        smech=0
        hmech=0
        tmech=0

!       Print out yielded sliders due to volumetric swelling
        do r=1,4

          IF(sflag(r)) smech=smech + icode
          IF(hflag(r)) hmech=hmech + icode
          IF(tflag(r)) tmech=tmech + icode

          icode = 10*icode

        end do
        WRITE(23,*) iter, State, Sat*100, State/(1+State), smech, hmech, tmech
        Qstemp =  Stress(1) - Stress(3)
        Qhtemp =  Qh(1) + Qh(2) + Qh(3) + Qh(4)
        CSig    = (CStress(1) + CStress(2) + CStress(3))/3.0
        iter    = iter + 1
        Eps(1,1) = Eps(1,1) + Ds(1)

        siter = 0
        IF (State .GT. 3.0) THEN
          EXIT
        END IF

      END DO
      WRITE(33,*)
      WRITE(23,*) 'Vol Strain =', (State-InitState)/(1+InitState)*100
      WRITE(33,*) '----------------------END of FREE SWELL--------------------'
      WRITE(23,*) 'Final Saturation =', Sat
      WRITE(23,*) 'Final Suction   =', Suc
      WRITE(23,*) 'Final Void Ratio =', State

      ENDIF

!************************************** END FREE SWELL TEST *********************************
!
!     STOP
!
!******************************** APPLY CONFINING PRESSURE TO SAMPLE **********************

    CSig = (CStress(1) + CStress(2) + CStress(3))/3.0
```

```
      WRITE(23,*) 'SigInit before loading =',CSig
      WRITE(23,*) 'Confining pressure    =',SigC

      SigError = 0.0
      IF (SwellType .EQ. 'LS' .or. SwellType .EQ. 'ls') THEN
      WRITE(*,*) 'Program is applying confining pressure'
       Ds(1) = D(1,1)
       Ds(2) = D(2,2)
       Ds(3) = D(3,3)
       Ds(4) = D(1,2)
       Ds(5) = D(1,3)
       Ds(6) = D(2,3)

!   Assume constant confinning stress. Save state data

       iter = 0
!   Increment the Volumetric Strain

       DO WHILE ((SigC - CStress(1)) .LT. 0.0)
         QsSave   = Qs
         QhSave   = Qh
         StateSave = State
         SflagSave = Sflag
         HflagSave = Hflag
         TflagSave = Tflag
         SucSave  = Suc
         SatSave  = Sat
         SwFlag   = 1
         dQ       = 0.0
         CSigSave = CSig
         Qhtemp = Qh(1) + Qh(2) + Qh(3) + Qh(4)

!        Small increment of axial strain is applied
         DirInit = -0.00005
         Ds(1)  = DirInit
         Ds(2)  = DirInit
         Ds(3)  = DirInit
         CALL Sand_Driver(Sat, Suc, Ds, State, Qs, Qh, Cstress, Stress, Sparms, &
                          SwFlag, Sflag, Hflag, Tflag, idump)
          dQ = Qh - QhSave

!   Assume constant water content so dtheta = 0
          Sat = (1.0 + State)/State * Theta
          IF (Sat .GT. 0.999) THEN
            Sat = 0.999
            Theta = Sat * State / (1 + State)
          END IF

          SwFlag = 4
          dSuc =  -SQRT(ABS(Suc/Qhtemp))*K2o/K1o*(dQ(1)+dQ(2)+dQ(3)+dQ(4))

        CALL EffStress(dQ,Qh,SigInit,CStress,Stress,Suc,dSuc,State,Sat,SwFlag,SParms)

!   Compute Error and iterate on confinning stress

        DsInc   = 0.5 * Ds(1)
        Dir     = DsInc
        DO siter=1,100

          Ds(1) = DirInit - Dir
```

```
      Ds(2) = DirInit + 0.5*Dir
      Ds(3) = DirInit + 0.5*Dir

!     Reset state to intial values
      Qs    = QsSave
      Qh    = QhSave
      State = StateSave
      Sflag = SflagSave
      Hflag = HflagSave
      Tflag = TflagSave
      Sat   = SatSave
      Suc   = SucSave
      CSig  = CSigSave

!     Compute new stress
      CALL Sand_Driver(Sat, Suc, Ds, State, Qs, Qh, Cstress, Stress, Sparms, &
                       SwFlag, Sflag, Hflag, Tflag, idump)
        dQ = Qh - QhSave
        Sat = (1.0 + State)/State * Theta
        IF (Sat .GT. 0.99999) THEN
          Sat = 0.999999
          Theta = Sat * State / (1 + State)
        END IF
        SwFlag = 5
        dSuc =  -SQRT(ABS(Suc/Qhtemp))*K2o/K1o*(dQ(1)+dQ(2)+dQ(3)+dQ(4))
      CALL EffStress(dQ,Qh,SigInit,CStress,Stress,Suc,dSuc,State,Sat,SwFlag,SParms)

!     Check for convergence
      IF(ABS(CStress(1)-CStress(3)) .LT. 1.e-07) THEN
        EXIT
      END IF

!     Check for change in sign of error. If changed, modify increment size
      IF(Dir*(CStress(1)-CStress(3)) .LT. 0)THEN
        DsInc = DsInc*ABS((CStress(1)-CStress(3))/(SigError-(CStress(1)-CStress(3))))
      END IF

!     Compute error correction increment
      SigError =  CStress(1)-CStress(3)
      Dir=SIGN(DsInc, SigError)

    END DO

    icode = 1
    smech=0
    hmech=0
    tmech=0
    do r=1,4

      IF(sflag(r)) smech=smech + icode
      IF(hflag(r)) hmech=hmech + icode
      IF(tflag(r)) tmech=tmech + icode

      icode = 10*icode

    end do
    Qstemp =  Stress(1) - Stress(3)
    Qhtemp =  Qh(1) + Qh(2) + Qh(3) + Qh(4)
    CSig   = (CStress(1) + CStress(2) + CStress(3))/3.0
    iter   = iter + 1
```

```
      END DO
      WRITE(*,*) 'Program has Finished applying the Confining Pressure'
      WRITE(33,*) '---------- END SEATING LOAD ----------'
      WRITE(33,*) 'Initial State and Saturation=',State, Sat
     END IF

     WRITE(33,*) 'CStress1  CStress3  Stress1  Stress3  Theta  State   Sat',&
     '   dSigma   SigInit   Suc'
     SigC = CStress(2)
     WRITE(*,*) '*****************************************************'
     WRITE(*,*)
     WRITE(*,*) 'Final state  =', State
     WRITE(*,*) 'Water Content =', Sat*State/2.74*100
     WRITE(*,*) 'Dry Density  =', 2.74*62.4/(1+State)

     DO r = 1,4
       WRITE(*,*) 'Qh(',r,')=',Qh(r)
     END DO

!************************************* END CONFINING PRESSURE ****************************
! **** Intialize the Pore Pressures in System
     IF (SwellType .EQ. 'LS' .or. SwellType .EQ. 'CT') THEN

     Ua = 0
     Uw = 0

    WRITE(14,10)
10   FORMAT(' Step',9x,'Strain',1x,'  Shear Stress' &
              ,' Mean Stress  ',6x,'R',8x, 'Void Ratio',8x,'Uw',8x,' Sig11'&
              ,7x,' Sig33',6x,' Yield')

     WRITE(23,*) 'State Before TX test begins = ', State
     WRITE(23,*) 'Deg Sat Before TX test     = ', Sat
     WRITE(23,*) 'Suction Before TX test     = ', Suc

!*********************************************************************************************
    BCheck = 0
!*********************************************************************************************
!   This routine determines Skempton's B Value for a triaxial test to assess the
!   compressibility of the soil
    IF (BCheck .EQ. 1) THEN
     D=0.0
     D(1,1) =  -0.0000001
     D(2,2) = D(1,1)
     D(3,3) = D(1,1)
     dSuc = 0.0
     Qh  = QhSave
     dQ  = 0.0
     CSig = (CStress(1) + CStress(2) + CStress(3))/3.0

     Ds(1)  = D(1,1)
     Ds(2)  = D(2,2)
     Ds(3)  = D(3,3)
     Ds(4)  = D(1,2)
     Ds(5)  = D(1,3)
     Ds(6)  = D(2,3)
     WRITE(*,*) '*******************************'
     WRITE(*,*)
     WRITE(*,*) 'Sig3 =', CStress(3)
```

```
      WRITE(*,*)
      Qhtemp = QhSave(1)+QhSave(2)+QhSave(3)+QhSave(4)
      CALL Sand_Driver(Sat, Suc, Ds, State, Qs, Qh, CStress, Stress, Sparms, &
                       SwFlag, Sflag, Hflag, Tflag, idump)
      dQ = Qh - QhSave
!     Assume constant water content
      Sat = (1.0 + State)/State * Theta
      IF (Sat .GT. 0.99999) THEN
       Sat = 0.999999
       Theta = Sat * State / (1 + State)
      END IF
      SwFlag = 4
      dSuc =  -SQRT(ABS(Suc/Qhtemp))*K2o/K1o*(dQ(1)+dQ(2)+dQ(3)+dQ(4))
      CALL EffStress(dQ, Qh, CSig, CStress, Stress, Suc, dSuc, State, Sat, SwFlag, SParms)
      CALL PorePressure(Sat, dSuc, State, StateSave, Uw, Ua)
      UwApp = Uw*Sat
      UaApp = Ua*(1.0-Sat)

      WRITE(*,*) 'Sig3 =', CStress(3) + UwApp + UaApp
      WRITE(*,*) 'PP   =', UwApp + UaApp
      WRITE(*,*)

      STOP

     END IF

!*************************************************************************************************
!*
!*                          TRIAXIAL TEST
!*
!*************************************************************************************************
!     This conducts a triaxial test on a soil either drained or undrained

!     Initialize incremental strain rate for constant volume
      D=0.0
      D(1,1) =  DeltaEps
      D(2,2) = -D(1,1)/2.0
      D(3,3) =  D(2,2)
      StateSave = State

!     Initialize strain tensor
      Eps   = 0.
      iprint = 1
      LCount = 1

      smech = 0
      hmech = 0
      tmech = 0

      Sigma(1,1) = CStress(1)  ! Stress changed to CStress to account for Qh terms
      Sigma(2,2) = CStress(2)  ! Stress changed to CStress to account for Qh terms
      Sigma(3,3) = CStress(3)  ! Stress changed to CStress to account for Qh terms
      Sigma(1,2) = Stress(4)
      Sigma(1,3) = Stress(5)
      Sigma(2,3) = Stress(6)

      IF (SwellType .EQ. 'CT' .or. SwellType .EQ. 'ct') THEN

       TStress = -Sigc - (Sigma(1,1) - Sigma(2,2)) / 3
       PorePress(LCount) = TStress + (Sigma(1,1)+Sigma(2,2)+Sigma(3,3)) / 3
```

```
      Sig11(LCount) = -Sigma(1,1) + PorePress(LCount)
      Sig22(LCount) = -Sigma(2,2) + PorePress(LCount)
      Sig33(LCount) = -Sigma(3,3) + PorePress(LCount)

     ELSE
      PorePress(LCount) = Uw + Ua
      Sig11(LCount) = -Sigma(1,1) + PorePress(LCount)
      Sig22(LCount) = -Sigma(2,2) + PorePress(LCount)
      Sig33(LCount) = -Sigma(3,3) + PorePress(LCount)


     END IF
     Sigma3 = Sig33(LCount)
     Sigma1 = Sig11(LCount)
     PoreP  = -PorePress(LCount)

!    Added for CModeler calculations
     WRITE(14,'(i4,2x,4(4x,f10.4),4(4x,f10.6),3(1x,i4))')im, -100. * (Eps(1,1)-Eps(2,2)),&
          -(Sigma(1,1)-Sigma(2,2)),&
          -(Sigma(1,1)+Sigma(2,2)+Sigma(3,3))/3.,&
          Sigma(1,1)/(Sigma(2,2)+0.01), State, PoreP, Sigma1,&
          Sigma3, smech, hmech, tmech

     Strain1(LCount) = -Eps(1,1)
     Strain3(LCount) = -Eps(2,2)

     Step(LCount) = im
     Strain(LCount) = -100. * (Eps(1,1)-Eps(2,2))
     VRatio(LCount) = State
     Y1(LCount) = smech
     Y2(LCount) = hmech
     Y3(LCount) = tmech
     LCount = LCount + 1
     idump = .false.

     WRITE(24,*) 'EffMean  ShearStress    Uw     Ua     AxStrain  ShrStrain'
     WRITE(24,*) '-------------------------------------------------------'

boss: DO im=1,Ntimes
!    Update strain tensor
!    Removed Eps calculator replaced in Drained routine

     CSig = (CStress(1) + CStress(2) + CStress(3))/3.0
     Ds(1)  = D(1,1)
     Ds(2)  = D(2,2)
     Ds(3)  = D(3,3)
     Ds(4)  = D(1,2)
     Ds(5)  = D(1,3)
     Ds(6)  = D(2,3)

     IF (SwellType .EQ. 'LS' .OR. SwellType .EQ. 'ls') THEN

!    Assume constant confinning stress. Save state data
     WRITE(23,*) 'Running Undrained Unsaturated TX Test'
       QsSave   = Qs
       QhSave   = Qh
       StateSave = State
       SflagSave = Sflag
       HflagSave = Hflag
       TflagSave = Tflag
```

```
      SatSave  = Sat
      SucSave  = Suc
      StateSave = State
      SwFlag   = 0
      dQ       = 0.0
      dSuc     = 0.0
      CSigSave = CSig
       UwSave  = Uw
      UaSave   = Ua

!     Elastic response is the initial guess.
      Qhtemp = QhSave(1)+QhSave(2)+QhSave(3)+QhSave(4)
      Ds(2) = -0.5*( 3.*BulkMod - ShearMod)/( 3.*BulkMod + 0.5 * ShearMod) * Ds(1)
      Ds(3) = Ds(2)

      CALL Sand_Driver(Sat, Suc, Ds, State, Qs, Qh, CStress, Stress, Sparms, &
                       SwFlag, Sflag, Hflag, Tflag, idump)
       dQ = Qh - QhSave

!      Assume constant water content
       Sat = (1.0 + State)/State * Theta
       IF (Sat .GT. 0.99999) THEN
        Sat = 0.999999
        Theta = Sat * State / (1 + State)
       END IF
       SwFlag = 4
       dSuc =  -SQRT(ABS(Suc/Qhtemp))*K2o/K1o*(dQ(1)+dQ(2)+dQ(3)+dQ(4))

      CALL EffStress(dQ,Qh,SigInit,CStress,Stress,Suc,dSuc,State,Sat,SwFlag,SParms)
      CALL PorePressure(Sat, dSuc, State, StateSave, Uw, Ua)
       UwApp = Uw*Sat
       UaApp = Ua*(1.0-Sat)

!     Use to conver to Cauchy stresses on surface
!*    CStress(1) = CStress(1) + Uw + Ua
!*    CStress(2) = CStress(2) + Uw + Ua
!*    CStress(3) = CStress(3) + Uw + Ua

!     Compute Error and iterate on confining stress
      DsInc = 0.1 * Ds(1)
      SigError =  CStress(2)+UwApp+UaApp-Sigc
      Dir= SIGN(DsInc, SigError)

!     Use up to 100 iterations
      DO iter = 1,100

!      Correct lateral strain
       Ds(2) = Ds(2) - Dir
       Ds(3) = Ds(2)

!      Reset state to intial values
       Qs   = QsSave
       Qh   = QhSave
       State = StateSave
       Sflag = SflagSave
       Hflag = HflagSave
       Tflag = TflagSave
       Sat   = SatSave
       Suc   = SucSave
       CSig  = CSigSave
```

```
          Uw   = UwSave
          Ua   = UaSave
          dQ   = 0.0
          dSuc  = 0.0
!         Compute new stress
          CALL Sand_Driver(Sat, Suc, Ds, State, Qs, Qh, CStress, Stress, Sparms, &
                           SwFlag, Sflag, Hflag, Tflag, idump)
            dQ = Qh - QhSave

!         Assume constant water content
          Sat = (1.0 + State)/State * Theta
          IF (Sat .GT. 0.99999) THEN
            Sat = 0.999999
            Theta = Sat * State / (1 + State)
          END IF
          SwFlag = 5
          dSuc =  -SQRT(ABS(Suc/Qhtemp))*K2o/K1o*(dQ(1)+dQ(2)+dQ(3)+dQ(4))
          CALL EffStress(dQ,Qh,SigInit,CStress,Stress,Suc,dSuc,State,Sat,SwFlag,SParms)
          CALL PorePressure(Sat, dSuc, State, StateSave, Uw, Ua)
          UwApp = Uw*Sat
          UaApp = Ua*(1.0-Sat)

!*        CStress(1) = CStress(1) + Uw + Ua
!*        CStress(2) = CStress(2) + Uw + Ua
!*        CStress(3) = CStress(3) + Uw + Ua

!         Check for convergence

          IF(ABS(CStress(2)+Uw+Ua-Sigc) .LT. 1.E-7) THEN

            EXIT
          END IF

!         Check for change in sign of error. If changed, modify increment size
          IF(Dir*(CStress(2)+UwApp+UaApp-Sigc) .LT. 0)THEN
            DsInc = DsInc * ABS( (CStress(2)+UwApp+UaApp-Sigc)/&
              (SigError-(CStress(2)+UwApp+UaApp-Sigc)) )
          END IF

!         Compute error correction increment
          SigError =  CStress(2)+UwApp+UaApp-Sigc
          Dir=SIGN(DsInc, SigError)

        END DO

        CSig = (CStress(1) + CStress(2) + CStress(3))/3.0
        QhSave = Qh
        QsSave = Qs
        StateSave  = State
        SatSave = Sat
        SucSave = Suc
        SflagSave = Sflag
        HflagSave = Hflag
        TflagSave = Tflag

!*************************CONSTANT VOLUME TRIAXIAL
TEST*********************************
!     If test is undrained then no volumteric strain is allowed,
!     and only pore pressures are calculated
```

```
      ELSE IF (SwellType .EQ. 'CT' .or. SwellType .EQ. 'ct') THEN
      WRITE(*,*) 'Running CT TX Test'
        CSig = (CStress(1) + CStress(2) + CStress(3))/3.0
        QhSave = Qh
        dSuc = 0.0
        State = StateSave
        SwFlag = 7

!       Standard constant volume test, all strains are known
        CALL Sand_Driver(Sat, Suc, Ds, State, Qs, Qh, CStress, Stress, Sparms,&
                         SwFlag, Sflag, Hflag, Tflag, idump)
        dQ = Qh - QhSave
        SwFlag = 0
!       Assume constant water content
        Sat = (1.0 + State)/State * Theta

        IF (Sat .GT. 0.99999) THEN
          Sat = 0.999999
          Theta = Sat * State / (1 + State)
        END IF
        CALL EffStress(dQ,Qh,SigInit,CStress,Stress,Suc,dSuc,State,Sat,SwFlag,SParms)

!       Do not need to call PorePressure routine, because system produces no excess pressure
        CALL PorePressure(Sat, dSuc, State, StateSave, Uw, Ua)
        UwApp = Uw*Sat
        UaApp = Ua*(1.0-Sat)

!********************** DRAINED CONSTANT LATERAL STRESS TRIAXIAL TEST
**********************

      ELSE
        WRITE(*,*) 'Running DCLTS TX'
        ! Condition for Drained, Constant Lateral Stress Behavior...needs to be
        ! Programmed Later
        WRITE(*,*) 'No Drained Lateral Stress Test Available'
        STOP
      END IF

      Sigma(1,1) = CStress(1)  ! Stress changed to CStress to account for Qh terms
      Sigma(2,2) = CStress(2)  ! Stress changed to CStress to account for Qh terms
      Sigma(3,3) = CStress(3)  ! Stress changed to CStress to account for Qh terms
      Sigma(1,2) = Stress(4)
      Sigma(1,3) = Stress(5)
      Sigma(2,3) = Stress(6)

!     Convert Ds array to D array and sum Total Strains
      D(1,1) = Ds(1)
      D(2,2) = Ds(2)
      D(3,3) = Ds(3)
      D(1,2) = Ds(4)
      D(1,3) = Ds(5)
      D(2,3) = Ds(6)
      Eps = Eps + D
      WRITE(24,'(4(f9.3,2x),4(f8.4,2x))') CStress(1), Cstress(1)-Cstress(3), UwApp, UaApp,&
              -100*Eps(1,1), -100*(Eps(1,1)-Eps(2,2)), Theta, Sat
      IF(im==iprint) then
        iprint = iprint + Numout
        icode = 1
        smech=0
        hmech=0
```

```
        tmech=0
        do r=1,4

          IF(sflag(r)) smech=smech + icode
          IF(hflag(r)) hmech=hmech + icode
          IF(tflag(r)) tmech=tmech + icode

          icode = 10*icode

        end do

!   Print data for an Excel file

!   Added for CModeler

      IF (SwellType .EQ. 'CT'.or. SwellType .EQ. 'ct') THEN

        TStress = -Sigc - (Sigma(1,1) - Sigma(2,2)) / 3
            PorePress(LCount) = TStress + (Sigma(1,1)+Sigma(2,2)+Sigma(3,3)) / 3
        Sig11(LCount) = -Sigma(1,1) + PorePress(LCount)
        Sig22(LCount) = -Sigma(2,2) + PorePress(LCount)
        Sig33(LCount) = -Sigma(3,3) + PorePress(LCount)

      ELSE
        PorePress(LCount) = -(UwApp + UaApp)
        Sig11(LCount) = -Sigma(1,1) + PorePress(LCount)
        Sig22(LCount) = -Sigma(2,2) + PorePress(LCount)
        Sig33(LCount) = -Sigma(3,3) + PorePress(LCount)

      END IF
!
          Sigma3 = Sig33(LCount)
      Sigma1 = Sig11(LCount)
      PoreP  = PorePress(LCount)

      WRITE(14,'(i4,2x,4(4x,f10.4),4(4x,f10.6),3(1x,i4))')im, -100. * (Eps(1,1)-Eps(2,2)),&
            -(Sigma(1,1)-Sigma(2,2)),&
            -(Sigma(1,1)+Sigma(2,2)+Sigma(3,3))/3.,&
            Sigma(1,1)/(Sigma(2,2)+0.01), State, PoreP, Sigma1,&
            Sigma3, smech, hmech, tmech

      Strain1(LCount) = -Eps(1,1)
      Strain3(LCount) = -Eps(2,2)

      Step(LCount) = im
      Strain(LCount) = -100. * (Eps(1,1)-Eps(2,2))
      VRatio(LCount) = State
      Y1(LCount) = smech
      Y2(LCount) = hmech
      Y3(LCount) = tmech
      LCount = LCount + 1
      If (LCount.eq.150) Then
                  LCount = LCount
          Endif
          If (LCount.eq.3000) Then
                  LCount = LCount
          Endif
    END IF
!************************ END STANDARD TRIAXIAL TEST ******************************
```

```
!************************ SET UP CYCLIC TRIAXIAL BEHAVIOR *********************************

!   Check for cyclic loading  and cycle if necessasary
    IF (Cyclic) THEN
!     if (strs_mode) WRITE(67,*) 'Stress Bounds are ',UBound,LBound,sigma(1,1)-sigma(2,2)
!     if (strn_mode) WRITE(67,*) 'Strain Bounds are ',UBound,LBound,Eps(1,1)-Eps(2,2)
!     if (combination) WRITE(67,*) 'Combo Bounds are ',
!      UBound,LBound,Eps(1,1)-Eps(2,2),sigma(1,1)-sigma(2,2)
      if (strs_mode .and. (-(sigma(1,1)-sigma(2,2)) .ge. ubound) .and. &
                          (.NOT. Cycle_Mode) )  Then
          Cycle_Mode = .true.
          Num_Cycles = 0
      end if
      if (strn_mode .and. (-(Eps(1,1)-Eps(2,2)) .ge. ubound) .and. &
                          (.NOT. Cycle_Mode) ) Then
          Cycle_Mode = .true.
          Num_Cycles = 0
      end if

      if (Combination .and. (-(Eps(1,1)-Eps(2,2)) .ge. ubound) .and. &
                          (.NOT. Cycle_Mode) )  THEN
         Cycle_Mode = .true.
         Combination = .false.
         strs_mode = .true.
         Ubound = -(sigma(1,1)-sigma(2,2))
         Num_Cycles = 0
!         Write(67,*) 'Combination Mode'
!         WRITE(67,*) 'Stress Bounds are ',UBound,LBound,sigma(1,1)-sigma(2,2)
      end if
      IF (Strs_Mode .AND. Cycle_Mode) then
       if ( (-(Sigma(1,1)-Sigma(2,2))  .GE. UBound) .or. &
          (-(Sigma(1,1)-Sigma(2,2))  .LE. LBound)  )  then
          D = -D
          Cycle_Mode = .TRUE.
          if (-(Sigma(1,1)-Sigma(2,2))  .LE. LBound) Num_Cycles = Num_Cycles + 1
!          WRITE(67,*) 'Doing the Recycle D = ',D
!          WRITE(67,*) 'Stress Bounds are ',UBound,LBound
       end if
      END IF

      IF (Strn_Mode .AND. Cycle_Mode) then
       if ( (-(Eps(1,1)-Eps(2,2))  .GE. UBound) .or. &
          (-(Eps(1,1)-Eps(2,2))  .LE. LBound)  )  then
          D = -D
          Cycle_Mode = .TRUE.
          if (-(Eps(1,1)-Eps(2,2))  .LE. LBound) Num_Cycles = Num_Cycles + 1
!          WRITE(67,*) 'Doing the Recycle D = ',D
!          WRITE(67,*) 'Strain Bounds are ',UBound,LBound
       end if
      END IF
      IF ( (Max_Cycles .GT. 0) .AND. (Num_Cycles .GE. Max_Cycles) ) THEN
       Cyclic = .false.
      END IF

     END IF
     END DO boss

     WRITE(33,*) '---------------------- END TRIAXIAL TEST ----------------------'
    END IF
     CLOSE (13)
```

```
      CLOSE (23)
      CLOSE (33)
!     CLOSE (67)

      CLOSE (14)
      CLOSE (24)

      END PROGRAM MAIN
!     END SUBROUTINE

!     ================================================================

      SUBROUTINE Sand_Driver(Sat, Suc, Ds, State, Qs, Qh, CStress, Stress, Sparms, &
                             SwFlag, Sflag, Hflag, Tflag, idump)

      IMPLICIT NONE

      INTERFACE
       FUNCTION Fy(Q)     ! An interface to yield function

       IMPLICIT NONE

       REAL (KIND=8), INTENT(IN):: Q(6)
       REAL (KIND=8) :: Fy

       END FUNCTION Fy
      END INTERFACE

      INTERFACE
       FUNCTION TDOT(A,B)

       IMPLICIT NONE
!
!      Function to compute scalar product of two symmetric tensors
!       given in 6 vector format
!
       REAL (KIND=8):: A(6),B(6), TDOT

       END FUNCTION TDOT
      END INTERFACE


      LOGICAL :: Sflag(4)
      LOGICAL :: Hflag(4)
      LOGICAL :: Tflag(4)
      LOGICAL :: Sflagd
      LOGICAL :: Idump, sdump

      INTEGER :: SwFlag, PoiFlag
      INTEGER :: r                ! Index for mechanism
      INTEGER :: i                ! index for stress component
      INTEGER :: counter

      REAL (KIND=8) :: Sparms(60)       ! Parameters
      REAL (KIND=8) :: Ds(6)           ! Strain increment
      REAL (KIND=8) :: Ds0(6)           ! Null strain increment
      REAL (KIND=8) :: State           ! Void ratio
      REAL (KIND=8) :: Qs(6,4)          ! Internal shear forces
      REAL (KIND=8) :: Qh(4)            ! Internal hydrostatic forces
```

```
      REAL (KIND=8) :: SigmaQ          ! Mean intergranular stress
      REAL (KIND=8) :: S(6)            ! Shear stress
      REAL (KIND=8) :: S0(6)           ! Initial shear stress
      REAL (KIND=8) :: Stress(6)       ! Stress
      REAL (KIND=8) :: Sig, Sig0       ! Mean stress parameter

      REAL (KIND=8) :: ShearMod        ! Elastic Shear Modulus
      REAL (KIND=8) :: BulkMod         ! Elastic Shear Modulus
      REAL (KIND=8) :: Poisson         ! Poisson's Ratio

      REAL (KIND=8) :: Fh, beta, Pe, Cr  ! Parameters defining volumetric state
      REAL (KIND=8) :: Mc              ! Shear-volume coupling parameter
      REAL (KIND=8) :: C               ! Normalized Cohesive Intercept Parameter
      REAL (KIND=8) :: Cohesion        ! Cohesion value
      REAL (KIND=8) :: Decay           ! Defines rate that PhiLim falls with OCR
      REAL (KIND=8) :: PhiRatio        ! Ratio of maximum and minimum PhiLim
      REAL (KIND=8) :: PhiR            ! Friction angle in radians
      REAL (KIND=8) :: SinPhi          ! Sine of friction angle
      REAL (KIND=8) :: PsiMax          ! Friction angle for Dilatant Surface at Mc
      REAL (KIND=8) :: PsiMin          ! Friction angle for low stress Dilatancy Surface
      REAL (KIND=8) :: Psi             ! Angle of Mc location in degrees
      REAL (KIND=8) :: PsiR            ! Mc angle in radians
      REAL (KIND=8) :: DecayV          ! Defines rate that Psi increases with pe
      REAL (KIND=8) :: Gamma

      REAL (KIND=8) :: Phi(4)          ! Fraction of PhiLim for each shear mechanism
      REAL (KIND=8) :: Ylimit(4)       ! Limit of internal shear mechanism
      REAL (KIND=8) :: Shear(4)        ! Shear modulus for internal mechanism
      REAL (KIND=8) :: Hlimit(4)       ! Limit of internal hydrostatic mechanism
      REAL (KIND=8) :: Tlimit          ! Limit of principal stress in tension
      REAL (KIND=8) :: Pfact(4)        ! factor to apportion mean stress to mechanism
      REAL (KIND=8) :: BulkRatio(4)    ! Distribution factor for Bulk Modulus to mechanism
      REAL (KIND=8) :: Bulk(4)         ! Bulk modulus for internal mechanism

      REAL (KIND=8) :: desp(6)         ! Plastic shear strain returned for rth mechanism
      REAL (KIND=8) :: despt(6)        ! Total plastic shear strain
      REAL (KIND=8) :: depd            ! Hydrostatic strain due to shear-volume coupling
      REAL (KIND=8) :: dEps            ! Total hydrostatic strain increment

      REAL (KIND=8) :: Lambda
      REAL (KIND=8) :: Sat, fSat
      REAL (KIND=8) :: Qe, Pew, Qsp
      REAL (KIND=8) :: Suc
      REAL (KIND=8) :: K1o,K2o,K3o
      REAL (KIND=8) :: Theta
      REAL (KIND=8) :: CStress(3)
      PoiFlag = 1
      counter = counter + 1
      WRITE(23,*) counter
!     Hydrostatic Strain increment
      dEps = Ds(1) + Ds(2) + Ds(3)
      desp = 0.

!     Account for void ratio
      State = (1.0 + State)* EXP(dEps) - 1.0

!     Fill in parameters
      beta     =  SParms( 1)
      Fh       =  SParms( 2)
      C        =  SParms( 3)
```

```
      Phi(1)    = SParms( 4)
      Phi(2)    = SParms( 5)
      Phi(3)    = SParms( 6)
      Phi(4)    = SParms( 7)
      Shear(1)  = Sparms( 8)
      Shear(2)  = SParms( 9)
      Shear(3)  = SParms(10)
      Shear(4)  = Sparms(11)
      Pfact(1)  = SParms(12)
      Pfact(2)  = SParms(13)
      Pfact(3)  = SParms(14)
      Pfact(4)  = SParms(15)
! *** Hlimit is calculated after Qe is determined
      BulkRatio(1) = Sparms(20)
      BulkRatio(2) = SParms(21)
      BulkRatio(3) = SParms(22)
      BulkRatio(4) = Sparms(23)
      Mc        = Sparms(24)
      Decay     = Sparms(25)
      PhiRatio  = Sparms(26)
      Gamma     = Sparms(27)
      Cr        = Sparms(28)
      PsiMax    = Sparms(29)
      PsiMin    = Sparms(30)
      DecayV    = Sparms(31)
      Lambda    = Sparms(32)
      K1o       = SParms(34)
      K2o       = SParms(35)
      K3o       = SParms(36)
      Poisson   = SParms(38)
      IF (PoiFlag .EQ. 0) THEN
        ShearMod = Shear(1) + Shear(2) + Shear(3) + Shear(4)
      END IF

!     Calculate current Pe states
      Pe  = 10**((Fh - State)*beta)

      Pew = -Pe*10**(Lambda*(1-Sat)*beta)
      IF (SwFlag .EQ. 8) THEN
        ! Produces small Qsp similar for saturated systems
        Qsp = 4.0 * (K2o / K3o)**2.0 * Suc
      ELSE
        ! Corrects Qsp for location in Q space
        Qsp = Qh(1) + Qh(2) + Qh(3) + Qh(4) - (CStress(1) + CStress(2) + CStress(3))/3
      END IF

!     Update Cohesion value due to new State and Pe
      Cohesion = C * Pe  !*** more strength due to higher cohesion

!     Hydrostatic stress parameter
      Sig    = Qh(1) + Qh(2) + Qh(3) + Qh(4) - Cohesion
      Qe     = Qsp + Pew

      Hlimit(1) = SParms(16) * Qe   !*** will strenghten the sliders
      Hlimit(2) = SParms(17) * Qe   !*** note negative sign is removed
      Hlimit(3) = SParms(18) * Qe
      Hlimit(4) = SParms(19) * Qe

!     Update Bulk Modulus Value
```

```
      BulkMod = ABS(Sig / Cr)
      Bulk(1) = BulkRatio(1) * BulkMod
      Bulk(2) = BulkRatio(2) * BulkMod
      Bulk(3) = BulkRatio(3) * BulkMod
      Bulk(4) = BulkRatio(4) * BulkMod

      IF (PoiFlag .EQ. 1) THEN
        ShearMod = 3.0 * BulkMod * (1.0 - 2.0*Poisson)/(1.0 + 2.0*Poisson)
        Shear(1) = Shear(1) * ShearMod
        Shear(2) = Shear(2) * ShearMod
        Shear(3) = Shear(3) * ShearMod
        Shear(4) = Shear(4) * ShearMod
      END IF

!     Convert friction angle to yield limit by building a principal stress
!     state at the limit and computing Fy for that state.
      DO r=1,4
        PhiR = (3.141592*Phi(r)/180.)*&
             ( PhiRatio + (1.0-PhiRatio)* EXP(Decay * (-Sig/Qe + C)))
             ! Friction angle is determined from Q/Qe effect
        SinPhi = SIN(PhiR)
        Stress= 0.0
        Stress(1) = (1. + SinPhi)/(1.-SinPhi)
        Stress(2) = 1.0
        Stress(3) = 1.0
        Ylimit(r) = Fy(Stress)
      END DO

!     Evaluate Mc based on Curvature of Psi Variables
      Psi = PsiMax - ( (PsiMax - PsiMin) * EXP(DecayV * (-Sig/Qe + C)))
             !*** Psi angle is determined from Q/Qe effect
      PsiR = Psi * 3.141592/180.
      Mc = ( 6 * SIN(PsiR) ) / ( 3 - SIN(PsiR) )

!     Initialize stress
      S    = 0.0
      S0   = 0.0
      SigmaQ = 0.0
      despt = 0.0
      desp= 0.0
      Sig0 = Sig

!     Update each sand shearing mechanism and shear accumulate stress
      DO r = 1,4

!       Save initial shear stress for stress dilatancy computation
        DO i=1,6
          S0(i) = S0(i) + Qs(i,r)
        END DO

        IF(idump) sdump = .true.
        CALL Ammos(Ds, Qs(1,r), Sig*Pfact(r), desp, &
                   Ylimit(r), Shear(r), Sflag(r), sdump)

        DO i=1,6
          despt(i) = despt(i) + Shear(r) * desp(i) / ShearMod
          S(i) = S(i) + Qs(i,r)
        END DO
      END DO
```

```
!   Shear coupling strain. Dilation is positive.
    depd = Gamma * ( TDOT(S0, despt)/(-Sig0) - Mc * SQRT( TDOT(despt, despt) ) )

!   Update each hydrostatic mechanism and accumulate hydrostatic stress
    sdump = .false.
    DO r = 1,4
      sdump=.false.

      Tlimit = Cohesion  * Bulk(r)/BulkMod

      CALL Hydros(dEps-depd, Qh(r), Bulk(r), Hlimit(r), Hflag(r),    &
                                  Tlimit, Tflag(r), sdump)
      SigmaQ = SigmaQ + Qh(r)
    END DO

!   Rescale shear stress to account for reduction in mean stress
    Sig  = SigmaQ - Cohesion
    Ds0 = 0.
    S=0.
    DO r = 1,4

      desp=0.0
      IF(idump) sdump = .true.
      CALL Ammos(Ds0, Qs(1,r), Sig*Pfact(r), desp, Ylimit(r),&
                    Shear(r), Sflagd, sdump)

      DO i=1,6
        S(i) = S(i) + Qs(i,r)
      END DO

    END DO

!   Only pass shear stresses since mean stress must be obtained from dQ
    Stress(1) = S(1)
    Stress(2) = S(2)
    Stress(3) = S(3)

  END SUBROUTINE Sand_Driver

!   ================================================================

    SUBROUTINE Ammos( Ds, Qs, Sig, desp, Ylimit, Shear, Sflag, sdump)

    IMPLICIT NONE

    INTERFACE
     FUNCTION Fy(Q)     ! An interface to yield function

     IMPLICIT NONE

     REAL (KIND=8), INTENT(IN):: Q(6)

     REAL (KIND=8) :: Fy

     END FUNCTION Fy
    END INTERFACE


    LOGICAL Sflag
    LOGICAL sdump
```

```
      REAL (KIND=8) :: Y              ! Value of yield function
      REAL (KIND=8) :: Sig            ! Mean stress
      REAL (KIND=8) :: Ylimit         ! Limiting value of yield function
      REAL (KIND=8) :: Shear          ! Shear modulus

      REAL (KIND=8) :: Ds(6)          ! Strain magnitude

      REAL (KIND=8) :: Id(6)          ! Identity tensor
      REAL (KIND=8) :: Qm(6)          ! Mean stress tensor
      REAL (KIND=8) :: Qs(6), Qs0(6)  ! Shear stress
      REAL (KIND=8) :: Q(6)           ! Stress
      REAL (KIND=8) :: des(6)         ! Shear strain increment tensor
      REAL (KIND=8) :: dem(6)         ! Volumetric strain increment tensor
      REAL (KIND=8) :: dQsE(6)        ! Elastic strain increment
      REAL (KIND=8) :: desp(6)        ! Plastic strain increment tensor

!     Identity tensor
      Id=0.0
      Id(1) = 1.0
      Id(2) = 1.0
      Id(3) = 1.0

!     Check for non-compression
      IF(Sig .GE. 0.0) Sig = -.001


!     Hydrostatic stress
      Qm = Id * Sig

!     Save initial value
      Qs0 = Qs

!     Initial yield surface
      Q = Qs + Qm

!     Hydrostatic increment
      dem = Id * (Ds(1) + Ds(2) + Ds(3))/3.0

!     Shear part
      des = Ds - dem

!     Apply elastic Law with coupling plastic strain
      dQsE = Shear * des

!     Updated deviatoric stress
!      WRITE(23,'(3(f8.4,1x))') Q(1),Qs(1),Qm(1)
      Qs = Qs + dQsE

!     Stress
      Q = Qs + Qm

!     Trial yield surface
      Y = Fy(Q)

!     Adjust stress for yield condition
      IF(Y .GT. Ylimit .OR. Y .LE. 9.0) THEN
!       Scale back stress
        CALL RadialReturn(Q, Ylimit, sdump)
        Qs  = Q - Qm
```

```
      IF(sdump) WRITE(13,*) q(1), q(2), q(3)

!     Plastic shear strain increment
      desp =( dQsE - (Qs - Qs0))/Shear

!     Signal that limit was hit
      Sflag = .True.

    ELSE
!     Plastic strain is zero
      desp=0.0

!     Signal that limit was not hit
      Sflag = .False.

    END IF

    END SUBROUTINE Ammos

!   ======================================================================

    FUNCTION Fy(Q)

    IMPLICIT NONE


    REAL (KIND=8), INTENT(IN):: Q(6)
    REAL (KIND=8) :: I1, I2, I3

    REAL (KIND=8) :: Fy

!   Invarients I1, I2, I3
    I1 = Q(1) + Q(2) + Q(3)

    I2 = Q(1)*Q(2) + Q(1)*Q(3) + Q(2)*Q(3) - (Q(4)**2 + Q(5)**2 + Q(6)**2)

    I3 = Q(1)*Q(2)*Q(3) - &
       Q(1)*Q(6)**2 - Q(2)*Q(5)**2 - Q(3)*Q(4)**2 + &
       2.0*Q(4)*Q(5)*Q(6)

!   Yield Function
    Fy = I1*I2/I3

    IF(Fy .GT. 500) Fy=500

    END FUNCTION  Fy
!   ======================================================================

    FUNCTION FGrad(Q)

    IMPLICIT NONE

    INTERFACE
      FUNCTION TDOT(A,B)

      IMPLICIT NONE
!
!     Function to compute scalar product of two symmetric tensors
!      given in 6 vector format
```

```
!
      REAL (KIND=8):: A(6),B(6), TDOT

      END FUNCTION TDOT
    END INTERFACE

    REAL (KIND=8), INTENT(IN):: Q(6)
    REAL (KIND=8) :: Iso(6)
    REAL (KIND=8) :: P(6)
    REAL (KIND=8) :: I1, I2, I3
    REAL (KIND=8) :: dFdI1, dFdI2, dFdI3
    REAL (KIND=8) :: dI1dQ(6), dI2dQ(6), dI3dQ(6)
    REAL (KIND=8) :: Pbar

    REAL (KIND=8) :: FGrad(6)

!   Mean tensor
    Iso=0.0
    Iso(1) = 1.0/3.0
    Iso(2) = Iso(1)
    Iso(3) = Iso(1)

!   Invarients I1, I2, I3
    I1 = Q(1) + Q(2) + Q(3)

    I2 = Q(1)*Q(2) + Q(1)*Q(3) + Q(2)*Q(3) - (Q(4)**2 + Q(5)**2 + Q(6)**2)

    I3 = Q(1)*Q(2)*Q(3) - &
       Q(1)*Q(6)**2 - Q(2)*Q(5)**2 - Q(3)*Q(4)**2 + &
       2.0*Q(4)*Q(5)*Q(6)

    dFdI1 = I2/I3
    dFdI2 = I1/I3
    dFdI3 = -I1*I2/I3**2

    dI1dQ = Iso

    dI2dQ(1) =  Q(2) + Q(3)
    dI2dQ(2) =  Q(1) + Q(3)
    dI2dQ(3) =  Q(1) + Q(2)
    dI2dQ(4) = -2.0 *Q(4)
    dI2dQ(5) = -2.0 *Q(5)
    dI2dQ(6) = -2.0 *Q(6)

    dI3dQ(1) =  Q(2)*Q(3) - Q(6)**2
    dI3dQ(2) =  Q(1)*Q(3) - Q(5)**2
    dI3dQ(3) =  Q(1)*Q(2) - Q(4)**2
    dI3dQ(4) = -2.0 *(Q(3)*Q(4) + Q(5)*Q(6))
    dI3dQ(5) = -2.0 *(Q(2)*Q(5) + Q(4)*Q(6))
    dI3dQ(6) = -2.0 *(Q(1)*Q(6) + Q(4)*Q(5))

    P = dFdI1 * dI1dQ + dFdI2 * dI2dQ + dFdI3 * dI3dQ

    P = P - (P(1)+P(2)+P(3))*Iso

    PBar = SQRT( TDOT(P,P) )

    Fgrad = P/Pbar

    END FUNCTION  FGrad
```

```
      SUBROUTINE Hydros(dEps, Sigma, Bulk, Hlimit, Hflag, Tlimit, Tflag, sdump)

      IMPLICIT NONE

      LOGICAL :: Hflag
      LOGICAL :: Tflag

      logical :: sdump

      REAL (KIND=8) :: dEps
      REAL (KIND=8) :: Bulk
      REAL (KIND=8) :: Hlimit
      REAL (KIND=8) :: Tlimit
      REAL (KIND=8) :: dSigmaE
      REAL (KIND=8) :: Sigma

!     Stress increment
      dSigmaE =  Bulk * dEps

!     Elastic stress
      Sigma = Sigma + dSigmaE
      IF(sdump) WRITE(13,*) dSigmaE, Sigma
      IF(sdump) WRITE(13,*) ' hlimit', Hlimit

!     Limit condition (note tension--positive convention)
      IF(Sigma .LT. Hlimit) THEN
!       Compression limit
        Sigma = Hlimit
        Hflag = .True.
        Tflag = .False.
      ELSE
        IF(Sigma .GT. Tlimit) THEN
!         Tension limit
          Sigma = Tlimit
          Tflag = .True.
          Hflag = .False.
        ELSE
          Hflag = .False.
          Tflag = .False.
        END IF
      END IF

      IF(sdump) WRITE(13,*) 'final sigma ',Sigma
      IF(sdump) WRITE(13,*)

      END SUBROUTINE Hydros

!     ======================================================================

      SUBROUTINE RadialReturn(Q, Ylimit, sdump)

!     Subroutine to perform radial return of stress point to yield function given
!     by Fy(Q) = I1 I2 /I3. A transformation is first performed to principal
!     stress space, then the return is performed such that I1 and (Pv2-Pv3)/(Pv1-Pv3)
!     are held constant. This these constraints, Fy=Ylimit becomes a cubic equation.
!     The stress tensor is computed from the eigen vectors and adjusted eigenvalues.
!     Therefore, the adjusted stress tensor has the same principal axes, mean stress,
!     and Lode parameter as the original stress tensor.
```

```
      IMPLICIT NONE

      LOGICAL sdump

      LOGICAL :: Reversed

      INTEGER :: i, j, iv, ib
      INTEGER :: it

      REAL (KIND=8) :: Qm1, Qm2, Qm3
      REAL (KIND=8) :: Qm
      REAL (KIND=8) :: Pmag
      REAL (KIND=8) :: I1, I2, I3, Bl
      REAL (KIND=8) :: A, B, C, D
      REAL (KIND=8) :: alpha, beta, gamma, omega

      REAL (KIND=8) :: m(3)
      REAL (KIND=8) :: fi(3)
      REAL (KIND=8) :: S(3,3)
      REAL (KIND=8) :: Pv(3), Ev(3,3)

      REAL (KIND=8) :: Q(6)
      REAL (KIND=8) :: Ylimit, Rmax

!     Initially principal values not reversed in order
      Reversed = .False.

!     First estimate the maximum eigenvalue using Gershgorin's theorem
      Qm1 = Q(1)     + ABS(Q(4)) + ABS(Q(5))
      Qm2 = ABS(Q(4)) + Q(2)     + ABS(Q(6))
      Qm3 = ABS(Q(5)) + ABS(Q(6)) + Q(3)

      Qm = MAX(Qm1, Qm2, Qm3)

!     ....Compute principal values

!     Invarients I1, I2, I3
      I1 = Q(1) + Q(2) + Q(3)

      I2 = Q(1)*Q(2) + Q(1)*Q(3) + Q(2)*Q(3) - (Q(4)**2 + Q(5)**2 + Q(6)**2)

      I3 = Q(1)*Q(2)*Q(3) - &
         Q(1)*Q(6)**2 - Q(2)*Q(5)**2 - Q(3)*Q(4)**2 + &
         2.0*Q(4)*Q(5)*Q(6)

!     Use Newton iteration to get largest eigenvalue
      it = 0
      DO WHILE(ABS(Qm * (Qm *(I1-Qm) - I2) + I3) .GT. 1E-15 .AND. it .LE. 50)
        it = it+1
        Qm = (Qm*Qm*(2.*Qm-I1) + I3)/(Qm*(3.*Qm-2.*I1) + I2)
      END DO

!     Compute other two values using quadratic obtained from synthetic division
!     A = -1.0
      B = I1 - Qm
      C = Qm * B - I2

      D = B*B + 4.0 * C
```

```
!   D can be <0 because of roundoff if there are repeated roots.
    IF(D .GT. 0.) THEN
      D = SQRT(D)
    ELSE
      D=0.0
    END IF

!   Put in order of compressive magnitude
    Pv(3) = Qm
    Pv(2) = MAX(B+D, B-D)/2.0
    Pv(1) = MIN(B+D, B-D)/2.0


    Pmag = MAX( ABS(Pv(1)), ABS(Pv(2)), ABS(Pv(3)) )

!   Check for null tensor
    IF(Pmag .LT. 1.E-12) RETURN

!   Check for near-hydrostatic conditions.
    IF( ( ABS(Pv(1)-Pv(2)) )/Pmag .LT. 1.e-3) THEN
      IF(( ABS(Pv(1)-Pv(3)) )/Pmag .LT. 1.e-3) THEN
!       Tensor is close to hydrostatic.
        RETURN
      END IF
    END IF

!   Save principal values in normalized form for use later
    fi(1) = -Pv(1)/I1
    fi(2) = -Pv(2)/I1
    fi(3) = -Pv(3)/I1

!   Compute principal directions. Note that by this point at least two eigenvalues
!    have been determined to be distinct. Order eigenvalues to insure the first
!    one is distinct. Note that they are now in order of magnitude. Thus Pv(1) and
!    Pv(3) cannot be equal because the hydrostatic case has been ruled out.

    IF(ABS(Pv(1)-Pv(2)) .LT. ABS(Pv(1)-Pv(3)) .AND.&
      ABS(Pv(1)-Pv(2)) .LT. ABS(Pv(2)-Pv(3)) ) THEN
!     Pv(1) and Pv(2) could be equal. Switch order

      Reversed = .true.
      A = Pv(3)
      Pv(3) = Pv(1)
      Pv(1) = A
    END IF

    DO i=1,2
     IF(i .EQ. 1 ) THEN
!      First eigenvector. First eigenvalue is distinct.
       iv = 1
     ELSE
!      Pick eigenvector with the "most distinct" eigenvalue.
       IF(ABS(Pv(1)-Pv(2)) .LT. ABS(Pv(1)-Pv(3)) ) THEN
          iv = 3
          ib = 2
       ELSE
          iv = 2
          ib=3
       END IF
     END IF
```

```
!     Set up the singular matrix
      S(1,1) = Q(1) - Pv(iv)
      S(1,2) = Q(4)
      S(1,3) = Q(5)

      S(2,1) = S(1,2)
      S(2,2) = Q(2) - Pv(iv)
      S(2,3) = Q(6)

      S(3,1) = S(1,3)
      S(3,2) = S(2,3)
      S(3,3) = Q(3) - Pv(iv)

      Pmag = Pmag * Pmag

!     Pick the appropriate set of equations for eigenvector components.
      IF(ABS(S(2,2) * S(3,3) - S(2,3) * S(3,2))/Pmag .GT. 1.E-5) THEN
       D = S(2,2) * S(3,3) - S(2,3) * S(3,2)
       A = 1.0
       B = (-S(2,1) * S(3,3) + S(3,1) * S(2,3))/D
       C = (-S(2,2) * S(3,1) + S(2,1) * S(2,3))/D

      ELSE IF(ABS(S(1,1) * S(3,3) - S(1,3) * S(3,1))/Pmag .GT. 1.E-5) THEN
       D = S(1,1) * S(3,3) - S(1,3) * S(3,1)
       A = (-S(1,2) * S(1,1) + S(3,2) * S(1,3))/D
       B = 1.0
       C = (-S(1,1) * S(3,2) + S(3,1) * S(1,2))/D

      ELSE IF(ABS(S(1,1) * S(2,2) - S(1,2) * S(2,1))/Pmag .GT. 1.E-5) THEN
       D = S(1,1) * S(2,2) - S(1,2) * S(2,1)
       A = (-S(2,2) * S(1,3) + S(2,1) * S(1,3))/D
       B = (-S(1,1) * S(2,3) + S(2,1) * S(1,3))/D
       C =  1.0

      ELSE
!      Repeated eigenvalue. Make a vector that is normal to first and direction m(i)
!      that is not colinear to Ev(i,1)

       IF(ABS(Ev(1,1)) .GT. ABS(Ev(1,2)) ) THEN
        IF(ABS(Ev(1,1)) .GT. ABS(EV(1,3)) ) THEN
         m(1)= Ev(3,1)
         m(2)= Ev(2,1)
         m(3)= -Ev(1,1)
        ELSE
         m(1)= -Ev(3,1)
         m(2)= Ev(2,1)
         m(3)= Ev(1,1)
        END IF
       ELSE
        IF(ABS(Ev(1,2)) .GT. ABS(EV(1,3)) ) THEN
         m(1)= Ev(3,1)
         m(2)= -Ev(2,1)
         m(3)= Ev(1,1)
        ELSE
         m(1)= -Ev(3,1)
         m(2)= Ev(2,1)
         m(3)= Ev(1,1)
        END IF
       END IF
```

```
        A = m(2) * Ev(3,1) - m(3) * Ev(2,1)
        B = m(3) * Ev(1,1) - m(1) * Ev(3,1)
        C = m(1) * Ev(2,1) - m(2) * Ev(1,1)
      END IF

!     Normalize vector
      D = SQRT(A*A + B*B + C*C)
      Ev(1,iv) = A/D
      Ev(2,iv) = B/D
      Ev(3,iv) = C/D
    END DO

!   Use cross product to find third eigenvector
    A =  Ev(2,1) * Ev(3,iv) - Ev(2,iv) * Ev(3,1)
    B = -Ev(1,1) * Ev(3,iv) + Ev(1,iv) * Ev(3,1)
    C =  Ev(1,1) * Ev(2,iv) - Ev(1,iv) * Ev(2,1)

!   Normalize vector
    D = SQRT(A*A + B*B + C*C)
    Ev(1,ib) = A/D
    Ev(2,ib) = B/D
    Ev(3,ib) = C/D

!   Adjust eigenvalues for yield condition assuming radial return in pi plane.
!    The radial return requires solution of the cubic equation that is obtained by
!    substitution of fi(1)+fi(2)+fi(3)=1 and Bl into the equation for the yield
!    function.  The root rendering the largest negative value (most compressive)
!    is the correct root. The cubic is in the form of
!     alpha * Qm**3 + beta * Qm**2 + gamma * Qm + omega  = 0

    Bl = (fi(2)-fi(3))/(fi(1)-fi(3))
    A = -(1.-Bl)/(2.-Bl)
    B = (2*Bl-1.)/(2.-Bl)
    C = -1./(2.-Bl)
    D = -(1.+Bl)/(2.-Bl)

    alpha = B*D*Ylimit
    beta  = B + B*D + D +(A*D+B*C)*Ylimit
    gamma = A + C + A*D + B*C + A*C*Ylimit
    omega = A * C

!   Use Newton iteration to get largest eigenvalue. Use approximation from Mohr-
!    Coulomb yield surface as first guess
    Rmax = 0.25 * ( (Ylimit - 5.) + SQRT((Ylimit-9.0)*(Ylimit-1.0)) )
    Qm = -Rmax/(Rmax*(Bl + 1.0)-(Bl-2.0))

    it = 0
    DO WHILE(ABS(Qm * (Qm *(alpha * Qm + beta) + gamma) + omega) .GT. 1E-7 &
                    .AND. it .LE. 50)
      it = it+1
      Qm = (Qm*Qm * (2.*alpha*Qm + beta) - omega)/&
                (Qm * (3.*alpha*Qm + 2.*beta) + gamma)
    END DO

!   Revised principal values that meet yield condition
    fi(1) = Qm
    fi(2) = A + B*fi(1)
    fi(3) = C + D*fi(1)
```

```
!   Fill back in to eigenvalues
    IF(Reversed) THEN
      Pv(3) = -fi(1) * I1
      Pv(2) = -fi(2) * I1
      Pv(1) = -fi(3) * I1
    ELSE
      Pv(1) = -fi(1) * I1
      Pv(2) = -fi(2) * I1
      Pv(3) = -fi(3) * I1
    END IF

!   Rebuild tensor from its spectral decomposition
    DO i=1,3
      DO j=i,3
        S(i,j) = Pv(1)*Ev(i,1)*Ev(j,1) + &
             Pv(2)*Ev(i,2)*Ev(j,2) + Pv(3)*Ev(i,3)*Ev(j,3)
        S(j,i) = S(i,j)
      END DO
    END DO

!   Put into vector form.
    Q(1) = S(1,1)
    Q(4) = S(1,2)
    Q(5) = S(1,3)

    Q(2) = S(2,2)
    Q(6) = S(2,3)
    Q(3) = S(3,3)

    END SUBROUTINE RadialReturn


! ****************************************************************
! *                  * T D O T *                  *
! ****************************************************************
    FUNCTION TDOT(A,B)

    IMPLICIT NONE
!
!   Function to compute scalar product of two symmetric tensors
!    given in 6 vector format
!
    REAL (KIND=8):: A(6),B(6), TDOT
!
    TDOT = A(1) * B(1) + A(2) * B(2) + A(3) * B(3) +  &
             2.D0 * (A(4) * B(4) +  A(5) * B(5) + A(6) * B(6))
!
       RETURN
         END

!   ================================================================

    SUBROUTINE PorePressure(Sat, dSuc, State, StateSave, Uw, Ua)

     IMPLICIT NONE

     REAL (KIND=8) :: Sat          ! Saturation of Water as a fraction
     REAL (KIND=8) :: Ca, Cw       ! Compressiblity of Air and Water (units/psi)
     REAL (KIND=8) :: PRatio       ! Volumetric strain based on porosity
     REAL (KIND=8) :: PI           ! Initial Porosity
```

```
      REAL (KIND=8) :: dP              ! Change in Porosity over strain increment
      REAL (KIND=8) :: dUw             ! Change in pore water pressure
      REAL (KIND=8) :: dUa             ! Change in pore air pressure
      REAL (KIND=8) :: dSuc            ! Change in suction
      REAL (KIND=8) :: Uw, Ua          ! Initial and Final Air and Water Pore Pressures
      REAL (KIND=8) :: State, StateSave
      REAL (KIND=8) :: Poros

      PI    = StateSave/(1+StateSave)
      Poros  = State/(1+State)
      dP    = PI - Poros
      Ca = 0.0336
      Cw = 3.116e-6

      PRatio = dP / PI

      dUw = -1*((1-Sat)*Ca*dsuc + PRatio) / (Sat*Cw + (1-Sat)*Ca)

      dUa = dsuc + dUw

      Uw = Uw + dUw

      Ua = Ua + dUa

    END SUBROUTINE PorePressure

!   ======================================================================

    SUBROUTINE EffStress(dQ,Qh,SigInit,CStress,Stress,Suc,dSuc,State,Sat,SwFlag,SParms)

      IMPLICIT NONE

      INTEGER :: r
      INTEGER :: SwFlag, ThetaFlag

      REAL (KIND=8) :: dQ(4), Qh(4), dQsum
      REAL (KIND=8) :: Suc, dSuc, Suction
      REAL (KIND=8) :: State, Poros
      REAL (KIND=8) :: K(3)
      REAL (KIND=8) :: Theta, ThetaStar, ThetaInit
      REAL (KIND=8) :: dsigma
      REAL (KIND=8) :: dtheta, dthetastar
      REAL (KIND=8) :: SParms(60)
      REAL (KIND=8) :: Q, SigInit
      REAL (KIND=8) :: Stress(6), CStress(3)
      REAL (KIND=8) :: Sat
      REAL (KIND=8) :: Pr, Alpha
      REAL (KIND=8) :: B, C, Temp, a
      REAL (KIND=8) :: K1o, K2o, K3o
      Pr    = Sparms(33)
      K1o   = Sparms(34)
      K2o   = Sparms(35)
      K3o   = Sparms(36)
      Alpha = SParms(37)
      Poros = State/(1.0 + State)
      a     = 0.005

!   Calculate Thetastar to allow upper bound to saturated volumetric water content
      ThetaStar = Sat * (1.0  + a/(1.0-Sat)) * Poros
      ThetaInit    = Sat * Poros
```

```
      Q = Qh(1) + Qh(2) + Qh(3) + Qh(4)
      dQsum = dQ(1) + dQ(2) + dQ(3) + dQ(4)
!
      dsigma = 0.0
      dtheta = 0.0
      B     = 0.0
      C     = 0.0

! For Constant Volume Swell Test, SwFlag = 1

!   This block solves the coupled constitutive equations for given increments of suction and
!   intergranular stress for constant volume swell test
      IF (SwFlag .EQ. 1) THEN
        B = SQRT(ABS(Suc/Q)) * K2o / K1o * dQsum

        dthetastar = (dSuc + B)/(K3o*ABS(Suc)+0.000001)

        ThetaStar  = ThetaStar + dthetastar
        Temp = 1.0 + a + ThetaStar/Poros
        Sat  = 0.5*(Temp - SQRT(Temp*Temp - 4*ThetaStar/Poros))
        Theta = Sat * Poros
        dtheta = Theta - ThetaInit

        C = SQRT(ABS(Q*Suc)) * K2o * dtheta
        dsigma = dQsum - C
      ELSE

!   This block solves the coupled constitutive equations for given increments of suction and
!   intergranular stress for Free Swell and Triaxial tests

        IF (SwFlag .EQ. 8) THEN

          dsigma = dQsum
          dtheta = 0.0
          WRITE(*,*) 'Program running under dsig=dQ'
        ELSE
          B = SQRT(ABS(Suc/Q)) * K2o / K1o * dQsum
          ! To account for saturated conditions
          dthetastar = (dSuc + B)/(K3o*ABS(Suc)+0.000001)

          ThetaStar  = ThetaStar + dthetastar
          Temp = 1.0 + a + ThetaStar/Poros
          Sat  = 0.5*(Temp - SQRT(Temp*Temp - 4*ThetaStar/Poros))
          Theta = Sat * Poros
          dtheta = Theta - ThetaInit

          C = SQRT(ABS(Q*Suc)) * K2o * dtheta
          dsigma = dQsum - C

!         WRITE(*,*) 'Program running under TX conditions'

        END IF
      END IF

!   Updated effective stress is calculated for return to main program
      CStress(1) = Stress(1) + dsigma + SigInit
      CStress(2) = Stress(2) + dsigma + SigInit
      CStress(3) = Stress(3) + dsigma + SigInit
```

```
  IF (SwFlag .LT. 5) THEN
  END IF
  WRITE(33,'(4(F9.2,1x),1x,3(F7.5,1x),3(F9.2,1x))') CStress(1), CStress(3), &
   Stress(1)+Q, Stress(3)+Q, Theta, State, Sat, dsigma, SigInit, Suc

  Suc = Suc + dSuc

  IF (Suc .GT. 0.0) THEN
    Suc = -0.000001
  END IF

  SigInit = (CStress(1)+CStress(2)+CStress(3))/3

END SUBROUTINE EffStress
```

REPORT DOCUMENTATION PAGE

Form Approved
OMB No. 0704-0188

1. REPORT DATE *(DD-MM-YYYY)*	2. REPORT TYPE	3. DATES COVERED *(From - To)*
June 2004	Final report	

4. TITLE AND SUBTITLE

A Partially Saturated Constitutive Theory for Compacted Fills

5a. CONTRACT NUMBER

5b. GRANT NUMBER

5c. PROGRAM ELEMENT NUMBER

6. AUTHOR(S)

Ernest S. Berney IV

5d. PROJECT NUMBER

5e. TASK NUMBER

5f. WORK UNIT NUMBER
Work Package AT40

7. PERFORMING ORGANIZATION NAME(S) AND ADDRESS(ES)

U.S. Army Engineer Research and Development Center
Geotechnical and Structures Laboratory
3909 Halls Ferry Rd.
Vicksburg, MS 39180-6199

8. PERFORMING ORGANIZATION REPORT NUMBER

ERDC/GSL TR-04-4

9. SPONSORING / MONITORING AGENCY NAME(S) AND ADDRESS(ES)

U.S. Army Corps of Engineers
Washington, DC 20314-1000

10. SPONSOR/MONITOR'S ACRONYM(S)

11. SPONSOR/MONITOR'S REPORT NUMBER(S)

12. DISTRIBUTION / AVAILABILITY STATEMENT

Approved for public release; distribution is unlimited.

13. SUPPLEMENTARY NOTES

14. ABSTRACT

Partially saturated soil is the most common material encountered in the field of geotechnical engineering. Yet, mechanics of partially saturated soil lags far behind that of saturated soil. A partially saturated soil is a complex multiphase system consisting of air, water, and solid material whose response is a function of the stress state, moisture condition, and other internal variables present within the soil. From a thermodynamic viewpoint, a partially saturated soil can be best described by the free energy associated with each component of the soil and water mixture.

It is noted that many thermodynamic formulations have been proposed for soil plasticity. In the current research, a theory to capture the mechanical response of partially saturated materials was constructed from a saturated soil model by adding a term for the free energy of the capillary phase that includes coupling between the solid and water phases. In defining the free energy, a distinction is made between water in the capillary phase and mobile water that flows as an independent phase. This inherent relationship between the variables appearing in the free energy expression and their conjugate stress terms obviates the traditional problem of defining the effective stress. The principles of the theory are illustrated by extending an existing plasticity model for saturated soils, which is based on an internal variable formulation, by adding terms that account for free energy of the capillary phase. The model exhibits the tendency

(Continued)

15. SUBJECT TERMS

See reverse.

16. SECURITY CLASSIFICATION OF:			17. LIMITATION OF ABSTRACT	18. NUMBER OF PAGES	19a. NAME OF RESPONSIBLE PERSON
a. REPORT	b. ABSTRACT	c. THIS PAGE			19b. TELEPHONE NUMBER *(include area code)*
UNCLASSIFIED	UNCLASSIFIED	UNCLASSIFIED		322	

14. (Concluded)

of partially saturated soil to either swell or collapse, depending on the compaction state. Simulations of consolidated-undrained triaxial tests demonstrate the proper relationship between strength and the state as described by water content, void ratio, and total confining stress.

15. (Concluded)

Airfield pavements
Compacted fill
Constitutive model
Elasticity
Granular mechanics
Partially saturated soil
Pavement mechanics
Porous media
Soil suction
Subgrade material
Thermodynamics